Università degli Studi di Milano
Facoltà di Agraria
Graduate school in Plant Biology and Production
Curriculum: Agriculture and Environment, interactions and reciprocal influences
XXVI Cycle
Scientific Sector: AGR/02

ENVIRONMENTAL SECURITY AND SEASONAL VARIABILITY: REMOTE SENSING AND MODELING APPLICATION FOR THE MONITORING OF SAHELIAN NATURAL RESOURCES

Doctoral thesis

OF

Francesco Nutini

Department of Agricultural and Environmental Science
Faculty of Agriculture
Milan, Italy

Supervisor:
Chiar.mo Prof. Stefano Bocchi

Co-Tutor:
Dott. Mirco Boschetti, CNR-IREA

Coordinator:
Chiar.mo Prof. Bianco Piero Attilio

Milan, 2012-13

Ringraziamenti

Sono grato a chi mi ha permesso di affrontare questi tre anni avventura scientifica, al Dott. Pietro Alessandro Brivio e al Prof. Stefano Bocchi che mi hanno accolto nelle rispettive strutture di lavoro con piena fiducia nelle mie capacità di studente e ricercatore.

Un immenso grazie va al Dott. Mirco Boschetti, il suo fenomenale vulcanismo scientifico è stato molto più che un mero supporto per il mio lavoro.

Grazie a tutto lo staff dell'IREA-CNR sia per i preziosi consigli/confronti lavorativi sia per i momenti di svago, all'amministrazione per non aver cercato di uccidermi ad ogni mio ritardo nel presentare qualsiasi documento, ai colleghi Alberto, Giacinto, Ramin, Simone, Paolo, senza di voi sia arrivare sin qui non sarebbe stata la stessa cosa, sia dal punto di vista lavorativo che personale.

E grazie anche al personale del CNR e alla 1,3,7-trimetilxantina per aver assecondato i miei bioritmi.

Satellite's gone up to the skies

thing like that drive me out of my mind […]

RIASSUNTO

Il lavoro sviluppato in questa Tesi si è incentrato sullo studio dei sistemi pascolivi delle regioni del Sahel, Africa Occidentale, tramite tecniche e strumenti del telerilevamento satellitare.

L'area oggetto di studio è una fascia di savana semi-arida, rappresentate la zona di transizione tra il Sahara a nord e le foreste del golfo di Guinea a sud. La regione è caratterizzata da ana marcata stagionalità, con una breve stagione umida (da Giugno ad Ottobre) in cui concentra gran parte delle produzione di biomassa vegetale e di conseguenza la produzione di derrate alimentari, seguita da una lunga stagione secca (Novembre-Maggio). A seconda della distanza dal Sahara le precipitazioni medie annuali vanno dai 150 mm annui ai 500, con elevata variabilità tra le annate. In questo sistema così mutevole la pastorizia transumante è l'attività antropica che meglio si adattata alle dinamiche stagionali. Difatti le uniche fonti di cibo sono date dalla pastorizia e, ove possibile, da agricoltura di sussistenza di specie molto rustiche come il Miglio (*Pennisetum glaucum*).

Nonostante questi adattamenti la regione ha subito una serie di crisi umanitarie a partire dagli anni 70' del secolo scorso, causate da un brusco calo delle precipitazioni annuali. Il fenomeno climatico è risultato essere dovuto ad anomalie di temperature dell'oceano Atlantico, similmente al fenomeno de *El Niño.* Nonostante le piogge siano in lenta ripresa dall'inizio degli anni 90', ricorrenti crisi umanitarie continuano ad interessare l'area (l'ultima nel 2010), motivo per cui le strategie da adottare per incrementare la sicurezza alimentare dell'area rimangono questioni dibattute.

In particolare, essendo il Sahel un'area marginale a ridosso di una zona iper-arida, non vi sono gli estremi per attuare due comuni strategie di *food security*, l'incremento delle aree coltivate e l'intensificazione delle produzioni. In questo contesto, in cui strategie top-down sono inefficaci o dannose, è il monitoraggio del territorio che riveste un ruolo cruciale. In particolare in un'area semi-naturale vasta come quella Saheliana, gli strumenti del telerilevamento satellitare sono strategici grazie alla loro capacità di fornire dati spazializzati ed ad elevata risoluzione temporale.

Scopo del lavoro è stato quello di contribuire a due aspetti del monitoraggio delle risorse naturali: lo studio di serie storiche di dati satellitari per individuare zone sottoposte a cronico degrado e studiare parametri correlati allo sviluppo della biomassa vegetale ad al suo stato idrico. Mentre il primo lavoro vuole dare informazioni utili alla pianificazione della gestione delle risorse naturali, il secondo vuole fornire informazioni in grado di fotografare in tempo reale l'andamento della stagione corrente.

La prima parte del lavoro ha riguardo il confronto sull'intera Africa Occidentale tra il 1998 e il 2009) dei i trend delle cumulate stagionali di NDVI come *proxy* dello sviluppo vegetazionale, e delle precipitazioni in quanto variabile climatiche guida.

I risultati hanno confermato che larga parte del territorio saheliano ha visto queste due variabili come perfettamente concordi durante il decennio passato. Tuttavia sono state evidenziate aree in cui i trend di produzione vegetale non sono spiegati dalle piogge. Aree in cui le produzioni sono aumentate nonostante la sostanziale stabilità delle precipitazioni (*Anomalous Greening*, AG) risultano più frequenti nelle aree più meridionali dell'Africa Occidentale ove è preponderante l'attività agricola (*West Sudanian savannah*, 46% degli AG rilevati), mentre zone localizzate di anomalo decremento dell'NDVI (*Anomalous Degradation*, AD) sono state rilevate nelle zone più aride del Sahel (*Sahelian Acacia savannah*, 59% degli AD rilevati). La analisi condotte a scala più di dettaglio con immagini ad alta risoluzione (30 m) hanno mostrato come queste anomalie si correlino ad usi e coperture del suolo differenti, con l'AG in aree agricole l'AD in aree marginali ove è praticabile unicamente la pastorizia. Due casi particolari di AG hanno mostrato eventi particolarmente drammatici in Chad e in Sudan. Entrambi i fenomeni sono risultati, da remoto, in un incremento dello sviluppo vegetazionale non legato alle piogge, dovuto al ritiro delle acque del lago Chad ed all'abbandono delle terre di pascolo a seguito del conflitto del Darfur (2005-2006).

I risultati sino a qui ottenuti permettono di sviluppare una mappatura tematica di aree localizzate soggette a cronico degrado, evidenziando in un sistema semi-naturale largamente legato alle precipitazioni zone in cui altre variabili vanno ad incidere sullo sviluppo vegetazionale. Queste possono essere approfondite dagli esperi locali, in modo da verificare se una popolazione rurale in continua crescita demografia sia incidendo sulla capacità di carico dell'ecosistema.

La seconda parte del lavoro si è concentrata sullo stima dello stress idrico e della biomassa, due variabili fondamentali nel monitoraggio delle risorse naturali e pascolive in aree semi-aride.

Serie temporali di frazione evapotraspirativa (EF) a bassa risoluzione sono state ottenute grazie alla relazione tra albedo e temperature superficiale. L'EF è una componente del bilancio energetico ed è strettamente correlata con la disponibilità idrica per la pianta. Le stime risultano avere dinamiche spaziotemporali coerenti con quelle che sono le dinamiche ecologiche della regione (piogge, fase vegetativa etc.) . Inoltre, l'EF è risultata altamente correlata con flussi energetici misurati a terra da una stazione *eddy covariance* in Niger ($r^2 > 0.7$). Il metodo implementato è di sicura utilità per la stima dello stress idrico su vaste aree come quella Saheliana, frequentemente interessata da siccità e piogge scarse.

Stime di produzioni di biomassa sono state ottenute dal prodotto operativo satellitare *Dry Matter Productivity* (DMP) basato su di un modello di *Light Use Efficiency* (LUE). Le stime satellitari sono state valutate grazie al confronto con dati di produzione di biomassa pascoliva in 46 siti di misura in Niger lungo 10 anni (2000-2009). Le stime da remoto riportano valori di biomassa (kg/ha) in linea con le produzioni medie annuali dell'area, tra i 200 kg/ha (aree iper-aride in annate sfavorevoli) e i 2000 kg/ha (pascoli altamente produttivi). Tuttavia le correlazioni coi dati di campo risultano basse ($r^2<0.3$), ed il lavoro propone due approcci per incrementare l'accuratezza del modello satellitare.

La prima consiste nell'integrazione dell'EF come fattore di efficienza di disponibilità idrica, attualmente non considerata dal DMP. L'EF ha permesso di incrementare la capacità del modello di LUE di spiegare la variabilità dei dati di campo, specialmente su quei siti ove è più marcata la carenza idrica.

Inoltre è stato verificato che il modello può incrementare la sua accuratezza nel caso in cui diverse *Radiation Use Efficency* (RUE) siano considerate, e seconda delle differenti coperture vegetali presenti al suolo. Le biomasse di queste "unità ecologiche" presentano correlazioni staticamente differenti con le stime satellitari, e si differenziano tra di loro per la loro produttività media (max NDVI) e la loro fenologia (inizio della stagione, SoS).

In conclusione, una stima satellitare di biomassa corretta per la disponibilità idrica e l'efficienza d'uso della radiazione da parte delle diverse specie vegetali, una volta prodotta operativamente potrà fornire indicazioni sulla capacità di carico dei pascoli nel corso della stagione, permettendo, se necessario, di produrre tempestive indicazioni sulle aree soggette a criticità.

Abstract

The research thesis here discussed focused on the Sahelian semi-arid rangeland, a region characterized by strong rainfall seasonality, with few dry months followed by a long dry season. In that area rangeland vegetation and human livelihoods of pastoralism and rainfed crop relies on this peculiar climatic condition. Unfavorable years whit poor or erratic rain results in reducing food supply from agropastoral activities possibly creating food insecurity condition.

The work conducted address to main aspects of natural resources monitoring: long term study to identify critical condition that require further analysis to assess potential unbalanced human activities and near real time production of herbaceous biomass relate parameters to support on-going season early warning.

In order to achieve the first goal satellite time-series of vegetation index and estimated rainfall were exploited (1998-2009) to identify areas where the two variables have opposite trends. These areas of anomalous hot spots highlight situations where the trend in the development of vegetation is locally driven by other factors mainly linked to human activity, rather than climatic driving force. In the humid regions of the southern part of the study area an increase of NDVI was observed even in conditions where rainfall remained stable (i.e. no significant trend), or even decreased (anomalous greening). These patches of increased NDVI are associated to crop land and savannah land cover classes. A number of hot spots of anomalous conditions along the boundary between the Sahelian and the Sahelian-Sudanian zones were analyzed in details using multi-temporal Landsat TM/ETM+ images and a more detailed analysis was conducted on a test area in Niger analyzing the anomalies in terms in changes of land cover and land use through years.

The analysis of changes occurred between pairs of images acquired over the same area confirmed at local scale the trends of land degradation or recovery identified at the coarser resolution of 1km. It is important to underline that these anomalous situations are driven by local causes. Anomalous greening occurring north of Lake Chad is indicative of a critical environmental situation: the shrinking of Lake Chad has uncovered new lands colonized by new agricultural fields.

On the contrary, small pockets anomalous degradation have been identified mainly in the Northern part of the study area, in the belt from West Mali to the Chad-Sudan border, which is well-known as fragile zone, where increasing population and human activity (rainfed agriculture,

pastoralism and wood exploitation) are in instable equilibrium. Their strong dependence on climatic conditions determines frequent humanitarian crises due to food shortage.

In Niger anomalous greening corresponds to the intensification of cropping in a fertile floodplain, whereas in Western Sudan it is associated to the abandonment of agro-pastoral land as a consequence of Darfur conflict. In areas where anomalous vegetation degradation is observed, the demographic framework and associated increase of the exploitation of environmental resources provide the general framework but are not sufficient to explain the local patterns.

This result would be a support for natural resources exploitation planning, highlighting local chronic rangeland condition that need detailed analysis to identify causes and specific strategies to compensate the negative effect.

The second part of the thesis focused on the estimation of two crucial variables in rangeland monitoring, the water availability for vegetation and the biomass production.

Time series of evaporative fraction (EF), strongly linked to the vegetation water status and able to increase the performances of biomass estimation , were estimated from low resolution satellite data exploiting the albedo vs. land surface temperature relation. EF satellite derived resulted highly correlated to flux tower evapotranspiration (ET) measurements. In order to monitoring regional biomass the reliability of an operational LUE based product called Dry Matter Productivity (DMP) was evaluated in Niger rangeland thanks to ground biomass measurements on 46 sites over 10 years.

In order to improve this useful biomass prediction at large scales the contribution of EF as a water stress efficiency in DMP algorithm was tested. Moreover the DMP performances were analyzed in relation to different ecological units, homogeneous in terms of vegetation cover and vegetation seasonal behaviour.

Results suggest and discuss feasible LUE modelling improvement over the Sahel, taking into account satellite estimation of water availability and different radiation use efficiency for distinct plant communities.

In conclusion, satellite biomass estimation corrected by water availability and including eco-types radiation use efficiency, once operationally produced and validated, could provide the necessary information for i) the creation of near real time bulletin of ongoing season and ii) if the case, the identification potential critical situation occurrence due to food shortage.

INTRODUCTION

Environmental security and natural resources monitoring: a Millennium Development Goals

Many international organisations that work on food security and natural hazard in developing countries stress the importance of acting in the direction of enhancing environmental security, that represents the freedom from social instability due to environmental degradation caused by natural or human processes. *Environmental security* has been defined as a state in which an ecosystem is able to support the healthy pursuit of livelihoods by the people living in that system (Thrupp and Megateli, 1999). Hence the environmental insecurity is the terminology used to express the condition in which social systems interact with ecological systems in unsustainable ways, all individuals not have fair and reasonable access to environmental goods, and mechanisms do not exist to address environmental crises and conflicts. The main aspects of Environmental security are related to both food/ water and social security in relation also to both climatic (drought, erratic rainfall) and anthropic (overgrazing, agriculture practice) causes (Figure 1).

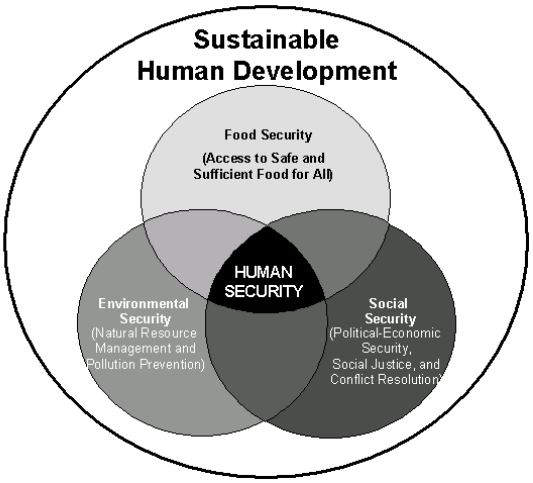

Figure 1. Linkages between food security, environmental security and social security in a sustainable development framework. Source: Thrupp and Megateli, (1999).

Role of agriculture and natural resources

Produce, increase or guarantee environmental security is one of the Millennium Development Goals (MDG), signed in New York on September 8th 2000 (un.org/millenniumgoals, last access December 2013), with the main aim to eradicate extreme poverty. The majority of poor and food insecure people live in rural areas where agriculture is the first step of economic development. Furthermore agriculture is likely to be the most affected sector to climate change, causing primarily a decrease of agriculture productivity and consequently food production that impact on

food security. Hence it has become urgent to develop adaptation processes to current and future shifts in the climate system because the most severe impacts are faced by rural population, due to their dependence on natural resources and their limited capacity to adapt to the effects of drops in agricultural production and productivity. Recently the Intergovernmental Panel for Climate Change (IPCC- www.ipcc.ch) - a committee of the United Nations that every five years collects and reviews the most important scientific contributions to the climate change - highlighted that higher frequency and diffusion of climate fluctuations are likely to produce more severe and frequent droughts and floods events, which already are the main causes of short-term fluctuations in food production in semiarid and sub-humid areas. Moreover there is an high probability of boosting temperatures in the tropics and subtropics region, such as in semi-arid rangelands, in the next 100 years, with dramatic impacts on agricultural productivity where there is no sufficient investments in adaptation (Battisti and Naylor, 2009).

In this context the opportunity to increase environmental and food security can be achieved by i) increasing the available cultivated surfaces and/or ii) improving natural and agriculture resource production efficiency. However in semi-arid area, like the Sahelian ones, there is no chance to increase areas of suitable land for agropastoral activities, and as stated by Foley et al. (2011) this marginal areas has no opportunity to increase their annual yields. Hence to achieved the MDG of increasing food security for these areas, a better management of existing resources is the most profitable option strategy. This can be achieved by both i) a better management of natural resources evaluating which human activities can be sustainable in relation to the carrying capacity of the analysed system and ii) supporting and providing early warning alarms of critical situation in order to prevent the effect on population of food crises.

Consequently it is of great importance to assess the carrying capacity of ecosystem, detecting also areas chronically deficient or in degradation, to improve monitoring programs and to provide better tools for natural resources management. In particular rangeland monitoring for a sustainable exploitation of these resources requires the capability to monitor vegetation behaviour and assess biomass production, especially where local livelihood depends on rangeland status (Ayantunde, 1999). Up to date information systems can be a key tool in supporting food security, providing services as early warning, monitoring, prediction and crop insurance (Brown and Funk, 2008).

The United Nations Office for Outer Space Affairs (UNOOSA) states that one of the most suitable way to perform natural resource monitoring is the exploitation of remote sensed data. These data source provide an unparalleled view of the Earth for studies that require synoptic or

periodic observations such as inventory, surveying, and monitoring in agriculture, hydrography, geology, mineralogy, land cover, land use and environment (www.oosa.unvienna.org/oosa/SAP/rs/index.html; last access December 2013). In particular remote sensing solution are strongly recommended where systematic acquisition of field data is not feasible and does not guarantee to properly describe wide areas spatial-temporal dynamics.

Earth observation from satellite

Remote sensing (RS) is the ability to estimate the properties of a surface by measuring and interpreting the amount of energy radiating from the object in particular portions of the spectrum. The exploitation of RS for agriculture and natural resources started in 1972 when was launched the first satellite (Earth Resources Technology Satellite ERTS-1, later renamed Landsat 1) for the global observation of earth surface. This was the first satellite for civil application designed to provide long-term, uniform global coverage for natural resources study. Optical passive[1] remotely sensed data are acquired by instrument called spectra-radiometer able to provide a quantitative measurement of the incoming radiation to the sensor in different portions of the spectrum.

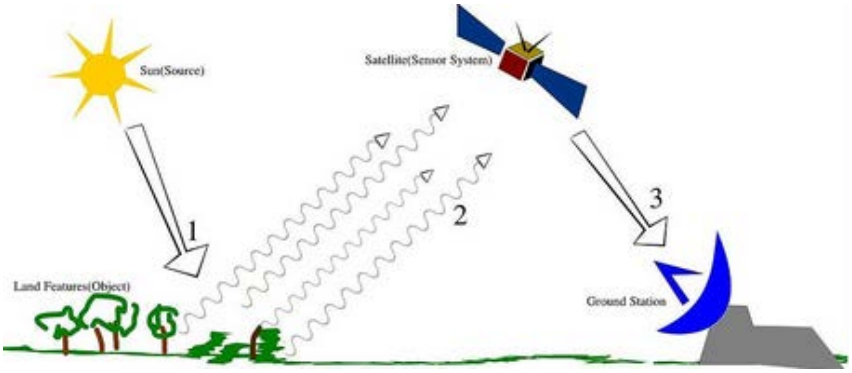

Figure 1- schematic procedure earth observation from satellite. Flux n°1 indicates incoming solar radiation, n°2 the reflected radiation and n°3 data acquisition.

Radiometers can be hand held for monitoring field plots (proximal sensing) or carried on board of aircraft or satellites to survey entire fields, farms, or agricultural regions (Brivio et al., 2006).

[1] There are two main types of remote sensing: passive remote sensing and active remote sensing. Passive sensors detect natural radiation that is emitted or reflected by the object or surrounding areas. Examples of passive remote sensors include film photography, infrared, charge-coupled devices, and radiometers. Active collection, on the other hand, emits energy in order to scan objects and areas whereupon a sensor then detects and measures the radiation that is reflected or backscattered from the target. RADAR and LiDAR are examples of active remote sensing where the time delay between emission and return is measured, establishing the location, speed and direction of an object.

The amount of radiation flux from an object (called radiance) depends on the properties (physical and chemical) of the object and the amount of incident radiation that reaches the object (irradiance). The basis of the relationship between radiation energy and surface characteristics is described by quantum mechanics and the atom resonance between two different quantum states. Many scientific field of work are based on the specific relation between molecules and radiation such as the spectroscopy physical and analytical chemistry, astronomy and remote sensing on earth.

The optical passive remote sensing uses the Sun as source of irradiance; since sun irradiance is not constant, varying with the time of day and atmospheric conditions, in order to study the physical properties of a surface apparent reflectance is requested. Reflectance is the ratio between the radiance "reflected" from an object (flux n°2 in Figure 1) and the irradiance reaching the object (flux n°1 in Figure 1). The primary remote sensing data exploited in vegetation application are acquired in the Visible (VIS; 400 – 800 nm) and Near Infrared (NIR; 800 – 1500 nm) portion of the spectrum. The characteristics of vegetation optical properties in those spectral region are here briefly described.

The relation of vegetation structure and solar radiation

Vegetation spectral characteristics

Light incident on a plant is either absorbed, transmitted or reflected depending on the wavelength and on the chemical and physical characteristics of single leaves (i.e. pigment content, leaf structure) and on plant structure related to leaf numbers (LAI) and spatial distribution (Mean Tilt Angle; MTA); all those interactions determine the typical vegetation spectra characterised by specific spectral features (Figure 2).

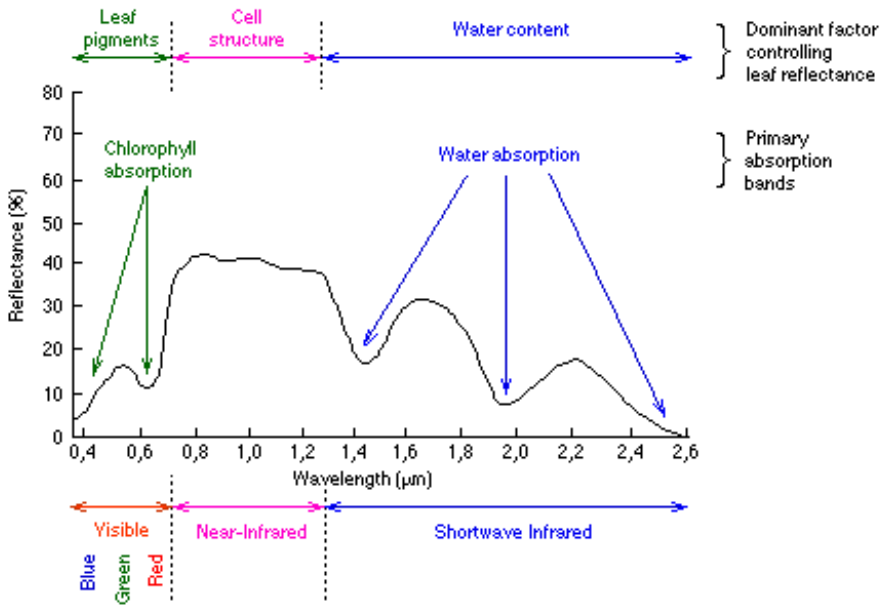

Figure 2- Spectral reflectance measured in a rice field in the VIS-NIR wavelength (nm).

Figure 2 highlights the portions of the spectra related to different leaf characteristics are highlighted. In particular the reflectance peak at 550 nm is typical of green vegetation, and it is the reason why human eye see green healthy leaf. Prominent features are also the dips at around 400 nm and 650 nm which correspond respectively to the absorption of blue and red light by foliar pigments. The concentration of foliar pigment will affect therefore the amount of red and blue light absorbed.

In addition Near infrared (NIR) light is not affected by foliar pigments. NIR energy penetrates deeper into the foliar tissue interacting with the cell structure. In the NIR (700-1500 nm), light is reflected and transmitted by plant leaves with very little being absorbed. About half the NIR light is reflected up from the spongy cell layer of the leaf while the remaining portion continues through the leaf. As the crop canopy grows becoming more dense (i.e. increase in biomass and Leaf Area Index) the NIR reflectance will increase. Healthy plants will generally reflect more NIR energy than a plant of the same species whose spongy layer is unhealthy. The amount of NIR energy reflected by a plant will be far greater than the amount of visible light. As a result detectors which are sensitive to NIR energy offer greater opportunity for detecting smaller changes in the health of a crop or in difference in plant growth than sensing systems which only detect visible light. This region of the spectrum also provides more opportunity for discriminating between different plant species as it is sensitive to the highly variable structure of plant leaves (Figure 3).

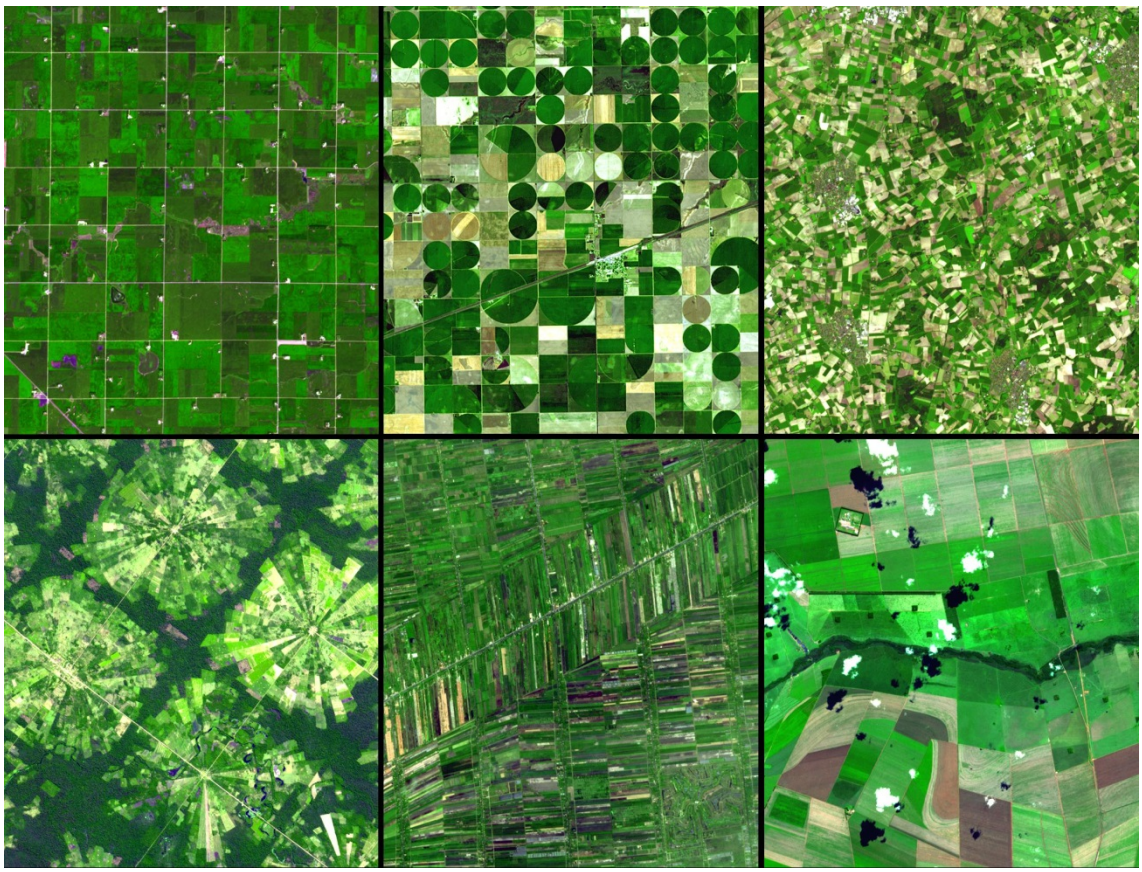

Figure 3- dense vegetated cultivated field, vivid green highlight great reflectance in NIR band compared to red (absorbed by chlorophyll type a).

Finally the short-wave infrared (1300-2600 nm) (SWIR), also called min-infrared, is the last region of Infrared exploited by vegetation RS. In this channels are clearly visible the water absorption.

Those characteristics are diagnostic of plant status and are therefore used to retrieve different crop information about health, production in term of LAI and biomass and phenological condition.

During the growing season the absorption of red and blue light tends to increase until the maturity when the chlorophyll content begins to stabilize. At the same time, the reflectance of NIR increases proportionally to the total leaf surface area due to the increasing number of cell walls and intercellular spaces. These reflectance characteristics remain relatively constant during the maturity stage unless external influences such as extreme temperatures or diseases cause a change in the overall biochemistry of the plant. When the plant reaches the senescence, the cell walls of the mesophyll tissue begin to desiccate and collapse, which results in a substantially reduced intercellular surface area and air space. The final result is a decrease in the level of green and near-infrared reflectance and an increase in reflectance of blue and red light which gives the

typical senescence yellowing aspect to leaves and the decrease in absorption id SWIR dominion due to lose of water from tissues (Figure 4).

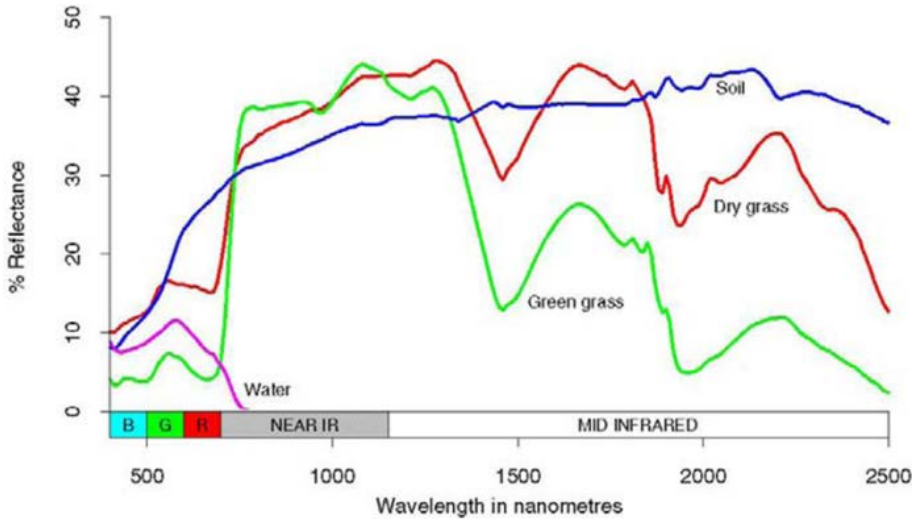

Figure 4- different spectral signature from a complete wet surface (water) to vegetation (healthy and drying) and bare dry soil.

Spectral vegetation indices

The measured spectral reflectance data are usually compressed into vegetation indices (VI), which are mathematical combination of spectral bands, able to emphasize the vegetation characteristic among the class and maximise the difference with the other surfaces. The vegetation indices are indicative of the activity of the absorbers components into the leaf (pigments, water, proteins etc.) and the total amount of foliage (LAI and biomass). In the literature more than dozen of vegetation indices are reported to show the correlation with several biophysical parameter such as fractional cover (Fc), leaf area index (LAI), total biomass, the fraction of absorbed photosynthetical active radiation (fAPAR) (Asrar et al., 1984), chlorophyll concentration (Haboudane et al., 2002), unstressed vegetation conductance and photosynthetic capacity. The best know vegetation index, widely used for monitoring the natural biome and agro-ecosystem, is NDVI (Normalized Different Vegetation Index) that is based on the difference between the maximum absorption of radiation in the red spectral wavelength and the maximum reflection of radiation in the NIR spectral wavelength (Tucker, 1979).

In agriculture monitoring crop spectral measurements can present a contamination related to the background condition (soil, water, weeds, etc.). Another source of variability is due to the atmosphere, the spectral signal has to pass through the atmosphere before reaching the analysed surface and in its reflected path to the sensor. For this reason different vegetation indices have been proposed to minimise background influence and atmospheric contamination.

Remote sensing for food security

In areas that face frequently food shortage it is important to have a tool to monitor environmental variables and crop production during the agricultural season, and to highlight where the ecosystem carrying capacity is endangered (Wang et al., 2013). The needed information on agricultural and pastureland production should i) cover large areas giving information on spatial dimension of phenomena, ii) provide information in near real time (NRT) of ongoing season in order to deliver alerts a few weeks before the harvest and iii) give quantitative estimation of agricultural production (Lambin et al., 1993).

Satellite RS can contribute significantly to such a system by collecting information on crops and on environmental variables on a wide geographical scale and with a high temporal frequency, exploiting both i) the remote sensors capability to detect vegetation presence and status and ii) the satellite capacity to frequently over pass on the same region.

Several national and international organization have developed RS tools, often combined with field survey, to monitor areas chronically affected by food shortage in order to produce early alarms on ongoing season. For example the Senegalese research institute *Centre de Suivi Ecologique* (CSE, svr-web.cse.sn/, last access December 2013) started in the Eighties, to exploit NDVI data derived from the Advanced Very High Resolution Radiometer (AVHRR) sensor in empirical correlation with field biomass data producing herbaceous biomass maps operationally used for rangeland monitoring (Beyè, 2010). This pioneering program was possible thanks to the first promising results obtained in the area by several studies (Tucker et al., 1983; Tucker, Townshend, et al., 1985).

International organizations currently produce periodic bullet on crop yield and natural resources status, combining RS, modelling and local expertize. Examples of these operational systems include the Crop Growth Monitoring System (CGMS) run by the MARS unit of the European Commission's Joint Research Centre (mars.jrc.ec.europa.eu, last access December 2013) and the Famine Early Warning System Network (FEWSNET, www.fews.net, last access December 2013) of the United States Agency for International Development (USAID). Also a series of international research projects worked on providing daily rainfall data (EPSAT-Estimation of Precipitation by SATellite, Lebel et al. 1992), meteorology modelling (HAPEX-Sahel, www.cesbio.ups-tlse.fr/hapex, last access December 2013) detailed land use mapping (DMP-GEF program, Hiernaux and Ayantunde 2004) and improving African environmental monitoring

capacity via RS data (NARMA-GeoLand2, www.gmes-geoland.info, last access December 2013).

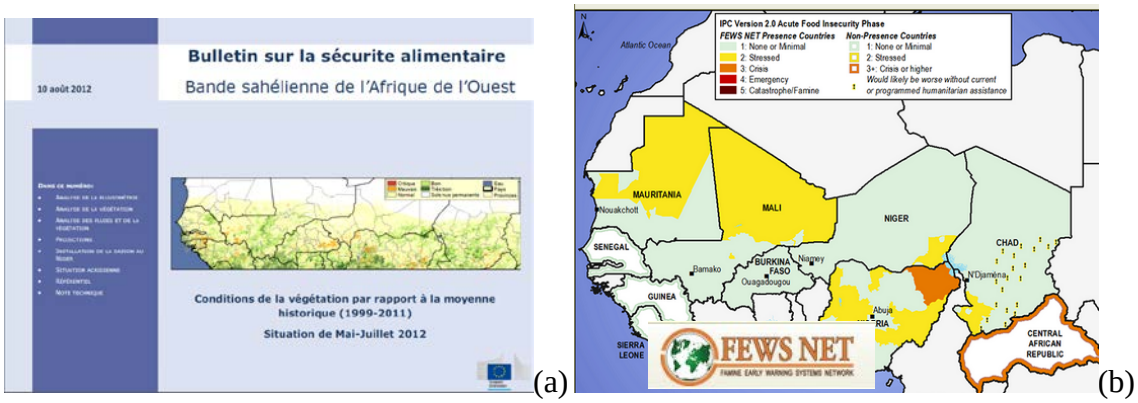

Figure 5- food security periodical bulletin in West Africa produced by MARS - mars.jrc.ec.europa.eu (a) and FEWSNET - www.fews.net (b)

The scientific challenge is to produce better information to improve existing monitoring tools for bulletins of rangeland status. Indeed the FAO communicated that the exploitation of satellite imagery by the Permanent Interstate Committee for Drought Control in the Sahel (French: *Comité permanent inter-État de lutte contre la sécheresse au Sahel*, abbreviated as CILSS, www.cilss.bf, last access December 2013) allowed in 2011 to determine that the amount of food produced in that year would have been sufficient to sustain local population. This analysis allowed to highlight how the 2011 food shortage problem was caused by food access by people with not enough money to buy the food that was available. Also the Regional Centre for Mapping of Resources for Development (RCMDR, www.rcmrd.org, last access December 2013) stressed the importance of remote sensing in drought monitoring critical baseline from which future changes can be spotted, and droughts anticipated before they happen.

Remote sensing application to support food policies and agropastoral development

Identification of anomalous situation and changes in land cover

Thanks to relation between surface characteristics and solar energy, and the particular behaviour of vegetation in optical and infrared domain, RS technique allows to analyse proxy of vegetation status in its spatial variability. However the study of natural resources needs to focus on the temporal dynamic of the systems, in order to explore vegetation behaviour within the growing season and/or through different consecutive seasons. The moderate resolution satellite images with quasi-daily revisiting cycle, routinely acquired over the same area are suitable to perform phenological monitoring and season growth analysis (Boschetti et al., 2009).

An example of phenological monitoring is provided in Figure 6; the graphs show the automatic identification of phenology stages in different rice cropping systems exploiting seasonal time series of EVI (Enhanced Vegetation Index) MODIS data. The figure demonstrates how from the analysis of temporal VI signal (black dotted lines) is possible to identify the occurrence of the start of season/crop establishment (red cross) and peak of season/flowering (green cross) in case of one, two and even three cropping seasons (respectively Figure 6a, b and c). For further details see Manfron and Crema (2012).

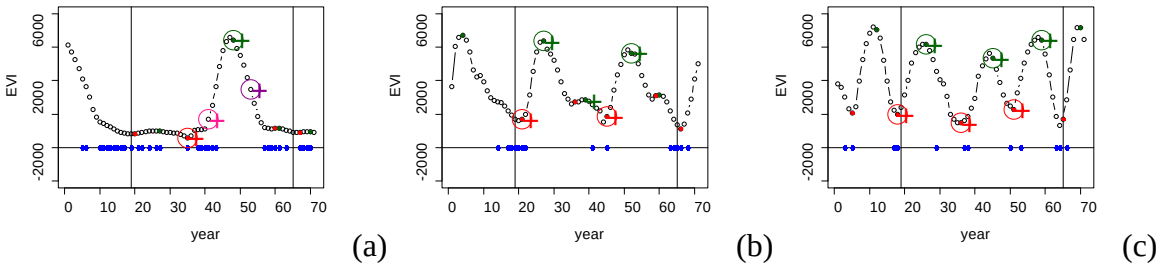

Figure 6- start of season (pink cross in a circle) and end of season (magenta cross in a circle) for each rice season detected (circled green and red crosses) mapped on smoothed MODIS-EVI data (black dotted line) for 3 selected rice cultivation in Philippines (a), Vietnam (b) and Spain (c). Vertical straight lines indicates one solar year.

The availability of long time series data such as 30 years of AVHRR (launch 1981), 25 years of SPOT-VGT (launch 1986) or 15 years of MODIS (launch 2000) resulted fundamental to study long term dynamics that involves the vegetation compound. Figure 7 displays the time series of NDVI vegetation index derived from SPOT-VGT data, over a savannah area. The grey line indicates 13 years of 10-days NDVI data, black line shows the mean annual behaviour and the red arrow displays the increasing trend in vegetation production.

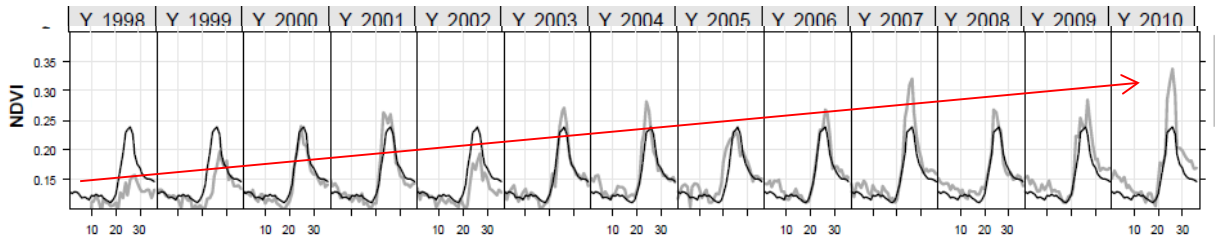

Figure 7- time series of 10-days NDVI over a savannah area (light gray line). Dark line indicates the mean decadal NDVI and red arrow indicates the increasing trend (Boschetti et al., 2013).

The importance of ecosystem dynamics studies are re-invigorated by environmental security issues linked to global change, such as desertification and land degradation processes that can be identified only using long-term spatial data analysis at an appropriate scale (Herrmann et al.,

2005). Multi annual time series of RS data were analyzed by Herrmann, Anyamba, and Tucker (2005) and Fensholt and Rasmussen (2011) to detect degraded vegetation in West Africa. These studies were able to identify local vegetation trend in accordance to climate variability and local critical areas where it can be assumed human-induced causes.

Vegetation mapping and change detection

The mapping of different vegetation cover and identification of land use is another common RS application. As exposed previously different natural surfaces (such as bare soils, cultivations, woodland, etc.) can be discerned by their spectral signature. These differences, both in VIS and IR channels, can be detected by automatic classification methods, based on statistics techniques able to separate surfaces by their spectral signature, resulting in thematic maps of land cover and land use (Brivio et al., 2006).

For example the satellite image in Figure 10 displays with RGB combination (false colour 543 TM bands) surfaces with different spectral signatures. In this case, thanks to NIR and SWIR bands, vegetation (green areas) bare soil (maroon) and water (dark spots) are clearly visible and can be automatically separated by an algorithm such as maximum-likelihood, IsoData, principal component analysis and so on. Currently a lot of thematic maps of land cover/use are produced in that way by public organization for planning agriculture purpose such as the Corine (G. Buttner, J. Feranec, G. Jaffrain, L. Mari, G. Maucha, 2004) or for natural resources management as the GlobCover (Arino et al., 2007) and GLC2000 products (Bartholomé and Belward, 2005).

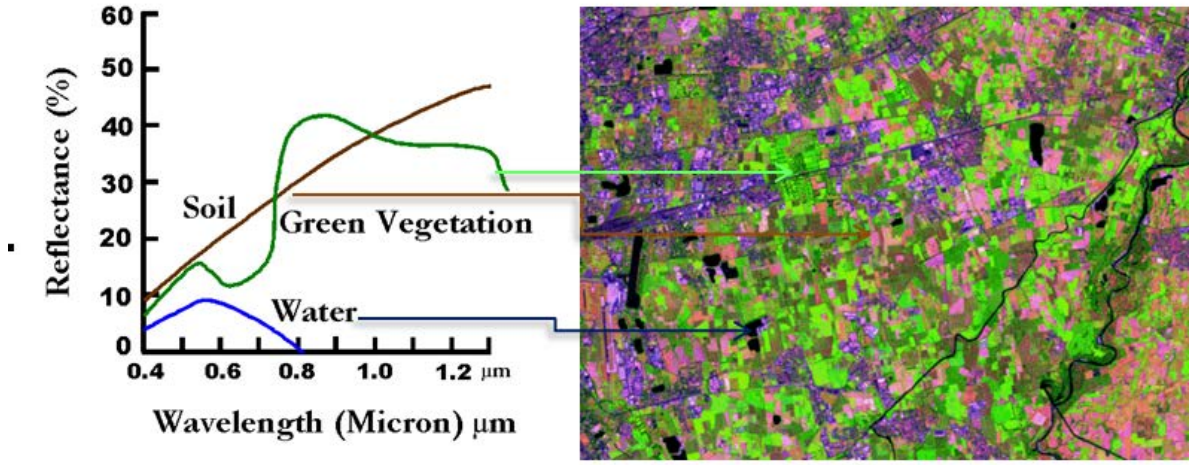

Figure 8- satellite image over Parco Agricolo Sud Milano in date 31/08/2009. Landsat 5 satellite, false color image TM bands 543 (Near-Infrared, Red). Graph reports the typical spectral signature of 3 surfaces (soil-brown, vegetation-green, water-dark blue).

Classification performance can be increased when several images are available during a growing season. For example Rasmussen and Reenberg (1992) used four images acquired during the year to discern crops from surrounding savannah on the base of different seasonal behaviour and visual interpretation techniques. Also Lasanta and Vicente-Serrano (2012) in the Mediterranean region used a combination of Landsat time series and local knowledge to detect 12 types of land-use changes such as intensification of agriculture, rural exodus and reforestation. The Figure 9 shows how the growing season in a semiarid savannah is monitored by time series of satellite images. This RGB combination (TM bands 432) highlights enhance vegetation cover in reddish. The Figure 9a shows homogenous bare condition (grey/maroon colours), Figure 9b shows in light red the starting of vegetation growth and Figure 9c shows the peak of vegetative phase (vivid red).

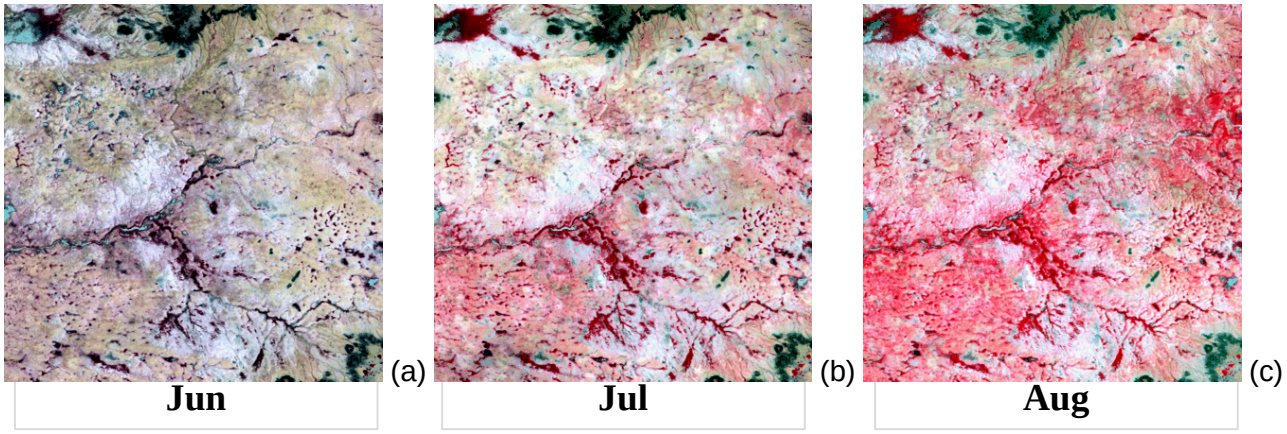

Figure 9- HR images (10 x10 km) over semi-arid savannah in Niger in June 2007 (a), July 2007 (b) and August 2007 (c). Landsat 5 satellite, false color image TM bands 432 (Near-Infrared, Red).

Moreover if images or maps referred to different years are available it is possible to detect the changes in vegetation cover by diachronic analysis. These changes can be related to human managements or climatic conditions. For example Brink and Eva (2009) detected changes in land cover and land use linked to degradation or improvements in agropastoral areas analysing changing of five thematic classes (shrubland, cultivated land, herbaceous vegetation, water body, and bare area) and Ruelland, Levavasseur, and Tribotté (2010) showed that West African croplands had been extended by 14% over the last 25 years of the twentieth century due to the increase in population, which effectively doubled in the period from 1970 to 2000.

The Figure 10 shows two typical vegetation types in semi-arid marginal area: a tiger bush (Figure 10a) and rainfed crops (probably Millet, Figure 10b). The former vegetation type between the 2 years (2000-2007) shows no evident changes in bush extension. On the contrary cropland (Figure 10b) shows a high change in field pattern due to human resources management.

This qualitative observation can be automatically extracted from the images exploiting algorithm of classification providing spatial thematic information of past phenomena and occurred changes.

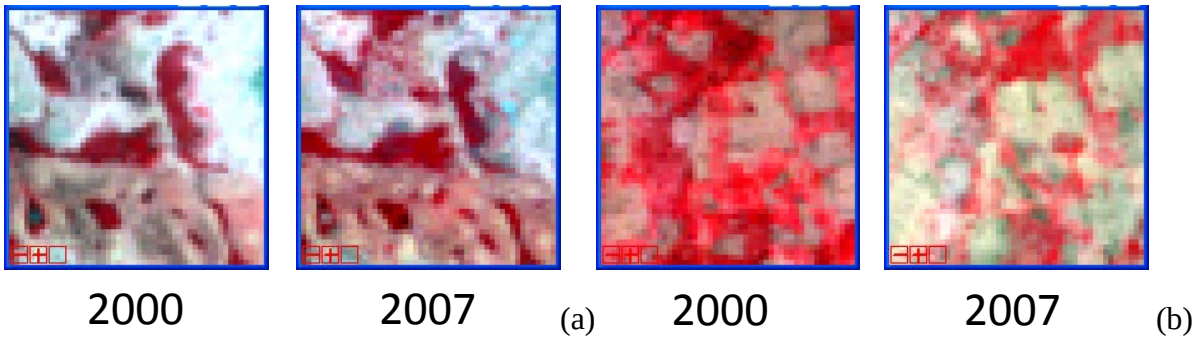

Figure 10- visualization (2x2 km) of a tiger bush area (a) and croplands (b) in semi-arid region of West Africa for year 2000 and 2007. Landsat 5 satellite, false color image TM bands 432 (Near-Infrared, Red).

Near real Time information to support agropastoral monitoring: Estimating of vegetation parameters from remote sensing modelling

Biomass estimation by Monteith' approach

Most of the rural poor population live in region where pastoralism and rainfed agriculture are the most important livelihoods. Especially extensive livestock system relies on forage availability that in semi-arid regions is the direct effect of annual climate condition (Ham and Fillol, 2010).

Due to the extension of the pastoral areas (Tucker, Vanpraet, et al., 1985), the very low demographic density (Ham and Fillol, 2010) and the difficulties to collect local data representative of the variability in space and time (van Vliet et al., 2013) satellite tools are necessary to monitor biomass production in the Sahel. Hence the lack of ground data could be overcome by exploiting remote sensing techniques (Prince, 1991).

A simple approach to estimate vegetation biomass was proposed by Monteith (1972) that experimentally demonstrated how the growth of a well-watered and fertilized annual crop is linearly related to the amount of solar energy that plants intercept over a growing season. This logic combined the meteorological constraint of available sunlight reaching a site with the ecological constraint of the amount of leaf area absorbing the solar energy, while avoiding many complexities of canopy micrometeorology and carbon balance theory.

The Monteith's model, also called Light Use Efficiency (LUE) model, defines the dry matter production (DM, g m^{-2}) for a given time period as total intercepted absorbed photosynthetically

active radiation (APAR; MJ m^{-2} d^{-1}) multiply by the RUE (g MJ^{-1}) coefficient as summaries in equation:

$$DM = RUE \times fAPAR \times PAR \qquad \textbf{Eq. 1}$$

where RUE is the coefficient that describe the efficiency of a plant in use radiation to produce dry matter, fAPAR is the fraction of absorbed PAR (fAPAR; -) by the plant and PAR is the photosynthetically active radiation (PAR - 300-700 nm; MJ m^{-2} d^{-1}) reaching the crop surface.

The success of the LUE model is due to the possibility of directly use of remote sensing data in its formulation as proposed by Kumar and Monteith, (1981). RS data can be used because fAPAR is a property directly linked to canopy reflectance (Daughtry et al., 1983; Asrar, G., Fuchs, M., Kanemasu, E.T., Hatfield, 1984; Gallo et al., 1985; Leblon et al., 1991). In a simple way vegetation light capture and absorption is generally not obtained directly by remote sensing instruments. However, the proportion of light absorbed is the complement of the proportion of light reflected (measured by remote sensors). The more light reflected in a given wavelength band means that less light is absorbed in that same band. fAPAR and canopy reflectance are therefore functionally interdependent because they depend by the same factors.

PAR absorption is a function of Leaf Area index (LAI), leaf optical properties (i.e. chlorophyll content), leaf angle distribution and optical properties of background (soil, water, etc.) and sun zenith angle. All these factors determine also the canopy spectral response acquired by the remote sensing instruments.

The effective of use remote sensing data in Monteith's equation depends on the availability of satellite overpass acquired during the growing season: three to four images are at least necessary to describe the crop growth. Many application of the Monteith's LUE model using remote sensing data are reported in scientific publication. This approach resulted particularly useful in assess net primary production in remote area were satellite data could represent a very useful (often unique) source of data (Bartholomé, 1990; Prince, 1991).

Specific model have been developed to directly use satellite data to provide global estimation of vegetation compound net primary productivity such as the CASA (Prince and Goward, 1995), SDBM (Knorr, W. Heimann, 1995), TURC (Ruimy et al., n.d.) and GLO-PEM2 (Goetz, 2000). For a faithfully comparison and discussion on these models, often developed for studies of carbon cycle and global climatic modification, refer to Cramer and Kicklighter (1999), Kicklighter and Bondeau (1999) and Ruimy, Kergoat, and Bondeau (1999).

LUE model is also widely used for crop production estimation at regional to local scale thanks to the availability of different Earth Observation (EO) data resolution. However, the majority of the application relies on the possibility of deriving fAPAR time series directly by NDVI data derived NOAA AVHRR (Advance Very High Resolution Radiometer). Turner et al. (2002) estimated corn and soybean biomass production using Monteith's model integrating 2 weeks composite data of 1 km resolution AVHRR. (Bastiaanssen and Ali, 2003) integrated the CASA model (Potter C.S. et al., 1993)based on 20 AVHRR NDVI data for dry biomass production with the surface energy balance model SEBAL (Bastiaanssen et al., 1998) to estimate crop growth in Pakistan. Kiniry et al. (2004) used weekly MCV (Maximum Value Composite) NDVI by AVHRR sensor to estimate crop fAPAR updating the RUE based model ALMANAC (Kiniry et al., 2004) to provide maize yield forecast. (Tao, F., M. Yokozawa, Z. Zhang, Y. Xu, 2005)compare the two above mentioned CASA and GLO-PEM model for regional maize yield estimation in China, the Authors derived fAPAR estimation from 10 days composite NDVI AVHRR data. (Leblon et al., 1991) used SPOT data to estimate fAPAR on rice to predict the final crop yield.

Lobell et al. (2003) produced reliable wheat yield estimation of Yaqui Valley in Mexico using 30 meter resolution Landsat 5 TM data. Since those satellite images are not available for each day the authors simply use the available dates to constrain a known crop development behaviour (from field studies of wheat) scaling the fAPAR profile and shifting planting date to fit the existing satellite observations.

The Monteith approach is therefore widely used for monitoring net primary production (NPP) above ground biomass (AGB) of natural ecosystem also for food security purpose, however its main drawback relies in a lack of description of the complex physiological and biological mechanism that control the plant growth and development (Hilker et al., 2008). LUE improvement still under scientific debate and they are discussed in V section of the manuscript.

Water status of vegetation compound from thermal and optical data

In semi-arid area the availability of water is considered the main driving force of vegetation growth and production (Le Houerou, 1980). Many scientific work were conducted on water availability in West African region, where water shortage and drought years impacting on rainfed food production systems have led to severe food crisis .

The recently capability to estimate rainfall events from satellite had stimulated the study of biomass production from satellite in relation to water (Herrmann et al., 2005; Olsson et al., 2005;

Heumann et al., 2007; Mertz et al., 2010; Fensholt and Rasmussen, 2011; Boschetti et al., 2013). The relation is so strong that in the Sahelian the soil moisture (Huber et al., 2011) and annual rainfall (Hein, 2006; Fensholt and Rasmussen, 2011) were proposed as proxy of vegetation production. The relation between rainfall availability and environmental security was so strong during the past century (Giannini et al., 2003) that several works used rainfall data to highlight production trends and anomalous spots in vegetation production (Herrmann et al., 2005; Heumann et al., 2007; Boschetti et al., 2013). However, the interpretation of this data is complicated by complex relation between climatic driving force, vegetation association and human management (Olsson et al., 2005; Mertz et al., 2012). Better understanding of rangeland production in relation to water availability is of interest for the implementation of operational policies aiming at reducing the socio-economic impacts of environmental stresses.

A possible improvement in study the ratio between rainfall and vegetated surfaces is the observing of evapotranspiration (ET), that is the loss of water from the ground and vegetative surfaces due to vaporization of liquid water. Evapotranspiration is both a heat balance component and a key component of the water budget and it's estimation is important for food security programs (Verstraeten et al., 2005) and improving water management (Bastiaanssen et al., 1998). Compared to the simple measuring of rainfall, the ET gives the possibility to study the relation between climate and vegetation.

Indeed ET it is one of the most important regulating factors of climate, both at local and global scales, linking energy, climate and hydrology (Ruhoff et al., 2012) and one of the main phases of the water cycle. One of its distinguishing factors is its role as a cornerstone between the energy and water cycles. Over highly vegetated area up to 80% of annual rainfall could be evapotranspirated (Orange, D., Wesselink, A.J., Make, G. and Feizure, 1997), hence ET knowledge is of great importance for water resources management in particular in areas marked by frequent water shortage.

In these context modelling and measuring of ET is of great relevance for supporting food-security programs (Bastiaanssen et al., 1999; Verstraeten et al., 2005) determining water needs to carry out new management strategies to improve efficiency in water uses (Ciraolo et al., 2007). For studies at field scale the measurement of evaporation of vegetation can be performed with field water balance, lysimeter, scintillometer and for landscape studies with eddy correlation techniques (Verstraeten et al., 2005). However it is not easy to quantify this flux; ET is highly dynamic in space and time because of complex interactions between soil, vegetation and climate (Allen et al., 2007) and furthermore quantification of this flux on a watershed or a regional scale

is much more difficult than at a specific site (Irmak et al., 2011). The traditional methods to estimate ET, such as the reference crop evapotranspiration assume homogeneous land coverage and structure and detailed spatial information of land cover, but these conditions are difficult to be founded for large regions (Li et al., 2012). In fact for regional and continental scales monitoring the solution of using models coupled with remote sensing is highly recommended, because this approach can cope with spatial and temporal dimension of evaporation processes (Verstraeten et al., 2005). Several data of surface characteristics such as albedo, vegetation coverage, land surface temperature, and leaf area index, can be retrieved from satellite providing data for ET estimation from space (Li et al., 2012). In practice, the estimation of ET from satellite may just be limited by the availability of input data. Several ET estimation were conducted over semi-arid areas with different methodology. Among them, ET maps obtained in arid regions of Iran (Muthuwatta et al., 2010) and China (Li et al., 2012) from low resolution data (MODIS and AVHRR respectively) allowed to produce spatialized information on water shortage, suitable for best water management. Hoedjes et al. (2008) tested a similar methodology based on EB but on HR data (ASTER) producing information on water stress for olive cultivation. Finally some works stress the link between ET and biomass production by empirical relationship (Novák and Genuchten, 2008) or as driving input in crop model (Roebeling et al., 2004) or LUE model (Sepulcre-cantó et al., 2013).

Case study: the Sahel

Eco-geography

The Sahelian[2] region is the eco-climatic zone of transition between Sahara desert at North and Sudanian savannahs at South. It is a semi-arid region that stretches across the West Africa (WA) and Sudan as displayed by gray belts in Figure 11. The Sahel is characterized by a savannah biome, which is typical of all transition areas between desert and forests, and is dominated by a marked rainfall seasonality and climate variability.

Figure 11- sahelian belt across Africa. Northern and Southern are define on the basis of annual rainfall.

The most common livelihood is pastoralism, because it can adapt to the un-stable climate taking advantage from nomadism and seasonal transhumance (Krätli, 2007). As a result, most of the people in the Sahel have been semi-nomads since last century, since rainfed farming and raising livestock in a system of transhumance is probably the most sustainable way of using the Sahel natural resources (Zorom et al., 2013).

[2] Sahel is an Arabic word which literally means *border, shore,* and it was a term traditionally employed by Saharan people to indicate the north (or west for ancient inhabitants of Mauritania) and broadly the direction to reach the Mediterranean sea and the Atlantic ocean. Still today the Tunisian coastal areas are named "Sahel".

Over the past fifty years the region was most renowned for a dramatic series of food crisis, mainly caused by prolonged drought (Mortimore, 2010). Some of these crisis resulted in tensions, and armed conflicts for the natural resources between herders and farmers.

Many studies converged to the Sahel from different point of view: environmental and climatic, agronomic and management, as well social, economic and political. Specifically, the nature of food crisis in the Sahel has been analysed with the aim of understanding whether the causes of food crisis were climate or human induced and to produce early warning systems to face future crisis.

Ecosystem and Climate features

The Sahel is not clearly defined by physical barriers (rivers, mountains etc.), but it is a transition according to a biological gradient largely driven by rainfall (Le Houerou, 1980). The climate is characterized by a strong and marked seasonality, with a long dry season (November-May) and a short rainy period (June-October) (Nicholson and Tucker, 1998) whose consequence is the vegetation biomass production circumscribed in the short and unstable wet period.

The rainfall gradient produces a gradual shift in vegetation from annual herbaceous species typical of desert to forests without even having the impression of a strict biologic border (Monod, 1985). As a result the borders of the Sahel can be defined by human activities (limits of pastoral livelihoods) or by the different isohyet, as shown in Figure 12.

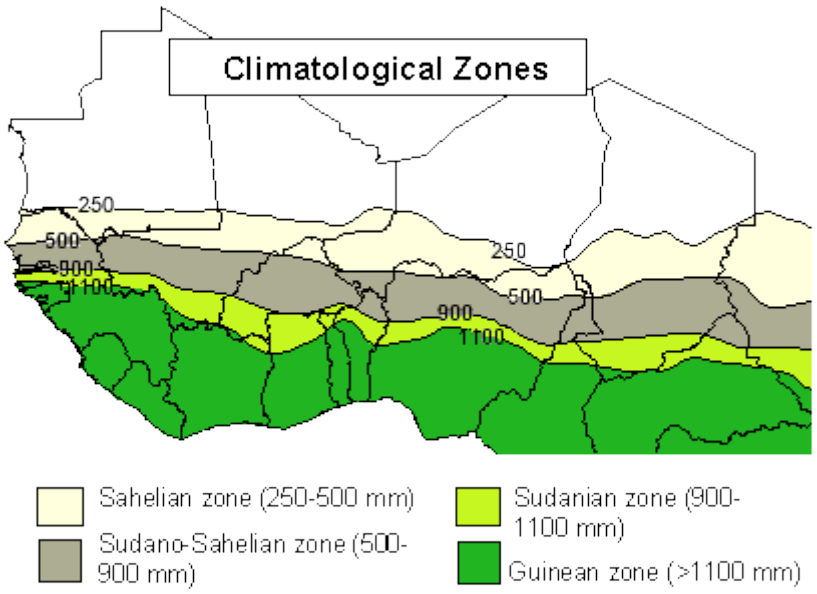

Figure 12- West Africa. Green, gray and light areas highlighted different eco-climatic zone as defined from mean annual rainfall from 1960 to 1990 (source: FAO).

The semi-arid Sahelian area has mean annual rainfall about 150-600 mm per year, comprised in 2 to 4 wet months. The Sahelian zone longitudinally extends from the Atlantic to Sudan, and it belongs to the "Sahara-Sindian" floristic region (Wickens, 1997). Latitudinally it can be derived in 3 different sub-regions, depending on mean rainfall, vegetation types and local livelihood. The first sahelian zone is the more arid where only pastoral activities are allowed. The central is characterize by strong link between pastoral and rainfed agriculture and the southern has pretty intensive agriculture and livestock breeding around cities.

Northern area – comprised between 100 m and 200 mm. Characterized by sandy soils and low tree density, herbaceous coverage of perennial Poaceae is dominant on severely poor soils. On soils composed by clay and loam, concentrated in depressions and valleys, productivity can reach 500 kg of dry matter per hectare but production lower than 300 kg/ha are more frequent (Justice and Hiernaux, 1986). Annual herbaceous species are the most common in this favourable zones providing an essential source of biomass for the Touareg's animals. The traditional animal production systems consist in nomadic pastoralism conducted over large pasturelands and goats are the most common specie since they can graze on poor and semi-arid pastures. Their weight has a strong seasonality as the surrounding environment, from 22 kg in June to 28 in November when there is the "better pastoral condition" (gray boxes in Figure 13). This area was the most affected by the great drought of 1973 (Zecchini and Cantàfora, 2010).

- Shrubs: *Acacia raddiana, Commiphora Africana, Leptadenia pyrotechnica, Balanites aegyptiaca, Maerua crassifolia and Ziziphus mauritanica*.
- Herbaceous: *Aristida hordeacea, Aristida funiculate, Cornulaca monacantha, Cornulaca aucheri*
- Cultivation: none
- Herding: nomadic pastoralism (mainly goat)

Central area - comprised between 200 mm and 350 mm of annual rainfall. Annual herbaceous species dominate these lands with spotted woody species, due to low rainfall and high wildfires frequency. On sandy soils the herbaceous coverage is quite homogeneous and the productivity of these grasslands can reach 1000 kg of dry matter biomass per hectare on richer soils (Justice and Hiernaux, 1986).

Here cropping activities and pastoralism are traditionally integrated. The livestock manure enhances soil fertility, and at the same time crop residues provide feed for herds in the dry season (Figure 14). Manure may come from farmer's own herd, from another farmer's one, or from transhumance pastoralists and represents the principal ways of enhancing crop yields (Mertz et al., 2012). Herds management vary according to the season. Animals can be free grazers or herded, depending on the intensity of management. Livestock move from south to north before the beginning of rain and move south at the end of wet season (Figure 13). Rainfed agriculture is possible in favourable areas, protected from wind and closed to water pools (Leblanc et al., 2008).

- Shrubs: *Acacia* (various species)
- Hebaceous: *Panicum turgidum, Aristida mutabilis, Cenchrus biflorus, Eragrostis tremula, Brachiaria xantholeuca, Schoenefeldia gracilis, Aristida funiculate, Cymbopogon schoenanthus.*
- Cultivation: rainfed, only in favourable areas. Pennisetum gluacum (Pearl Millet) and sorghum
- Herding: seasonal transhumance (mainly cattle Bororo and Azawak) strongly linked with rainfed agriculture

Southern area - below the limit of 350-mm isohyet. Productivity of grasslands, depending on floristic composition, can reach 3 tonnes of dry matter biomass per hectare (Schlecht and Hiernaux, 2006). On hydromorphic soils of lake Chad it is possible to find high productive grassland that provides pasture biomass through the whole year. In that area agriculture activities begins to be of great importance, due to supplementary water availability from rivers (Niger, Senegal) and dams. Livestock breeding is often close to town, due to the possibility to sell dairy products (Zecchini and Cantàfora, 2010).

- Shrubs: *Mimosaceae* and *Combretaceae*
- Herbaceous: *Therophytes Schoenefeldia gracilis, Aristida mutabilis and Cenchrus biflorus Panicum repens, Panicum porphyrrhizos, Sporobolus spicatus and Sporobolus helvolus,* while on sandy soils the dominant species are *Schoenefeldia gracilis* and *Echinochloa colon*a
- Cultivation: Millet, Sorghum, Maize, Onion. Groundnuts, cowpeas, rice, soya and cotton as cash-crops if water irrigation is available (i.e alongside Niger and Senegal rivers).
- Herding: per-urban farming linked with city market (mainly cattle)

The Figure 13 summarize the most important cropping and herding phases over the entire Sahelian region. The boxes along the timeline highlight a great temporal variability (up to 3 months) of pastoral and agricultural activities (transhumance, harvesting etc.). This is due to great inter-annual rainfall variability (Mertz et al., 2010), differences between southern and northern Sahel (Geesing, D., Djibo, 2001) and local personal choices (Krätli, 2008).

All the Sahelian livelihoods are linked to the rainfall seasonality (bottom blue box, Figure 13). Pastoralist move to north before starting of rain (April-June) and to south after the end of wet season (November-January), when animals are at their best condition (Krätli, 2008). Crops are seeded during the wet season (July-August) and in marginal areas seedling happens only after the starts of rain (Marteau et al., 2011).

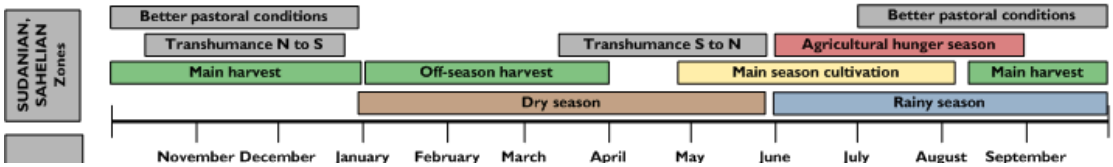

Figure 13- season calendar and critical period timeline for Sahelian agropastoral activities (Source: FEWSNET)

The most critical period are the months just before cropping (red box in Figure 13). If the previously year was poor, in these month food provisions would be finished and there is no ready cultivation to be yield. Erratic or late rainfall in these months can be troubling.

In conclusion the Figure 14 schematize the food supply system from typical sahelian agropastoral activities. All sources of food relies on annual rainfall, and there is a strong relation between pastoral and agriculture livelihoods thanks to manure and crop residues. Red colour highlight processes (vegetation growth, rainfall) of interest for food security programs and suitable to be satellite estimated.

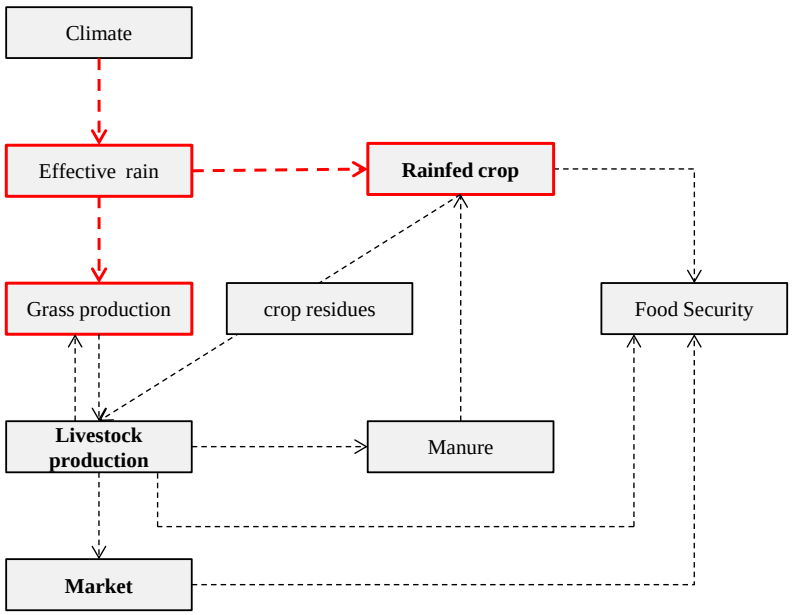

Figure 14- ecological–economic structure of Sahelian agropastoral livelihood. Red indicates variables and processes remote sensing derived. Bold text sources of food. Adapted from Hein et al., (2008)

Historical drought Crises and recent food security issues

In the 20th century, the Sahel region experienced three major drought periods including 1910–1916 (yellow arrow in Figure 15), 1941–1945 (orange arrow in Figure 15), and the long period of sustained declining rainfall, known as the "desiccation", that spanned from 1970s to the 1980s (red arrow in Figure 15). The *desiccation* was a dramatic episode for the young Sahelian nations, which had just gained their political independence through the decolonisation process (Mortimore, 2010).

The annual rainfall values of 1983 and 1984 were among the lowest ever recorded in the history of the Sahel. In 1984, drought severely affected all countries from Mauritania to Ethiopia, including several bordering countries on the southern edge of the Sahel (Tucker, Vanpraet, et al., 1985). In contrast, the 1973 drought was more localised and affected mostly Mali, Niger and Chad (Hiernaux et al., 2006). Histogram showed in Figure 15 highlight the mean rainfall during the past century over the entire sahelian area. Data are normalized on their mean. The beginning of the drought in 70's is evident as well as the 1984 crisis.

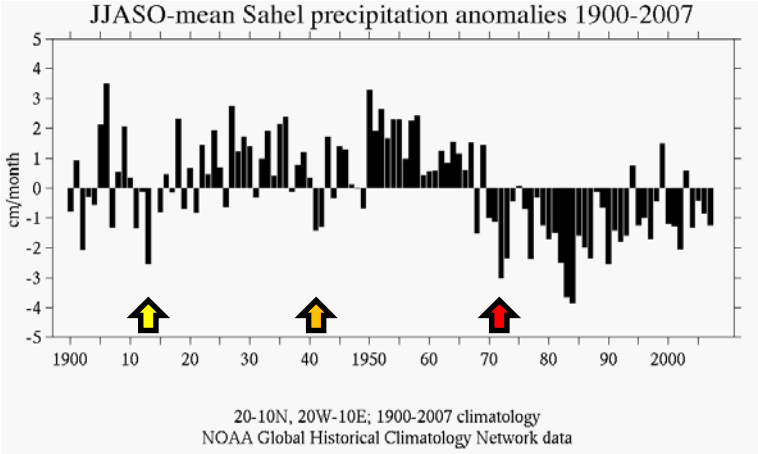

Figure 15- mean annual rainfall from 1900 to 2010 over the Sahelian area. Arrows indicate main drought occurrences (source: NOAA GHCD).

During the long period of drought local herds have experienced significant losses of livestock (50% of cattle, 36% of sheep, 27% of goats). These losses (particularly the cattle ones), have been more severe in pastoral areas than in agricultural ones: this factor increased the proportion of these herds in the South Sahel rather than the North. During this drought the nomadic Fulani have abandoned their usual migration path moving to cities or food distribution centres.

Only in 1977 the majority of pastoralists was able to restore usual route and in 1981 the 80% of cattle were restored. This long period of drought was followed by some favourable years, but it was always marked by a general lack of rainfall culminated in the catastrophic season of 1984. When the summer of 1984 was ending it became suddenly clear that biomass resources would not have been sufficient to provide enough livelihoods to the livestock and local governments advocated with pastoralists to make them leave pastoral areas in October. The pastoralists and their herds were moved from 150 to 250 km southern compared to their usual pastoral areas, often flocking to the cities and selling most of their animals. As a result, in the areas of Tahoua, Maradi and Agadez (Niger) as well as in other parts of Mali, the pastoralists do not own more than the 40% of the livestock that they herd.

This period of severe drought characterized the Sahel, reduced grasslands biomass and species composition as well. In some areas of Niger grasslands productivity of *Aristida mutabilis* and *Schoenfeldia gracilis* fell 50-70% between 1968 and 1985. In the area of Tedjira (north-east of Zinder, Niger) the herbaceous coverage before dry years was dominated by *Cymbopogon giganteus* (with a dry matter biomass productivity of 2.5 tonnes per hectare): this specie has disappeared and it has been replaced by *Aristida funiculata*, whose productivity barely targets 300 to 400 kg of dry matter biomass per hectare. Most of the perennial herbaceous species

almost disappeared (*Aristida sieberiana, Cymbopogon giganteus, Cymbopogon schoenanthus, Andropogon gayanus, Cyperus conglomerates)*. Other species, such as *Aristida mutabilis, Aristida funiculata* and *Schoenefeldia gracilis* have been replaced by species with a shorter life-cycle that is more adaptable to erratic rainfall, such as *Cenchrus biflorus*.

Despite the recent increasing in rainfall patterns (Mertz et al., 2012) local food shortage periodically characterized the Sahelian area. Maps in Figure 15 show the occurrence of humanitarian crisis from 2000 to 2008 both natural (floods, drought etc.) and anthropic driven. These localizes crisis are recurrent even if they don't affect the whole Sahel in the same time. Crisis are reported for administrative units, as were provided by FEWS-NET, UN-FAO, International Disaster Database (EM-DAT) and WHO databases. Each of these agencies provides different information on the crisis depending on the purposes for which it was established.

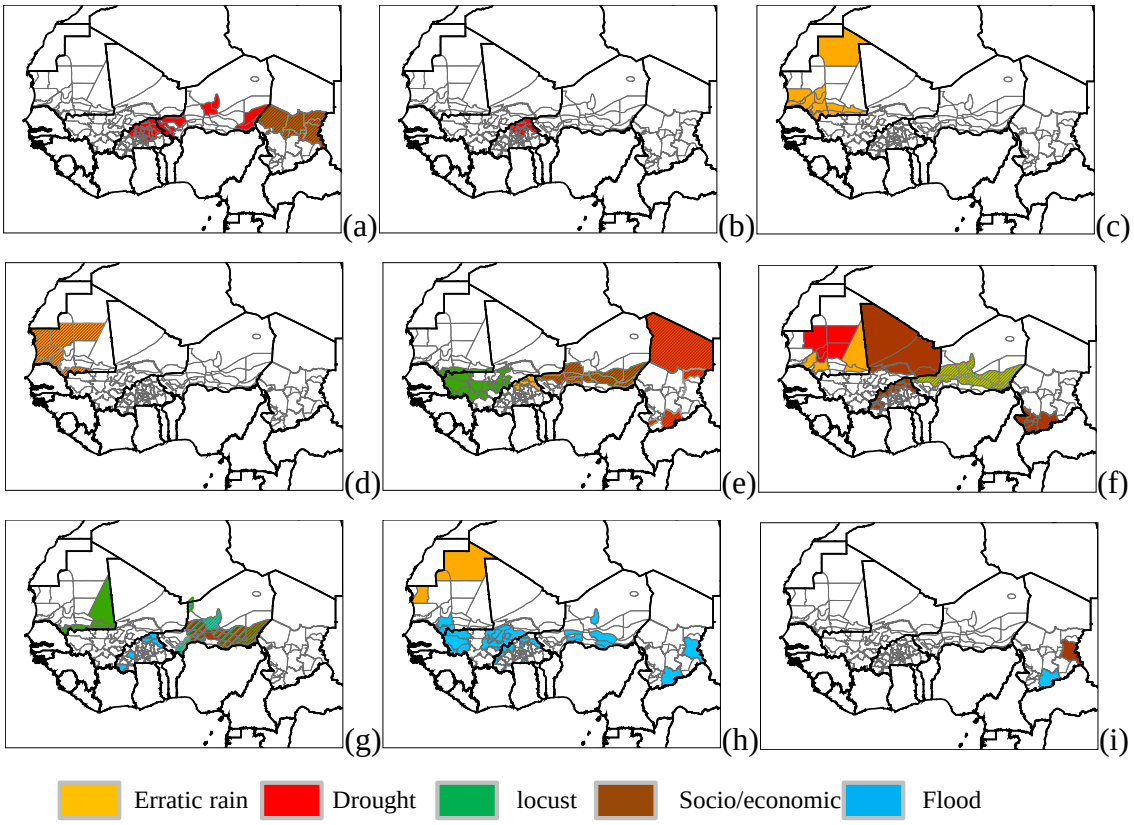

Figure 16- mapping of humanitarian crisis in WA from 2000 (a) TO 2008 (i). Sources: FAO, USAID, FAIS – WFP, EM-DAT database. Elaboration: Nutini et al. (2010)

Scientific studies on drought causes and effects

The progressive environmental degradation and food shortage during dramatic food crisis in the 70-80s have stimulated the international attention towards Sahel, which materialized in the United Nations Conference on Desertification (UNCOD), organized in 1977 and 1978. The conference has launched a debate that is still in progress, on the causes of drought and its impact on food security for the local population. The scientific interest focused a) on seeking climatic or anthropogenic driving factors for the extended drought and b) on assessing its impact on the environment and the agro-ecosystems (Herrmann et al., 2005). For what concern the interpretation of the causes of drought, there are two different schools of thought: one adheres to the hypothesis of a human-induced drought (Ibrahim, 1978) and the other one to the hypothesis that drought was caused by climatic variability on which human have a minor role (Nicholson et al., 1998; Olsson et al., 2005). These opposing hypotheses derived from the difficulty in identifying root causes of long term climate fluctuations. Some authors point to the relationship between rainfall and the anomalies of the ocean surface temperature, which is a phenomenon similar to El Niño occurring in the Pacific Ocean (Giannini et al., 2003; Nicholson and Grist, 2001), whereas others point to the relation between the monsoon season and the cold temperatures in the southern part of the Atlantic (Brooks, 2004).

Similarly the investigations on the drought consequences and impact have seen different interpretations. In the late 80s, Lamprey (1988) stated that the Sahelian region was witnessing an "irreversible and progressive desertification", but more recent studies based on satellite data show an increase in vegetation cover since the mid-80s (Eklundh and Olsson, 2003), which is correlated to an increase in large-scale precipitation (Herrmann et al., 2005; Heumann et al., 2007). This phenomenon, commonly referred to "greening" or "re-greening" has been interpreted as a recovery from the great Sahelian drought of the 60s and 70s (Anyamba and Tucker, 2005; Giannini et al., 2008; Olsson et al., 2005).

Although the extent of "greening" has not yet been extensively established with ground data, it questions previous theories about the "irreversible damage inflicted on the ecosystem Sahel" (Dregne, 1983; Middleton and Thomas, 1997). New technologies, like remote sensing, have allowed further analysis by the scientific community of climatic phenomena in their spatial and temporal dimensions and their relation with vegetation dynamics. Herrmann et al., (2005) compared trends of rainfall and Normalized Difference Vegetation Index (NDVI), a widely used proxy of vegetation production, and found a general increase of vegetation abundance in the Sahel between 1982 and 2003, thus refusing the presence of a large-scale irreversible

desertification. The same authors pointed out that locally the NDVI-rainfall relation differs from the expected trend, suggesting that other local factors have driven vegetation regrowth such as the improvement of agricultural activity by the population. A more recent research (Huber et al., 2011) confirms globally the recovery of Sahelian ecosystem but emphasizes this aspect highlighting differences of vegetation patterns and/or vegetation growth in relation to water availability. Some areas resulted especially interesting, because "*…the NDVI trends […] are opposed to those observed in the rainfall time series*", underlining local anomalous response of vegetation to precipitation. In particular, the authors discovered that the West Sahel (Senegal) shows a significant greening trend despite stable rainfall while East Sahel (Sudan) shows an opposite behaviour.

Even though, several studies based on time series of satellite data and, where available, also on ground data, confirmed the dynamics of the Sahelian ecosystems and their tendency to change with time, there is no general agreement on the entity of such changes and on the principal driving causes (Herrmann et al., 2005). Capecchi et al. (2008) verified the positive effects of increased rainfall on crop production and especially on the production of millet between 1986 and 2000. However, due to the lack of detailed information, it is hard to assess the real extent of the "greening" phenomenon in terms of ecosystem production. For example, the herbaceous savannah of Sahel has shown a strong greening when analysed with satellite data, however in field information indicates that locally the vegetation composition of these systems is changing. FAO indicates that rangelands have shown a phytosociological response of grassland to the prolonged droughts: loss of perennial herbaceous species as *Cymbopogon giganteus* and *Aristida sieberiana* and the expand of species with shorter phenological cycle (thus more resistant to drought) such as *Cenchrus biflorus* and *Aristida funicular*. In conclusion, a global greening could be due not only by ecosystem recovery but also to changes of herbaceous species composition. Some of these species are also palatable to animals but their low productivity (about 400 kg/ha compared with 2000 kg/ha of perennial herbaceous species) affects the livelihood of cattle (Geesing and Djibo, 2001).

If a general a regional "greening" is highlighted by time series of satellite data, it does not necessarily imply a recovery of the carrying capacity of these ecosystems. Several authors (Fensholt and Rasmussen, 2011; Herrmann et al., 2005; Seaquist et al., 2009) state that is not possible to exclude local processes of desertification and degradation and therefore it is necessary to conduct analyses at a finer spatial scale to highlight possible anomalous situations.

Objective of the research & Structure of the thesis

This work aims to the study of Sahelian rangeland[3], a wide semi-arid area characterized by lack in field data and recurrent food crisis. This dissertation exploited several RS data, together with local expertise, field data and bibliography information, to explore the rangeland status along past decade and to investigate potential tools to monitor the ecosystem carrying capacity. The manuscript is divided in two main sections, the first part (chapter 1 and 2) is related to environmental anomalies identification and interpretation via RS time series analysis while the second part (chapter 3 and 4) investigates the use of RS data in modelling to test methods for automatic vegetation parameters estimation.

Session 1: Identification of environmental anomalies to improve knowledge on rangeland status

Chapter 1 reports the research conducted to exploit time series of vegetation proxy (NDVI) and rainfall estimated from satellite. These maps were used to investigate the entire West Africa with a temporal resolution of 10 days from 1998 to 2010. Temporal behaviour of the two variables were analysed using non parametric statistics, looking for area where vegetation production is not correlated to the main driving force (water availability i.e. rainfall). In these areas NDVI and rainfall temporal trends were compared, highlighting anomalous situations where the rangeland behavior were not fully explained by water availability (driving force), suggesting that other factors are interfering with the phenomena. Possible interpretation of these situations are discussed thanks to availability of local expertize information, reference data and studying land cover changes in some test areas.

Chapter 2 provides a description of data analysis conducted to produce and interpret improved information on land cover/use changes with the final aim of explain anomalous zone, discovered in previous chapter, . The work investigates the optimal classification methodology for producing a LC map in a Nigerien marginal semi-arid region characterized by high climatic seasonality using multitemporal high resolution (HR) satellite data. The interpretation of phenological response to start of rainy season resulted crucial for the methodology. The produced maps were compared to

[3] This research was partially supported by the GEOLAND-2 project (contract n. 218795), which is a Collaborative Project (2008-2012) funded by the European Union under the 7th Framework Programme (http://www.gmes-geoland.info/).

obtain an overview of vegetation changes in the Sahelian context characterized by environmentally critical circumstances.

Session 2: Estimating rangeland biomass to support natural resource monitoring

Chapter 3 includes the studies conducted to set up an automatic methodology to produce maps of Evaporative Fraction(EF), an indicator of water availability for a vegetated system. . This variable, strongly related to vegetation status and soil moisture, has been calculated over the sahelian area of Niger every 8 days from 2000 to 2009 using satellite products of albedo and land surface temperature. The estimated variable is proposed in literature, and tested in the chapter, as a remote sensed water sufficiency indicator. Evaluation and discussion of the estimation were conducted via a comparison with thematic maps, ancillary information and energy fluxes measurements acquired on a eddy covariance tower in Niger.

Chapter 4 reports the analysis conducted to test a new method for biomass estimation in semi-arid environment exploiting a water stress indicator in LUE modelling approach. First of all an existing operational biomass estimation product was qualitatively evaluated in terms of spatio-temporal variability (using available thematic maps), and quantitatively assessed thanks to a comparison with field measurement (savannah annual biomass production from 2000 to 2009 over 46 field sites). In this chapter was tested the contribution of remote sensed EF as a water stress efficiency factor in biomass estimation as suggested by results of previous studies conducted on ground eddy covariance data. Statistical comparison was conducted between the standard biomass estimation and the improved ones, in order to check the suitability of water stress estimation in a LUE model.

Finally chapter 5 summarise the results of the PhD activities and experimental results in the framework of environmental security.

SESSION 1: Identification of environmental anomalies to improve knowledge on rangeland status

CHAPTER 1: Identification of hot spots of environmental anomaly in West Africa from time series of NDVI and Rainfall

1.1. Abstract

Studies of the impact of human activity on the vegetation dynamics in the Sahelian belt of Africa have been recently re-invigorated by new scientific findings that highlighted the primary role of climate in the drought crises of the 70-80s. Time series of satellite observations allowed identifying re-greening of the Sahelian belt that indicate no noteworthy human effect on vegetation dynamics at sub continental scale from 80s to late 90s. However, several regional/local crises related to natural resources occurred in the last decades despite the re-greening thus underlying that more detailed studies are needed. This study contributes to the understanding of climate and human impacts on the vegetation in the Sahelian region in the last decade (1998-2010). The use of time-series of SPOT-VGT NDVI and FEWS-RFE rainfall estimates allowed us to analyze vegetation and rainfall trends and to identify local anomalous situations. Trend analysis has been conducted to map a) areas where vegetation has been significantly decreasing or increasing due to changes in rainfall patterns and b) anomalous hot spot zones where vegetation dynamics could not be fully explained by changes of rainfall patterns. Multi-temporal analysis of Landsat images allows us to evaluate the reliability of the identified trends and to provide an interpretation of some example hot spots. The frequency distribution of the anomalous situations among the land cover class of the GlobCover map shows that, at the regional scale, environmental degradation occurs mainly in herbaceous vegetation covers where pastoral and cropping practices are often critical due to low and very unpredictable rainfall. The results of this study show that even if a general positive re-greening trend due to increased rainfall is evident for the entire Sahel, some local anomalous hot spots exist and can be explained by human factors such as population growth whose level reaches the ecosystem carrying capacity as well as population displacement leading to vegetation recovery.

1.2. Introduction

The West African Sahelian area saw a drought crisis in 1973, followed till 80s by several years of low rainfall, causing dramatic famine in agropastoral areas. The effects of this prolonged drought was exacerbated by no collective awareness amongst governments, or international agencies, of the kinds of climatic shocks (Mortimore and Adams, 2001). Indeed there were no

early warning systems. The progressive environmental degradation and food shortage during those years have stimulated the international attention towards Sahel, on the causes of drought and its impact on food security for the local population. Recent studies based on satellite data show an increase in vegetation cover since the mid-80s, which is correlated to an increase in large-scale precipitation (Herrmann et al., 2005; Heumann et al., 2007) (Figure 1). This phenomenon, commonly referred to "greening" or "re-greening" has been interpreted as a recovery from the great Sahelian drought of the 60s and 70s (Anyamba and Tucker, 2005; Giannini et al., 2008; Olsson et al., 2005).

The principal cause of this fluctuation is the relationship between rainfall and the anomalies of the ocean surface temperature, which is a phenomenon similar to El Niño occurring in the Pacific Ocean (Giannini et al., 2003; Nicholson and Grist, 2001). Although the extent of "greening" has not yet been extensively established with ground data, it questions previous theories about the "irreversible damage inflicted on the ecosystem Sahel" (Dregne, 1983; Middleton and Thomas, 1997).

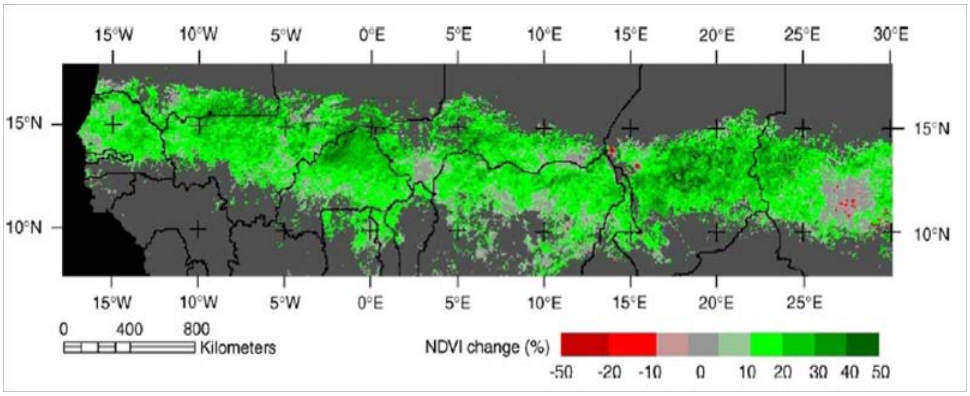

Figure 1- trends in vegetation greenness throughout the period 1982–2003. Source: (Herrmann et al., 2005)

New technologies, like remote sensing, have allowed further analysis by the scientific community of climatic phenomena in their spatial and temporal dimensions and their relation with vegetation dynamics. Herrmann et al., (2005) compared trends of rainfall and Normalized Difference Vegetation Index (NDVI), a widely used proxy of vegetation production, and found a general increase of vegetation abundance in the Sahel between 1982 and 2003, thus refusing the presence of a large-scale irreversible desertification. The same authors pointed out that the NDVI-rainfall relation differs from the expected trend, suggesting that other local factors have driven vegetation regrowth such as the improvement of agricultural activity by the population.

Huber et al. (2011) highlighted that differences in vegetation pat- terns are also related to water availability into the soil and not only to rainfall quantity. Some areas resulted especially interesting, be- cause ‘‘...the NDVI trends [...] are opposed to those observed in the rainfall time series’’, underlining local anomalous response of vegetation to changes in the precipitation amount. In particular, the authors found that Western Sahel (Senegal) shows a significant greening trend despite stable rainfall while Eastern Sahel (Sudan) shows an opposite behaviour. Several studies based on time series of satellite data and, where available, on ground data, confirmed the dynamics of the Sahelian ecosystem and their tendency to change with time, although there is no general agreement on the entity of such changes and on the major driving factors (Herrmann et al., 2005). Capecchi et al. (2008) confirmed the positive effects of increased rainfall on crop production and especially on the production of millet between 1986 and 2000. However, due to the lack of detailed information, it is hard to assess the real extent of the "greening" phenomenon. For example, the information provided by FAO on pastures shows a phytosociological response of grassland to the prolonged droughts: loss of perennial herbaceous species as *Cymbopogon giganteus* and *Aristida sieberiana* and the expand of species with shorter phenological cycle (thus more resistant to drought) such as *Cenchrus biflorus* and *Aristida funicular*. Some of these species are also palatable to animals but their low productivity (about 400 kg/ha compared with 2000 kg/ha of perennial herbaceous species) affects the livelihood of cattle (Geesing and Djibo, 2001). Therefore, the scientific community generally agrees on the hypothesis of a recovery of the Sahelian ecosystem, although the local effects of the environmental crisis are still to be explored due to human and environmental adaptation to climate vulnerability. If a general "greening" is highlighted by time series of satellite data, it does not necessarily imply a recovery of the carrying capacity of these ecosystems. Several authors (Fensholt and Rasmussen, 2011; Herrmann et al., 2005; Seaquist et al., 2009) state that is not possible to exclude local processes of desertification and degradation and therefore it is necessary to conduct analyses at a finer spatial scale to highlight possible anomalous situations.

This study aims to contribute to the understanding of climate and human impacts on the status of natural vegetation in the West African Sahelian belt in the last decade (1998-2010). Trend analysis of SPOT-Vegetation (VGT) NDVI and FEWS-RFE (Famine Early Warning Systems Network Rainfall Estimates) has been conducted to map a) areas where vegetation has been significantly decreasing or increasing due to changes in rainfall patterns and b) anomalous hot spots where vegetation dynamics could not be fully explained by changes in rainfall patterns.

The spatial distribution of the identified hot spots was analyzed according to land cover categories and discussed with other ancillary information in order to understand chronic situations where the carrying capacity of the ecosystem is endangered. Finally, a set of multitemporal Landsat TM images, with high spatial resolution (30 m) compare to medium resolution SPOT-VGT, have been used to evaluate the method and to interpret locally the results

1.3. Study area

The study area covers the sub-Saharan West Africa between 4° N to 18° N of latitude and -18° E to 25° E of longitude. The area of interest is the Sahel: a transition zone between Sahara to the north and the sub-humid tropical savannas to the south, which is marked by a steep north–south gradient in mean annual rainfall. The boundaries of this area are not clearly defined by physical barriers (i.e. rivers, mountains). The climate of the Sahel is characterized by the strong seasonality of rainfall, with a long dry season in winter and a short summer rainy period. The effect of this climate is the abundance of herbaceous species with an annual cycle in particular in the Sahel *sensu stricto,* and the consequence is that biomass production is possible only during the short and unstable rainy season. The gradient of precipitation causes a gradual change of vegetation from desert in the north to forests dominated by tree species of great value in the south (White, 1983; Monod, 1985). The Sahel borders are often identified with the boundaries of pastoral and agropastoral activities or with the position of rainfall isohyets (Geesing and Djibo, 2001). On the basis of these, the Sahel region is comprised between isohyet of 200 mm, the southern limit of desert herbaceous and bushy species like *Panicum turgidum* and *Boscia senegalensis* and isohyet of 600 mm, where tree species like *Isoberlinia doka* become dominant (Wickens, 1997). The most common human activity is pastoralism, because unlike agriculture, it is able to move (taking advantage of seasonal transhumance) and to adapt to interannual climate variability typical of the area. Agriculture in the Sahel is possible only in particularly favourable areas and relies on rustic species like *Pennisetum glaucum* (pearl millet) (Suttie et al., 2005). Most of the population lives south of the 300–350 mm isohyets, which are regarded as the lower limit for rainfed agriculture (Huber et al., 2011).

Agricultural surveys of the Sahelian countries pointed out that about one third of the total millet production, along with 15% of all sorghum and just under 10% of maize in 2000, was grown in vulnerable areas. These areas are characterized by persistently low and very unpredictable rainfall with a total rainfall varied by approximately 30% from year to year (ECOWAS-SWAC,

2006). These conditions determine potentially vulnerable situations that can lead to humanitarian crisis related to food shortage. This is the case of Niger and Chad that experienced several crises in the last decade (http://www.fews.net/, Last access May 2011).

1.4. Data

Satellite data time series

Satellite data are particularly suitable, and often represent the only available data source, for the analysis of large scale phenomena such as the vegetation dynamics of the sub-Saharan West Africa. The analysis of Sahelian vegetation development showed that the boundaries of this area may change even 150 km a year following rainfall pattern (Tucker and Nicholson, 1999). Thus the analysis of desertification and land degradation processes can be identified locally only using long-term spatial analysis at an appropriate scale (Herrmann et al., 2005). In this study a time-series of remotely sensed observations were used to identify areas of significant vegetation change in the pastoral and agricultural regions of the Sahelian and Sudanian savanna.

Time-series of NDVI data were obtained from the VGT sensor onboard the SPOT4 and 5 satellites and used as a proxy of vegetation production. The NDVI time series are 10-day maximum value composites (S10) at 1 km resolution and cover a 13-year period from April 1998 to December 2010. Data were made available in the framework of the Natural Resource Monitoring in Africa (NARMA) Core Information Service of the EU FP7 project Geoland2 through the NARMA eStation (Combal et al., 2010). Data available through the eStation are the latest version of VGT-NDVI: in 2010 the whole VGT archive has been reprocessed by the data provider in order to improve data consistency over time (http://www.vgt.vito.be, Last access December 2013).

Precipitation data were provided by FEWS of the United States Agency for International Development. Rainfall is estimated from satellite measurements (RFE) since a regional analysis based on direct measurement is not feasible due to the low number of rain gauges distributed over West Africa. RFE data are available at 8 km spatial resolution as 10-day temporal syntheses since 1996 and actually represent the most accurate rainfall dataset in terms of spatial resolution. In 2001, the REF 1.0 was replaced by the new enhanced algorithm REF 2.0 (NOAA CPC, 2001). For our study area the two versions of RFE data are comparable as demonstrated by Haas (2010).

RFE data are routinely resampled at 1km resolution and registered to VGT-NDVI data in the eStation .

Thematic maps and ancillary information

In order to interpret the results derived from satellite time series, ancillary information on land cover, environmental properties, agricultural activities as well as other socio-economic properties of local populations and humanitarian crises was used. The regional GlobCover (GC) map for Africa is derived from data acquired by the ENVISAT Medium Resolution Imaging Spectrometer (MERIS) with a 300 m spatial resolution (Arino et al., 2008). For sub-Saharan West Africa only 14 of the GlobCover classes cover more than 1% of the total area. The most relevant ones are grassland, shrubland and cropland, which form the Sahelian typical land cover (Figure 2). In addition these classes are the more interesting ones for human activities such as pastoralism, wood exploitation and agriculture.

The cartographic product EcoRegions (Olson et al., 2001), available at http://www.worldwildlife.org/science/data/item6373.html (last access December 2013) was used to delineate biogeographic units of land that contain a distinct assemblage of natural communities sharing a large majority of species, dynamics, and environmental conditions. This product, including a general description of each ecological region, outstanding and distinctive biodiversity features, current status and types and severity of threats to the natural habitats, is suitable for ecological analysis of the study area.

The “Global Cropland and Pasture Data from 1700-2007” (GCP_1700-2007) and the “Croplands in West Africa” (CWA) (Ramankutty, 2004) datasets available respectively at 0.5 degree and 5 minutes resolution were downloaded from http://www.geog.mcgill.ca/~nramankutty/Datasets/Datasets.html (last access December 2013) and used as a source of information on agricultural and pastoral activities.

Additional external information, such as the humanitarian crises database of the FEWS-NET (http://www.fews.net, last access December 2013), was also used to analyse hot-spots highlighted by trend analysis of satellite time series.

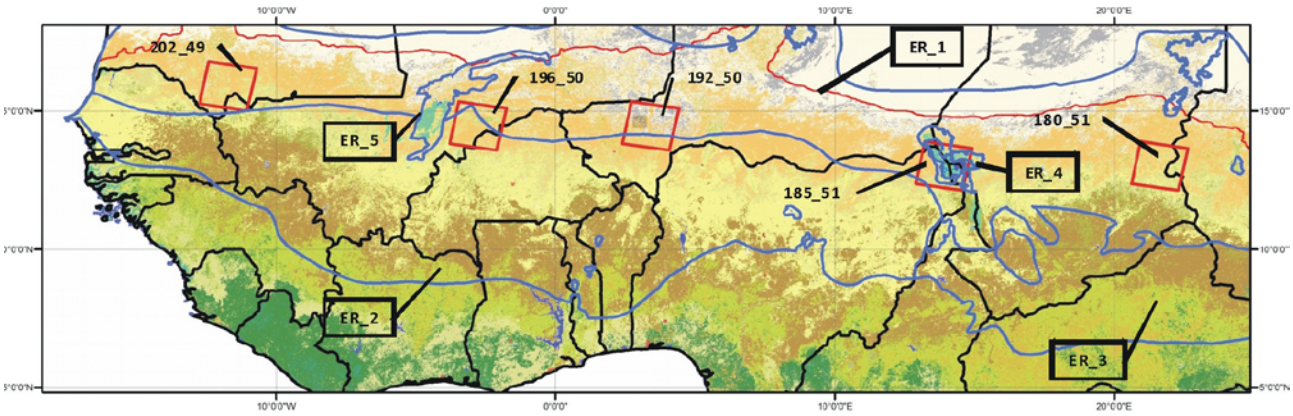

GC_code	Legend	Tot	ER1	ER2	ER3	ER4	ER5
			49%	38%	12%	1%	1%
14	Rainfed croplands	11%	3%	23%	4%	9%	3%
20	Mosaic cropland (50-70%) / vegetation (grassland/shrubland/forest) (20-50%)	6%	3%	10%	4%	8%	3%
30	Mosaic vegetation (grassland/shrubland/forest) (50-70%) / cropland (20-50%)	10%	9%	14%	1%	15%	10%
40/41	Closed (>40%) broadleaved evergreen and/or semi-deciduous forest (>5m)	0%	0%	0%	1%	0%	0%
60	Open (15-40%) broadleaved deciduous forest/woodland (>5m)	6%	0%	7%	31%	1%	0%
110	Mosaic forest or shrubland (50-70%) / grassland (20-50%)	4%	4%	3%	5%	3%	5%
120	Mosaic grassland (50-70%) / forest or shrubland (20-50%)	1%	0%	0%	11%	0%	0%
130	Closed to open (>15%) (broadleaved or needleleaved, evergreen or deciduous) shrubland (<5m)	19%	4%	31%	44%	2%	1%
140/144	Closed to open (>15%) herbaceous vegetation (grassland, savannas or lichens/mosses)	19%	31%	10%	0%	16%	30%
180	Closed to open (>15%) vegetation on regularly flooded soil	1%	0%	0%	0%	33%	15%
200/201/202	Bare areas	12%	24%	0%	0%	9%	8%
	tot	*89%*	*78%*	*99%*	*100%*	*96%*	*75%*

Figure 2: The study area. GobCover Land cover classes for West Africa. Red line refers to the isohyet of 200 mm/year and blue lines to the boundaries of the five ecoregions analysed: ER1 (Sahelian Acacia savanna), ER2 (West Sudanian savanna), ER3 (East Sudanian savanna), ER4 (Lake Chad flooded savanna) and ER5 (Inner Niger Delta flooded savanna). Red squares indicate the Landsat scenes selected for the interpretation of anomalous hot spots.

1.5. Methods

Standardization of the time series

The 10-day NDVI values for the period July-October (JASO) were cumulated to produce the annual synthesis (ΣNDVI), which is a widely used indicator of vegetation production (Fensholt and Rasmussen, 2011; Fensholt et al., 2006; Seaquist et al., 2009). ΣNDVI was demonstrated to be correlated to annual (net and gross) primary productivity for semi-arid regions such as Sahel (Prince, 1991). The RFE data have been used to calculate annual cumulated rainfall (Y-Rain), which is considered as the most influential parameter on plant production in the study areas (Huber et al., 2011).

ΣNDVI and Y-Rain were standardized and converted to z-scores by subtracting to the pixel value the pixel long term average and then by dividing the result by the standard deviation. In the analysis of time series, the z-score is a dimensionless quantity (Barbosa et al., 2006; Helldén and Tottrup, 2008) adopted to convert variables with different scales to a common domain. The z-score provides a measure of the pixel's anomaly at a given time with respect to its normal behaviour (long term average); the anomaly is expressed in number of standard deviations. In this study, z-scores of ΣNDVI and Y-Rain are used to highlight anomalous decrease/increase of vegetation production and rainfall. All computations were kept at the 1 km pixel resolution.

Trend analysis

A non parametric test was adopted to identify significant monotonic increase/decrease trends in the time series of the standardized data (z-scores). The Mann-Kendall test for the significance of the Kendall's *tau* was deemed suitable since its validity does not require normality in data distribution.

This approach has been applied to seasonal data, mainly for hydrological analyses and, more recently, to NDVI time series (Huber et al., 2011; Martínez and Gilabert, 2009). The Mann-Kendall test quantifies the strength and the direction of a trend. Kendall *tau* rank correlation coefficient is in the range $-1 \leq tau \leq 1$ expressing increasing and decreasing trends for positive and negative *tau* values, respectively.

The magnitude of the observed trends (slope of the trend) was assessed using the Sen's non-parametric method (Sen, 1968). This method is resistant to outliers and therefore is suitable to process short or noisy series (Huber et al., 2011).

The *tau* coefficient, its statistical significance (*p*-value) and the slope of the trend were calculated using ad-hoc IDL (Interactive Data Language, ITT- Visual Information Solutions) codes. The output of the trend analysis are maps of *tau* (t) and slope (sl), while map of *p*-values were used to mask out the areas of no significant trend at the 90% level ($p > 0.1$). No autocorrelation was founded in data used for trend analysis (see §annex 1).

Hot spots identification

The long term trends of ΣNDVI and Y-Rain z-score were analyzed according to the interpretive scheme proposed in Figure 2. The slope of the trends and its significance (p-value) for the two variables were considered for mapping anomalous situations.

Four classes of possible combinations of rainfall and vegetation long term trends were defined: "climatic greening" (CG) when the increase in NDVI occurs in combination with rainfall increase (Figure 3 panel 1); "climatic degradation" (CD) when both NDVI and rainfall decrease (Figure 3 panel 3); "anomalous greening" (AG) when NDVI increases with either a significant decrease of rainfall or a stable rainfall trend (i.e. no significant changes) (Figure 3 panel 2); "anomalous degradation" (AD) where NDVI decreases and rainfall either increases significantly or remains stable (Figure 3 panel 4).

The final map provides information only for those pixels with NDVI trend significant at the 90% level ($p < 0.1$) and with a trend slope < -0.126 or > 0.126 of z-score unit per year. Situations with slope below/above these values represent cases where, within the analyzed time frame of 13 years, the ΣNDVI z-score resulted in extreme increase/decrease categories at the 90% significant level. These situations can be considered as extremely anomalous with respect to values at the beginning of the time series therefore they identify with a very high level of confidence hot spots of environmental anomalies.

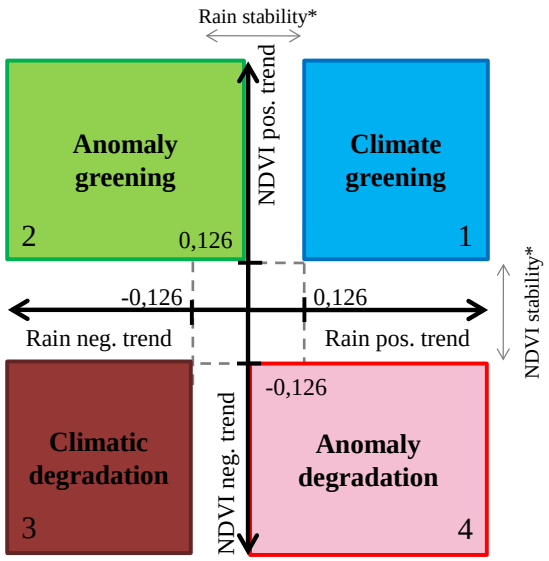

X = Rain trend slope Y = NDVI trend slope
* no signicant trend or low slope trend

Hot spot class	Y-Rain		ΣNDVI
Climatic greening	Stat. signif. Pos. Trend *tau* > 0; *p* < 0.1; Sl > 0.126	AND	Stat. signif. Pos. Trend *tau* > 0; *p* < 0.1; Sl > 0.126
Climatic degradation	Stat. signif. Neg. Trend *tau* < 0; *p* < 0.1; Sl < -0.126	AND	Stat. signif. Neg. Trend *tau* < 0; *p* < 0.1; Sl < -0.126
Anomalous greening	Non Stat. signif. Trend p> 0.1 OR Stat. signif. Neg. Trend *tau* < 0; *p* < 0.1; Sl < -0.126	AND	Stat. signif. Pos. Trend *tau* > 0; *p* < 0.1; Sl > 0.126
Anomalous degradation	Non Stat. signif. Trend *p*> 0.1 OR Stat. signif. Pos. Trend *tau* > 0; *p* < 0.1; Sl > 0.126	AND	Stat. signif. Neg. Trend *tau* < 0; *p* < 0.1; Sl < -0.126

Figure 3- Interpretation scheme for the hot spot map.

Hot spots regional analysis

The method described above allows highlighting anomalous behaviour with the same scale (z-score) for the entire study area; therefore, the map produced provides a regional picture of the analyzed phenomenon. However, the correct interpretation of these results requires considering additional information on distribution of different eco-climatic condition and land cover types. For this reason, we summarized and interpreted the results in term of land cover as derived from

the GlobCover map (Arino et al., 2008) and for ecologically homogeneous areas as derived from the EcoRegion layer (Olson et al., 2001). Five different ecological regions (ER) were selected: the Sahelian Acacia savanna (ER1), the West Sudanian savanna (ER2), the East Sudanian savanna (ER3), Lake Chad flooded savanna (ER4) and the Inner Niger Delta flooded savanna (ER5) (Figure 2).

The use of the EcoRegion layer allowed us to analyse the vegetation trends on the basis of a more spatially detailed stratification criteria, related to different ecosystem attributes, with respect to the use of simple rainfall isoline zonation. For example, both the West and East Sudanian savannas are included in the 500-1000 mm rainfall range but the East Sudanian savanna is a more forested area with less agriculture and rangelands than the Western region. Even though the ER4 (Lake Chad flooded savanna) and ER5 (Inner Niger Delta flooded savanna) cover just 2% of the study areas, they were considered separately due to their peculiarity and importance. For each ecological region, the occurrence of the four hot spot categories within each of the GlobCover class (Figure 2) was analyzed. Areas with average annual rainfall below 200 mm were masked out, because according to FAO (White, 1983), below this limit only desert species can exist.

Landsat TM data analysis

In order to interpret the hot spots, a set of high spatial resolution Landsat TM/ETM+ satellite images (30 m) from the USGS GLOVIS archive (http://glovis.usgs.gov/, last access December 2013) were selected under the requirement that at least two cloud free acquisitions, one at the beginning and one at the end of the study period, were available. A total of five couples of images were downloaded over the study area: four in correspondence with the Sahelian Acacia Savana (ER1) and the West Sudanian savanna (ER2) and one over the Lake Chad flooded savanna (ER4) (Figure 2). TM/ETM+ images were selected preferably at the end of the rainy season for a better discrimination of vegetated areas. In correspondence with the hot spots, identified by the temporal trend analysis, a window of at least 1300 x 1300 TM pixels was extracted and classified into land cover classes with an unsupervised isodata classification following the approach proposed by Brink and Eva (2009). Isodata clusters were labeled by photo-interpreting different colour composites of the TM images and by exploiting ancillary information. The final classification provides for each site a map at the TM spatial resolution with four classes: dense vegetation, sparse vegetation, bare areas and water. These classifications

were used for identifying land cover changes which could have led to a reduction or an increase in the amount of vegetation. For Landsat 7 ETM+ images acquired after May 31, 2003, when Scan Line Corrector technical problem occurred (SLC-off , http://landsat.usgs.gov/products_slcoffbackground.php, last access December 2013), no data values were masked out for the analysis, therefore changes were evaluated only on those pixels that were common to both images. Table 1 reports detailed information of the TM dataset and the typical land cover present in the areas as derived from the GlobCover map.

Table 1: Characteristics of Landsat images used for the hot spot evaluation and main GlobCover land cover classes present in the area.

Location	Path-Row	date 1	date 2	GC_14	GC_20	GC_30	GC_110	GC_140	GC_144	GC_180	GC_200	GC_201	tot
Mauritania	202-49	14/10/1999*	15/09/2009°	3%	6%	22%	5%	40%	17%		7%		100%
Mali	196-50	20/10/1999*	07/10/2009°	1%	3%	21%	6%	39%	22%		7%		100%
Niger	192-50	24/09/2000*	03/08/2007°				2%	25%	20%		30%	21%	98%
Lake Chad	185-51	25/09/2002*	17/10/2010^	6%	3%	22%	6%	12%	15%	25%			89%
Chad-Sudan	180-51	20/09/2000*	16/09/2010*	7%	11%	40%	3%	31%	7%				99%

* Landsat 7 ETM+ ° Landsat 4/5 TM ^ Landsat 7 ETM+ (slc off)

1.6. Results and discussion

Time series trend

Figure 4 shows the *tau* value of the Kendal correlation (a) and Sen's slope (b) for ΣNDVI over the 1998-2010 period; Figure 4c and d show the same parameters for rainfall (Y-Rain). For the analyzed period West Africa presents mainly a positive correlation between time and ΣNDVI showing a general increase of vegetation production. Pixels with negative correlation (orange to red colours) are located in the central belt of Sahel (15°-10° N).

In particular, large decrease of ΣNDVI trend (*tau* < -0.6) occurs in Chad and Niger and along the Burkina Faso/Mali and Chad/Sudan borders (Figure 4a). Less intense decreasing trends can be observed also near the Gulf of Guinea over peri-urban areas (i.e. Benin, Ghana), although these patterns are often not statistically significant (white areas in Figure 4b).

Time series of the cumulated rainfall (Figure 4c) show a strong increase (*tau* > 0.6) over West Africa (Senegal, Mali and Mauritania) and areas of significant decrease (*tau* < -0.6) mainly in Nigeria, in Sierra Leone and in Liberia.

The central Sahelian region presents patterns of slight decrease in rainfall (-0.4< *tau* < 0.0), surrounded by slight increase (0.0 < *tau* < 0.2), that geographically overlap with ΣNDVI decreases. However, only few of the above mentioned patterns in the central part are significant at the 90 % confidence level (Figure 4d).

In general, the study area does not appear to be significantly anomalous. Our results are in agreement with those recently published by (Fensholt and Rasmussen, 2011) for the period 1996-2007, although some local differences can be observed probably due to differences in the time period analyzed, in the spatial resolution of the datasets and in the method of analysis (Huber et al., 2011).

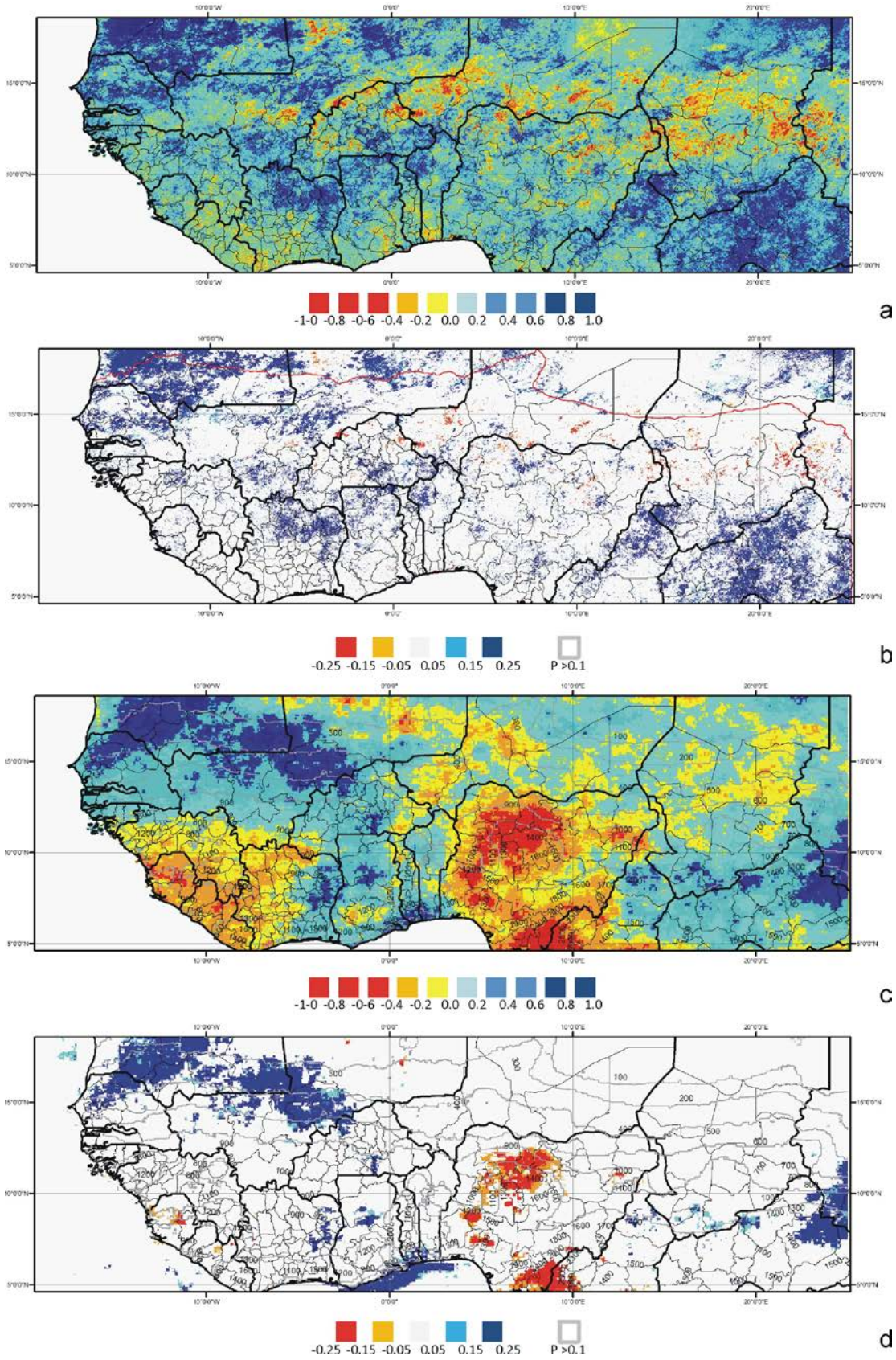

Figure 4: The Kendall *tau* rank correlation coefficient for ΣNDVI (a) and Y-Rain (c) and magnitude of trend significant slope value for ΣNDVI (b) and Y-Rain (d). White areas represent not significant trend at a level of 90% (p > 0.1).

Figure 5 shows the map of the combined analysis of NDVI and Rainfall according to the interpretation scheme that we proposed in Figure 2. Areas with average rainfall below 200 mm (red line in Figure 5) were masked out as well as areas where no significant ΣNDVI trends were identified (about 90 % of total area). Climatic greening (blue colour) covering 1.6 % of the area is located mainly in the southern part of Mauritania and in central Mali. Areas of climatic degradation (brown areas) cannot be appreciated at the regional scale because they cover less than 0.1 % and are concentrated mainly in Kano province, Nigeria. On the other hand, clear hot spots of anomalous greening (green colour, 7.8 %) and anomalous degradation (red colour, 0.6 %) can be identified.

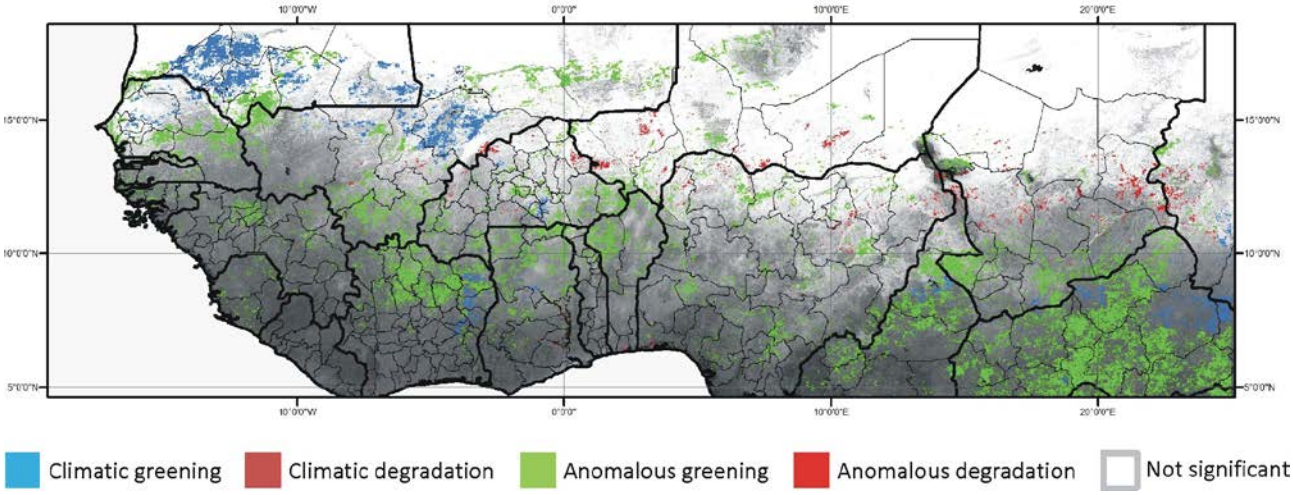

Figure 5: The hot spot map overlaid on a grey scale vegetation density map: climatic greening situation (CG), climatic degradation (CD), anomalous greening (AG) and anomalous degradation (AD) are represented respectively with cyan, brown, green and red key colours.

Anomalous degradation conditions are located in the central part of Sahel in an area covered by the typical Sahelian Acacia savanna (ER1) where the annual average rainfall is between 200 and 400 mm. On the other hand, anomalous greening is distributed mainly in two ecological regions: central part of West Sudanian savanna (ER2) for areas above 800 mm and forested areas of East Sudanian savanna (ER3) (Table 2). Some of the areas of anomalous greening (green patterns in Figure 5) correspond to locations surrounding inland water bodies such as the Senegal River, the Niger River and Lake Chad. In these regions the increase of vegetation production is likely to be related to the expansion of irrigated agricultural activities and/or to colonization of former water bodies (http://webworld.unesco.org/water/wwap/case_studies/senegal_river/index.shtml, last access December 2013; (Batello et al., 2004). The increase in ΣNDVI is particularly evident in

areas with intense agriculture such as rice cropping regions in Mali (Segou province around the town of Niono) along the border between Sudan and Cameroon (Mayo Kebi province) and between Mauritania and Senegal (Saint-Louis province, along the Senegal River). Finally, other, more localized, positive hot spots are highlighted in the northern part close to the desert in areas where rainfall increase is evident but not statistically significant.

On the contrary, red patterns in Figure 5 show decrease of the NDVI values that do not always correspond to areas where there are reported rainfall reduction. These areas are mainly distributed in Niger and Chad, where average annual rainfall is about 400 mm. In these conditions, even though no significant negative rainfall trend is highlighted by the analysis, it is possible that few years of low rainfall lead to a reduced vegetation production for several years (Figure 6c and d).

This zone is in fact considered the “Sahel’s fragile high-risk zone” because it suffers from both persistently low and very unpredictable rainfall (ECOWAS-SWAC, 2006). The comparison of our results with the livelihood crisis reported for Niger (FEWS-NET *alert* and GIEWS-FAO *Sahel Report* archive databases) demonstrates good agreement between areas of anomalous degradation (AD) and regions affected by humanitarian crises in the last ten years (2001, 2005 and 2010) which are the consequence of drought and unfavourable climatic condition of the previous years (see also Figure 6d) thus suggesting likely chronic environmental unfavourable conditions.

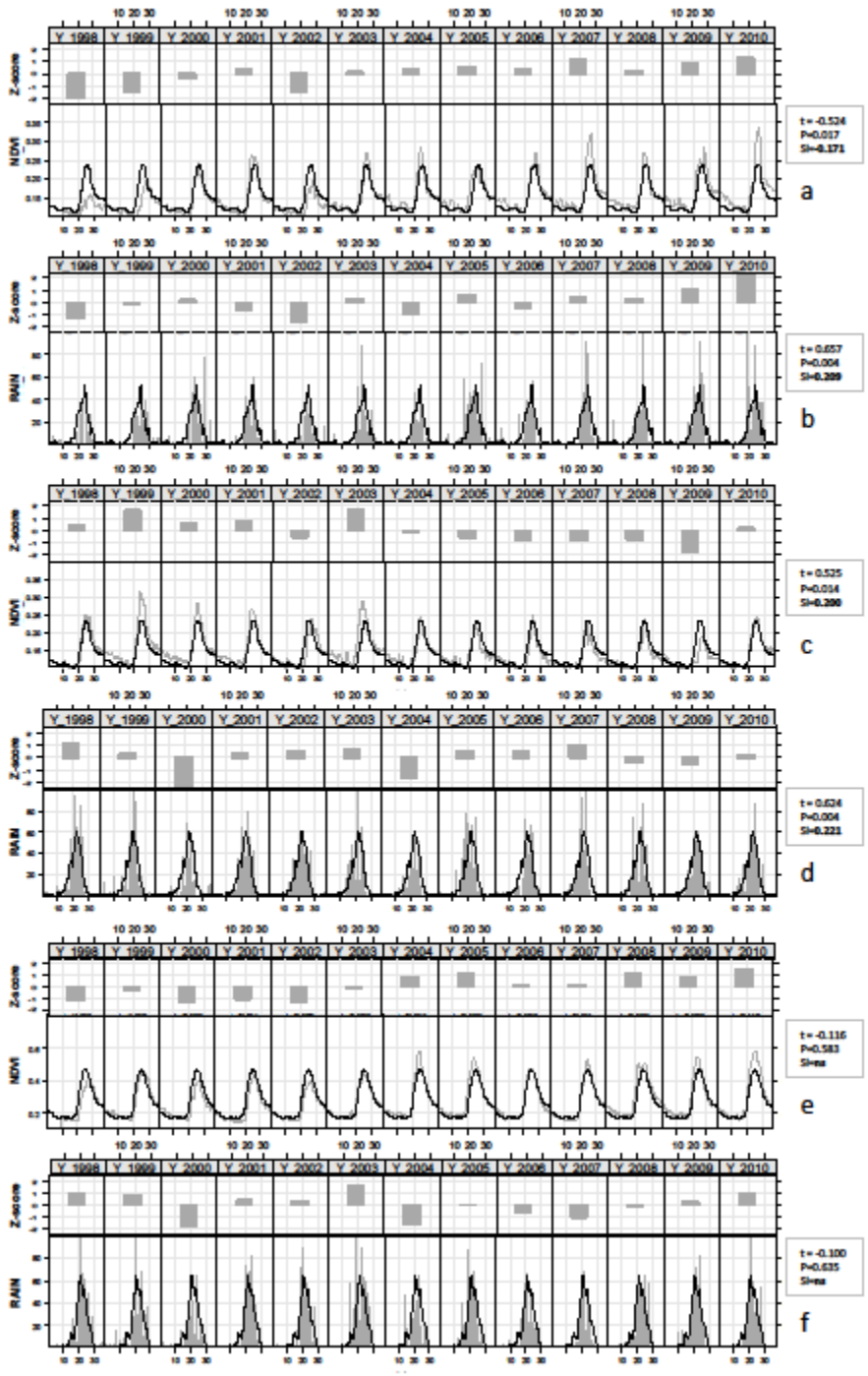

Figure 6: : Examples of the temporal trends of the decadal time series of NDVI and RFE and annual z-score for ΣNDVI and Y-Rain. Climatic greening (Mauritania-Senegal border, Lat 16.47, Lon -12.11, Landsat image 202_49) (a,b), anomalous degradation (Niger-Filinguè province, Lat 14.42, Lon 3.67; Landsat image 192_50) (c,d) and anomalous greening (Chad-Sudan border, Lat 13.31, Lon 22.29; Landsat image 180_51) (e,f). Next to the graphs are reported the values of Kendall t, P value and Slope (sl) of the trend analysis for each example.

Figure 6 shows some examples of 10-day time series for both NDVI and RFE for local conditions of climatic greening (Figure 6a and b), anomalous degradation (Figure 6c and d) and anomalous greening (Figure 6e and f). Grey lines (NDVI) and grey bars (rainfall) show the actual value compared to black lines that report the 13-year average values. Annual z-score for ΣNDVI and Y-Rain values are also reported to highlight the trend in the data and emphasize anomalous years.

Profiles in Figure 6a and b for the Assaba province, Mauritania, and show a significant increase of rainfall in the second half of the study period (see also Figure 8A, site 1). A consequent and correlated increase of NDVI ($p < 0.01$) can be appreciated since 2006 when the annual profile (grey line) is always above the mean (black line) and z-score is positive.

Figure 6 c and d identify the anomalous degradation, at least in term of vegetation production as represented by ΣNDVI, that is occurring in the Tillaberì province, Niger (see also Figure 8 3A, site 3). This area is a typical Sahelian semi-arid savanna (GC_140) with localized presence of agricultural activities (< 20% of cultivated areas in 5 minutes grid, source CWA; Ramankutty, 2004). The long term profiles show the NDVI response to increase in rainfall between 1998 and 2003; after 2003 a progressive NDVI decrease is observed (negative z-score).

Figure 6 e and f refer to an example of anomalous greening where a sensible increase in NDVI (*tau* = 0.624, $p < 0.05$) occurs despite a not significant decrease in rainfall, which can therefore be assumed as stable (*tau* = -0.100, $p > 0.6$). This area is located along the Ouadi Kadja river in Sudan close to the border with Chad (see also Figure 8 5A, site 7). The GlobCover map identifies this area as a mosaic of cropland and natural vegetation and the GCP_1700-2007 data set reports that, in the last decade, about 40% of the area is exploited for agriculture.

Hot spots regional distribution

In order to provide some hypotheses of the likely processes which have driven anomalies, a regional analysis of the hot spots in relation to EcoRegions and Land Cover has been conducted.

Anomalous greening (AG) is the more manifest process (Figure 5) accounting for about the 90% of all identified hot spots; in addition, the two anomalous classes AG and AD are distributed in a different way in the study area (Table 2): about 60% of the hot spots of anomalous degradation (AD) fall in the typical Sahelian Acacia savanna (ER1), the rest (35%) is mainly in the West

Sudanian savanna (ER2). On the contrary, anomalous greening (AG) is distributed primarily in ER2 (46%) with a strong presence in ER3 (30%).

Table 2: Distribution of Anomalous Degradation (AD) and Greening (AG) hot spots in the different ecological regions.

EcoRegion	code	AD [%]	AG [%]
Sahelian Acacia savannah	ER1	59	22
West Sudanian savannah	ER2	35	46
East Sudanian savannah	ER3	2	30
Lake Chad flooded savannah	ER4	3	1
Inner Niger Delta flooded savannah	ER5	0	1
Other	-	1	0

Figure 7 reports statistics of occurrence of the two anomalous trends (AG in dark grey and AD medium grey) in the different GB classes. In this figure, data are normalized and analyzed for the entire study area (Figure 7 a) as well as for the three larger ecological regions (Figure 7 b, c, d).

Land cover classes are positioned in the radar charts from north (CG_140, Close to open herbaceous vegetation) to south (GC_60, Open forest) in a clockwise direction. This disposition helps the interpretation of spatial distribution of the hot spots in relation to possible climatic/human processes and their interactions. Land cover with hot spot presence lower than 2% are not shown in the figure. By analyzing the entire study area, AG and AD processes show to have different behaviours: the frequency of degradation patterns (light grey) decreases from north to south (clockwise) while greening (dark grey) has the opposite spatial distribution. Degradation occurs primarily in natural herbaceous vegetation (GC_140 and 30, together 65%) and over regions of rainfed agriculture (GC_14, 26%). On the contrary, anomalous greening occurs mainly in shrubland and forested areas (GC_130 and 60, together 50%) with an important percentage in cropland (CG_14, 24%). It is worth to notice that even though AG and AD present similar percentages in cropland (about 25%), the AD is represented by very localized hot spots in

the northern part of Sahel where agriculture is practiced in the savannah areas which offer suitable hydrologic conditions. Those areas are considered in danger due to chronic vulnerable conditions and fall in the "Sahel's fragile high-risk zone" where agriculture production depends on favourable precipitation season.

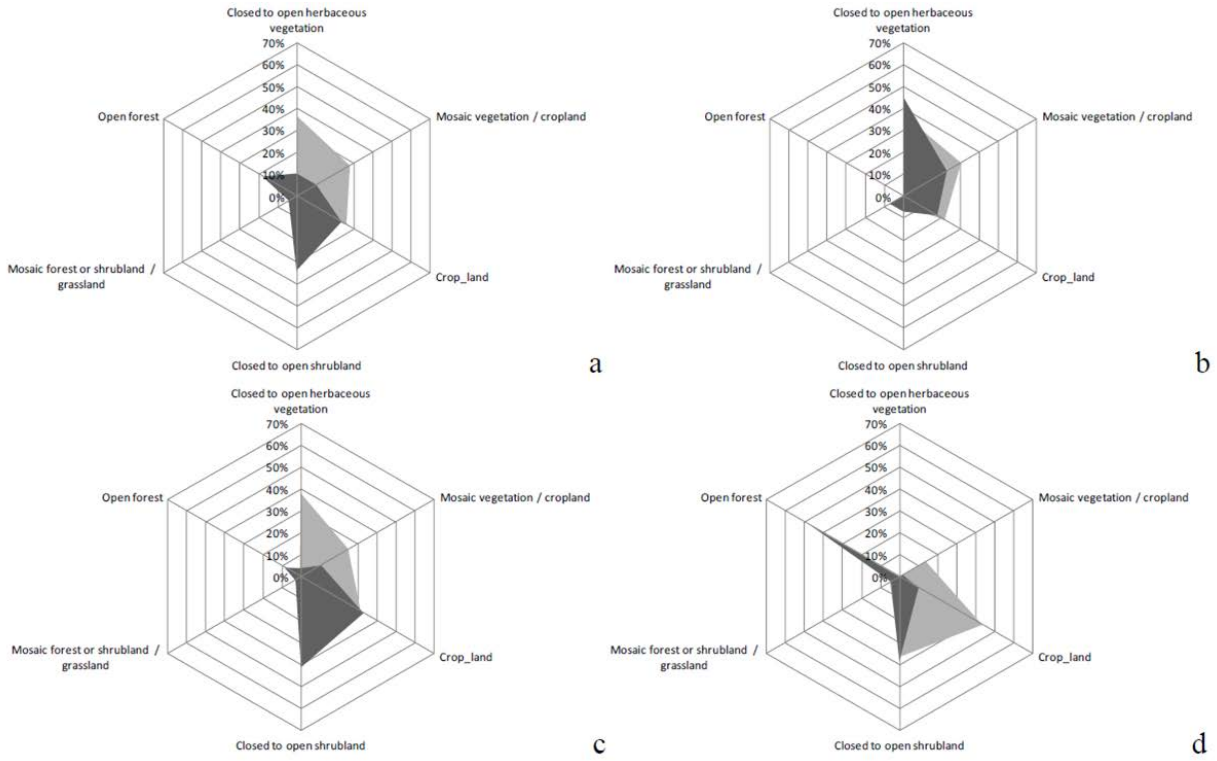

Figure 7: Distribution of hot spots of anomalous greening (dark grey) and anomalous degradation (light grey) in the GlobCover classes for the entire study area (a) and the ecological regions Sahelian Acacia savanna (b, 48% of surface), West Sudanian savanna (c, 38%) and East Sudanian savanna (d, 12%).

Interpretation of the anomalous hot spots

Figure 8 shows the hot spot maps for five Landsat scenes (boxes), which were acquired and classified. The hot spots of anomalous greening (AG) and anomalous degradation (AD) are identified by medium and dark grey, respectively, while climatic greening is reported by light grey (Figure 8, panels 1A to 5A). Eight sites, highlighted by black boxes in the figure, have been selected in correspondence to the hot spots. Results of the ISODATA classification on the selected boxes are shown on the right column Figure 8, 1B to 5B) where histograms report the proportion of change [%] for each vegetation cover class. All sites show cover changes consistent with the type of hot spot identified by our analysis at sub-continental scale. Anomalous greening (AG) always coincides with areas where isodata highlights either a

reduction of bare soil in favour of new vegetation cover or an increase of vegetation density (sites 1, 4, 5 and 7). On the contrary, anomalous degradation (AD) is always related to a decrease in the extent of vegetated areas (sites 2, 3, 6 and 8). Different nature of changes is highlighted by the analysis of Landsat images.

Site 1: Mauritania

Landsat scene of Site 1 (Figure 8 1A) represents an area showing a significant NDVI increase both climatic driven (light grey) and anomalous (medium grey). It is located at the border between Mali and Mauritania. It includes mainly the plain stretching between the Assaba and the Affolé Massifs, and drained by the Karakoro, a temporary tributary of the Senegal River.

The vegetation landscape is characterized by a steppe with a low density of bush species and an herbaceous stratum composed mainly of annual gramineous species. Locally dense woods of tree species can be observed along wadis and on screes along some slopes of the Assaba. Agriculture is limited in surface and concentrated on the wadi bottoms; a cattle breeding, instead, is very important for the local population in the Karakoro plain as well as for nomadic herders for which the area is a traditional migration corridor; as much as 90% of the population uses wood and charcoal for cooking. Therefore, both the herbaceous and the woody strata are threatened by the pressure of the population that ensures its sustainability by seasonal migration into cities as well as by permanent migration abroad. According to various studies (Ould Sidi, 2004; CMAP, 2004; ENDA-Diapol, 2007) it is rather stable area where population (about 10 inhab/km^2) tries to cope with limited environmental resources, and where no major short-term change, which could affect both the environment and the local human societies, is reported. Therefore, it is not surprising that the vegetation signal collected from satellite is mainly driven by the evolution of the rainfall pattern. In particular, the anomalous greening, occurring in an area primarily covered by grassland (GC_140) with some presence of cropland (GC_20 and 30, less than 1% of the surface; Ould Sidi, 2004), is confirmed by the histogram of cover change derived by TM analysis.

Site 2: Mali

The area displaying anomalous degradation in Site 2 (Figure 8 2A) is located at the border between Mali and Burkina Faso on the road between Mopti and Ouagadougou. The area is occupied by natural vegetation namely bush savanna on shallow soils developed on the

Continental Terminal and a tree savanna on aeolian sand deposits offering a good water storage capacity (Fontes et al., 1994). Agriculture is concentrated on alluvial deposits. The area on both sides of the border is subject to a significant population increase. Detailed statistics, at district and village levels, show that during the last 10 years the population has increased by 35 to 45 % on both sides of the border and current population densities are in the range 20-45 inhab/km^2 (INSD, 2008; INS, 2010). This situation clearly leads to an increased pressure on the environment. Local surveys among the population show that environmental degradation is well known but is mainly attributed to worsening climate conditions, and marginally to over-exploitation (Samaké, 2006). Also here quantitative assessment show that the need for firewood is greater than the production capacity: collecting dead wood does not cover anymore the demand for firewood and living trees are cut (DNCN, 2009). This general information is compatible with the local degradation observed, however it does not explain why this degradation is observed only locally. The results of photo-interpetation of high resolution satellite data confirm the increase of bare areas over the identified hot spots due to a reduction of vegetation cover as observed from Landsat TM analysis (Figure 8 2B).

Site 3 and 4: Niger

Figure 8 3A shows hot spot areas in Niger. This country experienced a rapid growth of population, a recent assessment depicts a situation of about 20 inhab/km^2 with a yearly increase rate of 3.3%, leading to a heavy pressure on the environment (World Bank, 2010). Two sites have been analyzed in Tillabery province, which is one of the most fragile zones because it relies on rainfall for farming and livestock and it is therefore highly vulnerable to climate variability. These conditions lead to a high proportion (about 30%) of households in severe food insecurity (World Bank, 2010). The anomalous greening (site 4) occurs in the valley of Dallol Bosso close to the town of Filingué. Even though this area is classified in GlobCover as grassland savanna (GC_144), the interpretation of Landsat images shows a significant proportion of croplands. The CWA data set also confirmed that 10 to 20% of the land is occupied by crops. The anomalous degradation of site 3 (Figure 6c and d) is located in areas of typically semiarid herbaceous vegetation where grazing is the major livelihood activity (GCP_1700-2007 data set). Humanitarian crisis, which are reported for this area in the last decades, occurred in 2001, 2005 and 2010; this region in fact belongs to the “Sahel’s fragile high-risk zone” (ECOWAS-SWAC, 2006). The Landsat TM analysis confirmed the contrasting behaviour of the two sites,

highlighted by the time series analysis, showing a decrease of vegetation cover for site 3 and an increase of vegetation density for site 4.

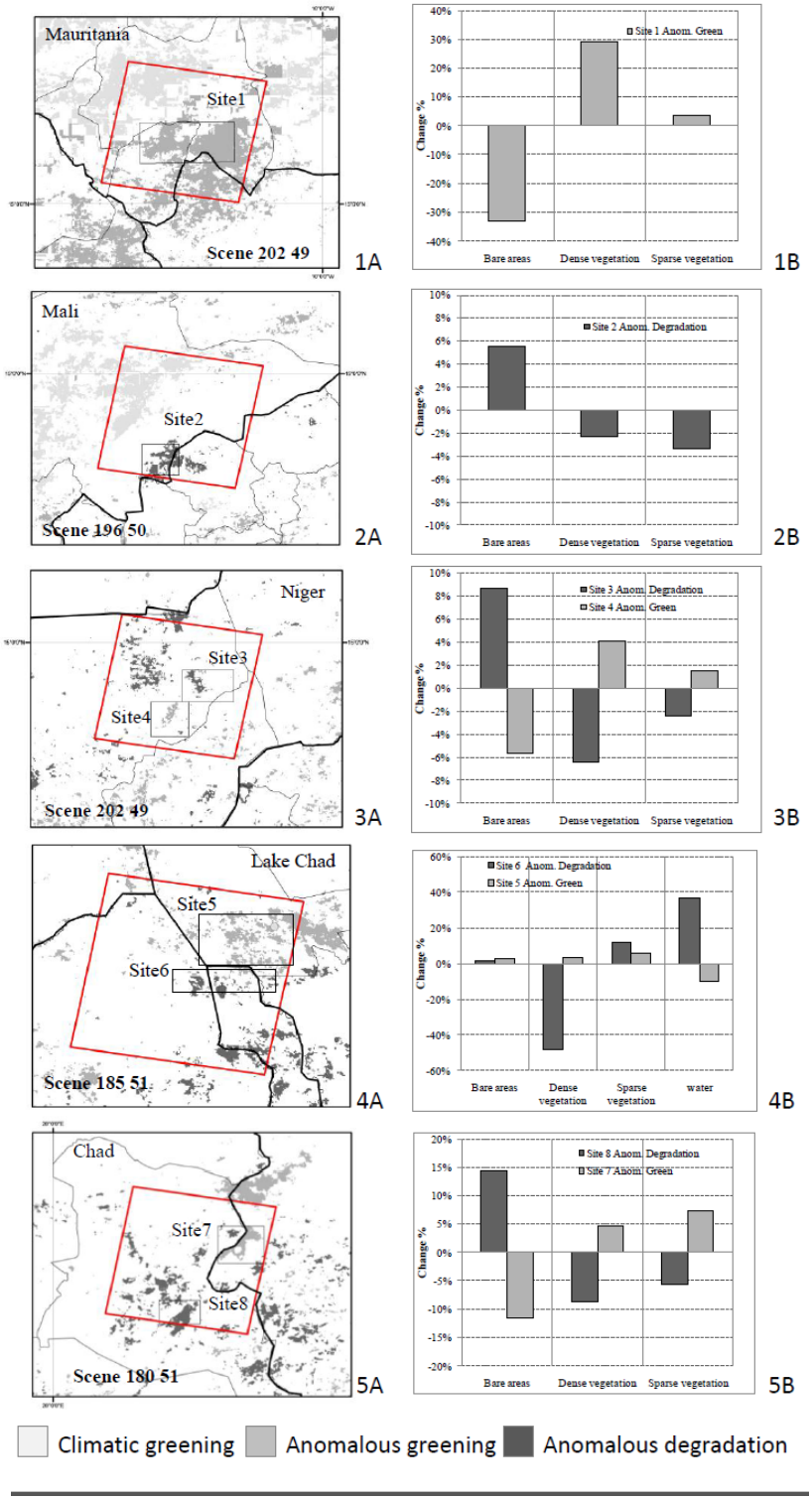

Figure 8: Maps of climatic greening (ligth grey), anomalous greening (medium grey) and anomalous degradation (dark grey) (A panels, left) and histograms showing the land cover change [%] (B panels, right) for the five Landsat TM/ETM+ images (red squares) used for local interpretation. Histogram indicates percentage cover change within the black boxes of the different sites (site 1 to site 8).

Site 5 and 6: Lake Chad

The Lake Chad basin is home to over 20 million people with the majority dependent on the lake and other wetlands for fishing, hunting, farming and grazing. The hot spot map presents two opposite conditions: anomalous greening for site 5 and anomalous degradation for site 6. The Landsat TM analysis revealed that the anomalous degradation in the southern part of the lake area is related to the expansion of the lake surface (Figure 8 4B, water increase > 30%). On the contrary, the northern part shows an increase of vegetation cover related to the expansion of agricultural areas (reported also by GlobCover) over previously flooded zones (decrease in water surface about 10%). This anomalous greening is predominant in the Lake Chad area (Figure 8 4A), however, it is likely to be a side effect of the well-known strong reduction of lake surface. Figure 9 display with two images at high resolution (central panel 2002, right panel 2010) the expansion of the lake surface (red circle) and the losses of water surface (blue circle)-

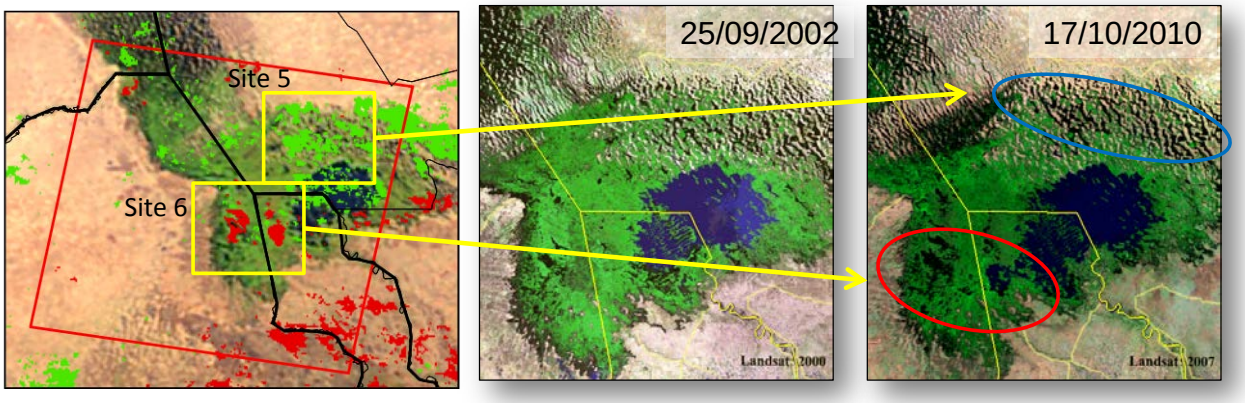

Figure 9- Maps of anomalous greening (green spots) and anomalous degradation (red spots). Landsat TM/ETM+ images (central and right panels) used for local interpretation.

Site 7 and 8: Chad-Sudan

Finally, Figure 8 5A reports the situation along the border between Chad and Sudan. The anomalous degradation patterns are located in the south-western region where agricultural is significantly diffused. The interpretation of Landsat images highlights several patterns of land degradation along steep watersheds that determines a persistent loss of vegetation cover (site 8), those areas are often interested by large wildfire. The region identified with a significant anomalous greening (site 7) belongs to the Western Darfur State, and is located in the Misterei Rural Council (HIC Darfur, 2004). The region stretches along the Wadi Kaja that makes up the

border with the neighbouring Chad in this area. The elevation ranges between 750 and 1000 m a.s.l., the average annual rainfall is about 600 mm, allowing a combination of rainfed agriculture and pastoral activities. Until 2004 the villages were concentrated mainly between Wadi Kadja and the paved road running in parallel from El Geneina to Beida. People have fled into refugee camps and are not able to crop their fields anymore and have lost most of their cattle that was looted by the militia (Schimmer et al., 2008). Our study shows a statistically significant vegetation increase since 2004 which cannot be explained by changes in rainfall patterns: in fact, over the last 10 years rainfall shows stability or a slight decrease (Figure 6e and f). As shown in maps published by the US Department of State (US Dept. of State, 2010) and by the Holocaust Memorial Museum (2009) also available as Google Earth layer most villages of this area have been destroyed between 2004 and 2006 during to the Darfur conflict. Figure 10 shows on very high resolution image the Anomalous Greening (green area) discussed in Figure 8 5A (Site 7). Red flames indicates destroyed or abandoned villages. Detected hot-spot shows the same shape of area affected by Darfur conflict. Beyond the border between Chad and Darfur (thin yellow line in Figure 10) no anomalous vegetation production was detected. This anomalous greening should be rather linked to abandonment of agriculture and cattle breeding due to forced population displacement. This statistically significant analysis confirms the observations made by Schimmer et al. (2008).

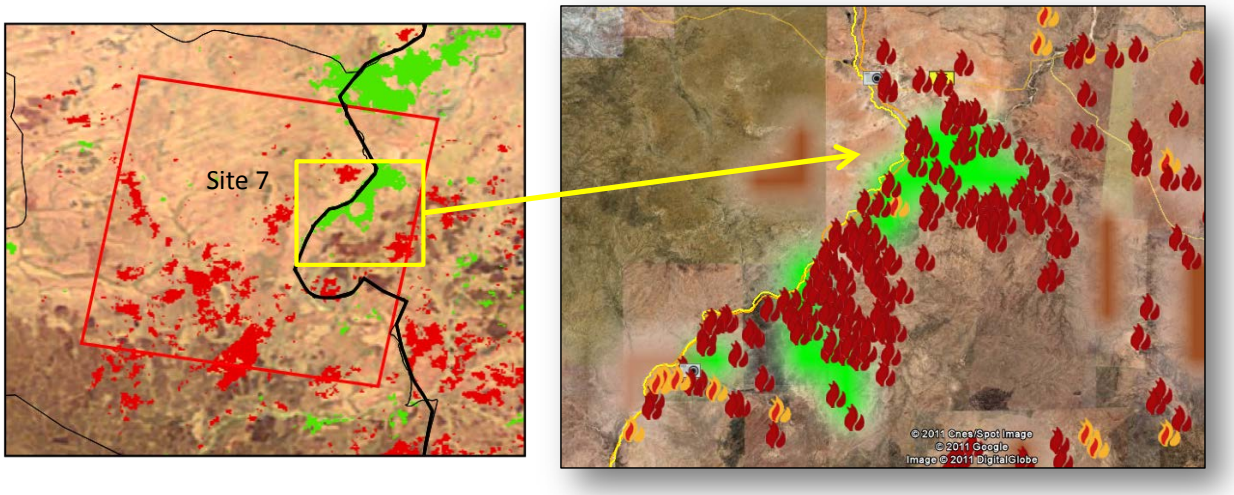

Figure 10- Maps of anomalous greening (green spots) and anomalous degradation (red spots) (left panel). In right panel Anomalous Greening hot-spot overlapped to very high resolution images in correspondence of destroyed (red flames) and damaged (yellow flames) villages during the Darfur genocide in 2004-2006.

1.7. Conclusions

This study aimed to detect anomalous situations where vegetation trends are not explained by changes of the climatic conditions in West African Sahel. Indeed, other anthropogenic or natural driving factors are involved in ecosystem processes. Long-term trend analysis of satellite derived NDVI and rainfall estimates showed that West Africa precipitations have been mainly stable over the period 1998-2010 thus leading to potentially favourable conditions; these results confirm that this area is still recovering from the effects of the drought occurred in the 70s and 80s and does not show an irreversible process of desertification. This finding is in line with the documented occurrence identified by several authors in the last 20 years. An evident increase of rainfall is observed in Southern of Mauritania, North Senegal and central Mali while significant decrease is observed in Nigeria. NDVI shows a general increasing trend with few localized areas of negative trend.

The combined analysis of NDVI and rainfall allowed us to identify those areas where vegetation follows the trend of rainfall (climate-driven increase of vegetation) and areas where the two variables have opposite trends (anomalous situations).

In the humid regions of the southern part of the study area an increase of NDVI was observed even in conditions where rainfall remained stable (i.e. no significant trend), or even decreased (anomalous greening). These patches of increased NDVI are associated to Crop land (GC_14) and close to open shrubland (GC_130) land cover classes of the GlobCover map.

On the contrary, small pockets anomalous degradation have been identified mainly in the Northern part of the study area, in the belt from West Mali to the Chad-Sudan border, which is well-known as fragile zone, where increasing population and human activity (rainfed agriculture, pastoralism and wood exploitation) are in instable equilibrium. Their strong dependence on climatic conditions determines frequent humanitarian crises due to food shortage.

A number of hot spots of anomalous conditions along the boundary between the Sahelian and the Sahelian-Sudanian zones were analyzed in details using multi-temporal Landsat TM/ETM+ images. The analysis of changes occurred between pairs of images acquired over the same area confirmed at local scale the trends of land degradation or recovery identified at the coarser resolution of 1km. It is important to underline that these anomalous situations are driven by local causes. Anomalous greening occurring north of Lake Chad is indicative of a critical

environmental situation: the shrinking of Lake Chad has uncovered new lands colonized by new agricultural fields. In Niger anomalous greening corresponds to the intensification of cropping in a fertile floodplain, whereas in Western Sudan it is associated to the abandonment of agro-pastoral land as a consequence of Darfur conflict. In areas where anomalous vegetation degradation is observed, the demographic framework and associated increase of the exploitation of environmental resources provide the general framework but are not sufficient to explain the local patterns.

Results of this study confirmed that most of the vegetation in the study area depends on climatic variability and more specifically is driven by changes in rainfall patterns at the sub-continental scale. However, there are areas of anomalous hot spots where the trend in the development of natural vegetation and crops is locally driven by other factors, mainly linked to human activity.

CHAPTER 2: Land use and cover change detection in a semi-arid area of Niger using multi-temporal analysis of Landsat images

2.1 Abstract

Recent studies using low resolution satellite time series show that the Sahelian belt of West Africa is witnessing an increase in vegetation cover/biomass, called re-greening. However, detailed information on local processing and occurring changes is rare or lacking. A multi-temporal set of Landsat images were used to produce land cover maps for the years 2000 and 2007 in a semi-arid region of Niger where anomalous vegetation trend have been previously detected. Several supervised classification approaches were tested: spectral classification of single Landsat data, temporal classification of NDVI time series from Landsat images and two-step classification integrating both these approaches. The accuracy of the obtained land cover maps ranges between 80% and 90% overall for the two-step classification approach. Comparison of the 2007-2000 maps indicates a stable semi-arid region, where some change hot-spots exist despite a generally constant level of rainfall in the area during this period. In particular the Dallol Bosso fossil valley highlights an increase in cultivated land, while a decrease in herbaceous vegetation was observed outside the valley, where rangeland is the predominant natural landscape.

2.2 Introduction

The Sahelian belt of West Africa is a region characterized by wide climate variations, which have an effect on the food security of local populations especially in rangeland areas. The most widely known example of this is the dramatic food crisis that occurred during 1970s and 1980s caused by severe drought. In this period Lamprey (1988) stated that the Sahelian region was witnessing an "irreversible and progressive desertification", caused by anthropogenic disturbances. Actually, more recent studies based on satellite data, have shown that there has been an increase in vegetation cover since the mid-1980s, associated with an increase in large-scale precipitation (Herrmann *et al.*, 2005; Heumann *et al.*, 2007).

This phenomenon, commonly referred to as "greening" or "re-greening" has been interpreted as a recovery from the great Sahelian drought of the 1970s (Anyamba and Tucker, 2005; Giannini *et al.*, 2008; Olsson *et al.*, 2005). Analysis of the time series of NDVI (*Normalized Difference*

Vegetation Index) data, obtained from low resolution NOAA-AVHRR (*Advanced Very High Resolution Radiometer*) images, clearly shows a positive trend in vegetation growth in the Sahelian region from 1982 to 2007 (Huber *et al*., 2011). In particular, the 1994-2003 period marks the changeover to a wetter rain season compared to the past, even if not so wet as the maximum period of rainfall recorded in Sahel from 1930 to 1965 (Anyamba and Tucker, 2005).

The extent of this phenomenon has not been comprehensively confirmed yet with ground data and local information. Some information given by Capecchi *et al*. (2008) demonstrates how a positive rainfall trend led to a considerable increase in agricultural land, mostly used for millet farming.

Over recent years, these issues have roused the interest of scientists to seek the climatic or anthropogenic factors that led to the extended drought and the re-greening and also to assess their impact on the environment and agro-ecosystems (Herrmann *et al*., 2005). Many of these studies, which were mainly conducted on a regional scale using low resolution data, underline the need for local information/analysis with higher spatial resolution, in order to improve the reliability of this "low resolution statement".

For example Hermann and Anyamba (2005) indicated that multi-temporal analyses performed on a local scale greatly facilitate the understanding of the current complex phenomena of greening and environmental degradation. Indeed, the modification in vegetation cover, involving the predominant clearing of natural vegetation, may have a long-term impact on sustainable food production, freshwater and forest resources and the climate and, last but not least, on human welfare (Foley *et al*., 2005). On the other hand, developing policy and cooperation actions produced local improvement of ecosystem services and agriculture production. These activities involve reforestation, agricultural land expansion or intensification. So, for a proper environmental monitoring of fragile area like the Sahel it is fundamentally important to reliably document at regular intervals the changes in land cover and land use linked to degradation or improvements in agro-pastoral areas (Brink and Eva, 2009).

One of the first land cover (LC) maps of the entire African continent was produced by Tucker *et al.* (1985) using principal component classification of NDVI from AVHRR images. Due to the coarse spatial resolution of the data (4 km) the Sahelian area is mapped in just three classes: desert, semi-desert, wooded grassland. The GLC-2000 initiative produced a further comprehensive and detailed map of African vegetation cover (Mayaux *et al*., 2004). This product has a spatial resolution of 1 km and it was produced exploiting SPOT–VGT (*Satellite Pour*

l'Observation de la Terre- Vegetation) satellite data; for the Sahel the map reports two class of cropland , four of grassland and stony desert areas. More recently, a regional map for Africa was derived in the GlobCover framework. This thematic layer is derived from data acquired by the ESA ENVISAT Medium Resolution Imaging Spectrometer (MERIS) with a 300 m spatial resolution (Arino *et al*., 2008). Despite the good thematic content of these two products the maps produced are not adequate for local studies that must depend on ad hoc processing of high resolution (< 30 m) multi-temporal images in particular when agriculture and pasture activities must be monitored.

Analysis with SPOT-HRV (*Haute Resolution Visible*) images (20 meter spatial resolution) were used in the Sahelian area with the specific aim to detect rain-fed agriculture. Rasmussen and Reenberg (1992) used 4 images acquired during the year to map millet on the base of digital and visual interpretation techniques. Following the same approach and exploiting multi-year data using aerial photograph and satellite images, Reenberg *et al.* (1998) trace the expansion of agriculture in Burkina Faso (1950-90); the analysis allowed to evaluate the relationship between the human use of land and alterations in the biophysical environment. In the Mali area of Inner Niger delta, Turner and Congalton (1998) mapped rice cultivation using 3 images within a multi-steps hybrid classification approach. SPOT data were also used to conduct a LC change analysis for the Taita Hills in the dry Serengeti plains (Kenya). The results linked with a soil model showed that an increase in the area of croplands has caused an enormous impact on soil-loss potential (Erdogan *et al*., 2011). This study highlighted that the transformation of natural vegetation into agricultural lands at an accelerated rate can endanger ecosystem services and increase soil-loss, which may trigger land degradation.

Landsat TM/ETM (Thematic Mapper/Enhanced TM, 30 m) provides also the right level of spatial resolution to map land cover changes (LCC) at a landscape level (Lillesand & Kiefer, 2000). In semi-arid areas of Mediterranean region, the combination between the Landsat time series and local knowledge has allowed to detect 12 types of land-use changes such as extensification of agriculture, rural exodus, reforestation, etc. (Lasanta & Vicente-Serrano, 2012). Concerning African landscape, a work conducted on a Sahelian area of Sudan, evaluated the desertification processes exploiting single images acquired in 1987 and 2008. Both desertified and regrown areas were detected, and it was established that in this case study the degradation is a direct result of human activity (Dawelbait and Morari, 2012), which has overexploited the natural resources beyond their ecological resilience capability leading to irreversible desertification (Hellden and Tottrup, 2008). LCC analysis was also conducted in the

lake Baringo catchment (Kenya) by diachronic comparison of single Landsat data acquired in the year 1986 and 2000 (Kiage et al., 2007). Images were first classified in six classes, with an accuracy of about 90%, and then Land cover map of the two dates analyzed (image differencing); results demonstrated to be an excellent tool for detecting land degradation in semi-arid environments. Finally, a recent LCC research conducted on the entire African continent and focused on agricultural activity showed that Sahelian croplands were extended by 14% over the last 25 years of the last century. The main driving force for this expansion would appear to be the increase in population, which effectively doubled in the period from 1970 to 2000 (Brink and Eva, 2009; Ruelland et al., 2010).

All these studies confirm the capability of Landsat and SPOT high resolution images to detect areas of rain-fed agriculture and highlight that availability of several images on the same year, or at least one image acquired in coincidence with the peak of cultivation cycle, is crucial to map the agriculture activities. Free availability of three decades of Landsat TM/ETM imagery can also be an important factor for LCC studies in semi-arid areas of African continent.

The aim of this paper is to provide improved information on land cover changes using multi-temporal Landsat images in the Tillabery province of Niger (West Africa) where detailed thematic maps are currently missing. The interest in this study area was stimulated by results of a previous study, conducted in the frame of EU FP7 Geoland2-NARMA (*Natural Resources Monitoring in Africa*) project, which focused on the analysis of climate/human interactions with vegetation patterns in the Sahel region during the decade 1999-2008 (Nutini *et al*., 2010). More specifically the area of Tillabery province presented “anomalous hot spots” where vegetation behavior is not fully explained by rainfall, indicating that other factors interfere in the dynamics of plant development. These area need local analysis for the interpretation of these phenomena.

The first step of the study was to identify the best classification methodology for producing a land cover map in a marginal semi-arid region characterized by high climatic seasonality using multi-temporal Landsat data. In the second phase, two land cover maps of the study area were produced for the years 2000 and 2007, and then were compared to obtain an overview of vegetation changes in Sahelian contexts characterized by environmentally critical circumstances.

2.3 Study area

The study area covers the Tillabery province in Niger, a Sahelian region of semi-arid savanna with localized evidence of agricultural activity (< 20% of cultivated areas; Ramankutty, 2004).

The country experienced a rapid growth in population and recent assessment indicates that there are about 20 inhab/km^2 with a yearly increase rate of 3.3%, leading to heavy pressure on the environment (World Bank, 2010). The area relies on rainfall for farming and livestock and is, therefore, highly vulnerable to climate variability. These conditions lead to a high proportion (about 30%) of households in severe food insecurity (World Bank, 2010). A number of humanitarian crises have hit this area over recent years; this region, in fact, belongs to the "Sahel's fragile high-risk zone" (ECOWAS-SWAC, 2006). The Centre for Research on the Epidemiology of Disasters (CRED) bulletins report that in 2000 the low rain (>300 mm/year) produced an important famine and in 2005 the drought and concomitant locust plague caused a reduction of 11% in cereal production and of 35% in the availability of forage. These events had a direct effect on 2.5 million people and caused a loss in livestock of more than 10,000 cattle (CRED, 2012).

(a)

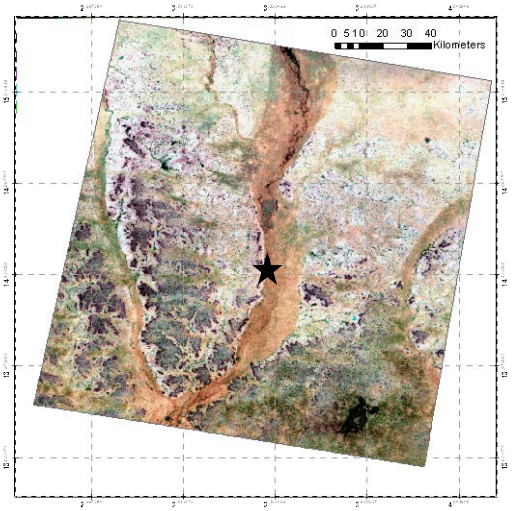

(b)

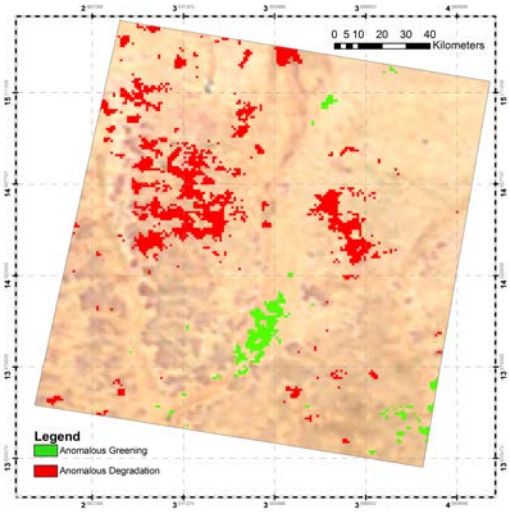

(c)

Figure 1- Study area in Niger, the black box is the area covered by Landsat imagery (path 192, row 50) (a). RGB (5:4:3) of Landsat image acquired in February 2007 and location of Filinguè city (b). Anomalous hot spots - Anomalous Greening (green) and Anomalous Degradation (red) – superimposed to VGT RBG image (c).

The central part of the study area (Figure 1a) is occupied by the Dallol Bosso valley, a relict braided river from a section of the ancient Azaouak River (Bui and Wilding, 1988). This is a fossil river valley which carries surface water in the rainy season. “Dallol” is the Djerma word which is equivalent to the Arabic word “Wadi” that refers to an ephemeral river that remains dry except during the rainy season, but maintains subsurface water during the rest of the year, making it a magnet for human population (Decalo, 1979).

Figure 1(c) shows the anomalous hot spots detected from the combined analysis of the low resolution time series of SPOT-Vegetation (VGT) NDVI and RFE (Rain Fall Estimate) from Famine Early Warning Systems Network (FEWS NET) during the period 1999 to 2008. Green and red spots represent areas of statistically significant increase (Anomalous Greening) or decrease (Anomalous Degradation) of vegetation cover that are not fully explained by rainfall variability (Nutini *et al*., 2010).

Considering the available LC maps, whole region is classified as natural area. In the GlobCover2005 map (Arino *et al*., 2008) this region is classified as savanna grassland, while in the GLC2000 map (Mayaux *et al*., 2004) it is classified as open and sparse grassland. However it is known that agriculture is possible in particularly favorable areas like the fossil river valley mentioned above, and that it relies on hardy species like *Pennisetum glaucum* (Pearl millet) (Geesing *et al.*, 2001; Suttie *et al*., 2005).

The study area is a “Sahelian fringe area” covered by typically semi-arid herbaceous vegetation and where grazing is the major livelihood activity.

Food production is highly unpredictable and depends exclusively on the quantity of erratic rainfall. The rainy season is essentially centered around the summer months, from July to September, with near-zero precipitation levels in the rest of the year (Figure 2).

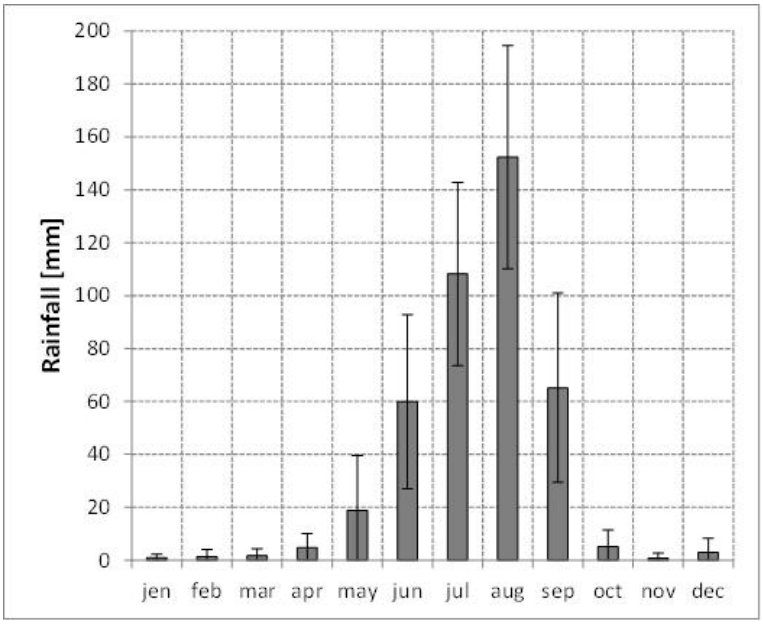

Figure 2- Mean rainfall values registered at Filinguè (14.20°N 3.20°E) from 1998 to 2008 (data: RFE Rainfall Estimate).

2.4 Materials

Satellite images used for this work were acquired by Thematic Mapper (TM) and Enhanced Thematic Mapper (ETM+) sensors mounted on US Landsat satellite series. These images are available free of charge at the USGS (US Geological Service) Global Visualization Viewer (http://glovis.usgs.gov/). However, the limited number of images, available through GloVis for areas outside the USA, and the cloud cover during the vegetation growing (wet season), had a significant effect on the number of available images.

Study area is covered by Landsat frame path row 195-50. Only two years (2000 and 2007) in the period between 1999 and 2008, during which anomalous hot spots were detected, present on GloVis enough images to cover dry (November-May) and rainy seasons (June-October). We selected and downloaded from GloVis six Landsat-7 images, from March to September, for the year 2000 and eight Landsat-5 and one Landsat-7 images, from February to August, for the year 2007 (Table 1).

Landsat images are distributed in GeoTiff format, with standard ground correction (Level 1T). Radiometric and geometric accuracies are achieved using control points extracted from available DEMs (STRM, NED, CDAC, DTED or GTOPO30). The images are provided resampled in UTM-WGS 84 geographic projection using the Cubic Convolution system (landsat.usgs.gov).

Table 1- List of Landsat images (path 192, row 50) with minimal cloud cover available and downloaded from GloVis. The Landsat-5 images are from TM and Landsat-7 from ETM+ sensor.

Year	Date	Satellite	Cloud cover from GloVis
2000	16 March	Landsat 7	-
	19 May	Landsat 7	-
	20 June	Landsat 7	-
	22 July	Landsat 7	1%
	23 August	Landsat 7	11%
	24 September	Landsat 7	9%
2007	08 February	Landsat 5	-
	24 February	Landsat 5	-
	12 March	Landsat 5	-
	31 May	Landsat 5	-
	16 June	Landsat 5	-
	02 July	Landsat 5	-
	18 July	Landsat 5	-
	03 August	Landsat 5	-
	28 September	Landsat 7	-

Other ancillary data used include time series of precipitation estimates and spectral vegetation index from course resolution data. For precipitation, we used RFE data, at 8 km spatial resolution and 10-day temporal composite, provided by FEWS NET, an agency that is part of US-AID (United States Agency for International Development). In addition time-series of NDVI data, obtained from the SPOT-VGT sensor and provided at 1 km spatial resolution in 10-day temporal composite, were used. These data allow us to compare in a spatially distributed way the timing of vegetation response to rainfall events and thus to understand the vegetation condition at the moment of Landsat acquisition. In particular, SPOT-NDVI data can outline the seasonal dynamic, and shows precisely in which period of the season the Landsat images were collected.

Both the NDVI and RFE time series were acquired under the Geoland2 Core Information Service NARMA (Combal *et al*., 2010).

2.5 Methods

Changes in land cover and land use linked to degradation or improvements in agro-pastoral areas can be analyzed through the identification of five thematic classes: Shrubland, Cultivated land, Herbaceous vegetation, Water body and Bare area (Brink and Eva, 2009). These five classes are suitable to describe the ecological conditions of vegetation cover in the Sahel and the analysis of the changes provides information on their relations with possible human activities. These five classes are used in this study, and a short description of their ecological features is reported in Table 2.

Table 2- Description of the five classes of interest.

Thematic Classes	Description	Typical species	Height [m]	Reference
Shrubland	Woody vegetation that formed well defined dark patterns like "tiger bush".	*Guiera senegalensis*	> 3	Kizito *et al.*, 2006
Cultivated land	Area close to villages, especially in the fossil valley with evident square patterns.	*Pennisetum glaucum*	2	Onyewotu *et al.*, 1998
Herbaceous vegetation	Natural vegetation useful for grazing with sparse arboreous species.	*Cenchrus biflorus*	1	Schlecht *et al.*, 2006
Water body	Bare areas flooded at the start of the rainy season.	-	-	Reenberg *et al.*, 1998
Bare area	Area with vegetation cover lower than 10% not usable for cattle grazing, or rocky area.	-	-	Brink and Eva, 2009

In order to obtain a reliable and accurate information on vegetation and LCCs, a pre-processing of multi-date sensor imagery is required taking into account and quantifying, among others, the sensor calibration, the atmospheric effects and the illumination conditions during each scene acquisition (Coppin *et al*., 2004). Digital number (DN) values were first converted into absolute spectral radiance units (W m^{-2} sr^{-1}) using appropriate calibration coefficients (Chander *et al*., 2009) and, secondly, corrected for the atmospheric effects using the Simulation of the Satellite

Signal in the Solar Spectrum (6S) code (Vermote *et al.*, 1997) to obtain ground spectral reflectance. The input to 6S was a tropical atmospheric profile and a desert aerosol model, with the Aerosol Optical Thickness (AOT) values, registered at the AERONET station of Banizoumbou, Niger (13°32'27" N e 02°39'54" E).

The Normalized Difference Vegetation Index (NDVI) (Rouse *et al.*, 1973) was then computed, using TM3 band (red, 0.63-0.69 µm) and TM4 (near infrared, 0.76-0.90 µm) in the following formula NDVI = (TM4-TM3)/(TM4+TM3). RFE data were also used to analyze and understand the dynamics of TM-NDVI evolution during the analyzed year.

In order to identify the best classification methodology for producing a land cover map in a marginal semi-arid region using multi-temporal Landsat data, three supervised approaches were tested: spectral classification of single date images, temporal classification of NDVI time series and two-step classification which includes both these approaches. The Maximum Likelihood algorithm was selected and applied to different Landsat datasets for the year 2007 in order to determine the best approach for obtaining a five-class LC map of the area.

Training set selection

The training sets for the supervised classification were selected with the following criteria: visual interpretation of Google Earth images, analysis of spectral features and temporal behavior, and expert knowledge of local conditions. Additionally, we exploited a comparison between NDVI temporal dynamics and the rainfall seasonality as an interpretive tool to further distinguish between different LC types.

- Shrub vegetation, dominated by *Guiera senegalensis* J.F. Gmel., *Combretum micranthum* G. Don and *Balanites aegyptiaca* Del. (Schlecht *et al.*, 2006, Saidou *et al.*, 2010), in this region forms regular patterns called “tiger bush” that are easy to be identified through visual interpretation (Galle *et al.*, 1999) of VHR images from Google Earth. From the phenological point of view, despite a general reduction of vegetation vigor, many shrubs maintain green leaf also during the dry season, due to the well-known capacity of roots to exploit deep water in arid ecosystems (Kizito *et al.*, 2006). Moreover, as expressed by local experts of Native Breeds at Risk of Extinction organization (R.A.R.E.), this photosynthetic vegetation is not always clearly visible in satellite images due to a thick layer of sand deposited at the base of the plant and on the leaves by desert wind (Trucchi and Semita of R.A.R.E., personal communication). When first rains come this layer is cleaned, resulting in a rapid increase in

the NDVI compared to previous satellite observation. Both these phenomena, presence of vegetation activity during the whole season and rapid NDVI increase, contribute towards the definition of TM-NDVI behavior rules for shrubland areas.

- Cultivated land, mainly rain-fed Pearl millet in the region (Geesing *et al.*, 2001), show a delay in the start of the season respect shrubs as consequence of agro-practices. Usually land preparation and sowing activities come after the start of the rainy season; Onyewotu *et al.* (1998) indicate that sowing occurs after " … *the first ten days in the season in which the amount of rainfall is equal to or greater than 25 mm, but with a subsequent ten-day period in which the amount of rainfall is at least equal to half the evapotranspiration demand*". So there is a time lapse of about 3 weeks at least between the start of effective rain and plant emergence and crop growing. The NDVI behavior shows a sensitive decreasing at the end of the wet season corresponding to the crop maturity and harvesting. In addition to this, the regular shape of cultivated fields can help in their visual identification and consequent selection of training pixels particularly if the images are taken at the peak of the season (Rasmussen & Reenberg, 1992; Reenberg *et al.*, 1998; Beguè *et al.*, 2011).
- Natural herbaceous vegetation, such as *Cenchrus biflorus* Roxb. (table 2), has a less intense growth rate compared to millet due to the absence of tillage and manure (Rufino *et al*., 2006, Schlecht *et al.*, 2006) and the effect of grazing. For these reasons, the natural herbaceous vegetation reaches a height of around 1 meter whereas herbaceous cultivated crops can reach 2 meters. The natural herbaceous vegetation does not have clear spatial patterns at Landsat resolution, and it was one of the most difficult classes to be identified by visual analysis.
- Bare area, defined where less than 10% of the surface are vegetated (Brink and Eva, 2009) corresponds to area where it is not appreciate seasonal variation of NDVI and its maximum value does not exceed 0.15.
- Water bodies, in the area are generally small and flooded in the wet season and dry out in the rest of the year (Reenberg *et al.*,1998). Consequently, training set for the “Water bodies” is selected where the NDVI progressively decreases at the beginning of the wet season dropping below 0 value.

Classification tests

On the basis of these training sets, seven supervised Maximum Likelihood classifications were applied on Landsat images from 2007: three spectral classifications on single date and four

multi-temporal classifications on NDVI. The single date spectral classifications were tested for one winter date (24 February), one spring date (02 July) and one summer date (8 August). These dates cover significant periods of Sahelian season and refer to the dry season, the start of the wet season and the vegetative peak respectively. Multi-temporal classifications of NDVIs were conducted starting with two dates (the first and last images of the year) and reaching up to nine (all dates available). The goal was to define the minimum cardinality and timing of multi-temporal NDVI acquisition that can guarantee the best mapping accuracy.

Thematic maps performance was assessed by comparing accuracy measurements such as overall accuracy (OA), kappa (K) statistics, and omission/commission errors (OE/CE) derived from the error matrices (Congalton, 1991). Reference test pixels were i) selected using a stratified random sampling scheme and ii) labeled by visual interpretations of Landsat images and using local information provided by the R.A.R.E. organization. The test reference cardinality is at least 60 pixels per class, in order to assure a significant level ($p > 0.1$) of accuracy assessment (Brivio *et al*., 1996).

The most accurate classification approach, defined with the 2007 dataset, was applied to Landsat images for the year 2000 and its accuracy was assessed. Finally the comparison between the two thematic maps (2000 and 2007) allowed to produce a LCC map (Kiage *et al.*, 2007; Dawelbait and Morari, 2012). The map reports 5 classes of changes (Increase cultivated, Decrease cultivated, Increase natural vegetation, Decrease natural vegetation, Stable area) and was analyzed in relation to the areas of Anomalous Greening and Anomalous Degradation derived by Nutini *et al*. 2010.

Area of cloud, shadow or affected by striping (Landsat-7 SLC-OFF problem) were masked out before the classification process using an unsupervised ISODATA algorithm (Tou and Gonzalez, 1974) and subsequent visual labeling. These no-data conditions were encountered only once for 2007 (24 September), but several times for the year 2000. For this reason, the classification of no-data areas that occurs in a specific date was obtained using all the other cloud free available images. Areas that are covered by cloud (or striping) more than one time in the year were excluded from the classification. This approach that exploit the multi-temporal data redundancy allowed us to sensibly increase the total classified surface.

2.6 Results and discussion

Test of classification approaches

Figure 3 shows the timing of Landsat acquisitions respect the 2007 vegetation season, as provided by SPOT-VGT NDVI temporal profile, and the rain occurrence recorded by RFE. The good temporal distribution of images is crucial for observing the seasonal behavior of the vegetation in relation to the timing of rainfall (Tucker *et al.*, 1985); the 2007 data set shows images well distributed in relation to the rainy season (see RFE histogram). Three images are representative of the dry season while the six remaining cover i) the start of wet season (three images), ii) the period close to vegetative peak (two images) and iii) the end of the rainy season (one image).

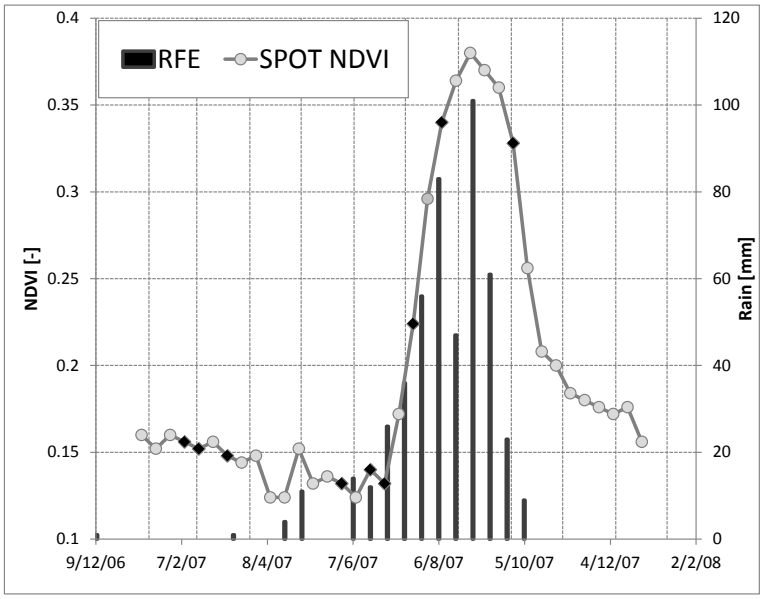

Figure 3- TM acquisitions (Black square) for 2007 in relation to precipitation (histogram of RFE data) and vegetation dynamics (SPOT-VGT NDVI, grey line)

Figure 4 displays the mean spectral signature of different classes, extracted from the selected training sets, in three topic periods of the season (dry season, start of rainy season, vegetative peak, panels *a*, *b* and *c* respectively) as well as the NDVI trends for the full annual period (panel *d*).

In Figure 4*a* the mean spectral response of the training sets present the typical soil spectral signature, as expected in the semi-arid African savanna where the vegetated area becomes arid during the dry months (October-May) (Brouwer, 2008) and the green shrubs reduce their vigor and are often covered by sand (Trucchi and Semita of R.A.R.E., personal communication). At

the beginning of the rainy season- (July)- (Figure 4*b*) the Water bodies start to be filled, and the spectra are able to show this event with a decrease in the reflectance response in the SWIR and NIR bands. The Shrub vegetative dynamics show the earliest response to rain, as underlined by its spectral signature (Figure 4*b*).

The third graph Figure 4*c* shows the spectral signature at the peak of rainy season (August). All the vegetated area displays the typical vegetation signature with an higher reflectance in NIR as a consequence of the well-developed canopy. Only the Bare area keeps the same signature as the previous dates.

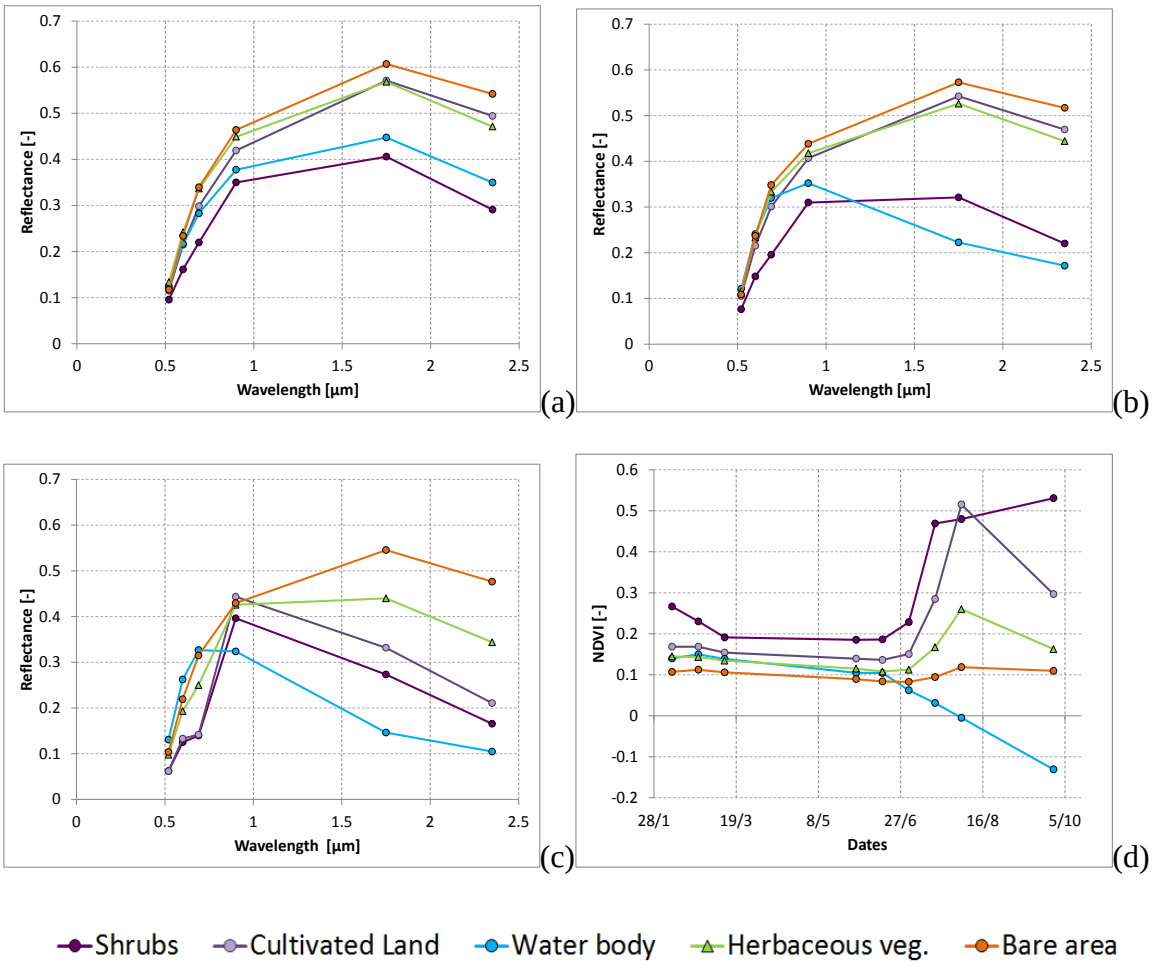

Figure 4- Training set characteristics: spectral signatures for dry season -24 February - (a), start of rainy season - 2 July - (b), vegetative peak 3 August - (c) and annual dynamic of NDVI (d).

Figure 4*d* displays the annual NDVI trends. All the classes except Shrubs have low NDVI values (NDVI ≈ 0.1) during the dry season (February-June). The Shrubs class (dark green) presents some permanent green canopy also during the dry season (NDVI ≈ 0.2) as confirmed by local studies (Saidou *et al.*, 2010; Trucchi and Semita R.A.R.E., personal communication). Being

partially vegetated and thanks to the early response to the rain (Kizito *et al*., 2006) the Shrubs NDVI values remain permanently higher compared to the other natural land-cover classes profiles until the end of the season in September. Only the Cultivated Land reaches NDVI values comparable to Shrubs ones (NDVI ≈ 0.5) at the growing peak.

The NDVI behavior of Cultivated land (Figure 4*d*, violet line) shows a later response to rain compared to Shrubs as a consequence of delayed sowing date (Onyewotu *et al.*, 1998) and a strong decrease in September due to physiological maturity of millet and/or harvesting (Soler *et al.*, 2008). It is interesting to note that crops have higher annual NDVI than natural Herbaceous vegetation, but lower values than shrubs, as showed in other Sahelian areas (Beguè *et al.*, 2011).

Table 3 reports the error matrixes for the classification approaches tested and accuracy metrics results are summarized in Figure 5. The spectral classifications show a good level of overall accuracy (OA = 81.1%) only for the August image (Figure 5 – TM Aug.).

In the other two spectral classification tests (Figure 5 – TM Febr. and TM July), the vegetation growth was not sufficient to distinguish between the different vegetated classes, causing a low overall accuracy of 60.3% and 58.7% respectively.

The error matrix of these two classifications presents major errors, mainly in Herbaceous vegetation and Water bodies. Herbaceous vegetation is often confused with Bare area, and the Water body with Shrubs and Bare soil because these temporary lakes are not yet flooded in this period. The spectral classification for August, despite the good level of accuracy (OA = 81.1%), has some problems in the separability between the Shrub and Herbaceous vegetation classes (Table 3-C) that are the most important in terms of natural resources.

Producer's accuracy for these classes is 59.2% and 62.2% respectively. Shrubs are confused with Herbaceous veg. (~25%) and Bare soil (~9%). Herbaceous vegetation are misclassified with Bare soil (~18%), Shrubs (~12%) and cultivated land (~8%).

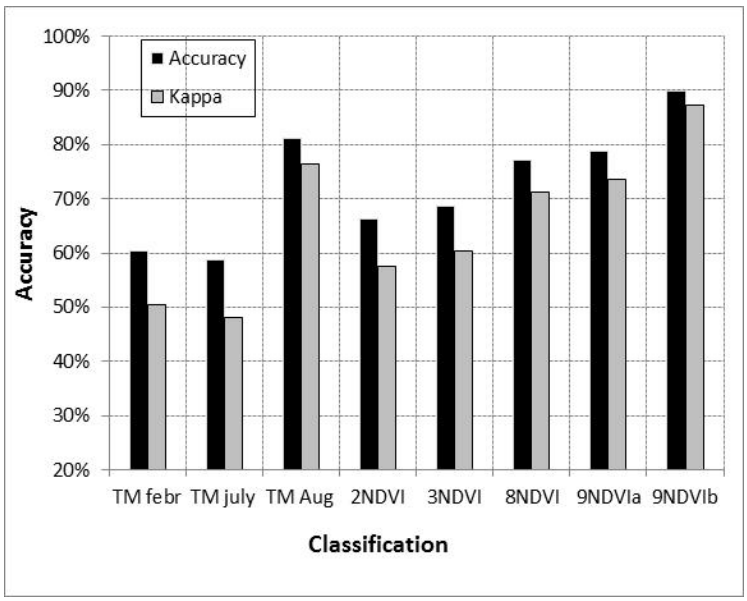

Figure 5- Comparison of accuracy performances of different classification approaches. 9NDVIb indicates the two step multi-temporal and spectral approach classification.

Figure 5 allows us to compare the accuracy metrics (OA and K coefficient) for the classifications based on the multi-temporal NDVI. The first classification (2NDVI) includes two images acquired in winter (24 February) and summer (3 August) respectively; the 3NDVI dataset adds one summer image acquired at the start of the season (2 July).

The 8NDVI exploits all the data except the end of the season image (28 September). The accuracy increases from around 60% for the first two cases to 72% for the 8NDVI classification, highlighting the importance of the availability of data acquired throughout the whole season. The classification that exploits all the available NDVI time series (9 dates) reaches a higher level of accuracy (OA = 78.9%) than the 8NDVI combination.

Even if this result is slightly lower that to one obtained with the spectral classification using August data (TM Aug.), the multi-temporal classification can be considered more promising than the spectral approach. The error matrix (Table 3-D) shows that the accuracy/error is more balanced as demonstrated by the producer's accuracy that is always higher than 70%, even for those classes that turned out to be inaccurate in the best spectral classification.

The Shrub land and Cultivated land have a low user accuracy of 62.0% and 65.7%, respectively. These classes are overestimated and the Cultivated land class sometimes includes Herbaceous vegetation (~19%) due to the similar temporal behavior. The Shrub class comprises some Water bodies (~24%), because often trees are very dense around small ponds, and these areas are flooded during the rainy season.

These two overestimated classes, Shrubs and Cultivated land, were re-classified thanks to the contribution of spectral information, using the same training sets previously used and the same classification algorithm.

Areas inside the Shrub class were classified using July Landsat data. In fact in Figure 4*b* it is possible to notice that in this date the spectral signature of the Shrubs training set is well separated from the other as a consequence of the rapid response to rain.

The same approach was applied to the areas of Cultivated land, using the August image, when the fields display the maximum growth rate and the signature difference is much more pronounced (Figure 4*c*). The results obtained within these two classes were then integrated into the final land cover map.

The matrix in Table 3-E shows the results of this two-step approach: OA reaches 89.9% because the user accuracy for Shrubs increases from 62% to 85% and Cultivated land from 65.7% to 88%. Globally, this error matrix confirms that the two-step classification reaches the highest OA. The information given by multi-temporal NDVI and spectra signals, collected on significant dates, allow us to obtain the most accurate map (Figure 5 – 9NDVIb).

The final land cover map for the year 2007 is displayed in Figure 7*b*. The area is mainly covered by Bare area (61% of the surface) and Herbaceous vegetation (32%). The other classes have a lower presence: 4.7% of Shrubs, 1.7% of Cultivated land and 0.4% of Water bodies. This division reflects the well-established environmental characteristics of this area. As expected, the Cultivated areas are grouped inside the valleys in the southern part of the study area, where rainfall is greater (up to 450 mm/year).

The Dallol Bosso valley shows the highest presence of Cultivated areas around the city of Filinguè (Lat 14°21′N Lon 3°19′E) (Figure 1*c*); in the Sahel logistics the distance from villages can be a further limiting factor for the agricultural activities, in addition the climatic conditions (Reenberg *et al.*, 1998; Hiernaux *et al.*, 2009).

Table 3- Error matrix of five different classification tests for 2007. Testing set is derived from a stratified random sampling and labelled by visual interpretation: Shrubs (81), Cultivated Land (77), Water body (87), Herbaceous veg. (90) and Bare soil (101).

		Reference data							
(a)	Image 24/02/2007	Shrubs	Cultivated Land	Water body	Herbaceous veg.	Bare soil	User's	OA	K
Spectral classification	Shrubs	60.49	7.79	32.18	6.67	3.96	52.69		
	Cultivated Land	6.17	77.92	1.15	25.56	8.91	61.22		
	Water body	12.35	0.00	54.02	0.00	1.98	79.66		
	Herbaceous veg.	12.35	2.60	8.05	42.22	16.83	51.35		
	Bare soil	8.64	11.69	4.60	25.56	68.32	61.61		
	Producer's	60.49	77.92	54.02	42.22	68.32		60.32	0.50
(b)	Image 02/07/2007	Shrubs	Cultivated Land	Water body	Herbaceous veg.	Bare soil	User's	OA	K
Spectral classification	Shrubs	74.07	2.60	35.63	1.11	6.93	59.41		
	Cultivated Land	2.47	70.13	0.00	12.22	8.91	71.05		
	Water body	9.88	0.00	32.18	2.22	1.98	70.00		
	Herbaceous veg.	4.94	16.88	10.34	53.33	16.83	52.75		
	Bare soil	8.64	10.39	21.84	31.11	65.35	51.56		
	Producer's	74.07	70.13	32.18	53.33	65.35		58.72	0.49
(c)	Image 03/08/2007	Shrubs	Cultivated Land	Water body	Herbaceous veg.	Bare soil	User's	OA	K
Spectral classification	Shrubs	59.26	2.60	0.00	12.22	0.00	78.69		
	Cultivated Land	4.94	94.81	0.00	7.78	1.98	84.88		
	Water body	2.47	0.00	93.10	0.00	0.99	96.43		
	Herbaceous veg.	24.69	2.60	1.15	62.22	1.98	69.14		
	Bare soil	8.64	0.00	5.75	17.78	95.05	77.42		
	Producer's	59.26	94.81	93.1	62.22	95.05		81.19	0.76
(d)	9NDVI time series	Shrubs	Cultivated Land	Water body	Herbaceous veg.	Bare soil	User's	OA	K
Temporal classification	Shrubs	82.72	12.99	24.14	5.56	4.95	62.04		
	Cultivated Land	14.81	87.01	3.45	18.89	2.97	65.69		
	Water body	0.00	0.00	71.26	0.00	0.99	98.41		
	Herbaceous veg.	2.47	0.00	0.00	71.11	7.92	86.49		
	Bare soil	0.00	0.00	1.15	4.44	83.17	94.38		
	Producer's	82.72	87.01	71.26	71.11	83.17		78.90	0.74

(continue)

(e)	9NDVI + Spectral	Shrubs	Cultivated Land	Water body	Herbaceous veg.	Bare soil	User's	OA	K
2 steps classification	Shrubs	91.36	3.90	0.00	6.67	3.96	85.06		
	Cultivated Land	2.47	94.81	0.00	6.67	1.98	87.95		
	Water body	2.47	0.00	98.85	0.00	0.99	96.63		
	Herbaceous veg.	3.70	1.30	0.00	81.11	7.92	85.88		
	Bare soil	0.00	0.00	1.15	5.56	85.15	93.48		
	Producer's	91.36	94.81	98.85	81.11	85.15		89.91	0.87

Land cover map for the year 2000 was produced using the same two-steps approach: first classifying the multi-temporal NDVI data and second using spectral information for refining the overestimated classes.

In addition to the smaller number of available Landsat scenes (6 instead 9), the main difference is given by the cloud cover, which was absent in 2007 but noticeable in 2000. The cloud cover reported by GloVis service (Table 1) is slightly underestimated respects the one obtained by image analysis: 25% of the entire study area has at least one date characterized by the presence of cloud.

The approach adopted to deal with no-data (see § Methods) allowed to classify a further part of the study area (11%) that was affected by cloud cover/striping only one time .

Figure 6 visualizes the excluded and analyzed areas. The black colors correspond to areas not classified because characterized by a presence of cloud cover in two or more dates On the contrary, the colored zones (green, yellow, orange and red) describes cloud contamination for a specific data.

These areas were analyzed using all the other cloud free dates.- The rest of the map (grey) was classified using the entire dataset.

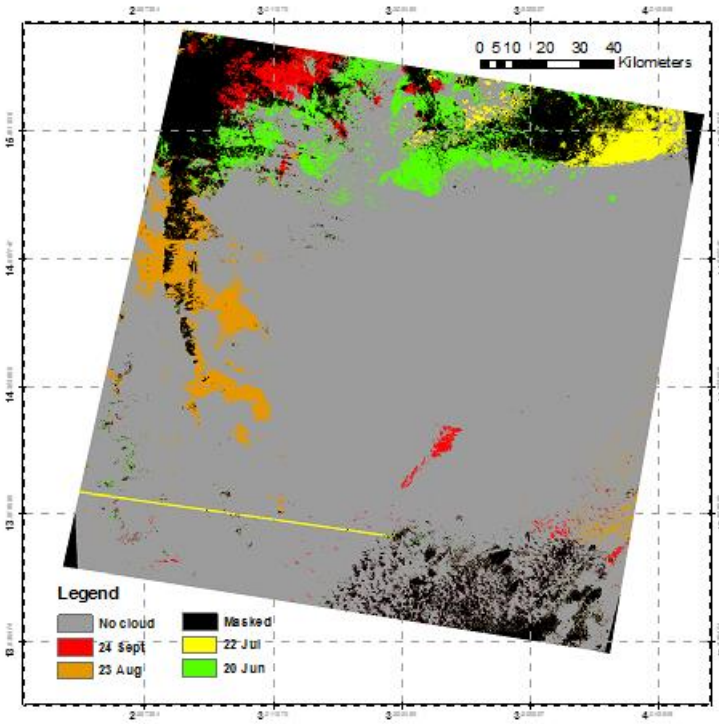

Code	16-Mar	19-May	20-Jun	22-Jul	23-Aug	24-Sep	Surface
	Clear	Clear	Cloud	Clear	Clear	Clear	4%
	Clear	Clear	Clear	Cloud*	Clear	Clear	2%
	Clear	Clear	Clear	Clear	Cloud	Clear	3%
	Clear	Clear	Clear	Clear	Clear	Cloud	2%
	Clear	Clear	Clear	Clear	Clear	Clear	75%
	Masked: Clouds at least for two dates						14%

* striping

Figure 6- Excluded and analysed surface of 2000 data set: entire dataset (grey), masked due to cloud at least in two dates (black). Coloured zone report cloud condition for one date. The table gives the percentage of each class.

Land cover maps and change analysis

The LC map for the year 2000 is shown in Figure 7*a*. Herbaceous vegetation and Bare areas are the most common classes covering 92% of the whole study area (32.5% and 60%, respectively). Table 4 reports error matrix; figures show satisfying performance described by an OA of 80 % and a K value of 0.74. Shrubs an Cultivated land classes are accurately represented (86 and

90.1% UA respectively), while Herbaceous vegetation and Bare soil classes are slightly overestimated (60.5% and 76% UA). In particular, commission errors for Bare areas with water bodies (16%) is related to the low rain condition of 2000 that reduce the surfaces of small lakes.

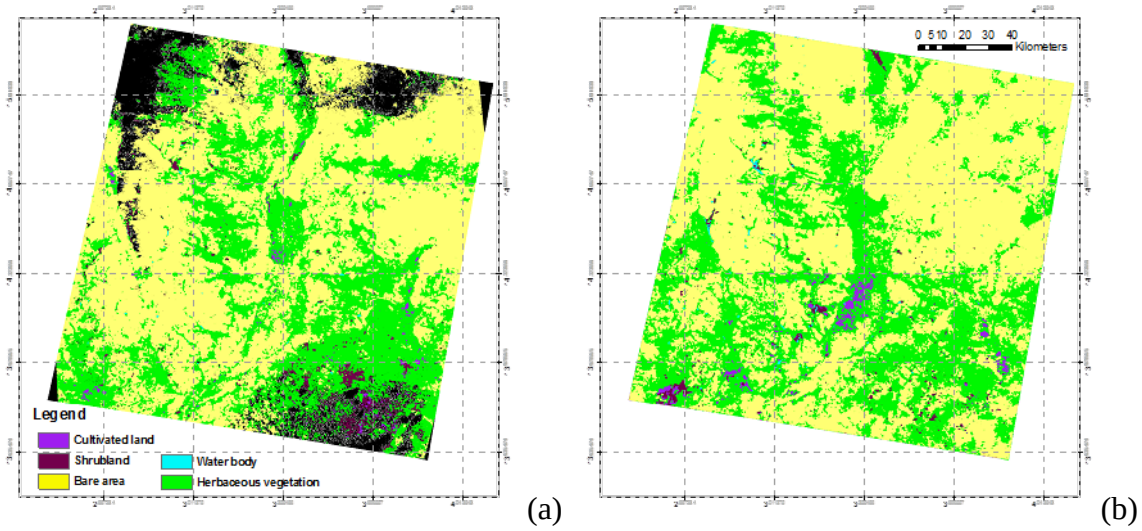

Figure 7- Land-cover map derived from two-step approach for year 2000 (a) and 2007 (b) for the study area in Niger. Black zones represent no-data areas.

		Reference data							
	6NDVI + Spectral	Shrubs	Cultivated Land	Water body	Herbaceous veg.	Bare soil	User's	OA	K
2 steps classification	Shrubs	82.69	1.85	6.00	5.49	1.20	86.00		
	Cultivated Land	1.92	67.59	0.00	6.59	0.00	90.12		
	Water body	0.00	0.00	77.00	0.00	0.00	100.00		
	Herbaceous veg.	12.50	29.63	1.00	82.42	3.61	60.48		
	Bare soil	2.88	0.93	16.00	5.49	95.18	75.96		
	Producer's	82.69	67.59	77.00	82.42	95.18		80.25	0.74

Table 4- Error matrix of classification for 2000. Testing set is derived from a stratified random sampling and labelled by visual interpretation: Shrubs (104), Cultivated Land (108), Water body (100), Herbaceous vegetation (91) and Bare soil (83)

Comparison between the two LC maps shows that in 2000 the shrubland area is larger and covers 5.7% of the total area, whereas Water body coverage is less (0.2% respect to 0.4% in 2007) due to the 2000 drier season. Finally, Cultivated land has a lower cover percentage (1.6% compared to 1.7% in 2007). Although these figures do not globally show any relevant

discrepancies compared to the year 2007, the two LC maps present significant differences in the distribution of LC pattern.

In order to underline these differences, a map of LCCs has been computed and is presented in figure 8. In this map the decrease/increase in Cultivated land is presented in red and blue respectively, while the increase/decrease in natural vegetation, both Shrub and Herbaceous, is depicted in green and orange respectively. The unchanged areas are showed in grey.

The portion undergoing LCC involved 34% of the area, while 66% of the surface remained stable from 2000 to 2007. The stable areas are mainly occupied by Bare area and Herbaceous vegetation. Also the pattern of tiger-bush and temporary water bodies, covering 3% of the entire region, remained stable in the considered period. Inside the area affected by changes, the increase in natural vegetation represents 38% of the changes (green), while blue highlights the increase in Cultivated area (4.6%). On the other hand the decrease in natural vegetation (orange) and Cultivated area (red) represents 43% and 4.1% of the changed respectively. Overall, the decrease of natural vegetation interested an extension of 297 km^2, and the increase of Cultivated land an extension of 43 km^2.

The valleys are characterized by an increase in Cultivated land (blue spots) and by an increase in natural (Shrubs and Herbaceous) vegetation (green areas). On the contrary, in the rangeland area, where agricultural activity is generally absent (Schlecht *et al*., 2006), there are some critical spots characterized by a decrease in natural vegetation (orange) despite the 2007 was a noticeable wet year.

In fact the 2007 was a pretty wet year as showed by RFE data, with 500 mm/year of rainfall, and the 2000 was drier (300 mm/year). Rangeland anomalous condition and unexpected response to rain could be the consequence of human activities, such as overgrazing (Schlecht *et al*., 2006). In order to define causes of this loss in natural vegetation cover ground observations are needed. However, identification of vegetation cover loss could confirms that forcing variables at local scale may cause land degradation even if phenomena on large scale (i.e. rainfall trend) have allowed a general recovery of the Sahelian ecosystem after the great drought of the last century (Dawelbait and Morari, 2012).

A possible explanation for the increase of Cultivated land might be found in the ACF (*Action Contre la Faim*) reports (Ham, 2011). From February to June cattle herds (mainly zebu Azawak) remain in the valley around Filinguè producing a high concentration of well manured fields. The use of manure is one of the principal ways to grow crop yield in the Sahel (Reenberg *et al.*, 1998;

Rufino *et al.*, 2006; Schlecht *et al.*, 2006; Brouwer, 2008; Hiernaux *et al.*, 2009; Mertz *et al.*, 2011) and could be one of the reasons for the identified crop increase/intensification.

However, the changes of cultivated areas in the Sahel are linked to a complex series of driving factors. As explained by Rasmussen and Reenberg (2012), the Sahelian field expansion is due to "individual decision making agents" and "large scale driving forces". Thanks to a series of interviews and questionnaires, authors report that field expansion during the last decade in Burkina Faso was undertaken for individual reasons of prestige rather than influenced by population growth, climatic variations and globalization.

In our case, the most important of the "large scale driving forces" (i.e. rainfall pattern) contributes to the expansion of cultivated area because the 2007 was wetter compared to 2000. The agriculture LCCs visualized in Figure 8 is probably due to a local decision linked to agro-climatic conditions and socio-cultural rationality.

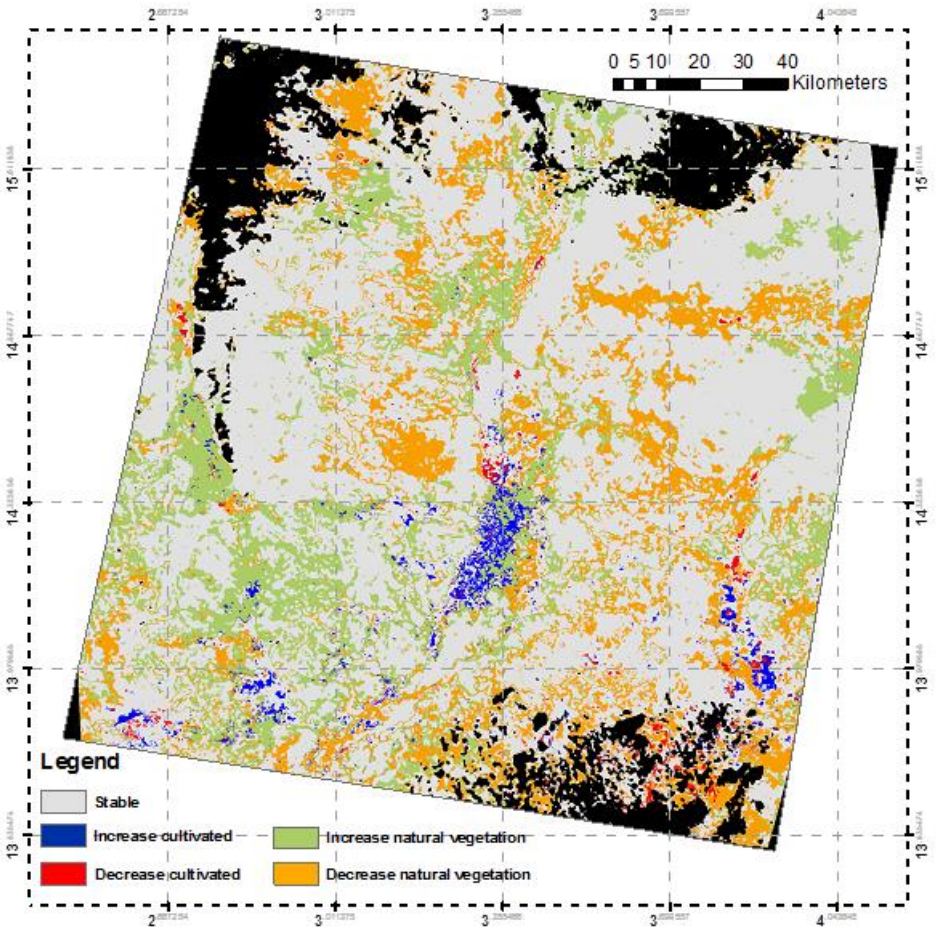

Figure 8- Map of land-cover change. Black zones represent no-data areas.

The 2000-2007 LCC map has been used to help in the interpretation of the anomalous vegetation cover behaviors detected with low resolution SPOT-VGT NDVI and FEWSNET-RFE from 1999 to 2008 (Nutini *et al.*, 2010). The distribution of the classes mapped in figure 8 were analyzed inside the areas of Anomalous Degradation/Greening shown in figure 1*b* that covers 8% of the entire study area.

The radar chart in Figure 9 shows the relative presence into the anomalous areas of the LCC classes: 4 classes of LCC (Increase cultivated, Increase natural vegetation, Decrease cultivated and Decrease natural vegetation) previously showed in blue, green, red and orange respectively and 3 classes of no change (Bare soil, Cultivated area and Natural vegetation) previously combined in grey. The classes linked with agriculture activities (Increase cultivation, Cultivation stable, Cultivation decrease) are on the right side of the radar chart while classes of natural landscape (Bare area, Natural vegetation decrease, Natural vegetation increase, Natural vegetation stable) are on the left. The "Anomalous Degradation" (red line) is mainly characterized by classes of natural vegetation, with an high presence of Bare soil (> 90%) and decrease of natural vegetation, both herbaceous and shrubs (85%), that accounts for about 154 km^2. On the other hand, the "Anomalous Greening" (green line) is characterized by an increase of Cultivated land (100%) and stable Cultivated land (> 95%).

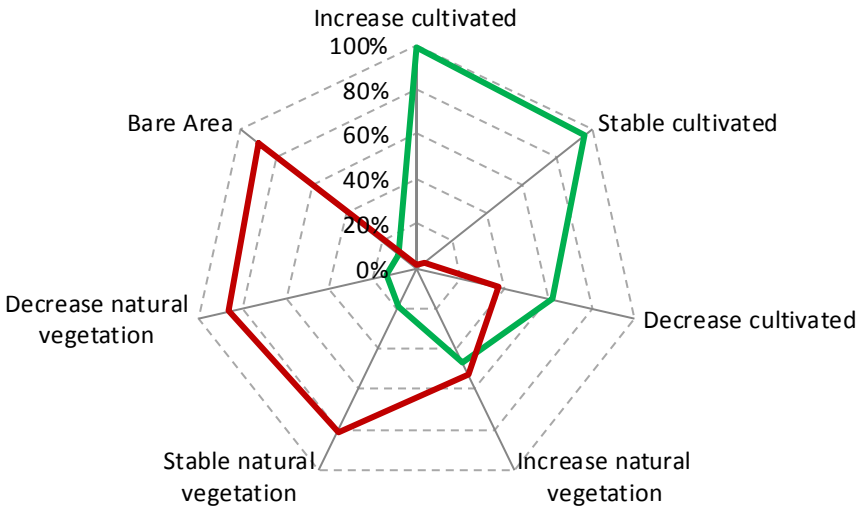

Figure 9- Distribution in percentage of classes of land cover change in the Anomalous Degradation (red border) and Anomalous Greening (green border) spot of figure 1.

The increase in cropping area correspond to about 32 km^2.The information on LCC at local scale produced by Landsat images analysis clearly highlight the two anomalous phenomena derived by

low resolution data analysis: Anomalous Degradation is mainly related to rangeland vegetation cover and relative changes while Anomalous Greening is related to crop cultivation area, concentrated in more populated zone. The Anomalous Greening could be explained by the conversion of fallow and rangeland into cropped areas as well as a general cropping improvement, a result in agreement for the Sahelian area with those of Beguè *et al.* (2011).

2.7 Conclusion

This work focused on the study of changes that occur in Sahelian environment using Landsat images, with the purpose of identifying a methodology to build a land cover map in marginal semi-arid regions characterized by high climatic seasonality. We focused on a test region in Niger, where anomalous vegetation dynamics were previously detected by low resolution satellite time series analysis.

The tests highlight that a two-step classification of Landsat data offers the most feasible way to detect important Sahelian LC classes such as rain-fed crops and natural vegetation. Best performance are obtained if satellite data cover start, peak and end of wet season. Analysis of multi-temporal NDVI data provides a good way to separate classes and spectral information can be further used to improve the thematic accuracy particularly for those land cover classes more prone to confusion.

The application of the methodology to two set of images for the year 2000 and 2007 allowed to produce a LCC map able to describe the main changes in vegetation cover occurred in the period. The map shows a stable semi-arid region, where some spots of change exist. In particular the Dallol Bosso fossil valley in the Tillabery province presents an increase in Cultivated land, suggesting the relevance of human intervention in some localized Sahelian areas, as hypothesized by Hermann *et al.* (2005). Despite the 2007 was wetter then 2000, a decrease in natural herbaceous vegetation was observed outside of the fossil valley where the rangeland is the predominant landscape. Overgrazing for thee area can be assumed. Nevertheless, ground information are needed in order to verify if local anthropic driving forces of these changes occurred.

The maps produced have been used also to interpret spots of local environmental anomalies detected with time series of low resolution data where significant vegetation variations (increase/decrease) are not fully explained by seasonal changes of rainfall. The combined analysis of the Landsat LCC and Spot-VGT anomalous map reveals that areas of Anomalous

Degradation occur in the arid natural environment (mainly bare or sparsely vegetated) characterized by an important reduction in vegetation cover (from herbaceous vegetation to bare soil). On the other hand, Anomalous Greening occurs mainly in the valleys where agro-practices, rainfed cropping, are stable ore improved in the period 2000-2007.

In conclusion, the mapping accuracy of the combined temporal and spectral classification approach, that we adopted, is rewarding and in line with other publications, and the methodology could be applied to other Sahelian semi-arid areas, where detailed information on land cover/use are lacking. These detailed cartographic products, together with ground information and interviews, are fundamental to interpret processes of changes that occurs in the area and that were detected al low resolution analyzing long time series of satellite data. Future expansion of this work will consist in the update of LCC map and new production for other areas exploiting for the past, Landsat archive data, and for the present new data acquired thanks to foreseen Landsat continuity mission and Sentinel-2 programs. These Earth Observation programs will guarantee operational acquisition of satellite images with an high revisiting cycle providing to the scientific community a new opportunity for multi-temporal analysis indispensable for a proper land-cover mapping of dynamic vegetated environment such as the Sahelian.

SESSION 2: Estimating rangeland biomass to support natural resource monitoring

CHAPTER 3: Analysis of EF contribution as an indicator of moisture condition and water stress status in rangeland ecosystems

3.1 Abstract

Rangeland monitoring services require the capability to investigate vegetation condition and to assess biomass production, especially in area where local livelihood depends on rangeland status. Remote sensing solutions are strongly recommended where systematic acquisition of field data is not feasible and does not guarantee to properly describe wide areas spatio-temporal dynamics. Recent research works on semi-arid rangelands have focused their attention on the estimation of Evaporative Fraction (EF), a key factor in the energy balance (EB) algorithm to estimate actual evapotranspiration. Water availability is in fact the major limiting factor of vegetation growing in semi-arid areas. EF is strongly linked to the vegetation water status and some works, conducted on eddy covariance stations, concluded to use this parameter to increase the performances of biomass estimation via remote sensing. In this chapter a method for estimating EF from low resolution satellite MODIS product of albedo (MOD43B3) and land surface temperature (MOD11A2), is tested and evaluated. Results show that the EF estimation from low resolution remote sensing data is feasible and EF satellite derived resulted highly correlated to flux tower ET measurements. Finally that the spatial and intra-annual dynamic of EF maps resulted in agreement with rainfall patterns and expected behaviors of different eco-regions.

3.2 Introduction

Despite the several adaptations of Sahelian population to erratic climate condition, food security still remains a concern, and an accurate estimations of regional yields play an important role in food security (Wang et al., 2013). The capability to estimate the biomass on ground just after the end of the rain gives a balance of the area for the current year (Ham and Fillol, 2010). Compared to its extension and spatial variability the Sahelian area has a lack of local and field information. The lack of ground data was usually overcome by exploiting remote sensing techniques, which allow to analyze climatic phenomena and vegetation condition in their spatial and temporal dimensions (Tucker et al., 1983; Prince, 1991).

Moreover the recently capability to estimate rainfall events had stimulated the study of biomass production from satellite in relation to main driver of this systems (Herrmann et al., 2005; Olsson et al., 2005; Heumann et al., 2007; Fensholt and Rasmussen, 2011; Boschetti et al., 2013) because in semi-arid area the vegetation production is closely linked with the seasonal cycle of

rain (Huber et al., 2011). The better understanding of rangeland production in relation to water availability is of interest for the implementation of operational monitoring systems to support policies and decisions aiming at reducing the socio-economic impacts of environmental stresses.

A possible method to study water condition of vegetated surfaces is the estimation /measurements of evapotranspiration, that is the loss of water from the ground and vegetative surfaces due to vaporization of liquid water. Evapotranspiration is both a heat balance component and a key component of the water budget and it's estimation is important for food security programs (Verstraeten et al., 2005) and improving water management (Bastiaanssen, Pelgrum, et al., 1998).

ET it is one of the most important regulating factors of climate, both at local and global scales, linking energy, climate and hydrology (Ruhoff et al., 2012) and one of the main phases of the water cycle. One of its distinguishing factors is its role as a cornerstone between the energy and water cycles. Over highly vegetated area up to 80% of annual rainfall could be evapotranspirated (Orange, D., Wesselink, A.J., Make, G. and Feizure, 1997), hence ET knowledge is of great importance for water resources management in particular in areas marked by frequent water shortage.

In drylands area modelling and measuring of ET is of great relevance for supporting food-security programs (Bastiaanssen et al., 1999; Verstraeten et al., 2005) determining water needs and necessary management strategies to improve efficiency in water uses (Ciraolo et al., 2007). For field scale studies the measurement of evaporation of vegetation can be performed with field water balance, lysimeter, scintillometer while for landscape studies eddy correlation techniques is the most appropriate method (Verstraeten et al., 2005).

However it is not easy to quantify this flux. ET is highly dynamic in space and time because of complex interactions between soil, vegetation and climate (Allen et al., 2007) and furthermore quantification of this flux on a watershed or a regional scale is much more difficult than at a specific site (Irmak et al., 2011).

The traditional methods to estimate ET such as the reference crop evapotranspiration assume homogeneous land coverage and structure but these conditions are difficult to be founded for large regions (Li et al., 2012). For regional and continental scales monitoring models coupled with remote sensing data is highly recommended, because they can cope with spatial and temporal dimension of evaporation processes (Verstraeten et al., 2005). Several data of surface characteristics such as albedo, vegetation coverage, land surface temperature, and leaf area

index, can be retrieved from satellite providing data for ET estimation from space (Li et al., 2012).

One of the wider applied method for ET estimation with satellite data is the energy balance. The land surface energy balance (EB) is the thermo-dynamic equilibrium between turbulent transport processes in the atmosphere and laminar processes in the sub-surface (Bastiaanssen, Menenti, et al., 1998). The basic formulation can be written as:

$$\boldsymbol{R_n = \lambda E + G_0 + H} \qquad \textbf{Eq. 1}$$

where Rn is net radiation, G_0 is soil heat flux, H is sensible heat flux and λE is latent heat flux.

Among these energy fluxes the sensible heat flux (H) is the more complex to be estimated from satellite because requires several local meteorological data such as wind speed, air temperature and surface temperature (Ciraolo et al., 2007). Several approaches aimed at daily ET estimation exploit the evaporative fraction (Sobrino et al., 2007; Hoedjes et al., 2008; Galleguillos et al., 2011), a the ratio between the latent heat flux and the available energy at the land surface:

$$\boldsymbol{\Lambda = \frac{\lambda E}{\lambda E + H} = \frac{\lambda E}{R_n - G_0}} \qquad \textbf{Eq. 2}$$

The Λ, a dimensionless number (it varies between 0 and 1), compares the latent heat flux (λE) to the total heat leaving the earth surface ($\lambda E + H$). This variable can ben satellite estimated as a combination between albedo and land surface temperature (Roerink et al., 2000). For detailed discussion on ET estimation please see §Annex 4.

The EF, estimated to calculate the daily ET, has a strong link with soil moisture availability because soil moisture is the limiting factor of latent heat flux (Gentine et al., 2007) and it is essentially controlled by water availability in the root zone (Bastiaanssen et al., 1997). Studies conducted in field demonstrated that there is a strong instantaneous correlation between air temperature, canopy temperature and EF (Gentine et al., 2007).

The EF variation is correlated to the amount of vegetation cover (Kustas and Schimugge, 1993), different lend cover (Teixeira et al., 2008), timing of rainfall events (Kurc and Small, 2004), succession of wet and dry period (Guyot et al., 2012), vapor pressure deficit and vegetation photosynthesis activity (Higuchi et al., 2000). Since EF describes the partitioning of net radiation into latent heat flux, this partitioning varies extremely with land wetness conditions (Bastiaanssen and Ali, 2003).

EF has been used in order to represent moisture availability for plants (Yuan et al., 2007; Sjöström et al., 2011), and the variable has an annual behaviour related to rainfall events, with

peaks during rainy season and a decreasing when soil is drying (Yuan et al., 2007). In fact a work conducted over paddy rice area shows that EF has always values closed to 1, because soil moisture was almost saturated (Higuchi et al., 2000).

Moreover the EF, derived instantaneously at time of remote sensing acquisition, is considered a constant daytime variable (Crago, 1996; Gomez et al., 2005; Verstraeten et al., 2005; Ciraolo et al., 2007; Gentine et al., 2007; Sobrino et al., 2007; Hoedjes et al., 2008; Venturini et al., 2008; Li et al., 2012; Yang et al., 2013).

In this framework, some recent works studied the Evaporative Fraction as a scalar factor of water stress in biomass modelling. Works conducted in correspondence of eddy covariance stations proposed the use of EF as an index of water stress to correct estimation of crop production. These works were carried out in North America (Yuan et al., 2007), in the northern Australia savannah (Kanniah et al., 2009) and also recently tested in the Sahelian region (Sjöström et al., 2011). The results show that the EF is able to increase the capacity of LUE model to estimate vegetation production.

Hence the main aim is to assess RS estimation of EF as a reliable proxy of water status for monitoring rangeland and specific objective are i) to set an automatic methodology to produce maps of Evaporative Fraction from MODIS data ii) to validate the estimation by eddy covariance data in Niger and ii) to evaluate if the spatial and intra-annual dynamic of EF maps are in agreement with rainfall patterns and the expected behaviours of different eco-regions. An estimation of EF, providing data on water stress in space and time, could be used to increase a remote sensed model of biomass estimation as suggested by Yuan et al., 2007, Kanniah et al., 2009 and Sjöström et al., 2011.

3.3 Materials and study area

The test area for EF estimation and evaluation is centered on Niger in West (Africa Figure 1). In this area are available different field data, useful for EF validation and for the next research steps.

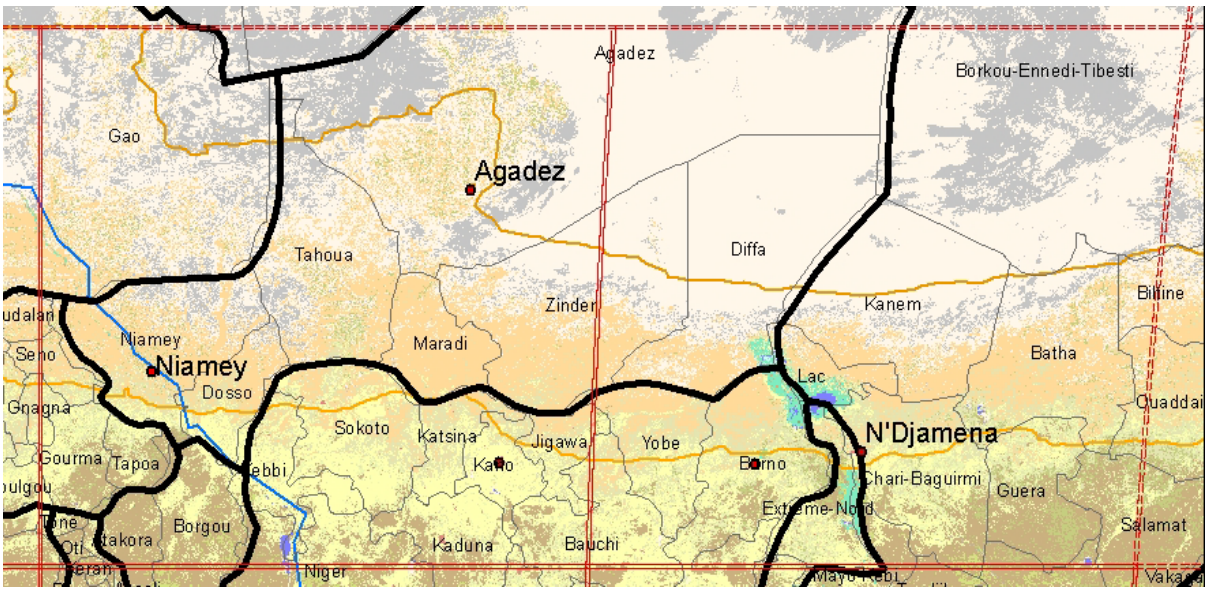

Figure 1-study area over sub-saharian savannah of Niger. Red boxes represent the area covers by 2 tiles of MODIS products (tile h18v07 on left, h19v07 on right). The orange lines indicates the boundaries of the isohyet 200–600 mm/year.

In particular, an eddy covariance tower is situated in SW Niger (§Materials of this chapter) and along the Nigerien Sahelian belt field biomass data are available, that will be exploited in the next section to test EF contribution in biomass estimation.

The Table 4 summarize the exploited data for EF calculation and validation. MODIS products, necessary for EF calculation, were downloaded for 2 tiles (h18v07, h19v07) in order to cover the entire Niger. All the local ancillary data, used for evaluation/validation purposes, are contained in that area (Land Cover, Eddy Covariance). The other ancillary information cover all the West Africa and were not a constrain in term of study area selection (RFE, VGT-NDVI, Ecoregions).

The first MODIS images were downloaded for year 2000, that is the start of MODIS program, and the last for 2009 covering the period where field data are also available (see next chapter). In this time frame all the reference data are comprised.

The ancillary data consist in satellite map of rainfall (RFE) of vegetation growth dynamics (VGT-NDVI) and maps of ecological units (eco-regions) and land cover classes (Land Cover). Finally the eddy covariance data supply data for quantitative evaluation of EF.

Table 1- summary of satellite products downloaded for EF estimation and data (field and satellite) for EF evaluation

Code	Type	Extent	Cardinality	time frame	Parameter	Use in relation to EF
MCD43B3	RS	h18v07	450 maps	2000-2009	Albedo	EF Estimation
	RS	h19v07	448 maps	2000-2009		
MOD11A2	RS	h18v07	450 maps	2000-2009	LST	
	RS	h19v07	448 maps	2000-2009		
VGT-NDVI	RS	Entire Africa	360 maps	2000-2009	Vegetation index	Vegetation dynamics analysis
RFE	RS	Entire Africa	360 maps	2000-2009	Rainfall estimate	Water availability dynamics
Ecoregions	TM	Entire Africa	1 map	2001	Natural communities	Ecological units analysis
Land cover	TM	Tillabery province (Niger)	1 map	2007	Land cover/use	Vegetation classes analysis
Eddy covariance	AD	Wankama (Tillabery province), Niger	1 site	2005-2006	Energy fluxes	Quantitative evaluation of EF

RS= Sattellite Remote Sensing data; TM= thematic map; AD= ancillary data

Earth observation data

MODIS surface parameters

The estimation of EF was performing using data from the MODerate resolution Imaging Spectroradiometer (MODIS), that is an optical sensor on-board the Terra and Aqua satellite vectors launched by NASA in December 1999. MODIS sensor explore land surface, biosphere, atmosphere and oceans and works on a circular, polar and eliosynchrony orbit, at 750 km of altitude. MODIS provides quasi daily global coverage in 36 spectral bands, which makes MODIS particularly suitable for global monitoring of terrestrial ecosystems.

The MODIS products used (MCD43B3, MOD11A2) results from the best pixels in a 8 days period, i.e. those pixels which show the most coherent data and clouds free condition. The 8-days composites results in 46 data for a complete year. These satellite products are free of charge and available on web (www.glovis.usgs.gov).

MODIS products are distributed in the HDF format (Hierarchical Data Format), composed by different layers giving different information and data as exposed by specific product user's guide (https://lpdaac.usgs.gov/products).

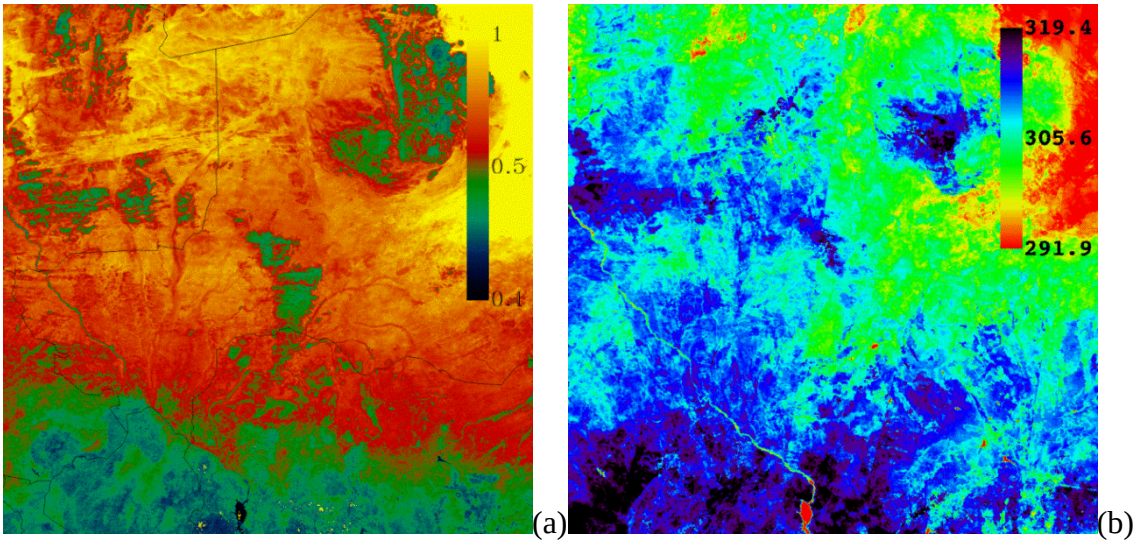

(a) (b)

Figure 2: Example of MODIS products for the tile h18v07 corresponding to the composite n°1 (01-01-2001) in dry season: Albedo map [-] (MCD43B3) for dry season period. Warm colors represent higher albedo values (a).Land Surface Temperature map [k] (MOD11A2). Warm color represents higher temperature values (b).

The MODIS Albedo product (MCD43B3) provides 1 km resolution data describing both directional hemispherical reflectance (black-sky albedo) at local solar noon, and bi-hemispherical reflectance (white-sky albedo). MOD43B3, is an MODIS standard product that began routine production in February 2000, shortly after the launch of Terra. MOD43B3 data consists of albedos of 7 spectral bands (MODIS bands 1–7) and 3 broadband (0.30–0.7, 0.7–3.0

and 0.3–5.0 nm). Black and white-sky albedos mark the extreme cases of completely direct and diffuse illumination. Downloaded albedo data has a temporal resolution of 8 days, since it is produced every 8 days calculating values from 16 days of acquisition MCD43B1 product whence MCD43B3 is derived.

Both Terra and Aqua data are used in the generation of this product, providing the highest probability for quality input data. These data products are archived in tiles of 1200x1200 pixels in sinusoidal (V004) and integrated sinusoidal (V003) projections. Albedo product were downloaded for the 2 MODIS tiles (h18v07 and h19v07) covering the entire study area. Overall 898 HDF albedo products were downloaded (Figure 2).

The MODIS product MOD11A2 of Land Surface Temperature (LST), and Emissivity is composed from the daily LST product (MOD11A1). Data are provided by the sensor on-board to Terra satellite with the spatial resolution of 1 km. This product is a 8-day composite, where data for every pixels is the average values of clear sky LST during the 8 days. 46 MOD11A2 data are available for every year, beginning from the February of 2000. 450 composite were downloaded for the tile h18v97 and 448 for tile h19v07 resulting in 10 years of LST data (2000-2009) as summarized in Table 1.

Estimated rainfall

Direct rainfall data by rain gauges are not sufficient in the Sahel to conduct regional analysis, since their number in Africa is too low and has considerably decreased during last 50 years.

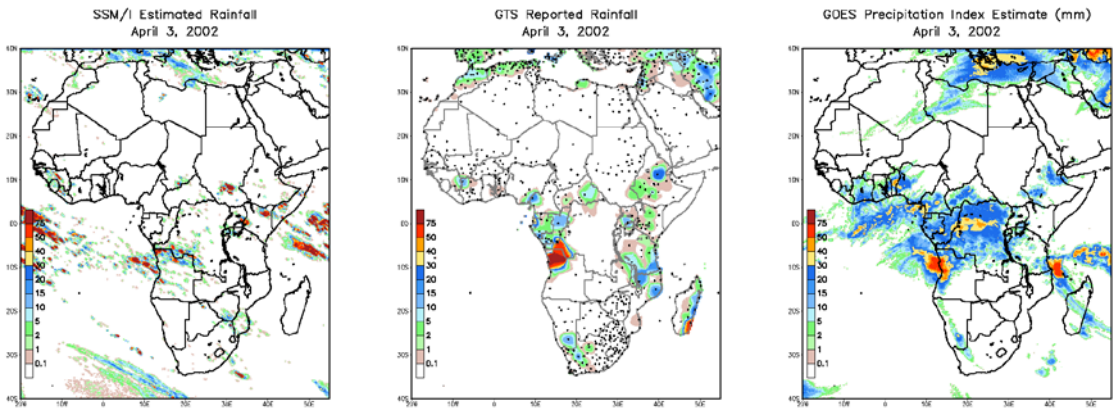

Figure 3: Input data for RFE estimation: microwave (SSM/I), field stations (GTS) and Meteosat data (GOES).

Therefore satellite estimation of rainfall is very suitable for study the behaviour of this critical variable in space and time. Satellite Rainfall Estimation (RFE) are produced by the U.S. Agency for International Development (USAID) Famine Early Warning Systems Network.

It is an information system designed to identify problems in the food supply that can potentially lead to famine or other food-insecure conditions in sub-Saharan Africa, Afghanistan, Central America, and Haiti. RFE is produced by a specific algorithm which uses as inputs three different precipitation measurements, both estimated and measured on field. These inputs are Meteosat satellite network infrared measurements, Global Telecommunications System (GTS) reports from on-field rain gauges and remote microwave observations (SSM/I). Figure 3 shows examples of these 3 types of input data for RFE estimation.

These inputs make it possible to obtain images with 8 km of spatial resolution and 10 days of temporal resolution. 360 RFE images were downloaded via the Geoland-2 project (www.gmes-geoland.info) (Table 1).

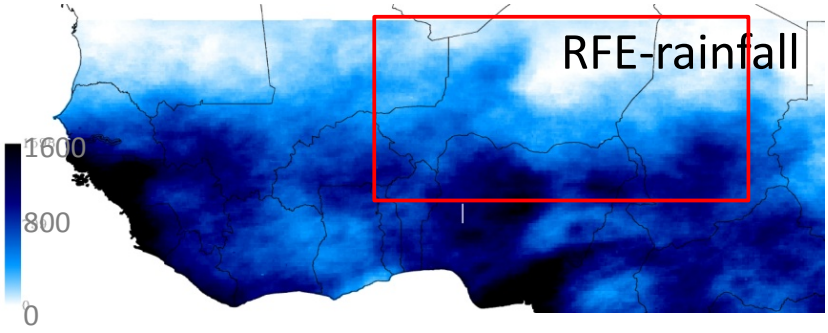

Figure 4- RFE map for the composite date 1/08/2009. Red box indicates study area where EF was estimated.

Vegetation Index

In this study NDVI (Normalized Difference Vegetation Index), data from the SPOT-Vegetation satellite sensor was utilized to study vegetation behaviour. The VEGETATION program is a collaboration between European partners and SPOT program, founded by Belgium, France and Sweden in 1978. It consists of two orbital observation instruments, VEGETATION 1 and VEGETATION 2, as well as ground infrastructures.

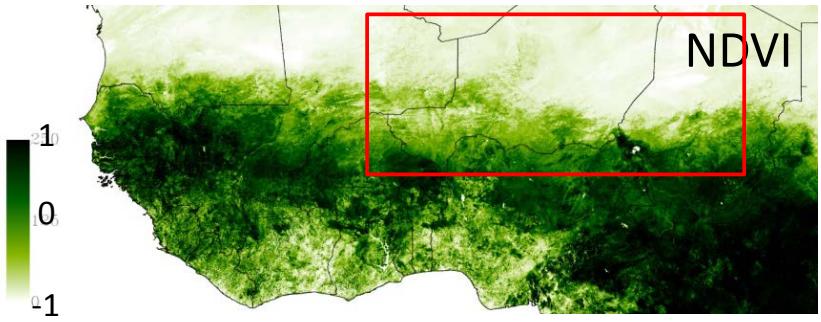

Figure 5- SPOT-NDVI map for the composite date 1/08/2009. Red box indicates study area where EF was estimated.

Data from SPOT-Vegetation sensor (VGT) are usually synthetize in 10-day composites, with a 1 km spatial resolution. Drops in the NDVI value across the ten-day series can be due to a lower signal strength as a result of cloud contamination. This composite is designed to minimize the influence of the clouds that contaminate the signal for each pixel, obtaining an image by selecting the best observation in the temporal window (www.vito-eodata.be, last access December 2013).

NDVI date were exploited to compare the EF temporal behavior with vegetation growth. 360 images were downloaded for the period between 2000 and 2009 (Table 1). These images cover all the West African area (Figure 5).

Ancillary data

Energy fluxes from eddy covariance tower

In order to validate the EF estimations eddy covariance fluxes from a tower included in the study area were downloaded (fluxnet.ornl.gov). Eddy correlation techniques offer the capability of measuring surface energy fluxes, including evapotranspiration and net radiation, at a footprint scale that is usually within a few hundreds of meters to 1 km (Kanniah et al., 2009).

The eddy tower is situated in the Wankama catchment (Fig. 1; 13.65N, 2.63E), 60 km east of Niamey, Niger (Figure 6a). It is a 1.9 km2 endoreic catchment, typical of the cultivated Sahel (Peugeot et al., 2003).

This site present the typical sahelian landscape with sparse savannah and millet fields (Figure 6b) and sahelian climate, with a long dry season and a short rainy period with a mean rainfall of 500 mm/year (Ramier et al., 2009).

Daily data of net radiation [W/m] and latent heat flux [W/m] were obtained for the tower situated over millet fields for the period between June-2005 and June-2007.

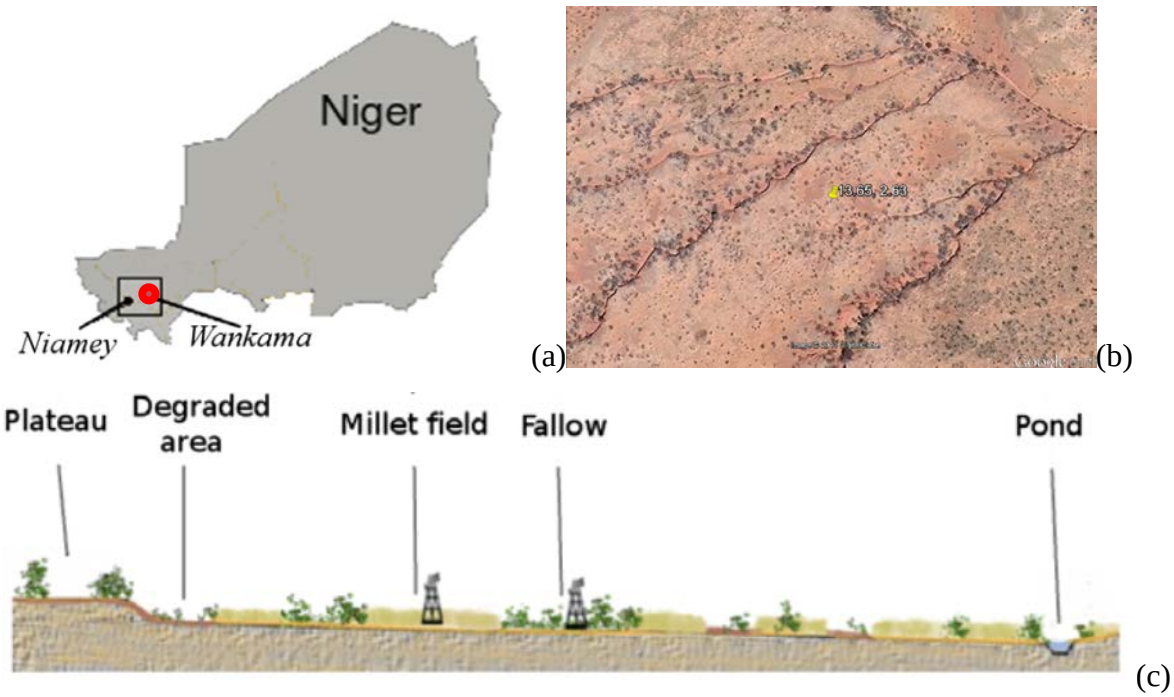

Figure 6- Localization of Wankama eddy covariance tower in Niger (red dot) (a), view from very high resolution image of the site – google earth- (b) and landscape characteristic (c) (Ramier et al., 2009)

Ecosystems units and Land cover maps

In order to interpret the results derived from satellite time series, ancillary data on land cover as well as information on eco-regions were exploited. The cartographic product Ecoregions (Olson et al., 2001), available at http://worldwildlife.org/publications/terrestrial-ecoregions-of-the-world (last access November 2013) was used to identify biogeographic units which contain a distinct assemblage of natural communities sharing a large majority of species, dynamics, and environmental conditions

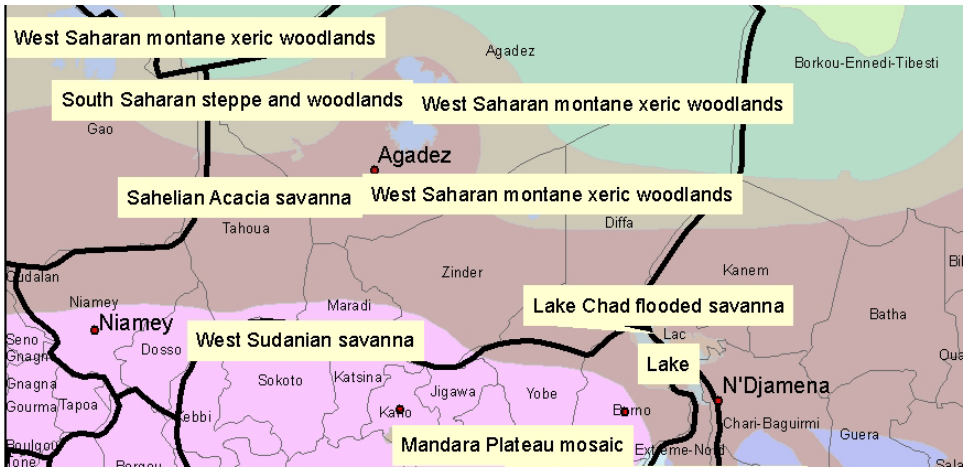

Figure 7- West african Ecoregions (ecozone: Afrotropic) across the study area.

This product, which includes a general description of each ecological region, its outstanding and distinctive biodiversity features as well as the current status and types and severity of threats to the natural habitats, is suitable for ecological analysis of the study area.

Finally a map of land cover and land used at HR (30 m) was exploited in order to study EF behaviour on different vegetation types. The map is included in the study area (Figure 8a) and supply information in 5 classes. The EF analysis over different LC condition was conducted over a random selection area highlighted by grid in Figure 8b. For further detail please see §Chapter2 and Nutini et al. (2013).

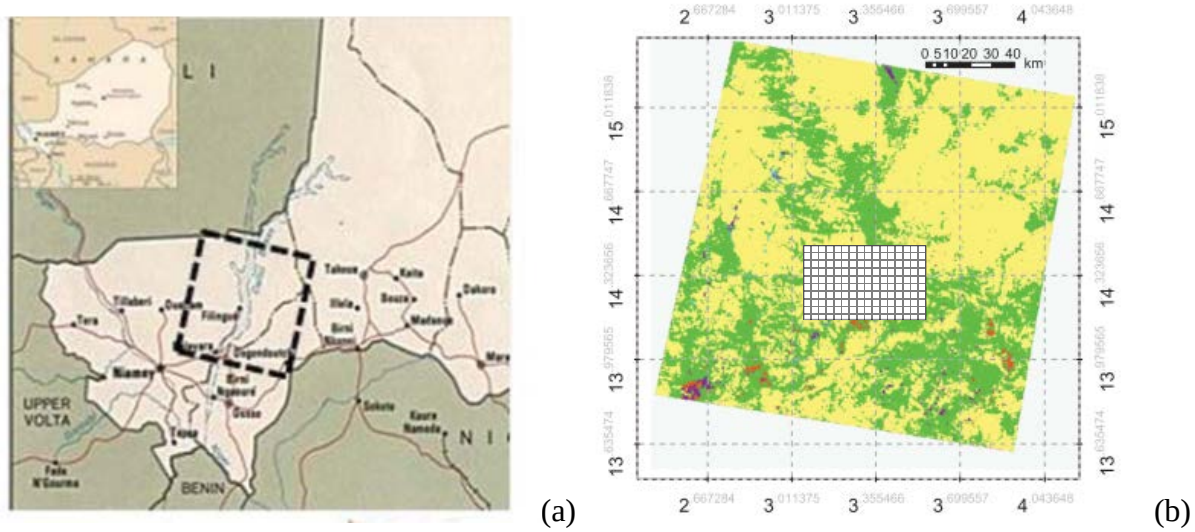

(a) (b)

Figure 8- Localization of HR Land Cover map in south Niger- the black box represents the area covered maps (a). Land cover map referred to year 2007 and subset of EF 1 km pixel analyzed – grey grid 80*130 km- (b). Source: (Nutini et al., 2013)

3.4 Method

Estimation of Evaporative Fraction

The Evaporative Fraction estimation were obtained following albedo - temperature correlogram method described in the literature (Roerink et al., 2000). Figure 9 provides a flow chart of the steps followed for EF estimation for each data of satellite products. Albedo and temperature data were obtained from MODIS products, MCD43B3 (HDF layer 10) and MOD11A2 (HDF layer 1) provide respectively the black –sky albedo (representing the hemispherical reflectance) and the Land Surface Temperature (LST) layer. Albedo and LST data were extracted from the Digital Numbers (DN) as indicated by the MODIS product description (lpdaac.usgs.gov/products) and information on data quality were derived from HDF layer 2 of the MOD11A2. Before starting the EF calculation pixels flagged as no-data or with low quality were masked out and excluded

from the analysis. From available data for a specific date Albedo-LST scatterplot was derived (Figure 10) and analyzed to extract min and max temperature values for albedo classes identified from statistical analysis (Sturges, 1926).

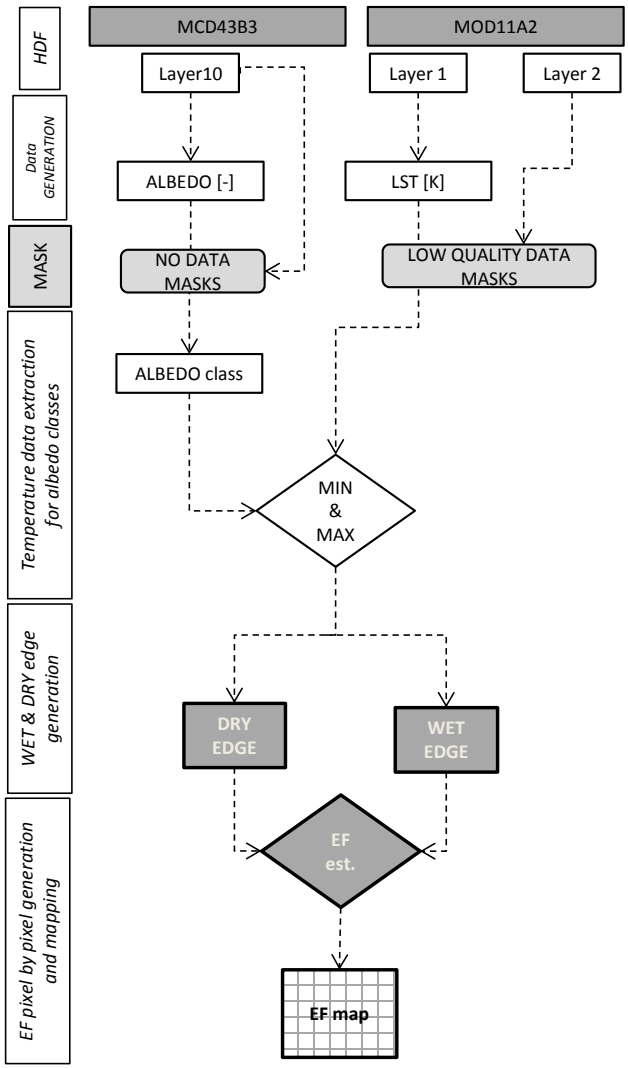

Figure 9- flowchart for Evaporative Fraction estimation from MODIS albedo and land surface temperature products

The series of LST maximum and minimum values for each albedo classes were used to calculate two regression lines, in order to identify dry and wet edge respectively:

$$\boldsymbol{dry\ edge}: \boldsymbol{T_H = m_{dry}\alpha_0 + q_{dry}} \qquad \textbf{Eq. 3}$$

$$\boldsymbol{wet\ edge}: \boldsymbol{T_{\lambda E} = m_{wet}\alpha_0 + q_{wet}} \qquad \textbf{Eq. 4}$$

where m and q represent the parameters (slope and intercept) of the two lines, α represents albedo and T land surface temperature.

Pixel whit albedo values lower than 0.2 were used for the calculation of the wet edge only (Galleguillos et al., 2011), because this threshold discriminate evaporative and radiative regimes

(Roerink et al., 2000). This threshold value is used to identify the maximum LST values to be used in the correlation between albedo and LST (Bastiaanssen, Menenti, et al., 1998). According to Verstraeten, Veroustraete, and Feyen (2005) and Galleguillos et al. (2011) this threshold wasn't take into account for the wet edge in order to reduce the noise influence.

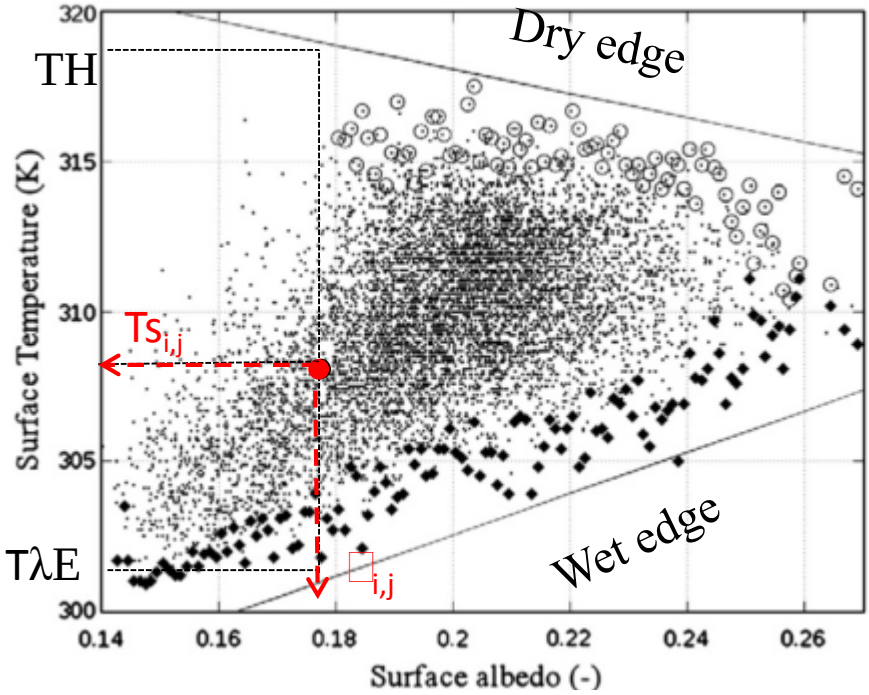

Figure 10- correlogram between albedo and LST. Full diamonds correspond to minimum temperature values of each albedo class to be used for computing the wet edge - lower limit of the graph- through linear regression. Empty circles correspond to the maximum temperature values for each albedo class, to be used for computing the dry edge - upper limit - through linear regression. TH and TλE represent the values used in the calculation of the EF for the pixel with αi,j and Tsi,j indicated by the red dot. Source: Galleguillos et al. (2011)

The EF can be calculated for every pixels, dividing the difference of TH and the temperature pixel by the TH and TλE distance:

$$EF = \frac{T_H - T_s}{T_H - T_{\lambda E}} \qquad \textbf{Eq. 5}$$

Where Ts is the pixel temperature value and TH and TλE are respectively the maximum and minimum temperature value derived by dry and wet edge functions for a given albedo value $\alpha_{i,j}$.

The EF equation can be rewritten as:

$$EF = \frac{(m_{dry}\alpha_{i,j} + q_{dry}) - T_S i,j}{(m_{dry}\alpha_{i,j} + q_{dry}) - (m_{wet}\alpha_{i,j} + q_{wet})} \qquad \textbf{Eq. 6}$$

where $TS_{i,j}$ and $\alpha_{i,j}$ are the temperature and albedo of the considered pixel and TH and TλE depend on the equation parameters (m and q) of the two lines.

The procedure described, automated with an appropriate code in IDL language (version 8.2, www.exelisvis.com), was applied iteratively for each pixel of the image and on each date available for both MODIS tiles h18v07 and h19v07. The resulted maps at the same dates were mosaicked, obtaining EF maps of 122x2400 km covering the entire study area.

Evaluation of the estimated EF

The EF estimates from 2000 to 2009 were first of all evaluated in their spatial and temporal patterns analyzing monthly average EF value for the major eco-regions of the study area. This analysis was conducted to verify that the EF maps shows variability in according to expected ecological behavior.

Since it is well known that EF is related to rainfall events, soil moisture and land cover (Kustas and Schimugge, 1993; Higuchi et al., 2000; Gentine et al., 2007; Teixeira et al., 2008) we used the produced LC map (Nutini et al., 2013) at HR (30 m) to evaluate the EF estimation.

5046 1x1 km EF pixels, covering an area of 80x130 (see Figure 8b), were selected and analyzed over the land cover map extracting the percentage of land cover classes and time series of EF, VGT-NDVI and RFE.

The LC information allows us to study EF behavior in pure LC conditions and different percentage of vegetation cover. Rainfall and NDVI are used because EF timing is in relation to rainfall events and vegetation growth. Finally, EF estimations were validated using the eddy covariance tower data, included in the study area (see Figure 6).

Temporal behavior of EF, for one pixel in correspondence of the tower, was compared with measured variables of evapotranspiration and net radiation (Rn) for the years 2005 and 2006. Due to the different time step of satellite EF estimation and field fluxes measurements, for each 8-days composite the ET data closest in time respect was selected. In case of daily ET missing data the average ET value in the eight days composite window was considered (here after $ET_{8\text{-}days}$).

Estimation of daily ET for an 8-days composite was performed following Sobrino et al. (2007), Galleguillos et al. (2011), Gomez et al. (2005), Sun et al. (2011) and Ciraolo, Minacapilli, and Sciortino (2007):

$$ET^{est}_{8-days} = \frac{\Lambda_{8-days} * \sum_{1}^{8} \frac{Rn_{daily}}{8}}{\lambda} \qquad \textbf{Eq. 7}$$

and Rn is:

$$\boldsymbol{Rn_{daily} = \sum_{1}^{48} Rn} \qquad \textbf{Eq. 8}$$

where Λ is the EF of the 8-days composite, Rn_{daily} is the daily net ration received by the system (counted cumulating half hour radiation measurements) and λ (latent heat flux of vaporization [MJKg-1]) is the conversion factor needed to pass from radian [MJKg^-1] to evapotranspiration [mm] (approximately 2450 Jg^-1 H_2O at 20°C, Verstraeten, Veroustraete, and Feyen, 2005)). Finally, eddy $ET_{8\text{-days}}$ values were compared through correlation analysis with both $EF_{8\text{-days}}$ and ET_{8-days}^{est}.. Date from the tower measurements identified as outliers from statistical analysis and EF satellite estimation flagged as low quality were excluded by the analysis.

3.5 Results

Multi-year EF products behavior on different eco-systems

The EF values vary between 0 and 1 for the 448 images produced, as expected. Figure 11 shows an example of 4 maps for the year 2009 , representing a the condition of in the dry season (Figure 11a) and 3 dates at the beginning, the middle and the end of wet season respectively (Figure 11b, Figure 11c and Figure 11d).

Maps show extended arid conditions in the dry period except for the southern subtropical savannah (Figure 11a) and high variation of EF during the rainy season (Figure 11b-d). The areas beyond the 17 ° N, corresponding to the arid Sahara, show low values of EF also during the rainy season (EF < 0.5). The black areas in Figure 11c, represent areas with no data due to cloud cover at the time of the data acquisition.

The savannah areas around Lake Chad (east of the maps), have high values of EF throughout the year (EF > 0.7), and it is surrounded by areas with a strong seasonality between dry season and wet season. The presence in the study area of wet areas (such as Lake Chad and subtropical savannas) and dry areas (such as the Sahara) guarantee that in any processed date the 2 extreme status of water condition were present. This is one of the conditions necessary for the application of the methodology (Bastiaanssen et al., 1998; Gomez et al., 2005).

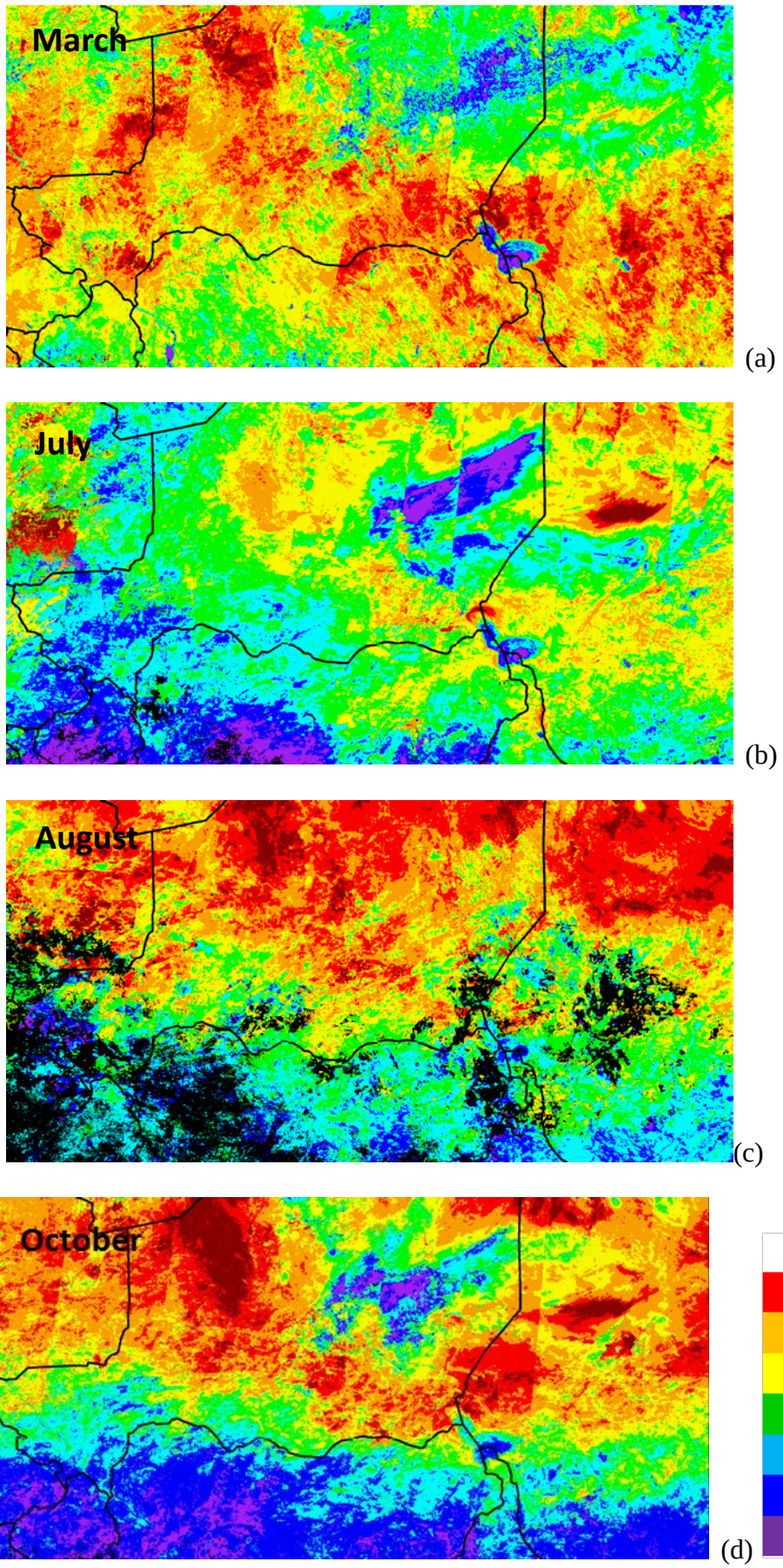

Figure 11- selection of 4 EF maps for the year 2009: dry season March (a), starting of wet season July (b), full rainy season August (c) and end of wet season October (c).

The EF behaviour was analysed deeply thanks to eco-region map. The most common ecoregions are West Soudanian Savannah, Sahelian acacia savannah and South Saharan steppe (see eco-region map in Figure 7). Other ecoregion, such as Lake Chad flooded savannah, West Saharan montane xeric woodlands and Tibesti montane xeric woodlands indicates highlight the presence of geomorphologic features such as lake Chad and Air mountains.

The boxplots in Figure 12 shows the monthly mean EF for the most common ecoregion in study area. EF shows a single season over savannah areas (Figure 12 a and b) and a double season over the tropical forest (Figure 12-c) following rainy season as expected from Guyot et al. (2012). The single savannah's season is linked to the rainy season that starts in May-June. Figure 12-a and Figure 12-b shows Soudanian and Sahelian savannahs.

The maximum EF values in boxplots (>0.8) show that Soudanian savannah, with more than 1000 mm /year of rain, is much more wetter than the Sahelian one, with 200-500 mm/year of rain. The southern forest (Figure 12c) shows a double season with EF peaks values of 0.8, due to two small dry seasons (of 3 and 1 months) in spring and autumn respectively (Stroppiana et al., 2011).

The area around lake chad (Figure 12-d), surrounded by the semi-arid ecoregion of Sahelian acacia savannah, has no seasonal behaviour due to the buffer effect of lake. Indeed the monthly mean EF remain high (>0.6) also during the dry season, when there is no rain and the EF of surrounded area drops to values of 0.3.

EF statistics over these area, for the years 2000-2009, showed the capability of the methodology to catch the temporal behavior of different ecosystems. Among the several West African eco-regions, the area of interest for the study correspond to the Sahelian acacia savannah region, which is the most populated among the arid eco-regions. The following evaluation of the produced EF where conducted in this semi-arid area, thanks to LC map and eddy data.

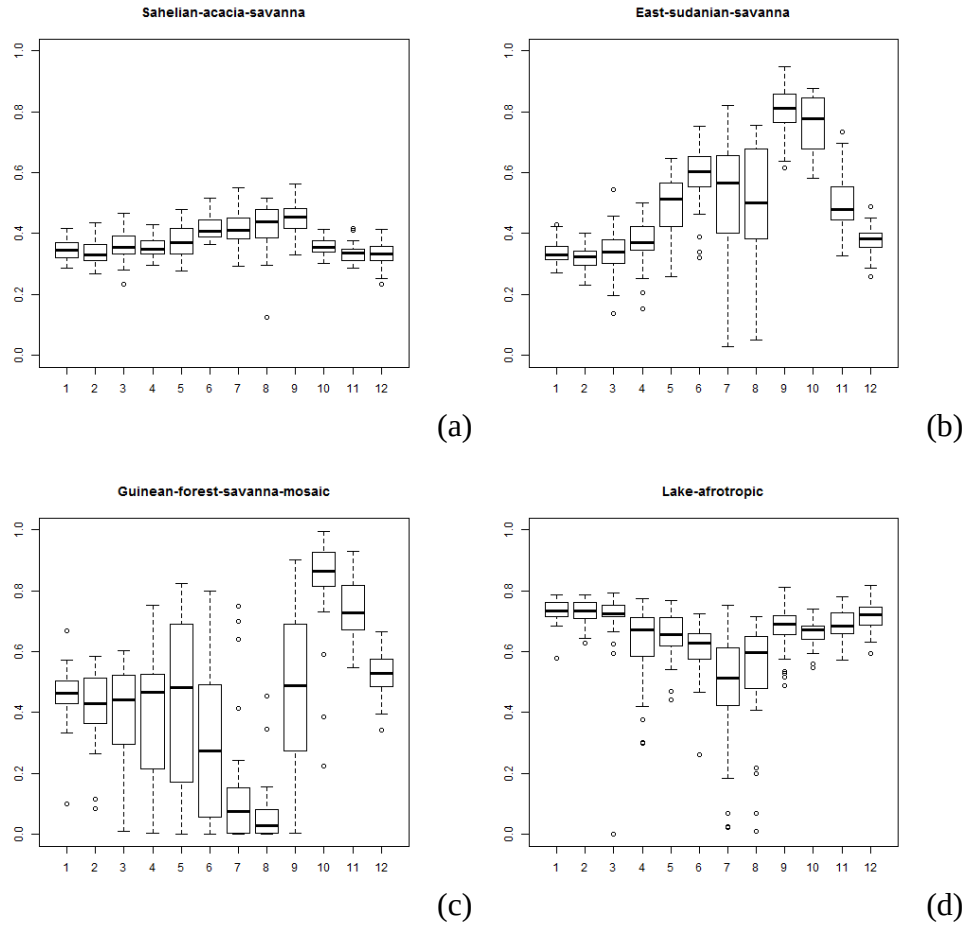

Figure 12- boxplots of monthly mean of EF (2000-2009) for the 4 main west african ecoregion.

EF seasonal dynamics in relation to Land Cover

Homogeneous pixel analysis

The study area of 80*130 km (5046 1 km pixels) analyzed shows a fragmented and heterogeneous land cover when analyzed at HR (30 m pixel). Pixels with homogeneous LC have been identified if more than 70% of the 1 km are is covered by the same class. Among the 5046 analyzed pixels about 1600 cases resulted homogeneous: 984 pixels of “bare area”, 691 “natural herbaceous”, 8 “agriculture” and 4 “shrubs”. These land covers make the typical Sahelian landscape, with predominant open herbaceous rangeland and sandy or rock areas with sparse vegetation. Pixels fully covered by water bodies were not selected because of lacking of large water pools.

Boxplots in Figure 17 shows the mean seasonal statistics of remote sensed Rainfall (first line), NDVI (second line) and EF (third line) variables in the four different pure land cover condition (Column “a” agriculture , Column “b” bare soli, Column “c” natural herbaceous vegetation and Column “d” shrub) for the year 2007. Rainfall is comparable on all the pixels with higher rainfall events of 120 mm (doy 241, 29 Aug). Fist rainfall events are reported at doy 120 (30 Apr).

NDVI behaviour highlights that vegetation growth started at doy 211 (30 Jul) in all homogeneous LC pixel. EF seasonal behaviour show a more scattered data compared to NDVI and RFE. Estimated EF has lower value on all pixels during the dry season (~0.2) and an increase with the start of rainy season in May (doy 131) reaching the peak in August (doy 213).

Figure 18 shows time series of EF, NDVI and rainfall, over 4 single pixel of homogeneous land cover. Each line show time series of EF, NDVI and RFE on the left panel and where the pixel is selected on right panel and black spots indicate low quality MODIS data. Right panel show the 1 km pixel in the multispectral Landsat image in a RGB false colour and in LC map. Figure 18a shows pixel localization and RS variables behavior in a homogenous agriculture, (b) in bare soil, (c) in natural herbaceous vegetation and (d) in shrubs.

The NDVI behaviour is in agreement with LCs, with lower values in homogenous bare soil (NDVI=0.2) and higher value for shrub (NDVI>0.4). Vegetation starts to growth at least 50 days later the first rain. EF reaches peak together with maximum of vegetation growth and rainfall events, about in August (doy 213-243) as stated by Kurc and Small (2004). EF series is less correlated with rainfall in the homogenous bare soil pixel, confirming the difficult in EF estimation over bare soil (Bastiaanssen, Pelgrum, et al., 1998).

Maximum EF during the season reaches values (> 0.7) comparable to published time series of this variable (Kustas and Schimugge, 1993; Kurc and Small, 2004; Teixeira et al., 2008; Guyot et al., 2012). Moreover black spots over on the top of the graph indicate that LST data, obtained from MOD11A2 product, are highly contaminated. This problematic is recurrent on bare area, and can affect the quality of the EF estimation.

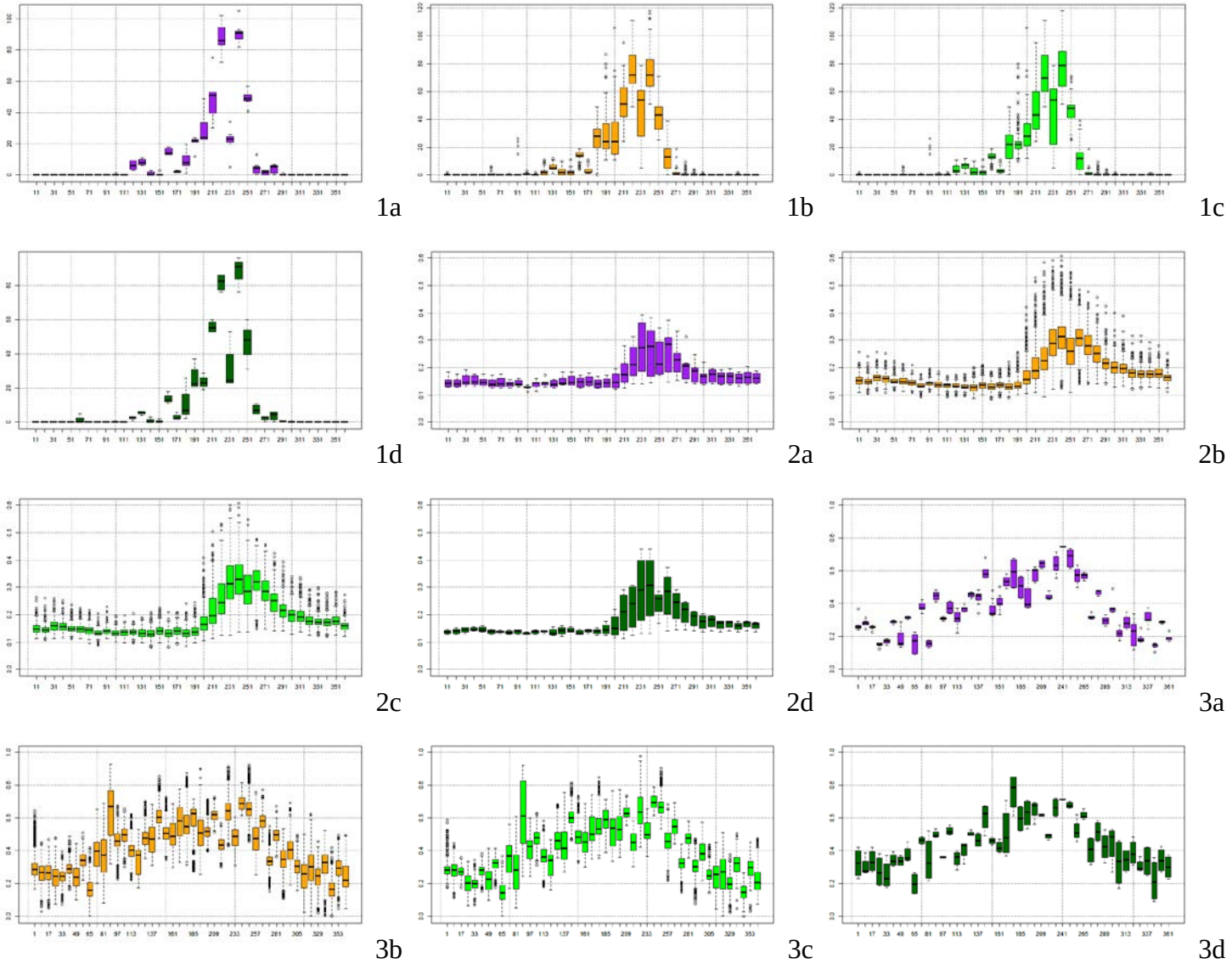

Figure 13- boxplot of monthly RFE, NDVI and EF (in first, second and third lines respectively) in pixel with homogeneous LC of agriculture (a), bare soil (b), natural herbaceous vegetation (c) and shrubs (d)

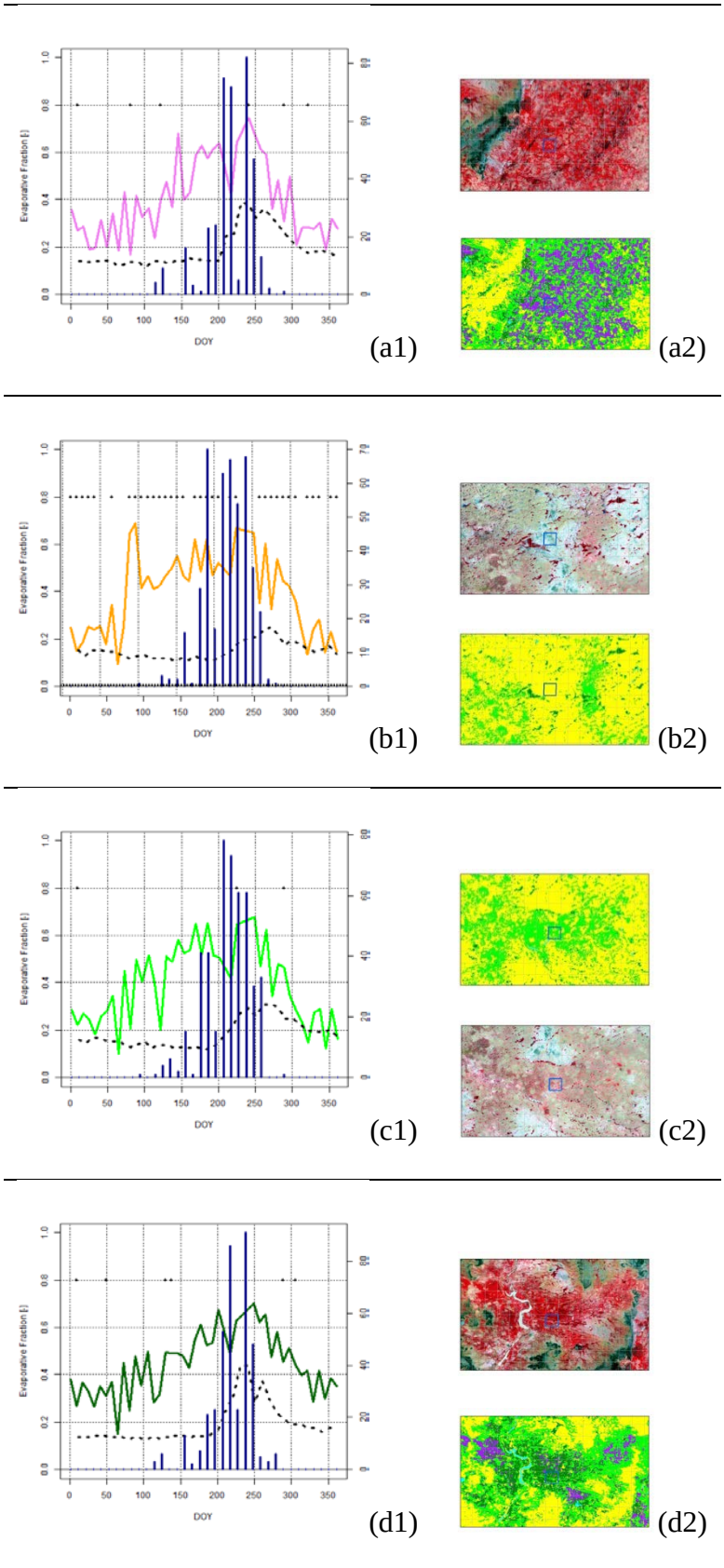

Figure 14- Cultivated areas (a), bare Soil (b), Natural Herbaceous Vegetation (c) and Shrubland (d).time series of remote sensed variables o: EF (coloured continuous line), NDVI (dottel line), rainfall (blue histogram). Right panels show the geolocalization of the pixel over RGB false color and land cover map (right panels).

Mixture land cover condition analysis

Finally an analysis of EF behaviour over the whole selection of 5046 pixel, also in mixture LC condition, has been conducted and synthetize in the ternary plot showed in Figure 15. The ternary plots, one for each months, clarify the behaviour of EF under different combinations of surface conditions.

The points in the plots that are close to one of the 3 vertices represent homogeneous land cover conditions for a specific class: top corner for soil, right corner for shrubland and left corner for herbaceous vegetation (both natural and cultivated).

Data are represented from warm (red to yellow) to cold (blue to light blue) which indicate low [0:0.5] to high [0.5:1] monthly EF values. The points shows the predominance of herbaceous and bare soil condition, as expected. Lower values characterized months from January to April (a-d), and after the end of wet season (October-December, k-m). This is the long dry season, where there is no rain and the Sahelian area becomes arid.

EF values grow up in May (e), reaching the top in August (i). During the middle of the wet (g) season pixel vegetated or partially vegetated have much higher EF values (dark blue) compared to pixels with no vegetation cover on top corner. Therefore estimated EF shows strong differences between dry and wet seasons, highlighting the months between May to September as the most humid (EF>0.7) (Guyot et al., 2012). Despite the work conducted by Teixeira et al. (2008) on eddy covariance data and Kustas and Schimugge (1993) on very HR data, smaller differences can be cached between different vegetation types due to moisture on vegetated area, as alluded by Kurc and Small (2004). Influence of vegetation types in EF estimation with low resolution data should be further investigated.

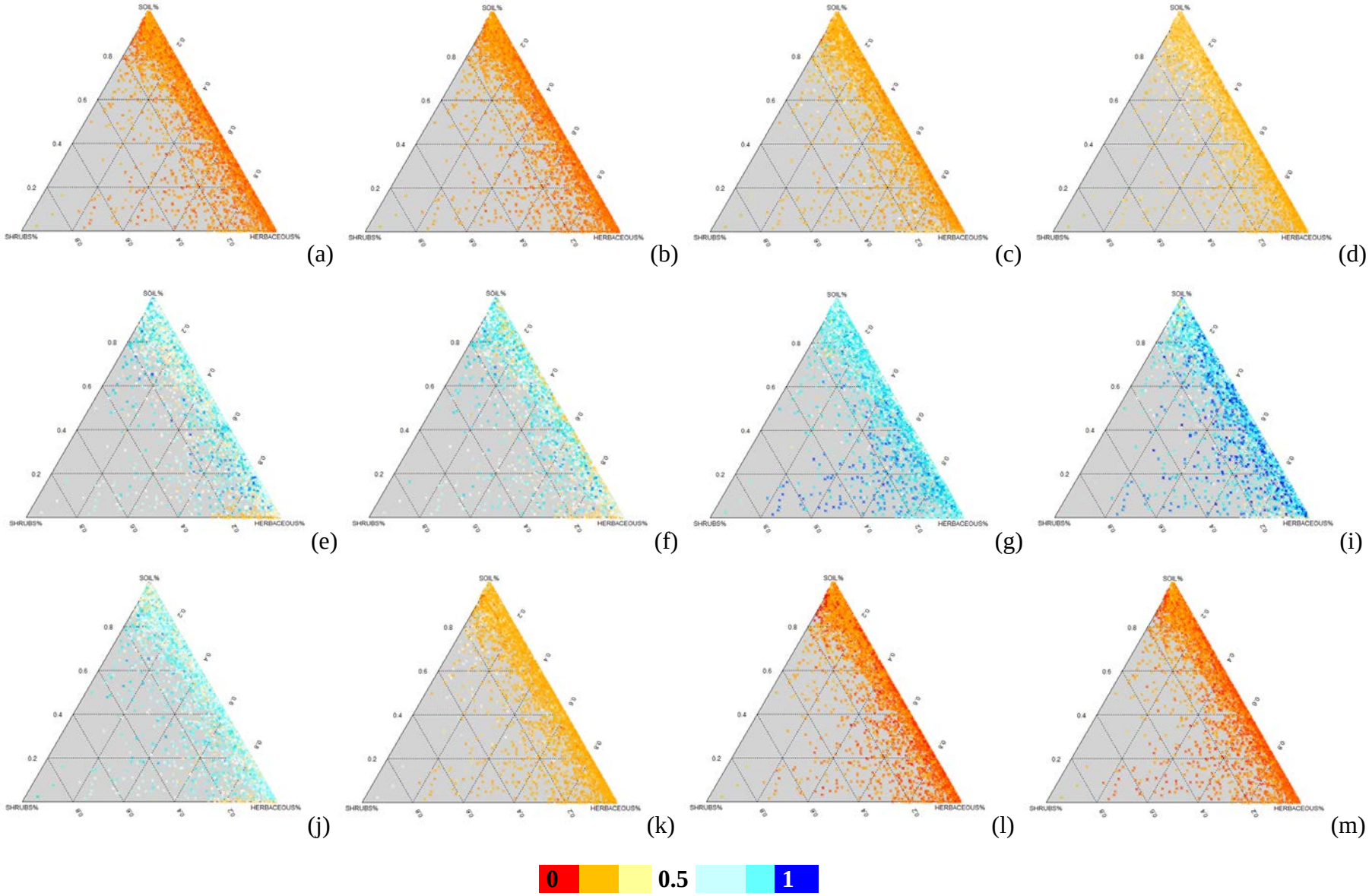

Figure 15 Ternary plot of EF monthly mean (Jan(a)-Dec(m)), where pure MODIS pixels are close to the vertices and pixels with mixture cover are spread in the plot area. Colour table is centered on 0.5 value (white), with warm and cold colors for low and high EF values, respectively.

EF quantitative evaluation with Eddy covariance data

Temporal dynamics of the variables

EF estimation on a single pixel were compared to eddy covariance evapotranspiration, since EF is the most important factor of ET estimation (Verstraeten et al., 2005). The Figure 16 compares the time series of measured ET with measured fluxes at eddy tower (ET and net radiation, black lines) and satellite time series of estimated EF (red line), RFE (blue histogram), NDVI (green line), albedo (cyan line) and LST (gold line). The eddy tower is placed on a semi-arid savannah (see Figure 6), and present the typical Sahelian behaviour of rainfall and vegetation growing. Vertical black lines indicate the Sahelian wet season from July to October. Figure 16 (a) shows the time series of remote sensed and measured variables for the year 2005. First eddy measurements was recorded in June (doy 160), after the beginning of rain. ET shows the peak (>4 mm/day) in August, as well as net radiation (Rn). RFE show an early start of rainy season, before the starting of eddy measurements, with an intense rainfall event of 60 mm in May (doy 155). Rainy season ended at doy 274 (1 October), after the peak of vegetation production (doy 234, 22 August).

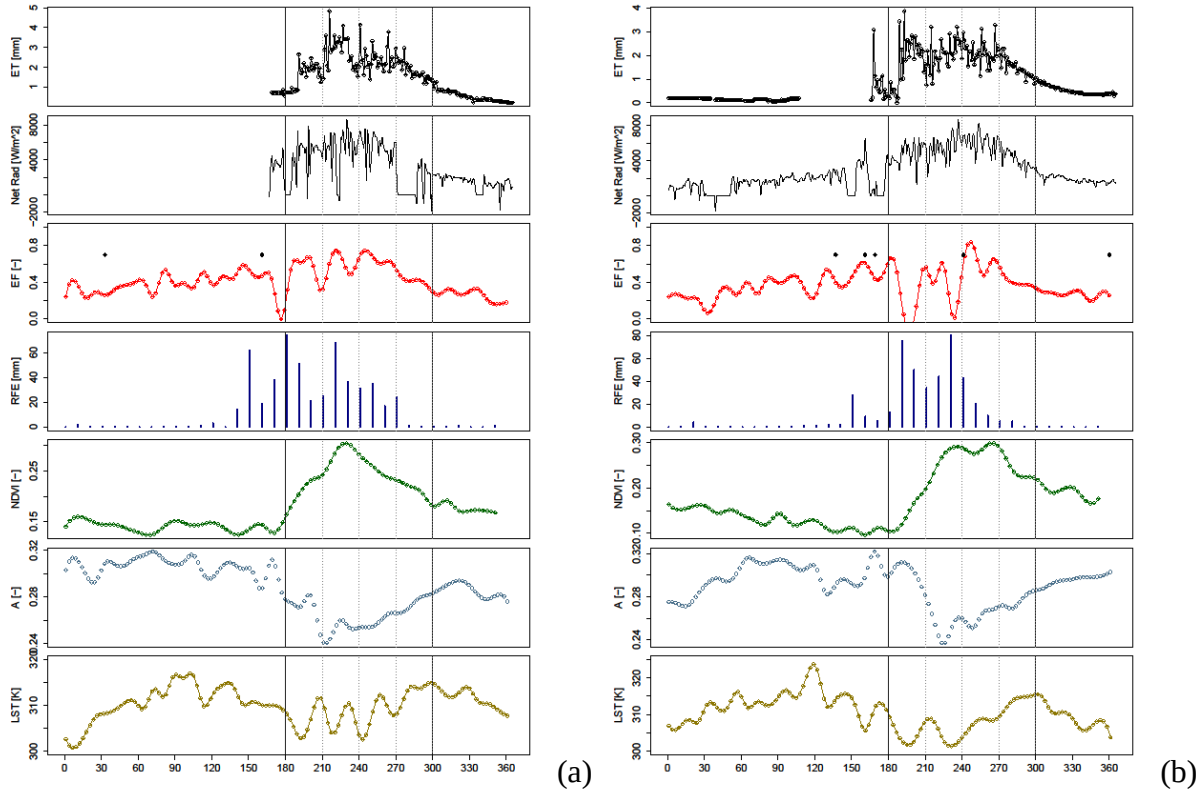

Figure 16- Temporal behaviour of decadal NDVI-VGT; 8days EF estimation from MODIS data and flagged data from MOD11A2 QF (black spots); daily evapotranspiration measured by Eddy Covariance tower at the Wankama site; decadal precipitation, 8days MODIS albedo and 8days MODIS temperature for years 2005 (a) and 2006 (b). Vertical dotted lines represent start and finish of wet season.

EF behaviour shows peak in correspondence of 2 main rainfall event, at doy 181 and 220, and 2 drops in correspondence of low ET value (doy 210 and 230). The drop at doy 180 is in agree with a rainfall event and could be caused by cloud cover condition. Finally after doy 270 both measured ET and estimated EF decrease linearly. The vegetation behaviour, highlighted by vegetation index NDVI, shows the start of season at doy 200 (19 July), 50 days after the start of because of the necessary time for germination.

NDVI has a specular behaviour compared to albedo, indeed some RS approaches estimate EF using VIs instead of albedo (Sandholt et al., 2002; Jiang et al., 2009; Tang et al., 2010). Last 2 graphs in Figure 16 (a) display time series of input data for EF calculation (albedo and LST). Both data show high value during the dry season, indicating a warm surface. Rainy season has medium radiance temperature of 310 K (~31°C) in wet season and 320 K (~47°C) during dry season because incoming energy during wet season is exploited by evaporative and transpirative processes. LST time series decease after the start of rain, and albedo decrease since start of vegetation growing.

Figure 16 (b) shows the same variables for the year 2006. Eddy ET shows a drier year compared to 2005 (max ET<0.4 mm/day), indeed rainy period go on only 2 month from doy 190 (June) to doy 240 (end of August). Estimated EF reaches peak of 0.8 at doy 240 (28 August) and during the season outline a plateau, comparable to ET behaviour. Two main EF drops are visible (doy 200 and 230) in correspondence of 2 main rainfall events. Cloud cover made noise satellite data acquisition and can be the cause of these drops. Both EF and ET rapidly decrease their values at the end of the wet season (doy 270).

Peak of vegetation occurs in late September (doy 270), and NDVI continue to show a presence of vegetation also in November-December (doy 300-360, NDVI ~0.2) even if EF and ET shows that is area is completely dry. The temporal behaviours of measured and satellite data for 2006 are comparable with data showed for the year 2005, with high variability between dry and wet months. EF estimated seems to be in accordance to ET and Rn temporal behavior, drops in estimation can be caused by cloud cover. To avoid this problem automatic procedure can be applied to mask of flag these data following Manfron et al., (2012) or Ruhoff et al., (2012).

Correlation analysis

Figure 17 display the correlation between estimated EF estimated (y-axis) and ET measured by eddy covariance tower (y-axis) for the two analyzed years: 2005 (Figure 17a) and 2006 (Figure 17b).

EF resulted significantly correlated to ET in both year (p<0.005), regressive coefficient are 0.62 and 0.45 for 2005 and 2006 respectively.

For the year 2006 the accordance between measured (ET) and estimated (EF) variables increases reaching a correlation coefficient > 0.55, comparable with 2005, if data from January to May are excluded from the analysis.

During these months (indeed not measured in 2005) correlation is biased by EF variation in the dry season, when no rain and no vegetation are present. Moreover EF estimation over bare soil is reported as problematic, the EF variable is only useful for the monitoring of vegetated land cover (Bastiaanssen, Pelgrum, et al., 1998).

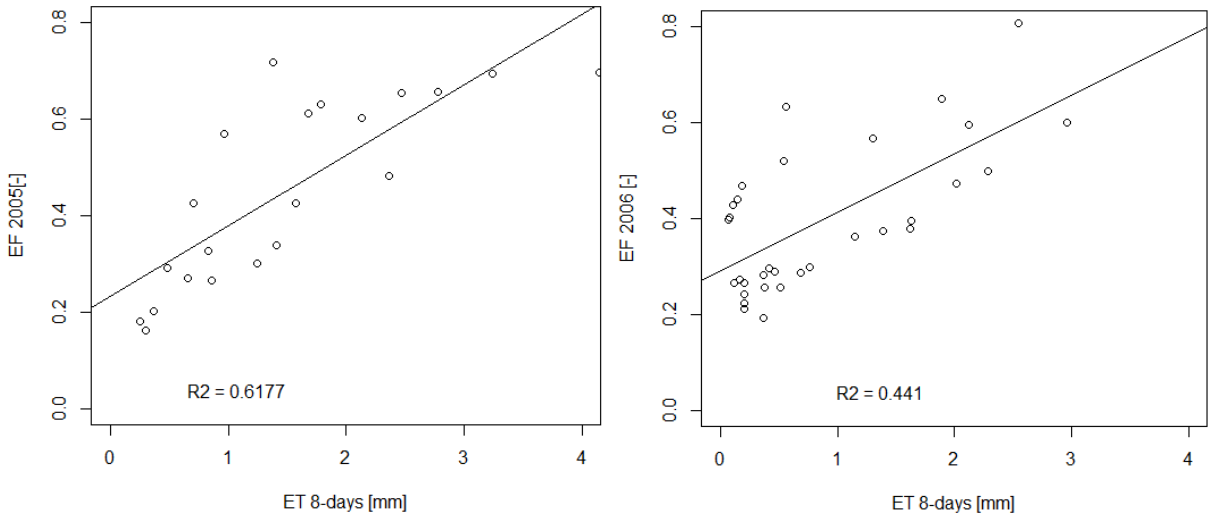

Figure 17- correlation between estimated EF (y-axis) and measured ET (x-axis) for years 2005 (a) (n=24) and 2006 (b) (n=36)

The Rn measured at eddy station allowed to exploit estimated EF to calculate ET, following the Eq.7 (Gomez et al., 2005; Ciraolo et al., 2007; Sobrino et al., 2007; Galleguillos et al., 2011; Sun et al., 2011).

Figure 18 reports the scatter plots of ET measured at the tower ($EF_{8\text{-}days}$) and estimated by satellite (ET_{8-days}^{est}) respectively for 2005 (a) ad 2006 (b).

For both years, the regression between the variables shows significantly high coefficient of determination (r^2 > 0.7).

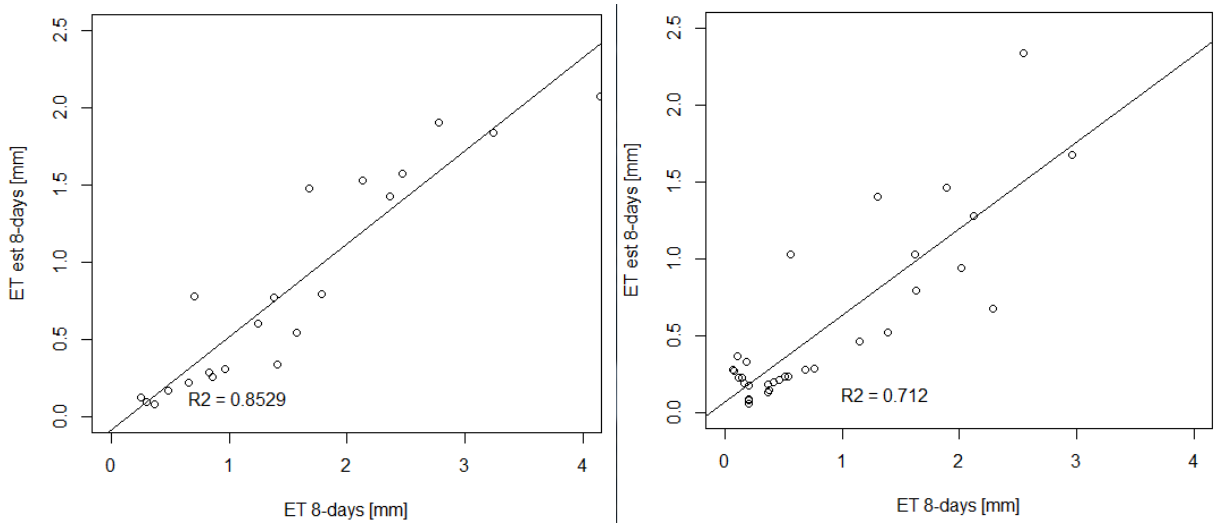

Figure 18- correlation between ET measured by Eddy Covariance tower at the Wankama site (x-axis) and ET calculated with estimated EF and field measured net radiation (ET^{est}_{8-days}) (y-axis) in the same site for 2005 (a) (n=24) and 2006 (b) (n=36).

Despite this good results the satellite ET provides lower estimates respect the tower measurements. The correlations between estimated and measured fluxes is not statistically different between the 2 years ($p>0.005$), hence the satellite estimation of ET is robust between different seasons. It is important to remember that the EF data is derived by 1 km albedo and LST products; this aspect can strongly limited the comparison with field data acquired on small plots in an heterogeneous environment.

3.6 Discussion and Conclusion

The Evaporative Fraction, the ratio between the latent heat flux and the available energy at the land surface, is a variable used in remote sensing studies to estimate daily evapotranspiration (Roerink et al., 2000; Gomez et al., 2005; Verstraeten et al., 2005; Sobrino et al., 2007). This ratio between energy fluxes is linked with moisture availability for plants (Guyot et al., 2012), and for this reason it has been recently exploited also as a proxy of vegetation water condition in biomass estimation models. The physical meaning of this variable and the opportunity to estimate it from satellite data, candidate this parameter as a suitable proxy of water stress to be used in biomass estimation model. An automatic procedure to estimate EF from satellite data was developed on the base of previous scientific work. Up to now, this is the first time that multiyear (2000-2009) maps of EF estimation from satellite data were produced for Nigerien sahelian. A total of 448 8-days EF maps were produced and analyzed.

Multi-year analysis revealed that the estimated data are able to reproduce the expected dynamics of sahelian ecosystems. The maps show seasonal variation in agreement with the typical

Sahelian succession of wet and dry period. The analysis on homogenous land cover pixels showed that EF temporal behaviour depend on rainfall events while EF absolute values are also influenced by vegetation typology and density.

EF estimation results strongly correlated to energy fluxes measurements acquired by an eddy tower in Niger. ET estimation obtained from satellite EF data and in situ net radiation measurements are able to describe the seasonal ET dynamics with correlation up to 0.85. However, satellite ET estimation resulted underestimated. These results indicate that the methodology described in bibliography for the estimation of EF can be followed to assess a water stress proxy. These satellites maps, calculated every 8 days with spatial resolution of 1 km, can be used to test improvement in an savannah biomass estimation. EF can be exploited as an efficiency factor in light use efficiency model that utilize remote sensing data. Up to now this approach have been conducted only on Eddy covariance data (Yuan et al., 2007; Kanniah et al., 2009 and Sjöström et al., 2011). From an operation point of view the EF monitoring, as a proxy of water availability for vegetation, could be integrated with a phonological analysis conducted on vegetation index time series (Boschetti et al., 2009). Automatic detection of the start and end of season can be used to constrain the analysis and interpretation of EF values as indicator of water stress.

CHAPTER 4: Contribution of EF in LUE modelling approach to estimate biomass in semi-arid environment

4.1. Abstract

Herbaceous savannah biomass estimation on Sahelian area is of great importance for rangeland monitoring and food security programs. In this area livelihoods rely on agro-pastoral activities and rainfed agriculture, which are dependent on the seasonal erratic rainfall.

Since the first multispectral satellite image were made available, they were exploited to develop methodology to estimate vegetation biomass on wide area. Feasible remote sensed approaches use the Light Use Efficiency (LUE) concept to estimate aboveground biomass. The LUE algorithms are a potentially effective approach to monitoring regional biomass production using low resolution satellite images providing useful predictions at large scales.

In this chapter the reliability of an operational LUE based product called Dry Matter Productivity (DMP) originally developed by Flemish Institute For Technological Research (VITO) for MARS program (Monitoring Agricultural Resources) was evaluated. DMP is a spatial estimation of dry matter obtained from SPOT-VEGETATION and meteorological data. The evaluation of DMP was carried out thanks to the *Action Contre La Fame* (ACF) field work, who provided the ground biomass measurements for the period 1998-2009. The analysis conducted shows the correlation of DMP with field measurements of herbaceous biomass, and discusses the differences among the different sites where data were collected. In this section was conducted a test of Evaporative Fraction (EF), estimated from MODIS products, as a water stress efficiency term (ε_{water}).

The site-specific performance of basic DMP and DMP integrated with water stress are compared thanks to an assessment with ground biomass data from 46 sites in Niger. Additionally, in order to take into account the differences in ε_{LUE} between varied ecosystems and vegetation types, the satellite estimation performances were studied via different ecological units separated by classification tree techniques.

Results show that incorporation of water availability correcting factor in the DMP model significantly improved the estimation of a Sahelian rangeland productivity. Moreover the regression among sites suggest that efficiency factor of ε_{LUE} should be include in the DMP

algorithm, in order to provide reliable estimation among vegetation types with distinct efficiencies in the conversion of light into biomass.

4.2. Introduction

The Sahelian region is characterized by large savannah area whose productivity depends on spatial and temporal rainfall variability. This system is typically dedicated to pastoralism, that suffered more than other livelihood practices the erratic climate. Most of the population survives thanks to extensive livestock systems characterized by extensive inter-seasonal movements linked to the availabilities of water and pasture (Justice and Hiernaux, 1986; Powell, 1996; Ayantunde, 1999; Hein et al., 2008; Ham and Fillol, 2010; Mortimore, 2010). For this reason pastoral food security is dependent on livestock and thus the livestock feed balance in the region (Ham and Fillol, 2010). Due to the extension of the pastoral areas (Tucker et al., 1985), the very low demographic density (Ham and Fillol, 2010) and the difficulties to collect local data representative of the variability in space and time (van Vliet et al., 2013) satellite tools are profitable to monitor biomass production in the Sahel. Hence the lack of ground data could be overcome by exploiting remote sensing techniques, which allow us to analyze climatic phenomena in their spatial and temporal dimensions, and give us further possibility to monitoring the Sahelian ecosystem (Boschetti et al., 2013). A better understanding of rangeland production is of interest for the implementation of operational policies aiming at reducing the socio-economic impacts of environmental stresses: long-term monitoring programs need to combine remotely sensed data with field data on vegetation structure, composition and productivity (Hein et al., 2011).

One of the most widely applied approaches to assess vegetation biomass at large spatial scale based on the Light Use Efficiency (LUE) concept (Monteith, 1972). According to the Monteith approach, vegetation growth is completely defined by the incoming energy (solar shortwave radiation) and a number of conversion and efficiency factors. Since the first satellite multispectral images were available several LUE approaches have been developed because allow us to monitor in space and time changes in ecosystems Net Primary Production (NPP), carbon uptake and anthropogenic influence in global carbon cycle. These approaches, such as the CASA (Potter et al., 2012), GLO-PEM (Prince and Goward, 1995), SDBM (Knorr, W. Heimann, 1995) and TURC (Ruimy et al., n.d.) were specifically developed for global application. For a faithfully comparison and discussion on these models refer to Cramer and Kicklighter (1999), Kicklighter and Bondeau (1999) and Ruimy, Kergoat, and Bondeau (1999).

On the Sahel several authors tried to produce local and regional empirical estimation of vegetation biomass, focusing on the importance of biomass production in food security (Tucker et al., 1985; Bartholome, 1988), also by applying the Monteith concept (Bartholomé, 1990). These first estimations were and despite the simple algorithms formulations obtained acceptable results (Seaquist, 2003). Also Rasmussen (1998) obtained an high empirical relation (r^2 up to 0.8) between field measurements in Senegal and LUE model based on remote sensing inputs. He also stated that these empirical correlation are of limited use because they changed from each years, highlighting that a LUE model can be improved considering a measure for water stress and a growth efficiency depending on different ecosystem (Rasmussen, 1998b; Seaquist, 2003).

In addition to these LUE models developed for research purpose, also operational Net Primary Production (NPP) estimation, such as MOD17 derived partly from MODIS data (www.ntsg.umt.edu/project/mod17, last access December 2013) and Dry Matter Productivity (DMP) product derived from SPOT-VGT imagery (Smets et al., 2010), have been produced for food monitoring purpose. The evaluation of MODIS product over the Sahelian rangeland shows that a LUE approach well explains observed measured biomass variation (r^2=0.77) but improvements in inputs quality and formulation of LUE efficiency factors are needed (Sjöström et al., 2013).

In fact the use of appropriate LUE efficiency terms is of key importance to improve the goodness of these models (Seaquist, 2003; Yuan et al., 2007; Garbulsky et al., 2010). As indicated by Rasmussen (1998), the two most studied efficiency terms are the biological efficiency in converting light in biomass and the limiting factor of water stress. The estimation of the first efficiency term is still under debate, and the specific literature gives opposite solutions. For example the MODIS product MOD17, consider different efficiency values for different vegetation types and biomes. On the other hand Yuan et al., (2007) developed a LUE model based on satellite derived inputs and an invariant biome-independent maximum ε_{LUE}. He also stated that the water availability is more important than an efficiency factor depending on vegetation types.

The most simple LUE model includes only temperature limitations while most recent models include also water balance. The water limitation can be estimated in different ways: water vapour deficit, evaporative fraction, soil moisture content, water holding capacity, spectral index and evapotranspiration. Input for the same parameter can be acquired via meteorology, eddy covariance or via satellite imagery.

A remote sensing based approach, followed by Fensholt et al. (2006) and Seaquist (2003) estimate the water availability exploiting a multispectral index as a proxy of soil moisture, the B2B7 MODIS bands combination (Key, C.H., Benson, 1999). They used this index as a multiplicative scalar by the difference between the potential and actual values, normalized by the potential value (Seaquist, 2003).

Although quite a number of models use vapor pressure deficit to describe water stress (Goetz, 2000; Zhao, 2005), recent research stressed that evaporative fraction (EF) or actual over potential evapotranspiration rate (ET) are the best Choices (Garbulsky et al., 2010). Indeed this approach has been followed by several recent work conducted in correspondence of eddy covariance tower, strongly proposing the evaporative fraction (EF) as an efficiency term of water stress to correct LUE models.

These work were carried out on eddy stations in North America (Yuan et al., 2007), whole European region (Verstraeten et al., 2006), North Australia Savannah (Kanniah et al., 2009), and were also re-invigorated by a test in the Sahelian region (Sjöström et al., 2011).

The results of these studies show that the EF is able to increase the capacity of a LUE model to estimate plant production. Yuan et al. (2007) exploited the evaporative fraction (EF) to evaluate moisture availability to plants, because decreasing amounts of energy partitioned into latent heat flux suggests a stronger moisture limitation. LUE model developed by Yuan exploited 4 variables, from remote sensing (fAPAR and NDVI), simulated (air temperature), and eddy covariance derived (EF). The comparison with MODIS biomass estimation highlight the approach as good candidate for mapping biomass at the regional scale. Moreover the author underline that all the used variables can also be estimated from satellite.

Also Kanniah et al. (2009) exploited EF in a biomass estimation because it is a relatively simple variable to be calculated. Author works in correspondence of eddy tower in semi-arid Australian savannah, replacing a VPD factor with EF as a moisture index in LUE model. The eddy covariance based model has higher performance compared to MODIS biomass estimation if EF is considered, highlighting that the effect of soil moisture needs to be adequately represented in the LUE algorithm.

Finally Sjöström et al. (2011) combined EVI with tower measured PAR and EF to improve the relationship between estimation and EVI at nine flux tower sites. This was the first test of EF improvement in biomass estimation aver a Sahelian area. The EF (used to represents moisture

availability to plants) improved the site-specific relationships of measured biomass and EVI at the majority of sites, confirming the results from Kanniah et al. (2009).

Both Kanniah et al. (2009) and Sjöström et al. (2011) stressed the difficulties to match eddy covariance studies with low resolution satellite product on wide region. The remote sensing approaches to estimate EF can be a suitable solution to this topic, thanks to the methodology developed to estimate ET at regional scale (Roerink et al., 2000; Sobrino et al., 2007; Galleguillos et al., 2011).

This new application, coping with LUE model and remote sensed EF, is promising in global application since it can now be applied in strongly water limited regions, like the Sahel (Verstraeten et al., 2006). In this scientific context the main aim of the present chapter is to study and define a remote sensing tool to monitor and estimate the annual vegetation production in semi-arid herbaceous ecosystem.

In detail the goals are i) to evaluate the quality of Dry Matter Productivity (DMP) product derived from satellite data for assessing the vegetal dry matter by a comparison with ground data of savanna biomass, ii) to test the contribution of remote sensed EF as a water stress efficiency factor in biomass estimation as tested by previous authors on eddy covariance data and finally iii) to check improvement on biomass estimation calibrating the DMP on different vegetation types.

4.3. Materials

Date used for the study are summarized in Table 1. These consist of remote sensed data of biomass estimation (DMP), water stress RS (EF) and field measurements of annual biomass production. In Table 1 are also summarized the data used to interpret the modelled biomass estimations. These data provide information on vegetation growth (SPOT-NDVI), rainfall patterns (RFE) and different land cover types or uses (GlobCover). Globally 10 years of data (2000-2009) are in common between the typology of data available for biomass estimation and regional evaluation (DMP, EF and field samples).

EF defines the start of analyzed period, because of the beginning of MODIS mission (2000) and the available last field sample defines the end (2009). Despite most of the available satellite products cover the entire West Africa (WA) the area analized cover the Sahelian belt of Niger, because of the spatial distribution of field sites (Figure 1Figure 6).

Table 1- satellite and field data characteristics for biomass estimation and model performance evaluation.

Data	type	resolution	Timing	info	Use	Time-lapse	Area	# data
DMP	Maps	1 km	10-days	Biomass	Model	1999-2010	W.A.	432 maps
EF	Maps	1 km	8-days	Water stress	Model	2000-2009	Central Sahel	448 maps
Field Sample	points	-	annual	Biomass	cal/val	1998-2009	Niger	537 records
SPOT-VGT NDVI	Maps	1 km	10-days	Veg. growth	Ancillary	1998-2010	W.A.	432 maps
RFE	Maps	8 km	10-days	Rainfall	Ancillary	1998-2010	W.A.	432 maps
GlobCover	Map	300 m	-	Land cover	Ancillary	2005-2006	W.A.	1 map

Field measurements and test area

The dataset of field measurements of grassland biomass [kg ha-1] cover the entire sahelian belt in Niger (Figure 1). In this area rainfall patterns changes from Saharan in the north, with 160 mm of rain to Sudanian in the south, where 500 mm of rain falls between June and September. Field data collected in Niger have been provided by Action Against Hunger (ACF), a global humanitarian organization committed to malnutrition problems and food security (http://www.actionagainsthunger.org, last access December 2013). These data were sampled by ACF exploiting the quick double-sampling technique (Mutanga and Skidmore, 2004) to calibrate/validate their satellite maps of available forage (Ham and Fillol, 2010). These field measurements of herbaceous biomass cover a period of eleven years (1998-2009) for a total of 98 different location sampled. Field sites sites are located in the northern border of the Sahel where the rainfall is erratic and the arid condition is much more pronounced (Huber et al., 2011). Sites are spread in an area of 1300 km x 300 km, where pastoralism is the most important source of food supply. Northern sites (17,5° Lat 7,7° Lon) are located around Agadez that is the upper limit of pasture activities (Justice and Hiernaux, 1986; Bonifacio et al., 1993). The ester sites are located around the lake Chad (13,5° Lat 13° Lon) and the easter around Niger river (14,8° Lat 0.8° Lon). The latitudinal variation is less pronounced, there are only 300 km from the northern site to the southern.

These sites were not sampled continuously, but on average about 40 sites with field measurements are available for every year in the period 1998-2009. Thirty-nine sites, about half

of total available sites, are characterized by land cover of grassland savannah (GC code 140, Figure 1) and 37 by bare area (GC code 200, Figure 1).

These ground samples provide indispensable information for the evaluation of DMP product and for the calibration and validation of regression model between field data and satellite estimation.

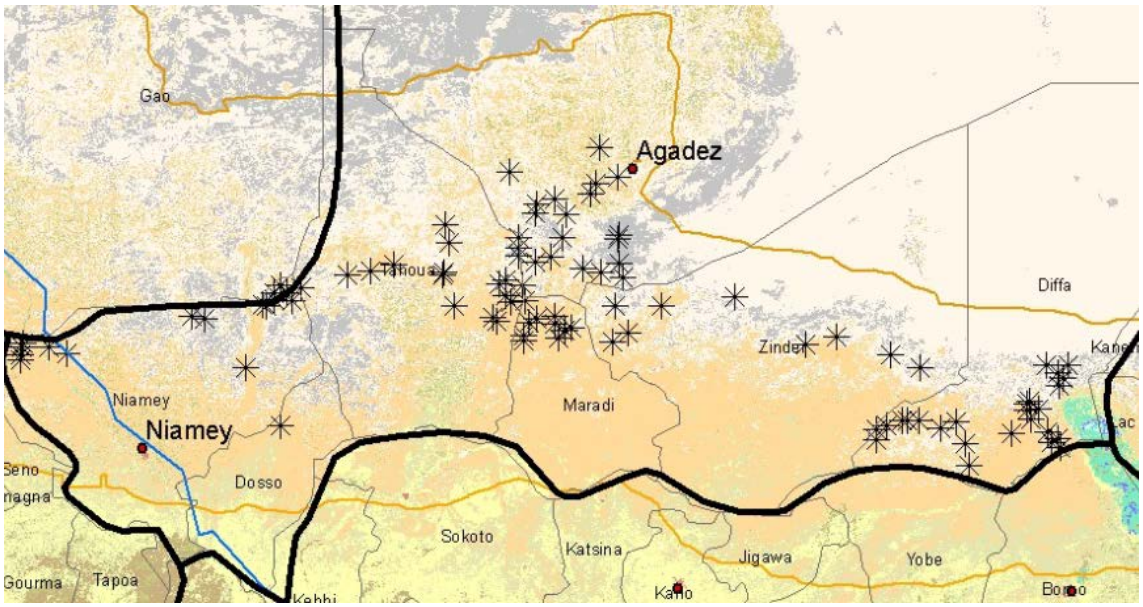

(a)

LC (GLC)			Field data	
Code_1	*Code*	*Description*	*# Site*	*# data*
14	10	Rainfed croplands	-	-
30	30	Mosaic vegetation (grassland/shrubland/forest) (50-70%) / cropland (20-50%)	-	-
110	110	Mosaic forest or shrubland (50-70%) / grassland (20-50%)	2	17
140	140	Closed to open (>15%) herbaceous vegetation (grassland, savannas or lichens/mosses)	39	240
	144	Closed (>40%) grassland	10	53
200	200	Bare areas	37	215
	201	Consolidated bare areas (hardpans, gravels, bare rock, stones, boulders)	8	32
	202	Non-consolidated bare areas (sandy desert)	2	16
		Tot	98	573

(b)

Figure 1- distribution of the 98 field sites in Niger (black stars). Background image is the GlobCover Land cover map for West Africa. The orange lines indicates the boundaries of the isohyet of 200–600 mm/year (a). Distribution of field sites within the land cover classes of GlobCover (b).

Satellite biomass estimation

Dry Matter Productivity is a satellite product based on the well-known model developed by Monteith (1972). According to the Monteith model, the amount of biomass over vegetated surfaces can be estimated from the incoming energy which is absorbed by vegetation (solar shortwave radiation) by applying a converting factor and a series of efficiency factors. The

Monteith's model was further developed from its original formulation at the Flemish Institute for Technological Research (VITO), in Belgium, with the collaboration of other European institutes like Monitoring Agricultural ResourceS (MARS) Unit Mission and INRA (National Institute for Agronomic Research). DMP quantifies the daily increase of dry biomass (growth rate) and is expressed as kilograms of dry matter (kg DM) per hectare per day (see §Annex 2). The DMP product used in this exercise is a 10-day estimation of dry matter derived from SPOT-VGT data at 1km spatial resolution for the period 1999 to 2010. The temporal resolution of 10 days allows us to well cover entire rainy seasons. Globally 360 DMP maps were used (Table 1). DMP data were made available in the framework of the Natural Resource Monitoring in Africa (NARMA) Core Information Service of the EU FP7 project Geoland2 through the NARMA eStation (Combal et al., 2010).

Satellite Water stress

The satellite estimation of water and condition stress is the Evaporative Fraction calculated thanks to MODIS products of albedo and LST (Gomez et al., 2005; Verstraeten et al., 2005; Sobrino et al., 2007; Galleguillos et al., 2011). EF data represents time series of water availability and soil moisture, suitable to asses vegetation status and therefore to improve LUE biomass estimation model (Verstraeten et al., 2006; Yuan et al., 2007; Kanniah et al., 2009; Sjöström et al., 2011). The produced maps cover the period between 2000 and 2009, with one image every 8 days except for date where input MODIS data are lacking. Globally 448 EF images were produced in the period where field data are available too (Table 1). EF maps cover an area of 1200x2400 km from eastern Mali to central Chad, with a spatial resolution of 1 km. The extension of EF maps is given by the merging of MODIS tiles h18v07 and h19v07. Resulted maps are centered on the sahelian area of Niger, where the field samples are located (Figure 6).

Ancillary data

SPOT-VGT NDVI

Time-series of NDVI data were obtained from the VGT sensor onboard the SPOT4 and 5 satellites and used as a proxy of vegetation productivity (Tucker et al., 1983; Ricotta et al., 1999). The NDVI time series are available as 10-day maximum value composites (S10) at 1 km resolution and cover a 13-year period from April 1998 to December 2010. Data were made available in the framework of the NARMA Core Information Service of Geoland2 (Combal et al., 2010). These data has the same spatial resolution of DMP and EF, and provides useful

information at high temporal resolution on vegetation growth. These data was use to extrapolate phenological metrics, in order to characterized the field sites.

Rainfall estimates

Precipitation data were provided by the Famine Early Warning System Network (FEWSNET) of the United States Agency for International Development. Rainfall estimates (RFE) are derived from satellite data since a regional analysis based on direct measurement is not feasible due to the low number of rain gauges available in West Africa. In the study area rainfall is the most important ecological variable and a limiting factor to vegetation growth (Huber et al., 2011), These data was analyzed in order to interprets the variation in annual biomass production. RFE data are available as 10-day cumulated values at 8 km spatial resolution since 1996 and currently represent the most accurate rainfall dataset in terms of spatial resolution. RFE data are routinely resampled at 1km resolution and registered to VGT-NDVI data in the eStation (Combal et al., 2010).

Thematic map of land cover and land use

In order to interpret the results derived from satellite and to analyze the possible influence of the land cover type on biomass estimation, the regional GlobCover map (GC) for Africa was used: this land cover is derived from data acquired by the ENVISAT Medium Resolution Imaging Spectrometer (MERIS) with a 300 m spatial resolution (Arino et al., 2007). GC land cover classes over the sampled sites are shown in Figure 1. The most relevant ones are grassland (GC 140) and bare soil (GC 200), which form the typical land cover of northern Sahel. These classes highlight the presence of marginal semi-arid rangeland, where pastoral activity is the most important source of food income. Bare soil class in 300 m GC represent area with very low but not absent, vegetation cover. in this area pasture activity is commonly conducted. Indeed these sites were selected and monitored by ACF because they represent typical pastureland.

4.4. Method

Figure 2 provides a flow chart of the steps followed for satellite data treatment and evaluation with ground data. Dark gray boxes indicate steps where ground data are involved. The data handling, allow to extract RS data in correspondence of field site. These RS data were managed in order to produce biomass estimation, and DMP were integrated with EF in orfer to produce biomass estimation corrected with water stress factor. The biomass estimation were compare

with ground data from selected sites, previously managed in order to delete outliers and sites with few data.

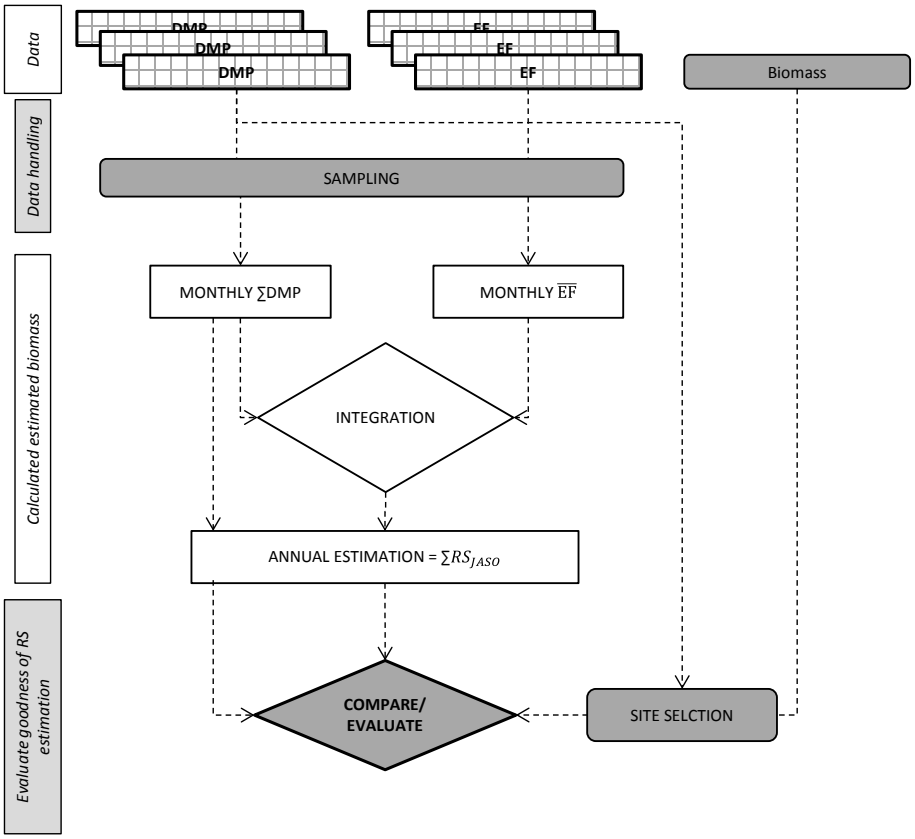

Figure 2- flow chart of biomass estimation and evaluation with field data from data selection (top of graph) to data management and evaluation (bottom of graph).

Satellite data handling

In order to compare satellite data with field samples, EF and DMP were extracted in the correspondence of the 98 field sites. A buffer of 1 km around every sites locations were considered, as displayed in Figure 3. The buffer was selected because field campaign schema doesn't report exactly the area sampled and at least one site reports a geo-localization with a potential shift of 200 meters. Time series of DMP and EF data were extracted from buffer areas around each sites. Buffer area include from 2 to 4 pixels, depending on site location, mean value were calculated. Globally were extracted 79184 records, 43904 of EF and 35280 of DMP data.

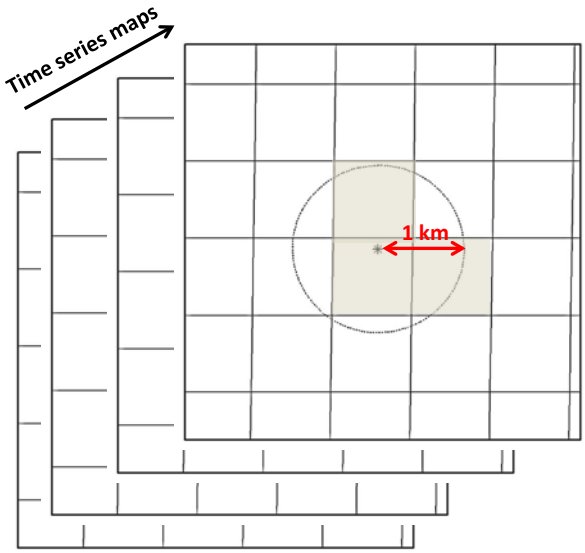

Figure 3- satellite data sampling. The circle line is the buffer of 1 km around field site (black star), gray grid the pixels of DMP and EF and. Maroon shaded area identifies pixels selected within the buffer.

The 10-day DMP estimation for the period July to October (JASO) were cumulated to obtain the annual syntheses of dry matter production (ΣDMP_{JASO}). The ΣDMP_{JASO} provides an indicator of annual rangeland production (Seaquist, 2003; Fensholt et al., 2006; Fensholt and Rasmussen, 2011) which can be compared to the available ground data, used to validate satellite biomass estimation, that represents total annual herbaceous production measured in field at the end of the season. For semi-arid regions such as Sahel is demonstrated that the NDVI cumulated on JASO is correlated to annual Net Primary Productivity (NPP) (Anyamba and Tucker, 2005). The months of July and October were selected to represent respectively the start and the end of the growing season, even though the start of the growing season might slightly vary across the regions from year to year (Anyamba and Tucker, 2005; Heumann et al., 2007; Huber et al., 2011).

The following equation gives the annual DMP expressed in [kg/ha] comparable with ground measurements:

$$\boldsymbol{DMP_{JASO}} = \sum_{i_{1,12}} \frac{10 * DMP_{10-days}}{k} \qquad \textbf{Eq. 1}$$

where JASO is the rainy period in west Africa, from July to October, $DMP_{10\text{-days}}$ is the 10-days satellite product, 12 is the number of decades in JASO period (4 month*3 decades) and k is converting factor to obtain physical value of agronomic interest (kg/ha).

Monthly values of DMP and EF were calculated in order to get improvement of water availability/stress factor in LUE model of biomass estimation. Because DMP and EF couldn't be directly integrated because they have different time-step (10 and 8 days respectively), on every months (*m*) for every sites (*s*) were calculated the mean of EF values ($\overline{\text{EF}}$) representing the average water condition:

$$\overline{\boldsymbol{EF}}_{\boldsymbol{s,m}} = \frac{\sum \boldsymbol{EF}_{\boldsymbol{8-days}}}{\boldsymbol{n}} \qquad \textbf{Eq. 2}$$

where $\text{EF}_{8-\text{days}}$ is the estimated water stress and *n* is the cardinality of 8-days EF data in one month and was calculated the monthly sum of DMP ($\sum$DMP) to represents the total dry biomass produced during every month:

$$\sum \boldsymbol{DMP}_{\boldsymbol{s,m}} = \sum \boldsymbol{DMP}_{\boldsymbol{10-days}} \qquad \textbf{Eq. 3}$$

where $\text{DMP}_{\text{10-days}}$ is the 10-days biomass estimation product.

The two monthly variables were than monthly integrated following the equation:

$$\boldsymbol{DMP} * \boldsymbol{EF}_{\boldsymbol{s,m}} = \overline{\mathbf{EF}}_{\boldsymbol{m,s}} * \sum \mathbf{DMP}_{\boldsymbol{s,m}} \qquad \textbf{Eq. 4}$$

where $\overline{\text{EF}}$ is the monthly EF mean, $\sum$DMP the monthly cumulated DMP, *m* is the month and *i* the site.

For every sites, 12 data (once for every month) of biomass estimation (DMP) rescaled by water status (EF) were obtained. Overall, 11760 records of $\sum$DMP corrected by $\overline{\text{EF}}$ were calculated (DMP*EF). This multitemporal data was annually cumulated by the procedure followed for the DMP product

$$\boldsymbol{DMP}_{\boldsymbol{JASO}} = \sum_{\boldsymbol{i}_{\mathbf{1,12}}} \frac{\mathbf{10} * \boldsymbol{DMP}_{\mathbf{10-days}}}{\boldsymbol{k}} \qquad \textbf{Eq. 5}$$

Statistical instruments for DMP quality assessment

To quantify the goodness of the remote sensing biomass estimation, difference-based statistics (Loague, K.M., Green, 1991) together with regression analysis were used for the comparison between observed and estimated biomass values. The results allowed the identification of the usefulness and the reliability of the DMP and EF effects. The root mean square error (RMSE) and the relative RMSE (RRMSE), expressed in percentage, provide information about the absolute and relative difference between the model's estimates and the ground measurements. Modelling efficiency (EF) quantifies the capability of the model to reproduce the trend of the

observed values and the coefficient of residual mass (CRM) quantifies the occurrence of overestimation (CRM < 0) or underestimation (CRM > 0) of data in the model. The indices used in this work are summarized in Table 2, reporting also the range and the best expected values.

Table 2- Indices of agreement between measured and computed values derived from difference statistics

Name and acronym	Min	Max	Best
Root mean square error (RMSE)	0	+∞	0
Relative Root mean square error (RRMSE)	0	+∞	0
Modeling efficiency (EF)	-∞	1	1
Coefficient of Residual Mass (CRM)	-∞	+∞	0
Coefficient of Determination (R^2)	0	1	1

The analysis of Covariance (ANCOVA) was also conducted to study the influence of land cover typology, isohyets and yearly variation on the relation (linear regression) between ground data and estimates. This method, which is a type of generalized linear model (GLM), allows the introduction of categorical variables as further explanatory variables in a linear regression model. Finally during the study linear regressions between variables were studied exploited the ranged major axis (RMA) method in order to obtain the most robust fit between field data and RS estimation (see §Annex 3).

Analysis of model response over different ecosystems

DMP has been analyzed where has homogeneous response to field biomass. This homogeneous ecological units were detected analyzing variable variables of land cover, geographical position of sites, average maximum NDVI as a proxy of vegetation production vegetation growth and average phenological metrics. These variables describe the sites in terms of vegetation dynamics and productions, highlighting area with different vegetation cover and associations.

To perform this analysis, a decision tree implemented in R (rpart package, Therneau and Atkinson 2013) was used to identify the best performing thresholds. The partitioning is based on minimal error fitting on the data set and it identifies the values on different remote sensed variables that best discriminate sites with different relation between DMP and ground data. The statistical significance of identified groups was checked by ANOVA analysis.

The splitting techniques allowed to calibrate a remote sensing vs. field biomass regression model on statistically different areas and to validate the estimation by the metrics summarized in Table 2.

Retrieval of phenological metrics

The phenological metrics, used in the decision tree, where estimated thanks to PhenoRice algorithm (Boschetti et al., 2009; Boschetti and Nelson, 2012; Manfron and Crema, 2012) developed by IREA institute to perform rice detection and rice seasonal monitoring by analyzing the continuous temporal signal of spectral indices. It is a rule based method able to identify rice crop when a clear and unambiguous flood condition is detected and a consistent rapid crop growth is recognized. Once rice is detected the phenological monitoring is performed analyzing the temporal behavior of vegetation spectral index (Boschetti et al., 2009).

For a more detailed description of this method please refer to Manfron et al, (2012). In this case the methodology was modified in order to avoid rice mapping and to report only the phenological estimation.

The algorithm involves two processing steps. First of all the *smoothing of temporal signal* of NDVI time series of 10 years (2000-2009) for every sites. Using a local polynomial function that weight observation in relation to cloud contamination on the based on Savitzky-Golay filter (Chen et al., 2004; Luo et al., 2005) the NDVI series were smoothed, in order to eliminate spikes, no data and small drops of data that are un-related to vegetation growth but linked to noise and atmosphere interference (such as cloud cover).

After that the signal analysis has been conducted. In this step first derivative of the smoothed signal is calculated and all points of local (relative) minima and local (relative) maxima identified. Crop minima (MIN) and maxima (MAX) points are then automatically identified using a series of criteria and then a temporal analysis is performed to derive the occurrence of the starting of rice growing season (Start of Season - SoS) end maturity (End of Season - EoS). In order to avoid the detection of false seasons, not referred to pasture growing, detected MAX was deleted if characterized by NDVI values lower than the 2th percentile of the entire NDVI population of this site.

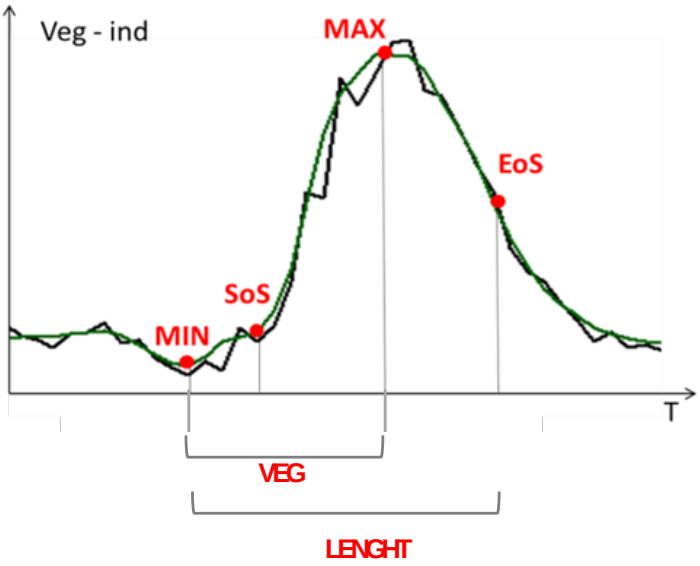

Figure 4: timely occurrence and representation of phenological stages (MIN, MAX, SoS, EoS).

These four metrics are able to provide important interpretations on the phenology of savannah for the analysed seasons (Figure 4). The output of the algorithm is constituted by 4 different date of phenological stages (MIN, MAX, SoS, EoS) on each analyzed years.

Furthermore they were used to calculate the length of vegetative phase as the different between MAX and MIN (VEG) and the length of season as the difference between EoS and MIN (LENGTH) (Figure 4). These phenological data, together with land cover (LC), latitude and longitude and average maximum NDVI, were used to classify the database sites into groups with statistically differences in DMP response to field biomass variability (i.e. potentially differences in ε_{LUE}).

4.5. Results

Field site selection

The available dataset of field data was firstly managed in order to delete outliers and sites with few data. among the total 98 field sites, only 87 present at least one data in the period 2000-2009. The other 11 sites were eliminated because they report data only for the years 1998 and 1999, when MODIS products were not already set. Among these 87 sites, 65 were kept because of sufficient cardinality (i.e. more than 4 samples in 10 years) to significantly analyze a site-specific correlation between satellite and field data, resulting in 453 biomass data (light blue bars in Figure 5). Above the 65 sites, 46 show significant correlation between measured and remote

sensed estimated biomass. The other 19 sites were deleted from the analysis in order to avoid field data with low quality, not robust date or not representative for analyze RS data. In conclusion, 46 field sites with 320 records of annual savannah production were exploited to evaluate the biomass estimation from satellite (blue bars in Figure 5). The dataset allows to perform a quantitative comparison between annual ∑DMP and ∑DMP*EF with ground biomass measurements.

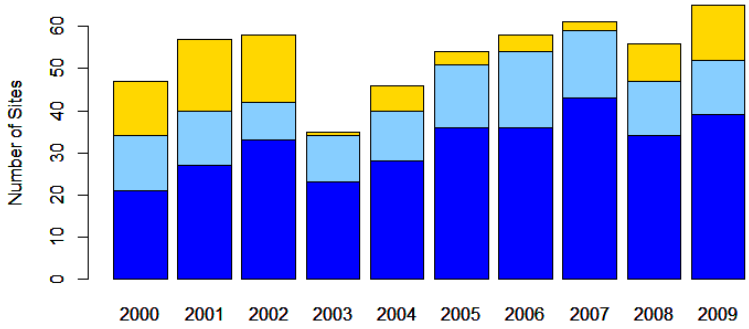

Figure 5- cardinality of sites with field data along the 10 years (orange bars, 87 sites). Available field sites after deletion of site with few data (light blue bars, 65 sites) and with no correlation with DMP (blue bars, 46 sites).

The selected field sites are mapped in Figure 6 with dark dots, the deleted with gray dots. The chosen 46 sites are equally distributed among the study area (Figure 6). Meanly 30 sites are available on each years. Each site has, on average, 6 to 9 years sampled between 2000 to 2009. Most of the eliminated sites are grouped in Agadez and Tahua regions.

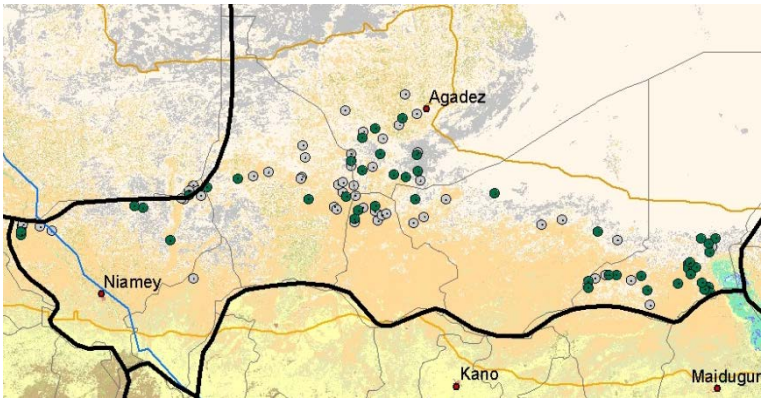

Figure 6-spatial distribution of 46 selected field sites (dark green dots) and eliminated ones (gray dots). Background image is the GlobCover Land cover map for West Africa. The orange lines indicates the boundaries of the isohyet of 200–600 mm/year.

These areas are the closet to the desert border and weren't frequently sampled during the 10 years. Moreover, due to the very sparse vegetation, the field samples are not easy representable

from 1 km resolution data. As an example is reported one eliminated field site from the analysis (Figure 7).

In that case the sampled area is located in the tiger bush well visible by HR image. The yellow box f 1 km^2 indicates that the area covered by low resolution pixel is much more wider, and not representative of the vegetation sampled. These vegetation surrounded by bare soil were sampled by ACF because they are meaningful for local pastoral activities.

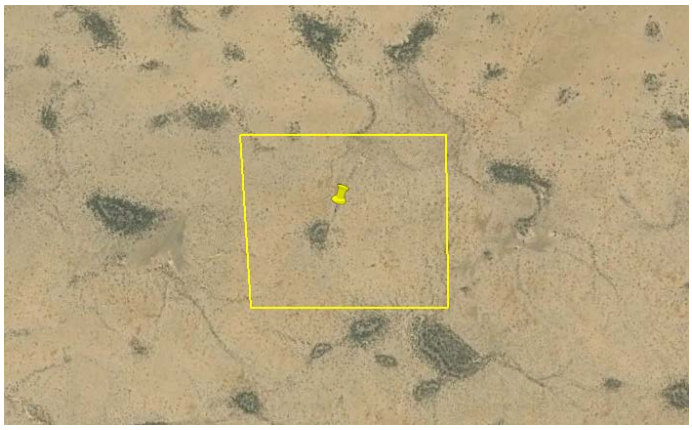

Figure 7- geolocation of one field sample eliminated from the analysis (field code A34, Location Mayata, Thoua region). Yellow box indicates an area of 1 km^2 around the sampled area that correspond to DMP spatial resolution.

Descriptive statistics of ground reference biomass data

The available biomass data are plotted in the histogram in Figure 8. The most common biomass measured in the field, about 200-600 kg/ha per year, with maximum of 2700 and minimum close to zero, appears comparable with values reported in the literature for Sahelian pastureland productions.

Campbell and Stafford Smith (2000) indicates that the mean pasture production in Sahel is comprised between 500 and 2500 kg/ha/year, and a FAO report stated that over the Sahelian steppe (situated between 250 and 500 mm of rainfall) the most productive pastureland areas have a mean productivity that varies from north to south between 1000 and 2000 kg/ha (Geesing, D., Djibo, 2001).

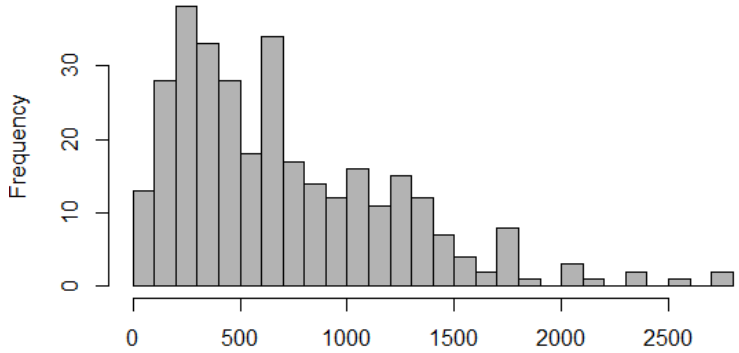

Figure 8- frequency distribution and descriptive statistics of field biomass values [kg ha^-1]over 46 sites and 10 years.

The Table 3 describes the selected biomass data according as land cover classes from GC map. Most of the 46 are characterized and equally distributed among of grassland savannah (GC_140) and bare area (GC_200).

Sites in GC_200 class report years with low production has about 50-300 kg/ha per year, as reported by Schlecht and Hiernaux (2006) and Begue (2002) in Nigerien marginal rangelands. Some seasons report no production at all as reported in hyper-arid area by Justice and Hiernaux (1986).

Table 3- field data cardinality and average sampled values of 46 selected sites depending on GC classes.

LC (GLC)			Field data cardinality			Field Biomass (Kg Ha-1)			
Code_1	*Code*	*Description*	*# Site*	*# data*	*AVG. Years*	*AVG*	*Min*	*Max*	*St.Dev*
14	10	Rainfed croplands	-	-	-	-	-	-	-
30	30	Mosaic vegetation (grassland/shrubland/forest) (50-70%) / cropland (20-50%)	-	-	-	-	-	-	-
110	110	Mosaic forest or shrubland (50-70%) / grassland (20-50%)	1	7	7	365.80	60	1319	439.25
140	140	Closed to open (>15%) herbaceous vegetation (grassland, savannas or lichens/mosses)	18	145	8	633.11	0	2019	413.97
	144	Closed (>40%) grassland	4	28	7	1168.61	53	2717	587.70
200	200	Bare areas	18	140	8	654.02	0	2303	461.73
	201	Consolidated bare areas (hardpans, gravels, bare rock, stones, boulders)	4	23	6	632.52	47	1762	525.68
	202	Non-consolidated bare areas (sandy desert)	1	9	9	623.75	292	1234	337.39
		tot:	46	320					

Higher productive years for GC_200 report 1200-2300 kg/ha are comparable with the 2 tons of biomass reported for high-productive pastureland (Geesing, D., Djibo, 2001; Schlecht and Hiernaux, 2006). The average production in GC_200 class of 650 kg/ha is analogous to the 600

kg/ha, reported by Ayantunde et al. (2008) in marginal rangeland areas typical for northern Sahel. The biomass variations for GC_200 is close to the range of 55-1093 kg/ha described for herbaceous production in northern Senegal by C. J. Tucker et al. (1985).

Sites with LC class GC_140, have slightly higher production. The mean of 1000 kg/ha is also indicated by Kandji et al., (2006) and Soler et al., (2008) for herbaceous biomass with high density of plants. Finally the highest annual production of 2700 kg/ha is perfectly in the same range of higher Nigerien production of 3000 kg/ha reported in particular areas where there are a lot of available water (Schlecht and Hiernaux, 2006; Ramier et al., 2009).

DMP product characteristics

Before comparing DMP biomass estimation with field data, the data were analyzed in its spatial variability thanks to the map of land cover (GC). Figure 9 shows the mean DMP production during the JASO period between 2000 to 2009. This map shows biomass varies that follow the typical north-south gradient determined by rainfall, ranging from 100 kg/ha for areas of bare soil to more than 7 t/ha for the woodland in Soudanian zone. The Nigerien Sahel region shows an estimate of the average production that varies between values lower than 200 kg(ha (red patterns) to values greater than 3000 kg/ha (green patterns), corresponding to typical woodland savannahs where water supply is no longer the major limiting factor to the vegetation growth (Geesing, D., Djibo, 2001). Spot of high biomass production can be seen around lake chad and in the correspondence of fossil valley where water availability is higher than the surrounded areas (Peugeot et al., 2003). Both areas are well known as favorable area of vegetation production in the Sahelian belt (Boschetti et al., 2013; Nutini et al., 2013).

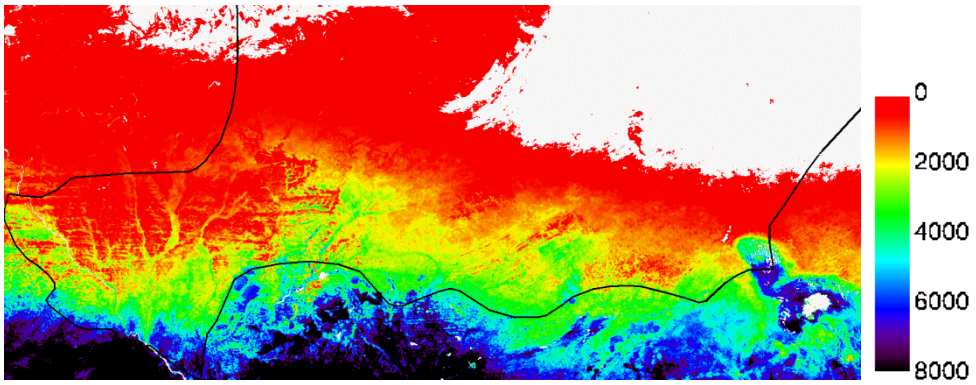

Figure 9- map of mean DMP between 2000 and 2009. Cold colors represent high production of woodland and humid savannahs (>4000 kg/ha) and warm color low production from semi-arid savannah (<2000 kg/ha)

The Table 4 shows the annual DMP values, compared with land cover information. The Table 4 shows that the LC classes of bare soil (GC_200, GC_201, GC_202) cover 76% of the study area, herbaceous savannah the 19% and only 4% is covered by cropland (GC_10, GC_30) and shrubs savannah (GC_110). Mean annual DMP values vary from about 3000 kg/ha on cropland (GC_14) to almost zero in bare areas (44.75 kg/ha, GC_202).

Sparse vegetation and bare area (GC_140, GC_144, GC_200, GC_201, GC_202) form the typical land cover characteristics of the northern Sahel. The DMP values for these classes are highlighetd by orange bars in Table 4, comparable with ground data highlighted by green bars. GC_144 display the higher productivity, both estimated (>1500 kh/ha) and measured (>1000 kg/ha). In the more arid LC classes the coherence between estimation and filed data decrease, as enphatized in Figure 10.

Table 4- GC percentage over the study area (red bars) and mean annual DMP for the different GC classes (orange bars).

	LC (GLC)			**DMP (Kg Ha-1)**	
Code_1	*Code*	*Description*	*%*	*AVG*	*St.Dev.*
14	10	Rainfed croplands	1%	3383.28	1013.05
30	30	Mosaic vegetation (grassland/shrubland/forest) (50-70%) / cropland (20-50%)	2%	2135.24	807.24
110	110	Mosaic forest or shrubland (50-70%) / grassland (20-50%)	2%	604.52	836.97
140	140	Closed to open (>15%) herbaceous vegetation (grassland, savannas or lichens/mosses)	**11%**	836.15	571.28
	144	Closed (>40%) grassland	**8%**	1547.49	533.60
200	200	Bare areas	**20%**	309.60	331.65
	201	Consolidated bare areas (hardpans, gravels, bare rock, stones, boulders)	**21%**	109.54	144.98
	202	Non-consolidated bare areas (sandy desert)	**35%**	44.75	65.54

Histogram in Figure 10 compare average and standar deviation of DMP anf ground biomass for the GC classes. The first two classes have no field data to be compared with. The 3 classes of shurbs and herbaceous savannah (GC codes: 110, 140 144) have estimated values in the same range of measurements, as highligth by standard deviation. ANOVA conducted for these classes demonstrated that DMP estimation are not statisticaly different from measurements. However, this correspondence is lost in bare area (GC codes: 200, 201, 202). Field sites collected in these area have average production greater than 600 kg/ha, at least 2 times greater than DMP (<300 kg/ha).

Hence DMP product shows globally biomass values comparable with field data and references information on savannah prodution. However, this first result suggest differencies of DMP goodness among different ecosysrems.

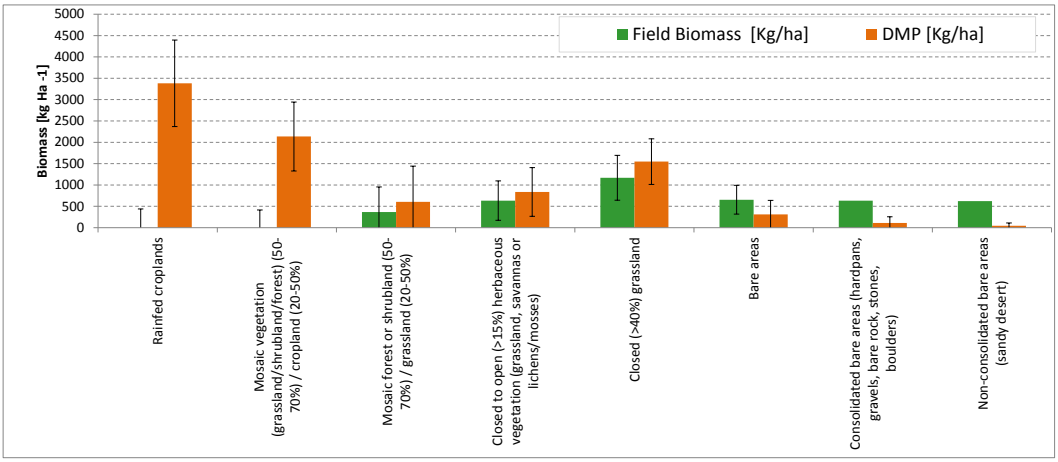

Figure 10- comparison, for each GC classes, of mean annual DMP and mean ground biomass.

Analysis of RS variables annually summarized in correspondence of selected field sites

The DMP data, together with the other analyzed remote sensing variables (NDVI, RFE, EF) were sampled in correspondence of field sites, cumulated over the wet season and compared with biomass data, as exposed in the §Method section.

Table 5 show descriptive statistic of cumulated RS variables while Figure 11 shows histograms of the frequency distribution. Annual rainfall data (ΣRFE) showed that study area presents a variability comparable to annual rainfall reported in bibliography (Anyamba and Tucker, 2005; Mertz et al., 2012), and ranges from lower than 100 mm in northern Sahel to 600 mm, first values represent the the minimum amount of annual rainfall for grassland growing and the second the southern limit of the Sahelian steppe.

Table 5- Descriptive statistics of field measurements and satellite-derived estimates expressed in kilograms per hectares [kg/ha]. In brackets the number of available data.

(n=320)	Σ DMP [kg/ha]	Σ DMP*EF [-]	Σ NDVI [-]	Σ RFE [mm]
mean	815	390	1.8	314
st.dev	524	302	0.2	97
median	703	293	1.8	317
min	58	28	1.1	94
max	2894	1607	2.5	604

Most of the annual rainfall are included between 200 and 350 mm per year, a typical range for northern Sahel (Justice and Hiernaux, 1986; Nicholson and Grist, 2001; Giannini et al., 2003; Hein, 2006; Mohino et al., 2010; Proud and Rasmussen, 2011; Mertz et al., 2012).

Concerning the DMP sampled data over the 46 sites (Figure 11a), values of the descriptive statistics for Niger are in the same range of field measurements, with a minimum close to 0 (bare areas) and a maximum close to 3000 kg/ha (equivalent to high productivity pastureland).

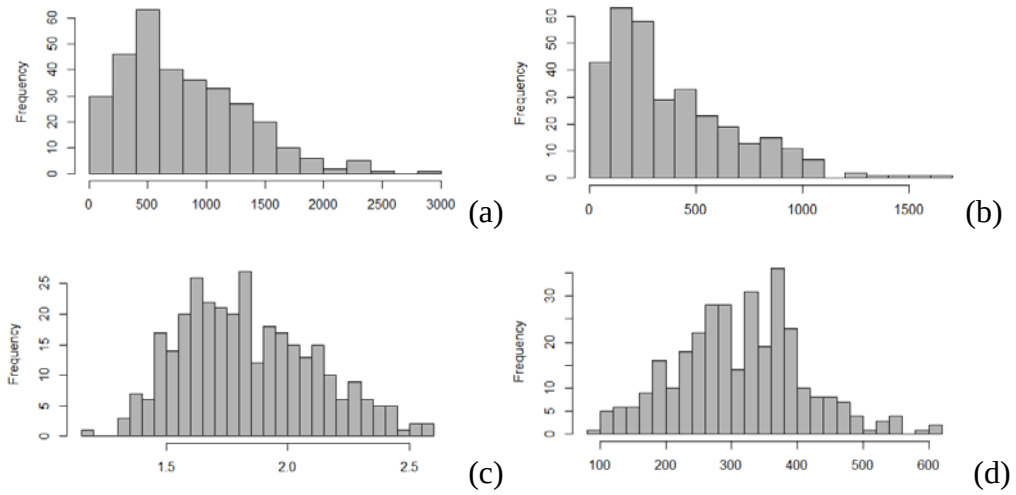

Figure 11- frequency distribution of remote sensed variables of biomass estimation of Σ DMP (a) and Σ DMP*EF (b), biomass proxy NDVI (c) and climatic driving force RFE (e) .

Correlation analysis of seasonal Remote Sensing variables with field data

All the cumulated RS variables, showed in Figure 11, considered as indicators (or estimation) of vegetation production were compared with annual sampled biomass over 10 years. The result from the analysis of correlation between field biomass and annual cumulation of remote sensed variables are plotted in Figure 12 and summarized in

Table 6. The plots represent the correlation between annual field data with cumulation of Σ DMP (a), Σ DMP*EF (b), Σ RFE (c) and Σ NDVI (d). The first two represent biomass estimations, Σ RFE is the main driving force for vegetation production and the latter a well-known biomass proxy currently used by Sahelian monitoring programs (AMESD, 2011).

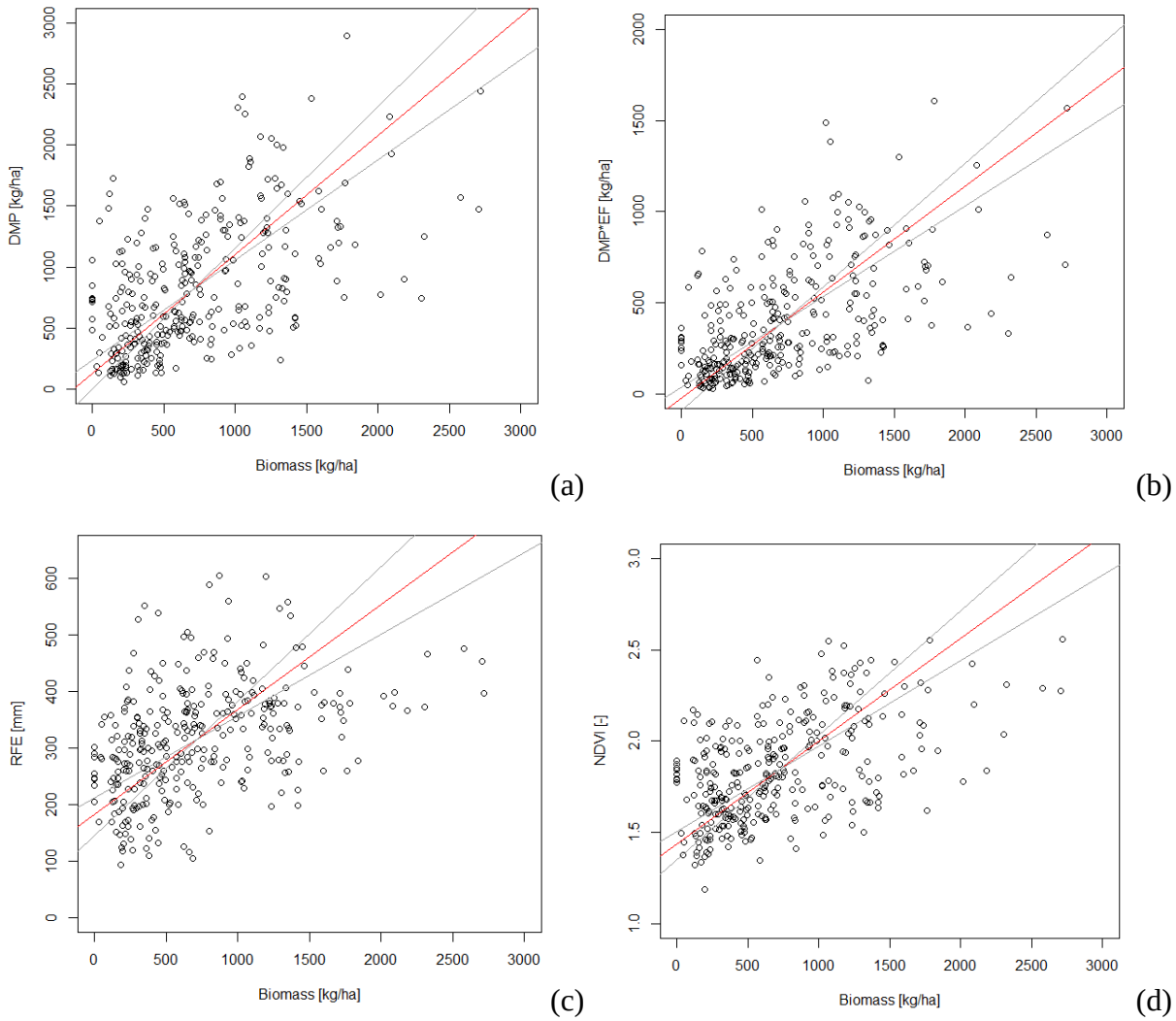

Figure 12- scatterplots of field biomass (x-axis) against LUE model estimation (ΣDMP (a) and ΣDMP*EF (b)) and proxies (ΣRFE (c) and ΣNDVI (d)). Lines represent the Ranged Major Axis regression between data, dotted lines the 95% confidence region. (n=320)

Data appear scattered and the coefficients of determination are less than 0.3 in all cases except for the DMP with ε_{water} (r^2 = 0.31). Despite the low correlation coefficients the correlations are significant in all cases. Among the 4 regression models the one with rainfall data is the less robust, confirming the this variable is not the best choice to predict annual production(Huber et al., 2011). The cumulative NDVI is correlated with field data, however LUE model overcome this proxy. This result confirm that 2 commonly used proxies of biomass production, NDVI and rainfall, can be overcome by a LUE model in detecting biomass variation (Seaquist, 2003). Moreover, globally, the EF seems to give a contribution to the biomass estimation (Figure 12a), even if these scatterplot shows an high rate of un-explained variability of field data.

Table 6- regression parameter between measured field data, satellite proxies (ΣRFE, ΣNDVI) and satellite estimation (ΣDMP, ΣDMP*EF). In bold best values.

Parameter	intercept	slope	R^2	Sign. of regression[α]
Range	[-∞, +∞]	[-1,+1]	[0, 1]	NS
Best	0	1	1	***
ΣDMP	431	0.55	0.26	***
ΣDMP*EF	150	0.34	0.31	***
ΣRFE	260	0.07	0.14	***
ΣNDVI	1.644	0.01	0.23	***

α *** < 0.001; ** < 0.01: * < 0.05; NS is not significant;

Correlation analysis for normalized data

The z-score allows us to compare in the same graph variable with different range values. Hence also the correlation plot can be compared. The z-score were calculated for annual biomass, ∑DMP, ∑DMP*EF for the 46 selected sites. The normalized data allows to remove the effect of local differences in the relation between LUE outputs and field biomass, visualizing only the overall model capability to detect the field data variance. The Figure 13 shows the correlation between normalized field data and ∑DMP (a), ∑DMP*EF (b).

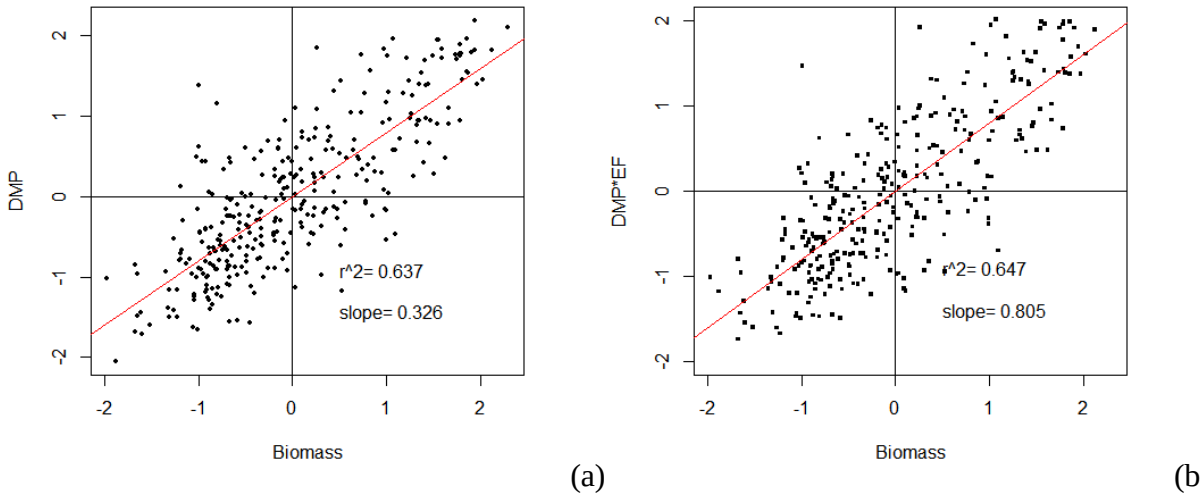

(a) (b

Figure 13 correlation between z-scores data of field biomass and ∑DMP (a), ∑DMP*EF (b), and RFE (c) for 320 annual data (46 field sites). The red line indicates the regression model.

Data closed to zero are near to the population average, while values data below or upper zero indicates a positive or a negative anomaly respectively. The top right and bottom left corners indicates years were estimated and measured variables data are in agreement. The top left and bottom right indicate respectively a negative and positive anomaly of field biomass corresponding to a positive and negative anomaly in LUE estimation. Both ∑DMP and ∑DMP*EF have most of the data in the "agreement corners" and along the 1:1 line. The main difference is provided by the field vs. biomass z-score. ∑DMP*EF shows a regression slope significantly different from ∑DMP ones and very close to the best value of the 1:1 line. This analysis highlight how the introduction of water stress factor (EF) improve model capability in monitoring and simulating annual accumulation of field biomass.

Site-specific correlation

Even if the scatterplots show an huge variability of field data definitely un-explained by the estimation, the ΣDMP has remarkable correlation on most of the single sites.

Statistics of site specific correlation for both ∑DMP and ∑DMP*EF, obtained over the all selected field sites, are summarized in Table 7. These 46 site-specific correlations are always higher than the global correlation showed in Figure 12, indeed the minimum regression coefficient is 0.33 for ∑DMP and 0.34 for ∑DMP*EF (Table 7).

In order to display site specific correlations and the effect of EF in the biomass estimation three site-specific regression are showed in Figure 14. These scatterplot show the correlation between sampled biomass and satellite estimation of ∑DMP and ∑DMP*EF models. The three sites represent situations where: Figure 14a) ∑DMP is low correlated with 6 measurements (r^2=0.49, Lon 10.9 Lat 13.7, Figure 14a), Figure 14b) the correlation shows medium value with 8 field data (r^2=0.51, Lon 12.8 Lat 13.95) and Figure 14c) ∑DMP highly correlated with 5 field measurements (r^2=0.66, Lon 6.8 Lat 15.8, Figure 14c).

Among the 3 sites the second one (Figure 14b) has the typical Sahelian inter-annual fluctuation of annual biomass, from un-favorable years (100 kg/ha) to years where the production is 10-times higher. Regression coefficient are permanently high and the differences in intercepts and slopes between these regression explain why the global correlation is always lower compared to the local regressions.

The slopes vary from average of 0.3 in Figure 14a1 and Figure 14c1 to average of 1.1 in Figure 14b1. Moreover the intercept is 1238 for the first regression (Figure 14a1), 919 in the second case and 393 for the case with higher correlation (Figure 14c1).

Table 7 summarize the correlation parameters (slope, regression, intercept) for the 46 regression models on each sites. Results from simple DMP model and with the EF improvement are showed. The empirical models between field and remote sensed variables change depending on sites. Regarding DMP, the average correlation coefficient is about 0.65, a pretty good results, with an average intercept of 437.08 and a slope of 0.55.

Variability of regression parameters across sites indicates that, despite the LUE model is able to detect the field biomass variability, it's not able to estimate biomass in robust way. Especially the differences in slopes indicate that, depending on site (i.e. different vegetation types, amount of rainfall etc.) the model overestimate or underestimate the field biomass.

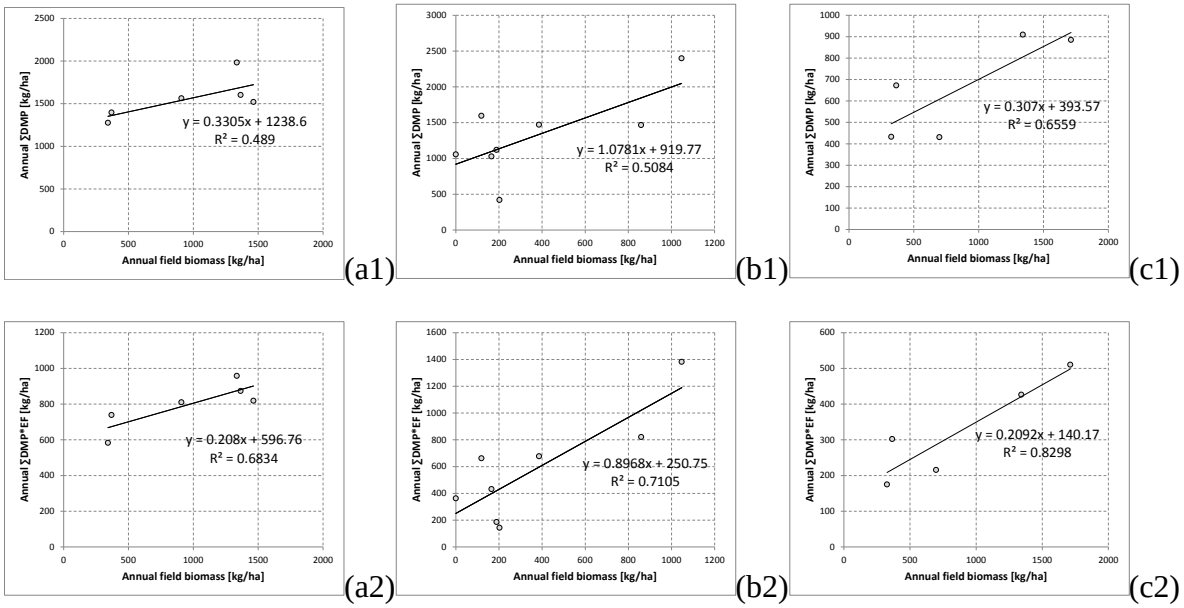

Figure 14- correlation between annual biomass samples and satellite estimation (∑DMP on top panels and ∑DMP*EF on bottom panels) for sites were the goodness of fit is low (a), medium(b) and high (c)

Furthermore the same analysis was conducted on the correlation with ∑DMP*EF, in order to investigate the contribution of water stress in biomass estimation. In Figure 14 the 3 plots showed, there is a general increase in the capacity of the remote sensing estimation to detect the variability of the field measurements if water stress is take into account, as indicated by increasing in regression coefficients. The EF has reduced the overestimation of the model for poorly productive years, as showed by intercepts closer to zero.

Globally when EF is take into account the regression models has and higher accuracy (r^2=0.67), an intercept closed to zero (151.43) confirming previous results (Sjöström et al., 2011) and less pronounced slope (0.3). However, minimum and maximum of these regression parameters highlight that huge varieties between sites is still present.

Table 7- summary of 46 regression coefficient (degree of freedom, intercept, slope and regression coefficient) for correlations between field biomass measurements and remote sensed estimations. Black stars indicate the significance of the difference between ∑DMP and ∑DMP*EF parameters.

	∑DMP			∑DMP*EF			
parameter	min	mean	max	min	mean	max	Differences
intercept	21.14	437.08	1238.59	-4	151.43	596.76	-
slope	0.08	0.55	1.36	0.02	0.35	1.09	-
r^2	0.33	0.65	0.97	0.34	0.67	0.97	***

α *** < 0.001; ** < 0.01: * < 0.05; NS is not significant

The regression coefficients obtained from ∑DMP and ∑DMP*EF models were compared in Figure 15. The blue dots indicate sites where the correlation increased, red where correlation decreased and in black the stable correlations. Globally in 18 cases the correlation increased by using the EF in the model (blue dots in Figure 15).

Plot shows that in 9 sites where the correlation decreased (red dots in Figure 15) the EF keep correlations a significative. The slope of the regression between al data (red line in the plot) highlight that sites with lower r^2 saw an increase of correlation between estimated and measured biomass if water stress is considered. Most of these sites have average low r^2, between 0.3 and 0.5, and reach with the water stress factor higher correlations, up to 0.7.

Eighteen of these sites (black dots in Figure 15) have no differences in regression coefficient (i.e. lower than 0.05).

Site characterized by an increasing in correlation seem to be more common in northern arid sites. Indeed sites with an increase in correlation coefficient have an average annual rainfall below 300 mm, and sites with the decrease in r^2 are in a average wetter condition with more than 375 mm of annual rainfall.

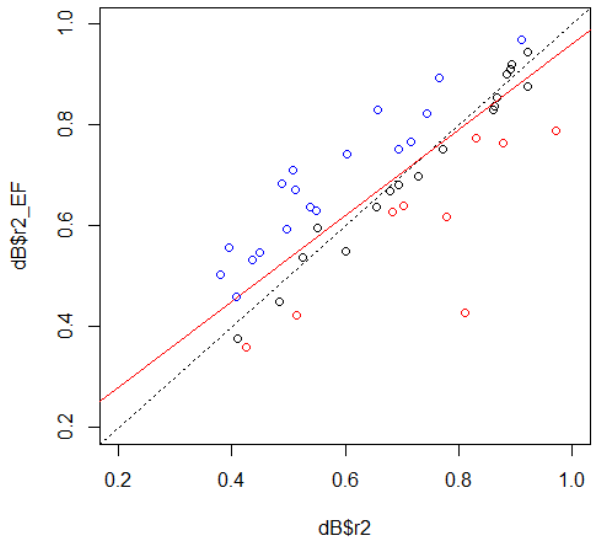

Figure 15- comparison between coefficient of determination of ∑DMP and ∑DMP*EF models. Blue dots indicate the 18 sites where the correlation increased, red the 9 cases where correlation decreased and in black the stable correlations. Red line indicates the regression between the two r^2 populations.

Probably sites situated in drier areas suffer of unfavorable years more than southern sites. The EF is able to detect the water stress , increasing the capability of satellite estimation to explain the variance of field sites.

Influence of ecology in remote sensing biomass estimation

Hence despite the EF increased the quality of DMP biomass estimation, the high variability of linear regression coefficient on single sites, showed in Table 7 and by data scattering showed in Figure 12, suggest that there are processes in biomass production not taken into account by LUE model. These results still underline that a calibration of DMP is needed.

In order to investigate this aspect, we analyze the spatial distribution of site-specific correlation of slope and intercept for all site-specific analysis.

Figure 16 shows 46 points, one for each selected sites, points size is proportional to latitude, northern sites are smaller and southern bigger. On the axis are represented the regression coefficient of slope (x-axix) and intercept (y-axis) for ∑DMP (Figure 16a) and ∑DMP*EF (Figure 16b). Northern sites are characterized by a lower slope (below 0.5 for ∑DMP and 0.3 for ∑DMP*EF) and lower intercept.

Indeed sites with bigger plot size constitute a cluster on the lower left corner in both graphs in Figure 16. Figure 16 suggest that there is the possibility to clusterized the field sites, by geographical of ecological features.

This preliminary result suggest that remote sensed model should be improved by a calibration that takes into account the spatial distribution of sites. Hence significant ecological variables were investigated to identify homogeneous patterns to further perform calibration of remote sensed LUE product.

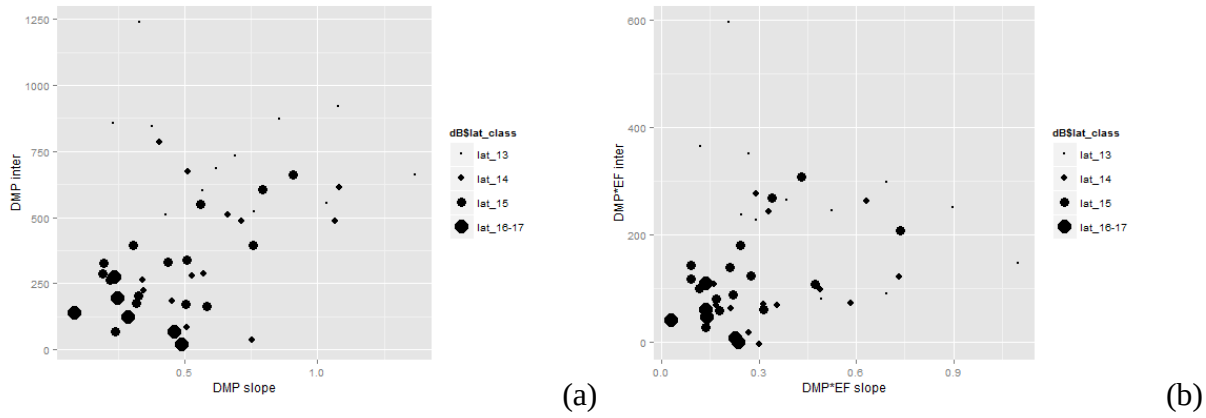

(a) (b)

Figure 16- slope vs. intercept scatterplot in relation to latitudinal position of 46 sites. Panels (a) shows coefficients of DMP vs. field biomass and panels (b) for DMP*EF. Symbol size in proportional to latitude (i.e. the bigger dot correspond to the northern site).

Estimating of phenological metrics

Phenological metrics were calculated as exposed in §Methods in order to investigate the effect of different vegetation in DMP estimation. These data allow to study when the vegetative period occurred in each site and for different year. The phenological information increase our knowledge on field sites behaviour, and give us the further possibility to discern the sites on the basis of ecological satellite derived information.

Estimated phenological metrics consist in the start of wet season/seedling (MIN), , the start of vegetative period/first leaf (SoS), plant heading/flowering (MAX), senescence (EoS), length of vegetative phase (VEG) and length of season (LENGTH). The graphs in Figure 17 shows the time series of 3 sites, as an example.

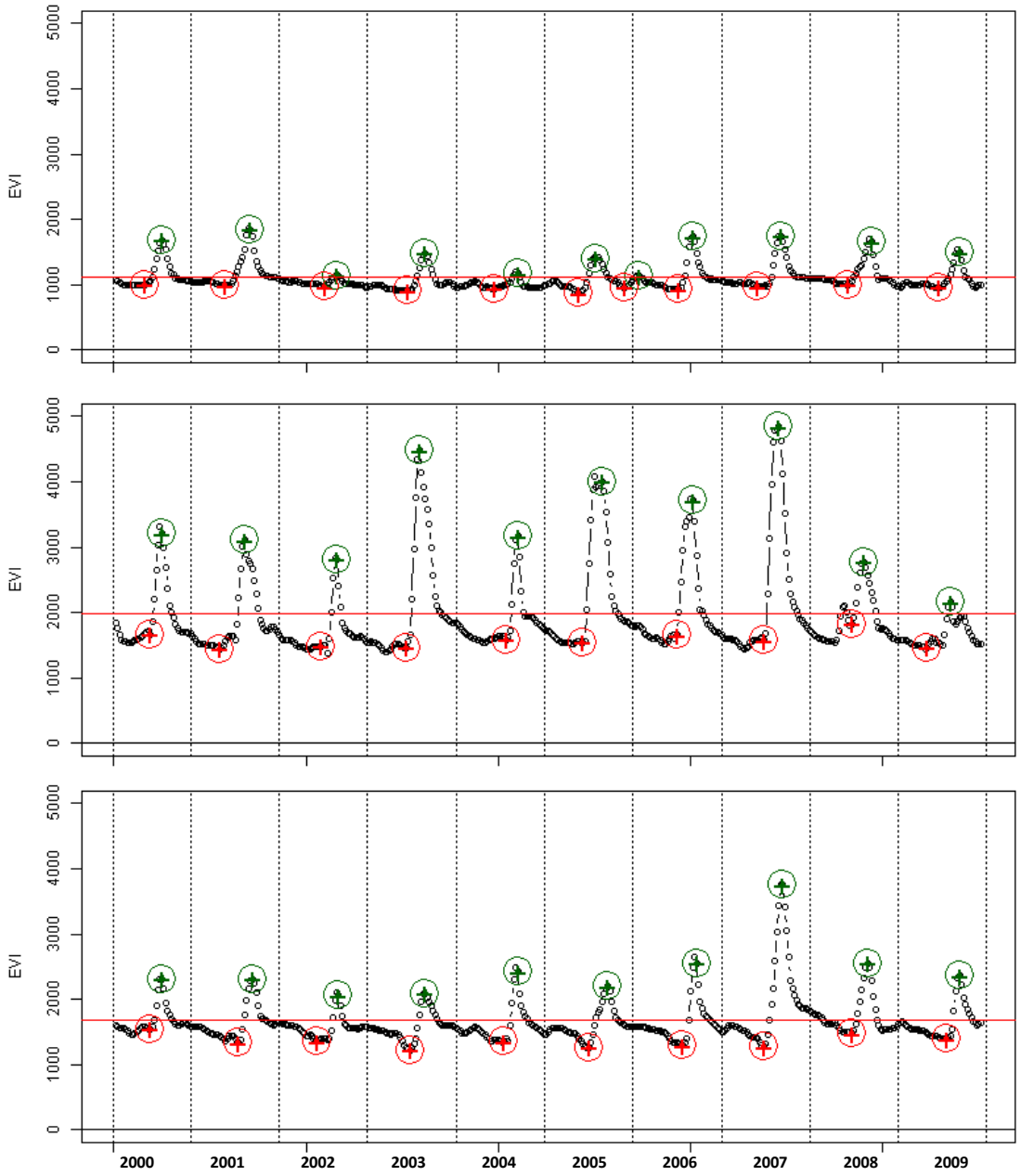

Figure 17- NDVI series with the occourrence of MAX (green stars) and MIN (red stars) for 3 sites. One hiper-arid (a), one southern more humid (b) and one with intermediate condition (c). Red line indicate NDVI threshold of minimum acceptable NDVI value for MAX phase.

The occurrences of MAX and MIN are plotted with green and red stars respectively, if automatically detected by the algorithm. In particular is showed one low productive site (a), one of the higher productive (b) and one with intermediate condition (c). The arid site shows a constant low vegetation growth during the 10 analyzed years. The wetter site (Figure 18b) shows a general high production level with single un-favorable year such as the 2009 (the latter of the series). Finally the last plot (Figure 18c) shows a general poor condition with an anomalous

positive production in the year 2007. These 2 anomalous year, 2007 and 2009, are reported as a particular wet year even with flooding events in Niger (the former) and a particular poor year that have caused a severe food crisis in 2010 (http://www.theguardian.com/commentisfree/2010/aug/03/eastern-sahel-food-crisis-aid, last access December 2013) (the latter). Most of the field site have the highest production in the year 2007. Moreover, most of the sampled data closed to zero happen in the year 2009.

Figure 18 reports the occurrence of phenological metrics calculated on 46 sites along 10 years shows that the earlier seasons started at the begging of June and the later almost in August (MIN) (blue bars in Figure 18), when also rain starts. The start of the plant emergence is comprise between the end and the start of July (SOS) (red bars in Figure 18). The peak of growing season, about flowering, occurs between the end of August and the beginning of September (MAX) (green bars in Figure 18). finally the end of seasons (EOS) happen mainly in October (gold bars in Figure 18).

Globally the length of seasons, comprised between the EOS and the SOS has the length of 3 month, from July to October. The vegetative phase (VEG), between MIN and MAX phases, where most of biomass production is concentrated, has on average the length of 2 month and a half. These estimated data confirm that all the field sites has the vegetative phase included in the JASO period confirming the result from Anyamba and Tucker (2005). Hence for a global study on huge area the JASO period can be considered as a sufficient proxy of vegetated period.

But our single sites can show a huge variation of phenological stages. In particular the former phases (MIN and SOS) have higher variation (up to 45 days) compared to the peak of season and the end of season (about 20 days). The differences of MIN occurrence between sites is the effect of variability of the beginning of wet season, that cause the beginning of vegetation growth. The less differences in MAX and EOS range indicates that vegetation with different MIN complete the life cycle at the same period. Hence vegetation that starts to growth one month later are even capable to reach the flowering before the end of wet season.

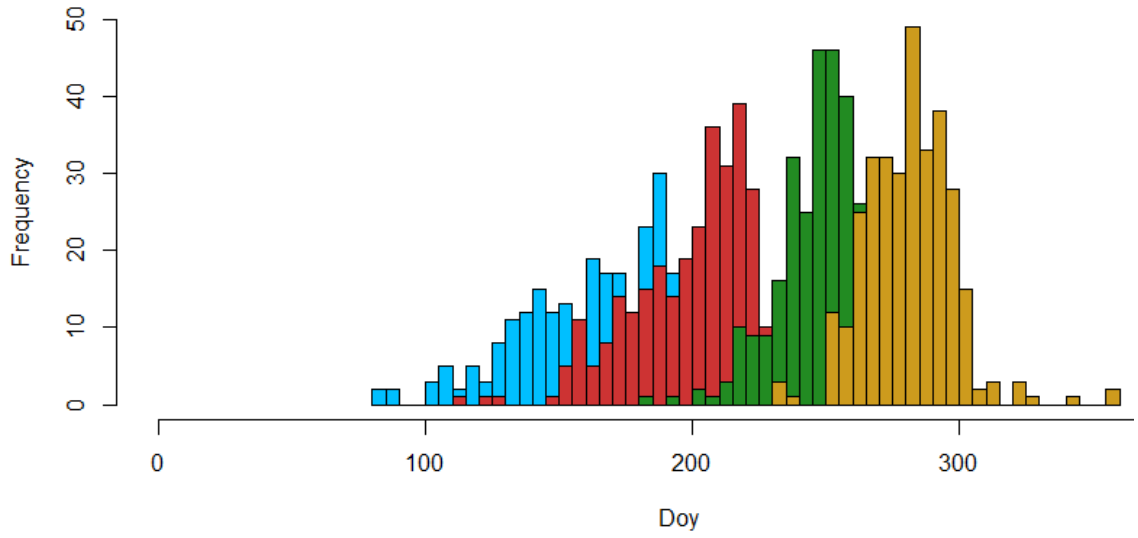

Colour code	Phenology metrics	meaning	Date of occurrence	range days
	MIN	Start of wet season	31 May -15 Jul	45
	SOS	Start of veg. growing	5 Jul - 8 Aug	33
	MAX	Flowering	28 Aug - 17 Sept	20
	EOS	Senescence	27 Sept – 19 Oct	22
-	LENGTH	Wet season	-	102-115
-	VEG	Vegetative season	-	72-82

Figure 18- description of phenological metric calculated on 46 field sites. Histogram represent the distribution of MIN (blue bar), SOS (green bar), MAX (yellow bar) and EOS (red bars) doy occurrence.

Analysis of RS estimation in different ecological units

All the selected sites were analyzed in order to identify closest similarity in term of biomass production efficiency. Phenological analysis, maximum NDVI, LC classes and geolocalization have been considered to identify homogeneous ecological groups for which DMP has homogeneous response to field biomass.

By using a decision tree technique of splitting, the 46 regression slopes of site-specific correlation between DMP and field biomass were clusterized by vegetation behaviour, longitude and latitude. Sites were automatically separated in 3 different groups, as display in Figure 19.

Only two variables were considered significant by the algorithm: the average maximum NDVI (proxy of vegetation density and total production) and the average date of the MIN occurrences (indicator of different ecotypes).

In detail the decision tree separated 15 sites (CL1) where the mean maximum NDVI is moderate high for a semi-arid region (max NDVI > 0.39). These sites are characterized by dense vegetation and are situated in southern part of the study area. A second group of 11 low productive sites (CL2) is located in northern study area and it is characterized by little vegetation production (max NDVI < 0.39) and a late start of season, that occurs after doy 182 (beginning of June). Finally the third group composed by 20 sites (CL3) shows low vegetation growth (max NDVI < 0.39) but an earlier start of season, before the beginning of June (doy 182), representing an average situation between the other 2 groups.

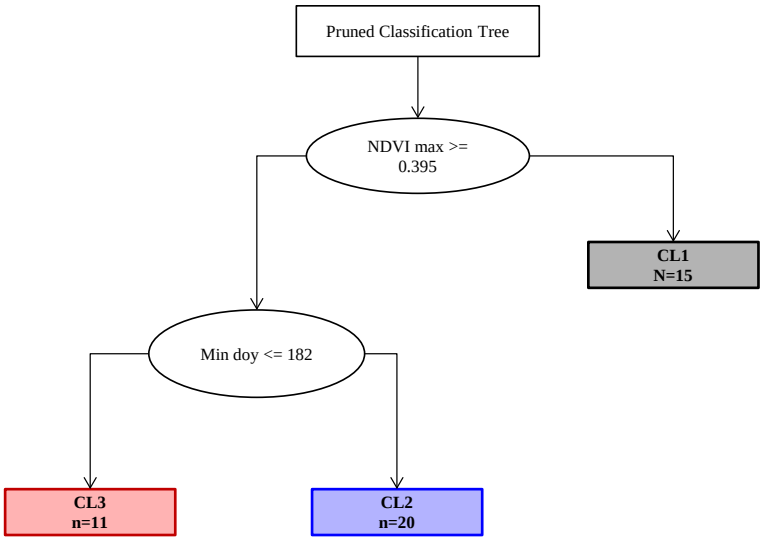

Figure 19- graphical representation of decision tree as obtained from the classification tree technique. CL1 indicated in black, CL2 in red and CL3 in blue. The target variable is the slopes of site specific regression between DMP and field biomass.

In order to further investigate the clusters identified by decision tree techniques the differences of regression slopes DMP between the 3 groups were analyzed by running ANOVA test and post-hoc test Nemenyi-Damico-Wolfe-Dunn (Hollander and Wolfe, 1999). The 3 groups have statistically different slopes at a level of significance of $\alpha=0.001$ ($p<0.05$). The plot in Figure 20 display the distribution of $\sum$DMP (a) and $\sum$DMP*EF (b) along the 3 groups. As expected the first group (CL1, black) includes the higher estimated biomass values (mean DMP > 1000 kg/ha per year) comparable to quite high productive pastureland (Schlecht and Hiernaux, 2006). The second group (CL2, red) is composed by lower biomass estimation (mean DMP < 500 kg/ha per year) comparable to marginal areas (Justice and Hiernaux, 1986) and the third (CL3, light gray) denotes an average biomass production.

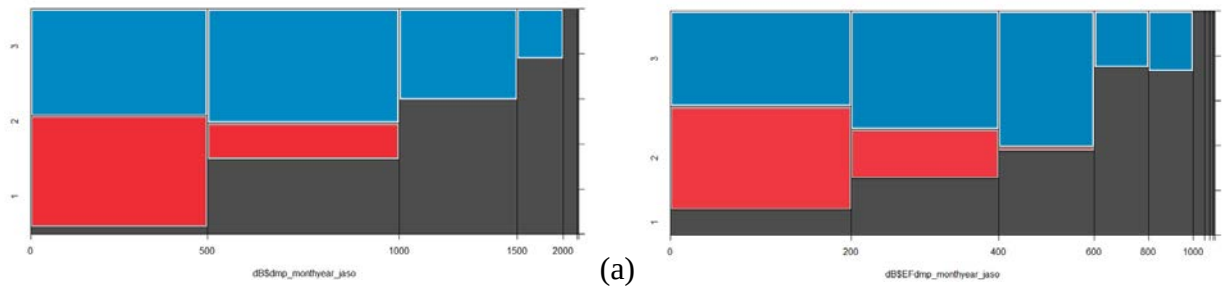

(a)

(b)

Figure 20- distribution of ∑DMP(a) and ∑DMP*EF (y-axis) data along the clusterized groups(x-axis): the first (CL1,dark gray), the second (CL2, gray) and the third (CL3, light gray).

The split on regression slope allow to separate 3 cluster with different DMP correlation to measurements. In Figure 21 the correlations of the 3 groups between ∑DMP (a), ∑DMP*EF (b) and field data represented. The correlation for each group is always higher than the overall correlation, analyzed in Figure 12. Regarding the DMP, when the global correlation has a r^2 of 0.29, reaches values of 0.42, 0.30 and 0.64 for CL1, CL2 and CL3 respectively. These values are slightly higher for DMP*EF model (CL1=0.46, CL2= 0.34, CL3= 0.68) (Figure 21b). Thus the splitting techniques highlighting sites where statistically different in slope between DMP and field measurements is present.

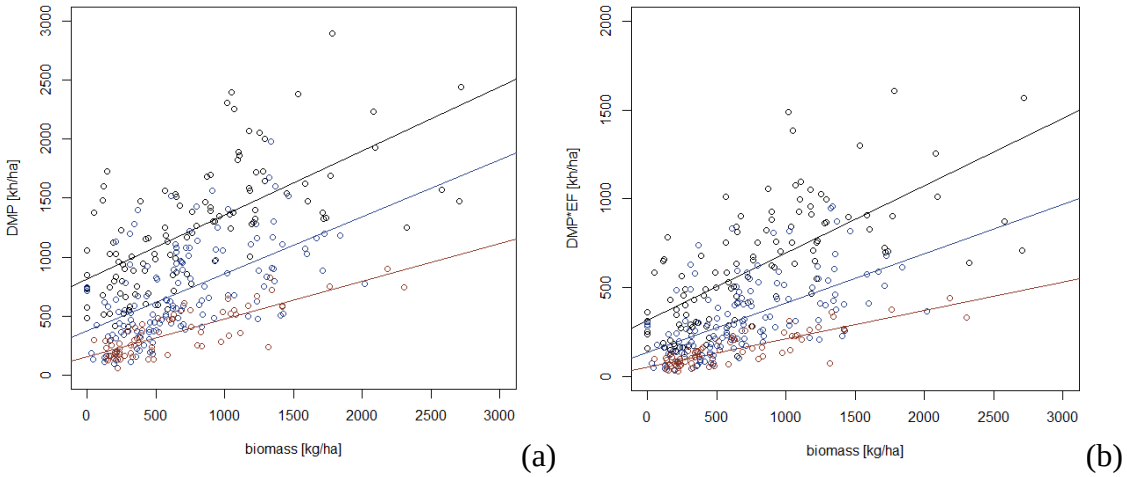

(a) (b)

Figure 21- correlation between ∑DMP (a) and ∑DMP*EF (b) annual cumulation (y-axis) with field biomass (x-axis) for the 3 clusterized groups. CL1 represented by black dots, CL2 red dots and CL3 blue dots (n=320)

Calibration and validation of empirical model for biomass estimation

The performance of ∑DMP and ∑DMP*EF were analyzed on these 3 groups. In order to assess if the water stress factor significantly improved the biomass estimation. Data plotted in Figure 21 were divided randomly in 2 groups for calibration and validation purposes. The 320 available

records of field data were randomly divided respectively in 159 and 161 datasets for the calibration and validation of regression model between remote sensing estimation and field data. The regression models for calibration purpose were set on each classes. The obtained coefficients of slope and intercept are exposed in Table 8.

Table 8- regression coefficients of slope and intercept for the calibration dataset

			∑DMP*EF			**∑DMP**		
cluster	Site	Cal Cardinality	Inter	slope	r^2	Inter	slope	r^2
CL1	20	55	203.16	0.56	0.48	635.36	0.82	0.42
CL2	11	34	29.84	0.21	0.73	101.80	0.45	0.68
CL3	15	70	-11.13	0.53	0.40	73.48	0.99	0.38
Tot	46	159	-	-	-	-	-	-

These coefficient obtained from 3 RMA equations, were used to calculated 161 simulated field biomass to be compared with validation dataset. The final result is summarized in Table 9. Estimated biomass from ∑DMP*EF data has the higher correlation respect ∑DMP in all CLs. The best model performance was obtained for CL2 with determination coefficient of 0.67. Also the indices of RRMSE and EF indicates that ∑DMP*EF based model produced higher quality estimations.

Only the CRM index indicates that ∑DMP*EF has higher overestimation on the 3 CL and especially on CL3 (CRM=0.12), compared to ∑DMP.

Finally scatterplots in Figure 22 shows the agreement between observed the simulated biomass, for ∑DMP*EF (a) and ∑DMP (b), obtained with calibration parameters reported in Table 8. The different color represent simulated data obtained from parameters of CL1 (black dots), CL2 (red dots) and CL3 (blue dots). Both scatterplots have higher correlation (0.44 ∑DMP*EF, 0.41 ∑DMP) compared to the data showed in Figure 12 and higher slope (slope: 0.61 ∑DMP*EF, 0.58 ∑DMP).

Table 9- Indices of agreement (RRMSE, EF, CRM, R2) between measured data and satellite estimate for ∑DMP and ∑DMP*EF. In bold best values comparing the two models.

	∑DMP*EF				∑DMP			
	RRMSE	EF	CRM	R2	RRMSE	EF	CRM	R2
Min	0.00	-inf.	-inf.	-inf.	0.00	-inf.	-inf.	-inf.
Max	+inf.	1.00	+inf.	+inf.	+inf.	1.00	+inf.	+inf.
Best	0.00	1.00	0.00	1.00	0.00	1.00	0.00	1.00
CL1	**67.96**	**0.39**	-0.09	**0.47**	70.00	0.35	**-0.08**	0.44
CL2	**43.23**	**0.67**	-0.03	**0.67**	44.63	0.65	**0.00**	0.65
CL3	**58.78**	**0.20**	0.12	**0.32**	61.05	0.14	0.12	0.27
Tot	**59.94**	**0.38**	**0.01**	**0.44**	62.12	0.33	0.02	0.41

Data are distinguishable around the 1:1 line (dotted lines in Figure 22), as suggested by CRM closed to zero (Table 9). Estimated biomasses from CL3 (blue dots) are the most spread in both graphs, and indeed CL3 has the lower regression (0.32) coefficient and EF (0.20).

This class is the "intermediate one", as resulted from decision tree (Figure 20), and has the widest distribution of DMP values. Probably this class can be further split by other significant ecological features in order to separate areas with more homogeneous DMP efficiency (Turner et al., 2002). As a general comment the inclusion of EF, water availability/stress factor, improve the biomass estimation increasing the goodness of fit of observed vs. simulated regression.

This approach, here applied on field site, can be extended for the entire study area. Satellite information of NDVI allow us to produce the needed information to split the study area in 3 region (CL1, CL2, CL3). Hence the equations extrapolated from calibration of field dataset and validated can be applied to every pixels of the DMP*EF maps.

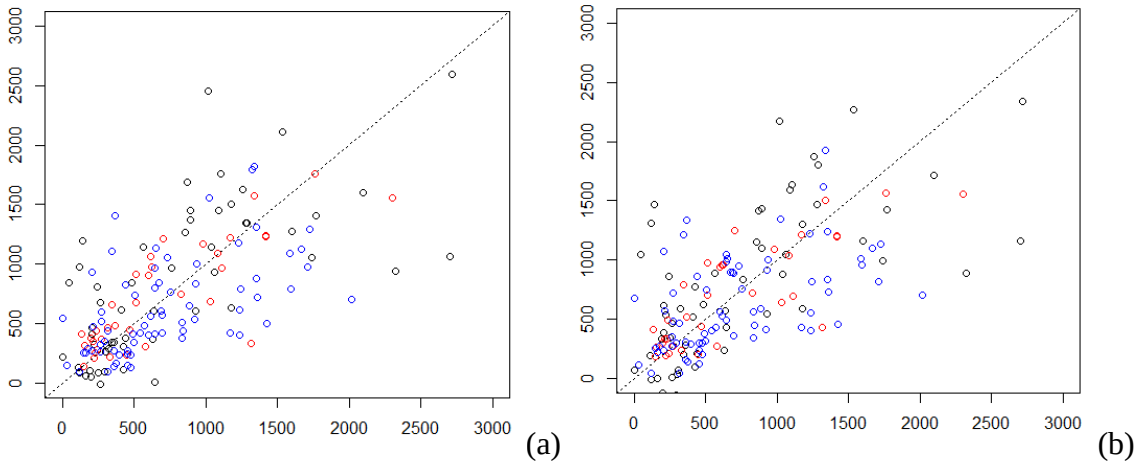

Figure 22- correlation between ∑DMP*EF (a) ∑DMP (b) simulates biomass (y-axis) obtained from calibrated regression models and field data (x-axis) from the validation dataset. (n=161)

4.6. Discussion and Conclusion

This work focused to the study of Sahelian pasture, with the purposes of evaluating the reliability of the Dry Matter Productivity (DMP) in a semi-arid region characterized by wide climate variations and periodic of food supply. The study wants to further test the contribution of remote sensed EF as a water stress efficiency factor in biomass estimation. The comparison of remote sensed DMP estimation on land cover classes with reference information from literature indicates these satellite estimation provides a reliable representation of Nigerien pastureland production in space and time when compared to field data. The satellite estimations evaluated on single site resulted highly correlated to biomass data, on the contrary when all sites are analyzed together the DMP vs. field data scatterplot resulted strongly disperse indicating that the simplified DMP model is not properly calibrated and not able to reproduce the different processes in vegetation compound. The variability of site specific DMP goodness of fit suggest that this LUE model should be implemented with efficiency factors depending on ecosystem units and vegetation types, that allows to group the data in significantly different eco-units. The calibration and validation of satellite estimation on area where vegetation compound has different behaviour allowed to produce significant biomass estimation. Moreover the EF, use to correct the LUE estimation, allowed to increase the goodness of biomass estimation. The results provide some hints on the direction to be followed to improve LUE model: the inclusion of an efficiency term related to water availability/stress and the definition of specific radiation use efficiency values for different ecological units. In particular the direct comparison between ∑DMP*EF and ∑DMP model, conducted thanks to normalized data, indicates that if EF is included the LUE model is more sensitive to biomass variability. This findings support the possibility of performing biomass estimation and rangeland monitoring in semi-arid region using appropriate RS technologies and modelling. The importance and influence of ecological variables should be further analyzed and investigated in order to better calibrate the remote sensed LUE product in relation to biomass data. In order to improve the evaluation of the results, maps of simulated biomass can be produced by applying the methodology on the entire Sahelian region.

CHAPTER 5: Conclusion

This work was directed to study the savannah rangeland ecosystem of Sahelian region, the semi-arid region of West Africa. This region is a transition belt between the Saharan desert on north and Soudanian forest on south, with a gradient largely driven by annual rainfall. Characteristic of the region is the strong rainfall seasonality, with a short wet season followed by a long dry season when precipitations are absent and most of the Sahel becomes arid with few or absent fresh herbaceous vegetation. Moreover, the seasonal rainfall is very erratic. Annual rainfall in the same Sahelian area can abruptly vary from 400 mm/y in one year to almost absence precipitation in another, with no chance to forecast this shift and serious impact on the livelihood that depend on productivity of rainfed natural ecosystems.

Vegetation growing and human livelihood strongly depend on this particular climatic condition. Herbaceous vegetation is constitute by C4 plants, capable to terminate their life cycle in few months. The presence of the different fodder species vary depending on climatic trend and fire occurrences. Also the shrubs are adapted to water scarcity forming the typical tiger bush pattern, vegetation is organised in facieses that alternate extremely open stands and dense thickets. The run-off on open stands make available more water for the dense vegetated spots. These herbaceous and shrub vegetation constitute the typical Sahelian landscape, with sparse trees and bushes surrounded by open area vegetated during the shot wet season.

In this ecosystem the predominant sources of food production are nomadic pastoralism, especially in northern areas closed to Sahara desert, and rainfed agriculture, strongly dependent to manure and profitable only in local favourable areas. Agropastoral activities has developed a series of effective strategies to cope with erratic climate, among which transhumance for pastoralist and manage the seedling time for farmers.

Despite these adaptations the area witnessed a dramatic food crisis in the 1970s–1980s, which was caused by prolonged drought, forced by anomalies of the Atlantic Ocean surface temperature. Despite a general increasing in annual rainfall during the last decades, local environmental crisis periodically occurs in the Sahel (the last one in 2010) and food security still remain a concern. Two approaches are commonly adopted to increase environmental and food security of an area, i) the increase of cropped areas and/or ii) improve the natural resource production efficiency. In the Sahel, as in other semi-arid area, it no possible to increase the arable land as well as it is difficult to improve production efficiency. Agropastoral livelihood are

already well adapted to this marginal eco-climate, and top-down policies can damage the Sahelian resiliency rather than increase it.

Hence a better management of existing resources is the most (only) profitable option strategy to increase food security in this context. This can be achieved by providing i) information to plan a better exploitation of ecosystem carrying capacity and ii) early warning alarms about the ongoing season. Satellite remote sensing can contribute significantly to these tasks by collecting information on crops and on environmental variables at a sub-continental geographical scale and with a high temporal frequency. In fact several food programs exploiting RS techniques, stressing the importance of satellite data in drought monitoring creating a baseline of thematic information to evaluate magnitude and direction of future changes in order to provide anticipated hints of new possible droughts.

The PhD research conducted can be subdivided in two main parts, referred to the different tasks for environmental security goals. First of all – Session 1 of this manuscript- satellite time series were analysed to identify and evaluate environmental anomalies with the final goal to improve knowledge on Sahelian rangeland status and then – Session 2 - a method to produce information on rangeland biomass and status to support natural resource monitoring were tested.

The identification of anomalies in the past decade was carried out by trend analysis of proxy of vegetation production (NDVI) and rainfall. The analysis confirm that the area is not facing a general land degradation, and rainfall is the main driving force and limiting factor in vegetation growth. However the hot-spots detected highlight area with increase in vegetation growth even in conditions where rainfall remained stable. Some of these spots correspond to the intensification of cropping in fertile floodplain (Niger) or rice district (Mali). This first result suggest that in local favourable area there is the opportunity to improve factors of production efficiency such as first of all irrigation but also manure management or use of new varieties. This result partially contradict well-known information that the Sahelian agropastoral area is so marginal that no gaps between measured and the ecosystem's potential yield exist. On the other hand, degradation hot-spots – detected where NDVI decreases with no relation to rain - were mostly located in the Sahelian fragile zone a region where it is well-known that food security strongly depend on climatic conditions. These small pockets of anomalous degradation have been identified mainly in rangeland area, where pastoralism is the most important livelihood activity.

These information can be a support regional scale management planning of natural resources exploitation. Indication of local chronic anomalous area where vegetation decrease over years, could allow local experts to further investigate and focused on specific zones prioritising field survey and intervention. The Sahel rural population is still growing, on the contrary of many other parts of the world, and locally human pressure such as overgrazing along transhumance itinerary and wood exploitation around villages can locally endangered the ecosystem carrying capacity if sustainable management is missing. Information on local chronic situation allows a feasible top-down approach in natural resources management, with no general intervention on local procedure in resources management but focusing on specific zones.

The second part of the present thesis focused on the estimation of crucial variables in rangeland monitoring, the biomass production and the water availability for vegetation.

Time series of water stress proxy – Evaporative Fraction EF - from low resolution RS data was obtained exploiting a methodology originally developed for evapotranspiration estimation. Despite the course resolution of satellite EF (1 km), seasonal estimation of this parameter show an un-expected good correlation with field measurement energy fluxes ($r^2 > 0.7$). This analysis was the first one that demonstrate the reliability of satellite EF estimation, as a proxy of water availability/stress, in semi-arid region of Sahel. The tested method to generate the water availability proxy is of extreme utility to support biomass estimation in the study area since the Sahel is well-known region characterized by shortage water.

The available DMP operation product of biomass estimation was analysed and evaluated to assess its suitability rangeland monitoring. Biomass maps can improve monitoring tools because give a quantitative evaluation of available vegetation on ground, increasing the qualitative information provided by commonly used vegetation proxies. Obviously quantitative biomass estimation can be directly linked with fodder needed for the herds currently presents in an area i) indicating if potential risk of overgrazing can occurs and ii) suggesting where is more convenient/sustainable to conduct pastoral activities. It is nice to note that areas indicated as bare soil by commonly available moderate resolution thematic map of land cover (e.g. Glob Cover or GLC) can have in reality a considerable amount of annual biomass production (up to 700 kg/ha).

Results from DMP analysis highlight that biomass estimation can be improved following two main guidelines. First of all the satellite derived water stress (EF) can be included in the LUE algorithm as an efficiency factor term, improving the goodness of model site specific biomass estimation. Secondly an improved LUE model can be obtained if different radiation use

efficiency values are taken in account, depending on ecological units indicating that different vegetation types and associations are present on ground.

This conclusion was achieved by analysing DMP model performance, exploiting classification tree techniques, in relation to different environmental/vegetation related variable. This investigation highlighted that DMP shows statistically different correlation with ground biomass in relation to different ecological units, identified thanks to phenology and proxy of vegetation production. RS data analysis can provide the operational method to spatialise significant ecological variables, hence to produce more robust biomass estimation maps on the entire Sahelian region. The importance and influence of ecological variables should be further analyzed and investigated in order to better calibrate the remote sensed LUE product in relation to biomass data. Moreover, currently RS estimation of annual vegetation production over the Sahel are obtained by considering a fix vegetative period between July and October. However, it is well known that vegetative seasons and plant productivity show a strong variability that change year by year within and outside the JASO period. Satellite base operational phenological estimation could be exploited to detect in time and space the occurrence of season start/end potentially improving the flexibility of biomass estimation and related monitoring system.

In conclusion, satellite biomass estimation corrected by water availability and including eco-types radiation use efficiency, once operationally produced and validated, could provide the necessary information for i) the creation near real time bulletin of ongoing season and, if the annual estimated production will not be able to sustain existing herds, ii) identification of early warning alarming of food shortage and consequent potential critical situation occurrence.

Further improvement on these analysis will concern in the extensions of hot-spot detection by extending the work done in the period 1998-2009 to current year. The anomalies can be further investigated also analysing the time series of biomass estimation provided by the new LUE model proposed. Biomass estimation gives the capability to explore the detected hot-spot in quantitative terms of biomass lost/increase. Hence giving estimation of the endangered carrying capacity of rangeland natural resources in the Sahel.

ANNEX

1. Annex: auto-correlation in time series

When studying natural processes, such as seasonal vegetation production, the more frequent the data points the more possible is the auto correlation in the data. Being aware of autocorrelation can avoid misinterpretation of trends. As said by de Jong and de Bruin, (2012) in case of seasonal data with a dense sampling interval, both starting phase and extent influence the linear model. They shows a NDVI time series demonstrating that the true change in NDVI (i.e. zero in the example) is only obtained by aggregation over complete cyclic periods.

As a rough guideline, daily series are usually strongly correlated, annual series are often approximately independent, and monthly values are intermediate (World Meteorological Organization, 2000).

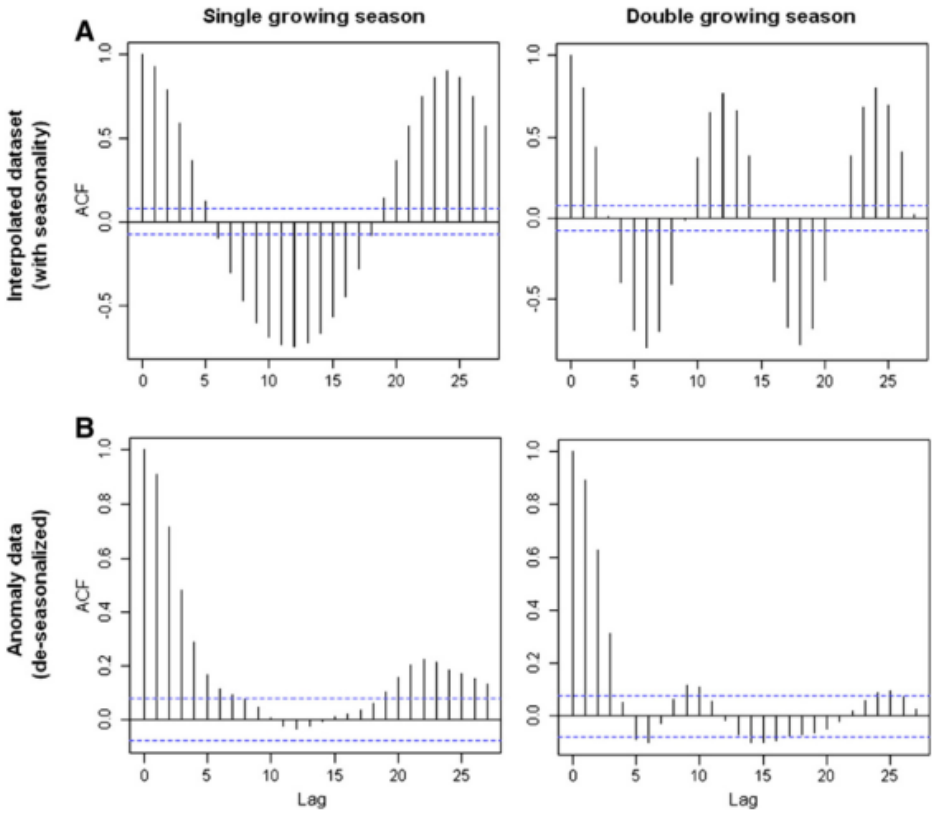

Figure 1- Average auto-correlation functions (ACF) of GIMMS data (A: interpolated, B: anomalies) with fortnightly lags (lag 24=1 year). Source: de Jong et al., (2011). Blue dotted line indicates the critical value.

Figure 1 shows that when the absolute values of the autocorrelation coefficients of lag-1 to lag-3 (i.e. the first 3 bars in the graphs) calculated for a time series observations is not larger than the typical critical value (5% significance level), then the observations in the time series can be considered as independent from each other (Bai et al., 2008). Figure 2 display that normalized

data are less auto-correlated. Following this example the test was conducted on NDVI time series in 3 Sahelian sites (Figure 2). Left panel reports 3 auto-correlogram for 11 years of 10-days NDVI (1998-2009). Since the bars outdo the critical value in every sites, data can be considered auto-correlated. The right panel reports the cumulated data, over the JASO period.

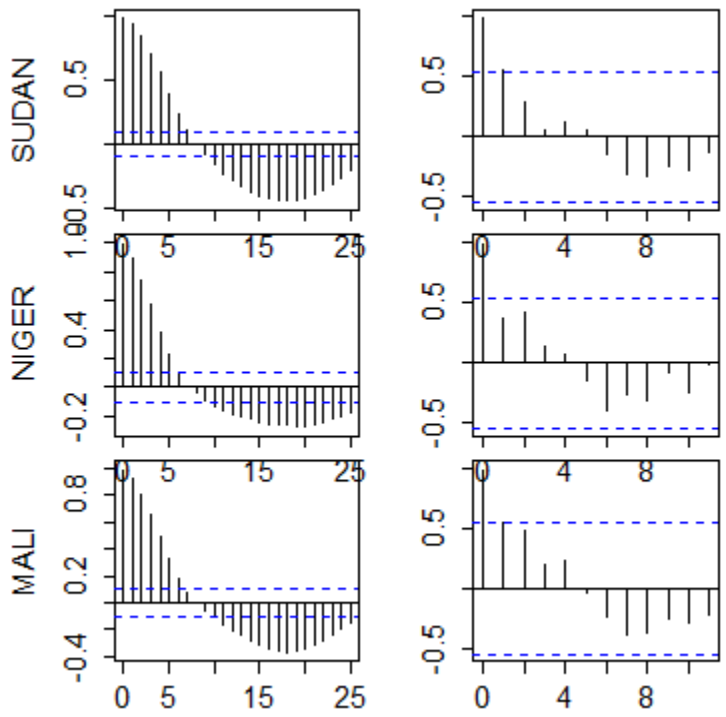

Figure 2- auto-correlogram for 3 NDVI time series. Left panels displays full 10-days data, right pales annual cumulates.

2. Annex: Dry Matter Productivity

Dry Matter Productivity (DMP) is a 10-daily data representing an estimation of dry matter, oriented towards agricultural crop monitoring and yield estimation. DMP reflects the daily increase of the dry matter biomass (growth rate) of vegetation and is expressed in kilograms of dry matter (kg DM) per hectare per day. The developer is Flemish Institute for Technological Research – VITO, situated in Belgium.

Product is based on well-known Light Use Efficiency (LUE) model developed by Monteith in 1972. He observed that vegetation growth is completely defined by the part of the incoming solar radiance that is absorbed for photosynthesis (APAR) and a number of efficiency factors (ε). Among them the most important is the actual efficiency of converting atmospheric CO2 into plant tissue. The Monteith Dry Matter Productivity can thus be expressed as follows:

$$\boldsymbol{DMP = APAR * \varepsilon 1 * \varepsilon 2 * \varepsilon 3 \ldots} \qquad \textbf{Eq. 1}$$

This simple formulation provides a functional modelling framework where single efficiency factors can be added to the basic formulation in order to improve modelling complexity. Monteith used his formulation to explain the variations in biomass accumulation between different vegetation types and climatic zones.

The quality of the final assessment depends on the efficiency factors accuracy. Over the years several Monteith-variants were developed and since remote sensing and weather modeling data were provided the LUE approaches has been exploited to produce regional to global biomass estimation.

The DMP approach exploits satellite and meteorological model derive data (ERA-Interim dataset) resulting in this formulation:

$$\boldsymbol{DMP = [R * 0,48] * fAPAR * \varepsilon(T) * \varepsilon(RUE)} \qquad \textbf{Eq. 2}$$

Where the terms are explained in Table 1:

Table 1- Individual terms in the DMP approach. All terms are expressed on a daily basis.

	Meaning	Value	Unit
DMP	Dry Matter Productivity	0 – 320	kgDM/ha/day
R	Shortwave incoming radiation (200 - 300 nm)	0 – 320	GJ_T/ha/day
0,48	Fraction of PAR (400 – 700 nm) in total shortwave	0.48	J_P/J_T
*f*APAR	PAR-fraction absorbed by green vegetation	0,0 ...1,0	J_{PA}/J_P
ε(T)	Efficiency term (function of temperature, autotrophic respiration and CO_2)	0,0 ...1,0	-
ε(RUE)	Radiation use efficiency	2,54	$kgDM/GJ_{PA}$

The efficiency term ε(RUE) accounts for the conversion of absorbed energy into biomass (Radiation Use Efficiency) and ε(T) for the losses related to temperature stress, the transport of photosynthetates, the maintenance of the standing phytomass, and other biochemical process (Veroustraete et al, 2002). The function is non-linear as show in Figure 3, and it reaches a maximum at a temperature of 22°C and approaches zero for temperatures below 0°C or above 40°C. The 3 lines represent the different efficiency due to the increasing of CO_2 concentration.

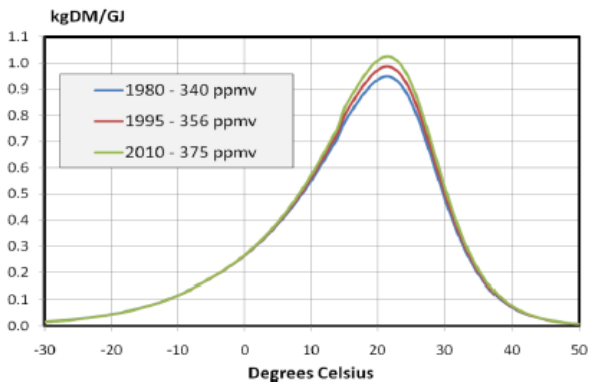

Figure 3- relation between DM[kg] temperature and CO_2 concentration. Behavior typical for C3-species. Source: VITO's comunications

VITO's practical approach

The practical approach of DMP estimation is based on 3 steps. DMP inputs are fAPAR, radiation, temperature and CO2 (actually a global constant). CO2 concentration is fixed at 355,61 ppmv, that is the global mean level of the year 1994. The DMP-software built function which automatically adjusts the CO2-level between the years, but in practice this has never been used.

First step generate DMP_{max} represents the maximum reachable DMP, for the (virtual) cases where fAPAR would be equal to one.

$$\boldsymbol{DMP_{max} = R * \varepsilon(T, RUE)} \qquad \textbf{Eq. 3}$$

Where R is the incoming short wave radiation of the sun (200-3000 nm) [GJ_T/ha/day] and $\varepsilon(T,CO_2)$ is the efficiency term [kgDM/JPAR] (Figure 4). DMP_{max} images have daily temporal resolution.

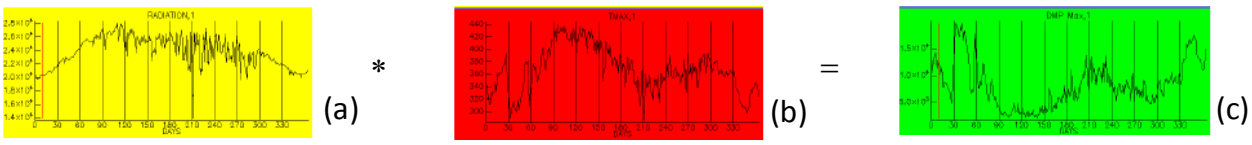

Figure 4- visual representation of DMP_{max} calculation for one pixel over a year in Malian rangeland. (a) Incoming solar shortwave radiation [kJT/m²/day], (b) Daily maximum temperature [deci-degrees], (c) DMP_{max} derived with the Monteith approach from the daily meteodata. Source: VITO's comunications

DMP_{max} represents the maximum reachable DMP for the (virtual) cases where *f*APAR would be equal to one. At the end of every decade (10 days), first a new image is computed as the mean of the 10 daily DMP_{max}.

$$\boldsymbol{DMP_{max,10} = \{\Sigma\, DMP_{max}\} / 10} \qquad \textbf{Eq. 4}$$

Where DMP_{max} is the daily product and 10 is the number of days (Figure 5).

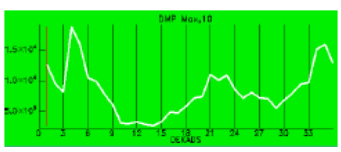

Figure 5- ten days DMP_{max} over a year (n=36).

The resulting image ($DMP_{max,10}$) is then resampled (bilinear interpolation) to the same resolution as the fAPAR image, derived from SPOT-VGT (1km). And next, both are simply multiplied to retrieve the final image with the DMP estimates.

$$DMP_{10} = fAPAR_{10} * DMP_{max,10} \quad \text{Eq. 5}$$

Where: *f*APAR is the PAR-fraction absorbed by the green vegetation [J_{PA}/J_p]. $DMP_{max,10}$ is the average DMP_{max} in a decade (Figure 6). The *f*APAR data is comprise between 1 and 0, whit low data corresponding to sparse vegetation and high data to dense vegetation.

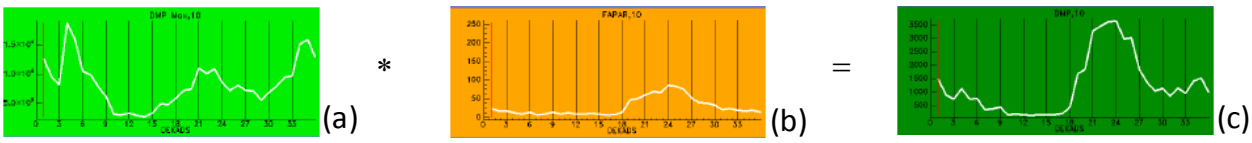

Figure 6- visual representation of DMP_{10} calculation for one pixel over a year. (a) DMPmax for one dekad, (b) fAPAR derived from the VGT-S10, (c) the final DMP is the product. Source: VITO's comunications

3. Annex: Linear regression models

In the ecological literature, method Ordinary Least Squares (OLS) is referred to as Model I regression and all other methods, including major axis (MA), standard major axis (SMA), and ranged major axis (RMA), are referred to as Model II regressions. The most widely used is the Least Squares Regression (OLS) that minimizes the sum of the squared vertical deviations. This model wasn't chosen in order to produce simulation biomass because the reference field data are characterized by errors and aren't normally distributed as showed by Lillie test of normality (p-value < 0.05) (Dallal and Wilkinson, 1986). Hence several approaches were testes to fit the best regression model. Major axis regression (MA) that minimizes the sum of the squared perpendicular deviations (also called orthogonal regression), the Reduced major axis regression (RMA) that minimizes the sum of the area of right triangles whose legs are the horizontal and vertical deviations (also called geometric mean regression or standardized regression) and the Ranged major axis regression (RMA in R) in which both the x and y-variables are first transformed by the equation. This last model is discussed in (Legendre and Legendre, 1998) who are its major proponents arguing that this protocol corrects the defects of MA and the defects of RMA making this the best method overall. They conclude that MA regression was appropriate when both variables are measured on the same scales with the same units, or are dimensionless. They described a modification of MA regression when firstly the variables are standardized by their ranges, the MA regression is calculated, and then the regression slope is back-transformed to the original scale. The advantage of ranged MA regression is that the variables don't need to be in comparable units. Because of dependent variable DMP is in the same range of field biomass but DMP*EF not RMA regression was exploited in order to use the same regression approach for both satellite estimations.

4. Annex: Evapotranspiration estimation

In-field ET measurement

Traditional ET measurements to support agriculture studies are based on pan evaporation, which is still widely used, or large scale weighing lysimeters (Vinukollu et al., 2011). A lysimeter is a measuring device which can be used to measure the amount of actual evapotranspiration which is released by plants, usually crops or trees. By recording the amount of precipitation and the amount of water lost through the soil, the evapotranspiration can be calculated. The lysimeter gives the amount of water lost by evapotranspiration by a difference between the weight of volume of land measured before and after the precipitation.

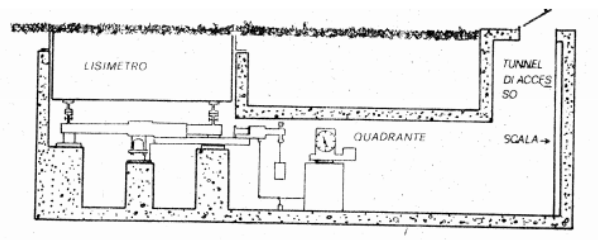

Figure 7- lysimeter scheme

The development of instrumentation for measuring scalar fluxes and vertical wind during the 1970s allowed to produce easily ET estimation. These fluxes are strongly linked to the capacity of atmosphere to transport heat and water vapour. The instruments that can measure these fluxes are cost efficient compared to lysimeter, such as eddy-covariance tower and scintillometer (Ciraolo et al., 2007; Vinukollu et al., 2011). Nowadays, hundreds of eddy-flux towers have been set up globally for constant measurements of surface water and carbon fluxes. Many of these stations are organized within the FLUXNET international program (fluxnet.ornl.gov). There are more than 140 eddy covariance sites on five continents in the FLUXNET network, that currently measure the exchanges of energy and water between the land surface and the atmosphere (Tang et al., 2013).

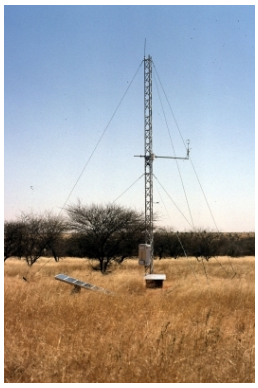

Figure 8- eddy covariance tower over a Sahelian savannah

However, these sparsely distributed tower sites are insufficient for regional, and global studies, due to the heterogeneity of the earth's surface. In spite of high accuracy of such techniques, their use over large areas can be limited due to the number of sites needed and the related expense (Irmak et al., 2011). However data from eddy tower are frequently used in order to calibrate new approaches of flux measurements (Yuan et al., 2007; Sjöström et al., 2011), to study plants physiology or ecosystem (Bagayoko et al., 2007; Gentine et al., 2007; Lindroth et al., 2008; Yang et al., 2013) or to validate an estimation obtained from model or remote sensing (Kurc and Small, 2004; Fensholt et al., 2006; Hadria and Duchemin, 2006; Kanniah et al., 2009; Galleguillos et al., 2011; Ruhoff et al., 2012; Sepulcre-cantó et al., 2013). One of the main constraints of this technique to validate remote sensing estimation is the fetch over which eddy-covariance towers can sample (Heinsch et al., 2006). The towers footprint has a range that vary between 30 and 1000 meters, depending on its height, wind condition and height of canopy, and how this footprint is representative of a satellite image pixels (such as MODIS 1 km) is an open issue (Chasmer et al., 2011). At any rate eddy covariance data have been considered enough robust to validate low resolution satellite estimation in semi-arid and savannah areas (Kanniah et al., 2009).

Remote sensing model-based estimation methods

Remote sensing provides a potential method to estimate ET at different spatial resolution and temporal steps. Development of satellite remote sensing techniques has been motivated by the limitations to measure ET at large scales using ground-based methods (Irmak et al., 2011; Ruhoff et al., 2012).

Satellite data are suited for deriving spatially continuous fields of ET. Furthermore, remote sensing is at present the only possible way to get completely-observational driven, spatially and temporally continuous ET products (Vinukollu et al., 2011).The challenge to the use of RS for

monitoring ET is that the phase change of water molecules produces neither emission nor absorption of an electromagnetic signal. Therefore the ET process is not directly quantifiable from satellite observations. It has to be assessed, taking advantage of information gained through the satellite about surface bioclimatic variables. For distributed ET estimation there are two major difficulties: the requirement of complex land surface model which must be interfaced with remote sensing data and the necessity of surface meteorological observations that are not readily available over large areas (Jiang et al., 2009).

Remote sensing provides and economical and reliable way to estimate ET over large heterogeneous areas. Several algorithms have been developed for estimating ET from remotely sensed rough data, such as Land Surface Temperature (LST, or T_s) and vegetation indexes (VI). Models to estimate terrestrial heat fluxes and ET adapted for remote measurement may be classified into three types: i) Penman-Monteith based models, ii) Priestley-Taylor based and iii) single source energy budget model (Verstraeten et al., 2005; Vinukollu et al., 2011).

Penman-Monteith approach

First approach for estimating evaporative flux by combining both the energy balance and mass-transfer approaches, without surface temperature data and surface resistance term, resulted in an equation valid for open water surfaces or vegetation without water limitations (Penman, 1948). Sixteen years later Monteith modified it considering that i) the internal leaf vapor (stomata) is saturated at the leaf temperature, ii) the leaf surface is at the vapor pressure of the surrounding air and iii) there is a resistance that controls the transfer of vapor from the leaf to the surrounding air. This resistance is integrated up to the canopy resistance (Monteith, 1964).

The extended Penman-Monteith equation combines aerodynamic resistance (ra), surface resistance (rs) along with the available energy ($R_{net} - G_{\text{flux}}$).

$$\boldsymbol{\lambda E = \Delta(R_{net} - G_{flux}) + \frac{\rho_a C_p \frac{VPD}{r_a}}{\Delta + \gamma\left(1+\frac{r_s}{r_a}\right)}} \qquad \textbf{Eq. 1}$$

where, ρa is density of air, Cp the specific heat of air at constant pressure, VPD the Vapour Pressure Deficit, Δ is the slope of the saturated vapour curve $\left(\frac{hPa}{^\circ K}\right)$ and γ is the psychrometric constant $\left(\frac{hPa}{^\circ K}\right)$. A shortcoming of the Penman-Monteith approach stays in the parameterization

of the resistances. The Priestley-Taylor approach starts out from the need of coping with this problem.

Priestley-Taylor approach

This methodology is intended to avoid complicated parameterizations that involve heat and momentum resistances to energy transfer for ET estimation, and to avoid numerous correction procedures (Jiang et al., 2009). The Priestley-Taylor approach was developed in 1972 for well watered surfaces, like for Penman one (Priestley, C. H. B., & Taylor, 1972). This introduces the unit-less constant α, with a standard value set to 1.26 for well-watered surfaces, representing the temperature and aerodynamic terms. This multiplier's role is replacing all the atmospheric demand. Its value is empirically related to soil moisture, and from its standard for water stressed surfaces. The Priestley-Taylor equation is:

$$\boldsymbol{\lambda E = \alpha \frac{\Delta}{\Delta+\gamma}(R_{net} - G_{flux})} \qquad \textbf{Eq. 2}$$

Where γ is the psychrometric constant $\left(\frac{hPa}{^{\circ}K}\right)$ and Δ is the slope of the saturated vapor pressure at the air temperature $\left(\frac{hPa}{^{\circ}K}\right)$.

This equation is considered valid only for potential ET (PET), rather than actual ET, but it is shown that it can be adapted to estimate Daily Actual ET (DAET) relying on remotely sensed simple inputs (Jiang et al., 2009). This methodology is based on commonly used energy balance formulation of ET and a contextual relationship between remotely sensed temperature and vegetation index. However, there is the need of using this equation not only under the ideal conditions of well watered surfaces, so it becomes necessary to estimate the α value. It has been shown that this coefficient is a function of Λ, Δ and γ, as shown below:

$$\boldsymbol{\alpha = \Lambda \frac{\Delta+\gamma}{\Delta}} \qquad \textbf{Eq. 3}$$

A more direct way to estimate the value of α is recurring to the following equation, which relies on reference radiometric temperatures:

$$\boldsymbol{\alpha \approx \alpha_{max} \frac{T_{max}-T_s}{T_{max}-T_{min}}} \qquad \textbf{Eq. 4}$$

This methods estimates the actual α value starting from its standard value, α_{max}, equal to 1.26. Tmax and Tmin may be derived by the following way: it has been shown that T and NDVI exhibit a characteristic triangular pattern whose boundaries constitute limiting conditions for the fluxes.

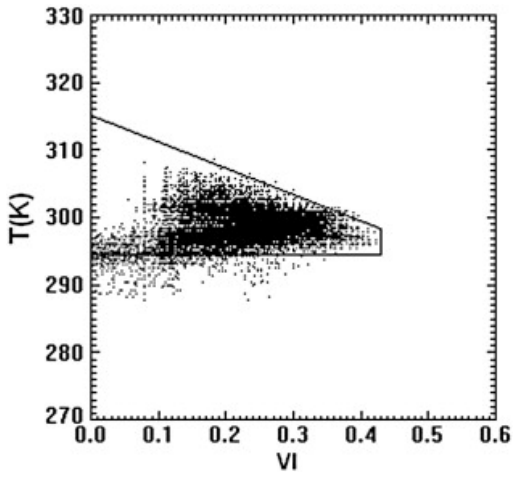

Figure 9: Example of a scatterplot between temperature and a VI (Sandholt et al., 2002).

After plotting remotely derived T vs. NDVI, it can be found that such trapezoid or triangular T–VI space exist for almost all days except heavily cloudy days. Sandholt et al., (2002) also show how a scatterplot of remotely sensed surface temperature and a vegetation index often results in a triangular shape (Figure 9).

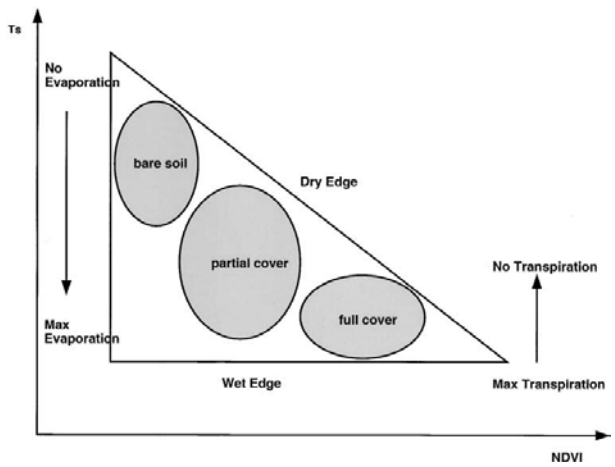

Figure 10: Graphical scheme explaining how to get information from the T/VI scatterplot *(Fensholt et al., 2006)*

Figure 10 in particular explains how to interpret the information contained in the triangular T-VI space. T_{max} and T_{min} are considered the intercepts between respectively the dry edge and the wet edge with the vertical axis. Priestley-Taylor approach has been used to estimate ET from several remote sensing sources, such as MODIS (Venturini et al., 2008; Tang et al., 2010; Vinukollu et al., 2011), AVHRR (Seaquist, 2003; Jiang et al., 2009) and GOES (Mecikalski and Diak, 1999) to produce maps at high temporal resolution.

Energy Balance approach

The land surface energy balance (EB) is the thermo-dynamic equilibrium between turbulent transport processes in the atmosphere and laminar processes in the sub-surface (Bastiaanssen, Menenti, et al., 1998). The basical formulation can be written as:

$$\mathbf{R_n = \lambda E + G_0 + H} \qquad \textbf{Eq. 5}$$

where Rn is net radiation, G_0 is soil heat flux, H is sensible heat flux and λE is latent heat flux.

This formulation doesn't take into account the energy required for photosynthesis and the heat storage in vegetation (Bastiaanssen, Menenti, et al., 1998) because this is just a small and negligible percentage of the whole surface energy balance (Verstraeten et al., 2005). This formula shows that all the incoming solar radiation, both shortwave and longwave (that is the net radiation) can be split in process of soil heating, evapotranspiration and energy flux exchanged between air and surface depending on difference in temperature between them Figure 11). Above these elements latent heat flux (λE), that is the energy required for evaporating water, is of great importance for different applications in hydrology, agronomy and meteorology because it's linked with vegetation presence and status. Since it is always accompanied by vapour transfer, it represents actual evapotranspiration.

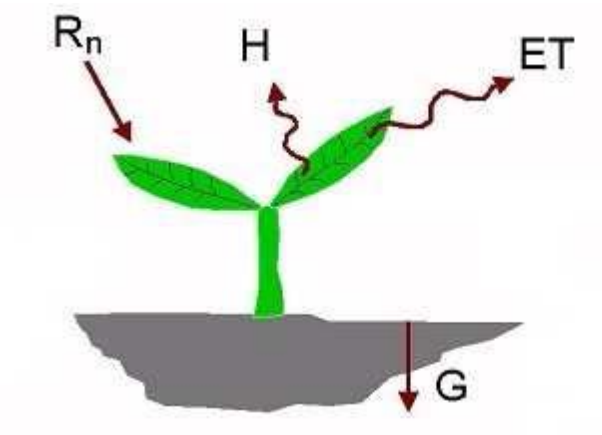

Figure 11: A conceptual representation of the EB in the soil-plant-atmosphere system. Rn is net radiation, G_0 is soil heat flux, H is sensible heat flux and λE is latent heat flux.

Each term of the relation is expressed as $\frac{W}{m^2}$. λE, H and G_0 are considered positive when oriented to the opposite side of the earth surface. The final goal of calculating λE can be reached by estimating the value of all EB terms. To achieve this goal it may be useful to rewrite the EB in the following way:

$$\mathbf{\lambda E + H = R_n - G_0} \qquad \textbf{Eq. 6}$$

Between 1990 and 2005 several energy balance based models were developed for remote sensing approach (Vinukollu et al., 2011). These approaches are summarized in the Table 2.

The aim of such algorithms is to estimate latent heat fluxes and ET at both local and regional scales, using remote sensing with complementary meteorological data.

All of these models require multispectral visible and infrared and thermal information, hence that models can only be used with images acquired on cloud-free days.

Table 2: Some model approaches for ET estimation from remote sensing data and field observations

Acronym	Complete Name	Developers
ALEXI	Atmosphere-Land Exchange Inverse	(Anderson, M. C., Norman, J., Diak, G., Kustas, W., and Mecikalski, 1997)
SEBAL	Surface Energy Balance over Land	(Bastiaanssen, Pelgrum, et al., 1998)
S-SEBI	Simplified Surface Energy Balance Index	(Roerink et al., 2000)
SEBS	Surface Energy Balance System	(Su, 2002)
METRIC™	Mapping Evapotranspiration with Internalized Calibration	(Allen et al., 2007)

G0 estimation

Several remote sensed approaches have been developed to estimate the soil heat flux. The heat flow into the soil appears as a thermal gradient in the upper layers. This gradient is influenced by the vegetation cover properties, the soil moisture and texture. The water in the soil affects the heat fluxes absorbing solar energy, so it is expected that dry soils conduct heat better than wet ones. Here below are proposed some G_0 equations from (Li et al., 2012) (Irmak et al., 2011) and (Bastiaanssen, 2000) which rely on inputs retrievable from remote sensing products (Table 3).

Table 3- proposed algorithm for soil heat flux estimation, where T_s (°K) is the land surface temperature, α_0 is the surface albedo, C_1 is a conversion factor to obtain the daily average surface albedo from instantaneous values (default = 1.1), NDVI is the Normalized Difference Vegetation Index, LAI the leaf area index. Rn is the net radiation and r_0 the broad band surface albedo.

$G_0 = R_n \left[\frac{T_s - 273,15}{\alpha_0}(0,0032C_1\alpha_0 + 0,0062C_1^2\alpha_0^2)\,(1 - 0,978NDVI^4)\right]$	(Li et al., 2012)
$LAI \geq 0,5 \quad G_0 = R_n(0,05 + 0,18e^{-0,521LAI})$ $LAI < 0,5 \quad G_0 = R_n\left(1,80\frac{T_s - 272,15}{R_n} + 0,084\right)$	(Irmak et al., 2011)
$G_0 = R_n \left[\frac{T_{TM6}}{r_0}(0,0038\alpha_0 + 0,0074\alpha_0^2)(1 - 0,98NDVI^4)\right]$	(Bastiaanssen, 2000)

The advantage of these equations (Table 3) is that they relies on satellite products routinely produced by several earth observation programs (MODIS, VGT, AVHRR etc.).

Net radiation estimation

The net radiation is defined as the difference between the incoming and outgoing radiation fluxes including both long- and shortwave radiation at the surface of Earth, and it is the amount of energy available at the surface (Bisht et al., 2005; Ciraolo et al., 2007). net radiation is at last the overall value of the energy balance of a surface, considering both long-wave and short-wave radiations.

Net radiation at the land surface can be expressed as the sum of its components:

$$\mathbf{R_n} = \left(\mathbf{R_S^{\downarrow}} - \mathbf{R_S^{\uparrow}}\right) + \left(\mathbf{R_L^{\uparrow}} - \mathbf{R_L^{\downarrow}}\right) \qquad \textbf{Eq. 7}$$

where $R_S^{\downarrow}$ and $R_S^{\uparrow}$ are respectively the incoming (or downward) and outgoing (or upward) shortwave radiation, $R_L^{\uparrow}$ and $R_L^{\downarrow}$ are respectively the incoming and outgoing longwave radiation. Long and short wave represents the two forms of net radiation reaching the surface after passing through the atmosphere. The first part of the equation can be expressed as:

$$\left(\mathbf{R_S^{\downarrow}} - \mathbf{R_S^{\uparrow}}\right) = (\mathbf{1} - \boldsymbol{\alpha_0})\mathbf{R_S^{\downarrow}} \qquad \textbf{Eq. 8}$$

and the second as:

$$\left(\mathbf{R_L^{\uparrow}} - \mathbf{R_L^{\downarrow}}\right) = \boldsymbol{\varepsilon}\left(\mathbf{R_L^{\downarrow}} - \boldsymbol{\sigma}\mathbf{T_s}\right) \qquad \textbf{Eq. 9}$$

where σ is the Stephan-Boltzman constant, equal to $5.67 \cdot 10^{-8} \frac{W}{m^{2} \cdot {}^{\circ} K^{4}}$ and ε is the land surface emissivity. Some Global Climate Models (GCM) consider this term a constant parameter.

The resulting and widely accepted R_n equation is then:

$$\mathbf{R_n = (1 - \alpha_0)R_S^{\downarrow} + \varepsilon\left(R_L^{\downarrow} - \sigma T_s\right)} \qquad \textbf{Eq. 10}$$

Sensible heat flux and estimation of evaporative fraction

The more complex flux to be estimated from satellite is the sensible heat flux (H),because requires several local meteorological data such as wind speed, air temperature and surface temperature (Ciraolo et al., 2007). Moreover H changes almost continuously with the solar elevation, hence instantaneous remote sensing based H flux could not be compared with daily integrated H-fluxes (Bastiaanssen, Pelgrum, et al., 1998). Several remote sensing approaches exploited the variable of Evaporative Fraction (EF, identified as Λ in formulations), because has the advantage of avoiding the complexity related to the determination of sensible heat (Bastiaanssen, Pelgrum, et al., 1998; Verstraeten et al., 2005). Evaporative fraction is the ratio between the latent heat flux (λE) and the available energy at the land surface (R_n –G_0):

$$\boldsymbol{EF = \Lambda = \frac{\lambda E}{\lambda E + H} = \frac{\lambda E}{R_n - G_0}} \qquad \textbf{Eq. 11}$$

The Λ, a dimensionless number (it varies between 0 and 1), compares the latent heat flux (λE) to the total heat leaving the earth surface $(\lambda E + H)$.

The algorithm for latent heat flux estimation can be rewritten as:

$$\mathbf{\lambda E = \Lambda(R_n - G_0)} \qquad \textbf{Eq. 12}$$

thanks to the estimation of EF the H component is not directly include in the calculation. Therefore, evapotranspiration can be assessed from remote sensing image by estimating the evaporative fraction, net surface radiation and the soil heat flux (Li et al., 2012). As EF is only derived once a day from remote sensing images. Since it's clearly impossible to obtain continue satellite measurements over the day, in order to obtain a daily estimation of latent heat flux (i.e. daily ET) the integration will be done by assuming that the evaporative fraction at the daily scale is similar to that derived instantaneously at time of remote sensing data (Crago, 1996; Gomez et al., 2005; Verstraeten et al., 2005; Ciraolo et al., 2007; Gentine et al., 2007; Sobrino et al., 2007; Hoedjes et al., 2008; Venturini et al., 2008; Li et al., 2012; Yang et al., 2013). The conservation of EF during the day allows us to estimate daily ET using instantaneous EF. This formula displays how daily remote sensed EF is useful in EB approach to calculate the daily actual ET:

$$\text{ET daily} = \Lambda \frac{\sum Rn\ daily}{\lambda} \qquad \text{Eq. 13}$$

where Λ is the EF, Rn is the total daily net radiation and λ is the latent heat flux of vaporization [MJKg-1]. In this formulation the soil heat flux can be considered as negligible (Gomez et al., 2005).

Both SEBAL, SEBS and METRIC models require anchor pixels (wet and dry) to determine the Evaporative Fraction. Wet pixel can be identified in open water bodies or un-stressed vegetation (such as well-irrigated areas) and dry pixel in correspondence of bare soil (Tang et al., 2013).

At dry limit, the whole area is assumed as dry. The latent heat (or the evaporation) then becomes zero due to the limitation of soil moisture and the sensible heat flux is at its maximum value. Under the wet limit, the whole area is assumed to be wet and evaporation takes place at its potential rate (Muthuwatta et al., 2010). At this limit it is reasonable to assume that the sensible heat flux takes its minimum value. Usually coldest and warmest pixels coincide with the wettest and driest land surface elements (Bastiaanssen, 2000). The dry and wet pixel called anchor pixels, are useful for the automatic self-calibration of the model for ET estimation (Tang et al., 2013). Hence for the SEBAL model the presence in the area of interest of high contrast in hydrological condition are necessary. The image resolution might affect the anchor pixels retrieving, since in a high-sized pixel both bare soil and vegetation could be present. In most cases, extremely dry or wet pixels may not exist in the low-resolution satellite view of the area of interest.

Another approach to estimate the EF from remote sensing was delineated by (Roerink et al., 2000), which stated that a simple graphical method to obtain EF is to combine albedo and land surface temperature. The correlation between albedo and temperature allow us to describe the contrast between wet and dry soil condition. In fact surface moisture affects both variables and a relation between them can be expected. An empirical relation between reflectance and surface soil moisture is demonstrated (Bastiaanssen, Menenti, et al., 1998).

Under wet conditions the reflectance in VIS-NIR can be 2–3 times lower than under dry conditions, as happens on wet sand on shoreline. On the other hand, dry areas (sand dunes and limestone plateaux) have the largest reflectance values and contains the warmest spots. Previous studies demonstrated (Bastiaanssen et al., 1998a,b; Rosema & Fiselier, 1990; Seguin et al., 1989) that albedo/temperature ratio has an increasing slope until a certain point of inflection, with a 3th order effect (Verstraeten et al., 2005).

The correlation between albedo and surface can be divided in two phases: evaporation and radiation controlled (Figure 12). Evaporation controlled is determined when the correlation slope is positive. In this phase wet surfaces will evaporate moisture to keep land surface temperature low, the same principle that maintain ours temperature low with the sweat. The process of evaporation raises albedo values, resulting in brighter land surface and slightly increase temperature. When moisture from the land surface is depleted, the evaporation process stops (Verstraeten et al., 2005). That happens generally at albedo values around 0.2 (Galleguillos et al., 2011), that is the stat of radiation controlled phase. At this point the increasing albedo cause a high reflectance of incoming solar energy, resulting in a reducing of surface temperature. That is the same effect exploited by white floor and roof commonly to be founded in hot countries.. Only when the evaporation term is excluded, hence when the radiation controlled phase is set up, the slope of correlation between albedo and temperature decrease with increasing of albedo.

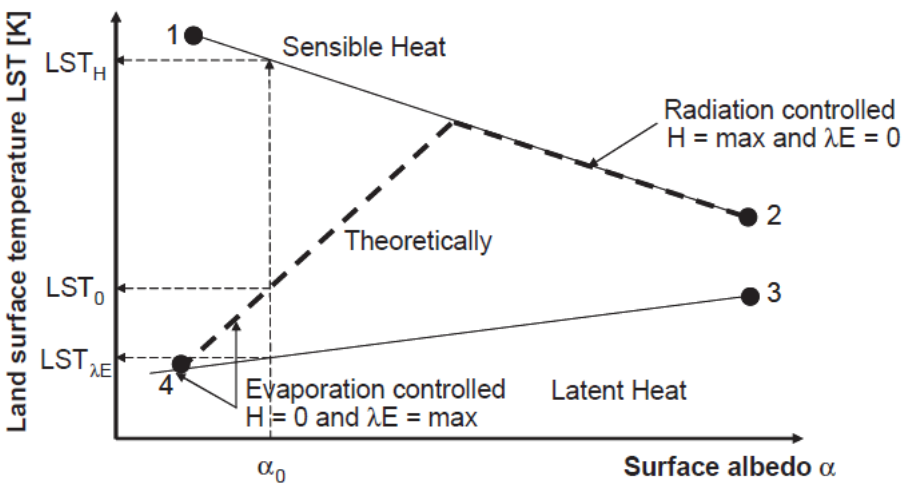

Figure 12- Graphical explanation of the process for obtaining EF estimation parameters from the albedo vs. land surface temperature scatterplot (Verstraeten et al., 2005)

This empirical relation have been exploited in order to estimate EF from satellite images, thanks to thermic sensor available on recently launched satellites (Gomez et al., 2005; Verstraeten et al., 2005; Sobrino et al., 2007; Galleguillos et al., 2011).

BIBLIOGRAPHY

Allen, RG, Masahiro Tasumi, and Ricardo Trezza. 2007. Satellite-based energy balance for mapping evapotranspiration with internalized calibration (METRIC)—Model. Journal of irrigation and drainage (August):380–94.

AMESD. 2011. AMESD Continental Environmental Bulletin.

Anderson, M. C., Norman, J., Diak, G., Kustas, W., and Mecikalski, J. 1997. A two-source time-integrated model for estimating surface fluxes using thermal infrared remote sensing. Remote Sens. Environ 60(2):195–216.

Anyamba, A., and C. Tucker. 2005. Analysis of Sahelian vegetation dynamics using NOAA-AVHRR NDVI data from 1981–2003. Journal of Arid Environments 63(3):596–614.

Arino, O., D. Gross, F. Ranera, and L. Bourg. 2007. GlobCover: ESA service for global land cover from MERIS. 2007. IGARSS 2007 2412–15.

Arino, O., Gross, D., Ranera, F., Bourg, L., Leroy, M., Bicheron, P., Latham, J., Di Gregorio, A., Brockman, C., Witt, R., Defourny, P., Vancutsem, C., Herold, M., Sambale, J., Achard, F., Durieux, L., Plummer, S., Weber, J.L., 2008. GlobCover. ESA service for global land cover from MERIS. IEEE International Geoscience and Remote Sensing Symposium, IGARSS 2007, pp. 2412-2415, Barcelona, Spain.

Arino, Olivier et al. 2007. GlobCover: ESA service for global land cover from MERIS. Pp. 2412–15 in International Geoscience and Remote Sensing Symposium (IGARSS 2007), Barcellona, Spain, July 23-27. IEEE.

Asrar, G., Fuchs, M., Kanemasu, E.T., Hatfield, J. L. 1984. Estimating absorbed photosynthetic radiation and leaf area index from spectral reflectance in wheat. Agronomy Journal 76:300–306.

Ayantunde, A. 1999. Selective grazing by cattle on spatially and seasonally heterogeneous rangeland in Sahel. Journal of Arid Environments 42(4):261–79.

Ayantunde, A., S. Fernández-Rivera, P. H. Hiernaux, and R. Tabo. 2008. Implications of restricted access to grazing by cattle in wet season in the Sahel. Journal of Arid Environments 72(4):523–33.

Bagayoko, Fafre, Samuel Yonkeu, Jan Elbers, and Nick van de Giesen. 2007. Energy partitioning over the West African savanna: Multi-year evaporation and surface conductance measurements in Eastern Burkina Faso. Journal of Hydrology 334(3-4):545–59.

Bai, Z. G., D. L. Dent, L. Olsson, and M. E. Schaepman. 2008. Proxy global assessment of land degradation. Soil Use and Management 24(3):223–34.

Barbosa, H.A., Huete, A.R., Baethgen, W.E., 2006. A 20-year study of NDVI variability over the northeast region of Brazil. Journal of Arid Environments 67, 288-307.

Bartholomé, E., and a. S. Belward. 2005. GLC2000: a new approach to global land cover mapping from Earth observation data. International Journal of Remote Sensing 26(9):1959–77.

Bartholome, Etienne. 1988. Radiometric measurements and crop yield forecasting Some observations over millet and sorghum experimental plots in Mali. 9(10-11):1539–52.

Bartholomé, Etienne. 1990. estimation of apar values from avhrr ndvi for regional crop yield assessment in west Africa, 587-590.

Bastiaanssen, W. G. .. 2000. SEBAL-based sensible and latent heat fluxes in the irrigated Gediz Basin, Turkey. Journal of Hydrology 229(1-2):87–100. Retrieved (http://linkinghub.elsevier.com/retrieve/pii/S0022169499002024).

Bastiaanssen, W. G. M., H. Pelgrum, et al. 1998. A remote sensing surface energy balance algorithm for land (SEBAL). Journal of Hydrology 212-213:213–29.

Bastiaanssen, W. G. M., H. Pelgrum, P. Droogers, H. a. R. de Bruin, and M. Menenti. 1997. Area-average estimates of evaporation, wetness indicators and top soil moisture during two golden days in EFEDA. Agricultural and Forest Meteorology 87(2-3):119–37.

Bastiaanssen, W. G. M., M. Menenti, R. a. Feddes, and A. a. M. Holtslag. 1998. A remote sensing surface energy balance algorithm for land (SEBAL). 1. Formulation. Journal of Hydrology 212-213:198–212.

Bastiaanssen, W. G. M., R. Sakthivadivel, and A. Van Dellen. 1999. Spatially Delineating Actual and Relative Evapotranspiration from Remote Sensing to Assist Spatial Modeling of Non-Point Source Pollutants. Pp. 179–96 in Assessment of Non-Point Source Pollution in the Vadose Zone, edited by American Geophysical Union.

Bastiaanssen, Wim G. M., and Samia Ali. 2003. A new crop yield forecasting model based on satellite measurements applied across the Indus Basin, Pakistan. Agriculture, Ecosystems & Environment 94(3):321–40.

Batello, C., Marzot, M., Touré, A.H., 2004. The future is an ancient lake: Traditional knowledge, biodiversity and genetic resources for food and agriculture in lake chad basin ecosystems. FAO-UN, Rome.

Battisti, DS, and RL Naylor. 2009. Historical warnings of future food insecurity with unprecedented seasonal heat. Science 323(January):240–44. Retrieved December 12, 2013 (http://www.sciencemag.org/content/323/5911/240.short).

Bégué, A., Vintrou, E., Ruelland, D., Claden, M. & Dessay, n. 2011, Can a 25-year trend in Soudano-Sahelian vegetation dynamics be interpreted in terms of land use change? A remote sensing approach. Global Environmental Change, 21, pp. 413-420.

Begue, Agnès. 2002. Télédétection et production végétale. Université Pierre et Marie Curie.

Beyè, Gora. 2010. Presentation du Centre de Suivi Ecologique. Dakar.

Bisht, Gautam, Virginia Venturini, Shafiqul Islam, and Le Jiang. 2005. Estimation of the net radiation using MODIS (Moderate Resolution Imaging Spectroradiometer) data for clear sky days. Remote Sensing of Environment 97(1):52–67.

Bonifacio, R., G. Dugdale, and JR Milford. 1993. Sahelian rangeland production in relation to rainfall estimates from Meteosat. International Journal of … 14(14):2695–2711.

Boschetti, M. et al. 2013. Identification of environmental anomaly hot spots in West Africa from time series of NDVI and rainfall. ISPRS Journal of Photogrammetry and Remote Sensing 78:26–40.

Boschetti, M., and A. Nelson. 2012. An automatic approach for rice mapping in temperate region using time series of MODIS imagery: first results for Mediterranean environment edited by European Geophysical Union. EGU General Assembly 14:14068–1

Boschetti, M., D. Stroppiana, P. a. Brivio, and S. Bocchi. 2009. Multi-year monitoring of rice crop phenology through time series analysis of MODIS images. International Journal of Remote Sensing 30(18):4643–62.

Brink, A.B., Eva, H.D., 2009. Monitoring 25 years of land cover change dynamics in Africa: A sample based remote sensing approach. Applied Geography 29, 501-512.

Brink, Andreas Bernhard, and Hugh Douglas Eva. 2009. Monitoring 25 years of land cover change dynamics in Africa: A sample based remote sensing approach. Applied Geography 29(4):501–12.

Brivio, P. A., G. Lechi, and E. Zilioli. 2006. Principi e metodi di telerilevamento. edited by Citta Studi.

Brooks, N., 2004. Drought in the African Sahel: Long-term perspectives and future prospects. Tyndall Centre Working Paper, 61.

Brouwer, J. 2008, The importance of within-field soil and crop growth variability to improving food production in a changing Sahel, (Niamey: ICRISAT Sahelian Centre).

Brown, Molly E., and C. C. Funk. 2008. Food security under climate change. Science 319.(5863):580 – 581.

Bui, E.N., Wilding, L.P., 1988, Pedogenesis and Mineralogy of a Halaquept in Niger (West Africa), Geoderma, 43, pp. 49-64.

Campbell, B. D., and D. M. Stafford Smith. 2000. A synthesis of recent global change research on pasture and rangeland production: reduced uncertainties and their management implications. Agriculture, Ecosystems & Environment 82(1-3):39–55.

Capecchi, V., Crisci, A., Genesio, L., Maselli, F., Vignaroli, P., 2008. Analysis of NDVI trends and their climatic origin in the Sahel 1986-2000. Geocarto International 23(4), 297 - 310.

Chander, G., Markham, B. L., Helder, D. L., 2009, Summary of current radiometric calibration coefficients for Landsat MSS, TM, ETM+, and EO-1 ALI sensors, Remote Sensing of Environment, 113, pp. 893-903.

Chasmer, L. et al. 2011. Characterizing vegetation structural and topographic characteristics sampled by eddy covariance within two mature aspen stands using lidar and a flux footprint model: Scaling to MODIS. Journal of Geophysical Research 116(G2):G02026.

Chen, Jin et al. 2004. A simple method for reconstructing a high-quality NDVI time-series data set based on the Savitzky–Golay filter. Remote Sensing of Environment 91(3–4):332–44.

Ciraolo, G., M. Minacapilli, and M. Sciortino. 2007. Stima dell'evapotraspirazione effettiva mediante telerilevamento aereo iperspettrale. J. of Ag. Eng. (482):49–60.

CMAP (Centre Mauritanien d'Analayse Politiques), 2004. Le diagnostic du secteur rural dans la Wilaya de Guidimagha. Comité Technique du CSLP. Nouakchott 50 p.

Combal, B., Bartholomé, E., Brivio, P.A., Boschetti, M., Stroppiana, D., Martini, M., 2010. The NARMA-geoland2 e-station an Earth Observation based decision support system tool for real time environmental monitoring in Africa. ISPRS GI4DM, Torino (Italy), 2-4 February 2010, CD, ISBN 978-88-903132-3-3

Congalton, R. G., 1991, A review of assessing the accuracy of classifications of remotely sensed data, Remote Sensing of Environment, 37, pp. 35–46.

Coppin, P., Jonckheere, I., Nackaerts, K., Muys, B., Lambin, E. (2004) 'Review Article. Digital change detection methods in ecosystem monitoring: a review', International Journal of Remote Sensing, 25:9, 1565 - 1596

Crago, Richard D. 1996. Conservation and variability of the evaporative fraction during the daytime. Journal of Hydrology 180(1-4):173–94.

Cramer, W., and DW Kicklighter. 1999. Comparing global models of terrestrial net primary productivity (NPP): overview and key results. Global Change Biology 5:1–15.

CRED, 2012. EM-DAT: The international disaster database: result for country profile. http://www.emdat.be/result-country-profile (accessed September 2012).

Dallal, G. E., and L. Wilkinson. 1986. An analytic approximation to the distribution of Lilliefors' test for normality. The American Statistician 40:294–96.

Daughtry, C. S. T., K. P. Gallo, and M. E. Bauer. 1983. Spectral estimates of solar-radiation intercepted by corn canopies. Agron J 75(3):527–31.

Dawelbait, M., Morari, F., 2012, Monitoring desertification in a Savannah region in Sudan using Landsat images and spectral mixture analysis, Journal of Arid Environments, 80, pp. 45-55.

De Jong, R., and S. de Bruin. 2012. Linear trends in seasonal vegetation time series and the modifiable temporal unit problem. Biogeosciences 9(1):71–77.

De Jong, Rogier, Sytze de Bruin, Allard de Wit, Michael E. Schaepman, and David L. Dent. 2011. Analysis of monotonic greening and browning trends from global NDVI time-series. Remote Sensing of Environment 115(2):692–702.

Decalo, S., 1979, Historical Dictionary of Niger, pp.31-179 (New York – London: Scarecrow Press Editor).

DNCN, 2009. Evaluation intégrée des écosystèmes: cas de la région de Mopti au Mali. Rapport Provisoire. Direction Nationale de la Conservation de la Nature, Bamako.

Dregne, H.E., 1983. Desertification of arid lands. Harwood Academic Publishers, New York.

ECOWAS-SWAC, 2006. The Ecologically vulnerable zone of Sahelian countries. Atlas on Regional Integration in West Africa, http://www.oecd.org/dataoecd/41/49/38409502.pdf.

Eklundh, L., Olsson, L., 2003. Vegetation index trends for the African Sahel 1982–1999. Geophysical Research Letters, 30(8), 1-4.

ENDA-Diapol, 2007. Diagnostic des économies ruralesdu bassin du Karakoro. Club du Sahel et de l'Afrique de l'Ouest, Paris. 69 p.

Erdogan, H. E., Pellikka, P. K. E., Clark, B., 2011, Modelling the impact of land-cover change on potential soil loss in the Taita Hills , Kenya , between 1987 and 2003 using remote-sensing and geospatial data. International Journal of Remote Sensing, 32 (21), pp. 37-41.

Fensholt, R., Rasmussen, K., 2011. Analysis of trends in the Sahelian `rain-use efficiency' using GIMMS NDVI, RFE and GPCP rainfall data. Remote Sensing of Environment 115, 438-451.

Fensholt, R., Sandholt, I., Stisen, S., 2006. Evaluating MODIS, MERIS, and Vegetation - vegetation indices using in situ measurements in a semiarid environment. IEEE Transactions on Geoscience and Remote Sensing 44, 1774-1786.

Fensholt, Rasmus, Inge Sandholt, Michael Schultz Rasmussen, Simon Stisen, and Alioune Diouf. 2006. Evaluation of satellite based primary production modelling in the semi-arid Sahel. Remote Sensing of Environment 105(3):173–88.

Foley, J. A, Defries, R., Asner, G.P., Barford, C., Bonan, G., Carpenter, S.R., Chapin, F.S., COE, M.T., Daily, G.C., Gibbs, H.K., Helkowski, J.H., Holloway, T., Howard, E. A, Kucharik, C.J.,

Monfreda, C., Patz, J. A, Prentice, I.C., Ramankutty, N., Snyder, P.K., 2005, Global consequences of land use. Science. 309, pp. 570-4.

Foley, Jonathan a et al. 2011. Solutions for a cultivated planet. Nature 478(7369):337–42.

Fontès J., Diallo A., Compaoré J. A. 1994: carte de la végétation naturelle et de l'occupation du sol – Burkina Faso au 1/1000000. ICIV, Toulouse.

G. Buttner, J. Feranec, G. Jaffrain, L. Mari, G. Maucha, and T. Soukup. 2004. The CORINE Land Cover 2000 Project, EARSeL eProc 3(3):331–46.

Galle, S., Ehrmann, M., Peugeot, C., 1999, Water balance in a banded vegetation pattern: A case study of tiger bush in western Niger. Catena, 37 (1–2), pp. 197-216

Galleguillos, Mauricio, Frédéric Jacob, Laurent Prévot, Andrew French, and Philippe Lagacherie. 2011. Comparison of two temperature differencing methods to estimate daily evapotranspiration over a Mediterranean vineyard watershed from ASTER data. Remote Sensing of Environment 115(6):1326–40.

Gallo, K. P., C. S. T. Daughtry, and M. E. Bauer. 1985. Spectral estimation of absorbed photosynthetically active radiation in corn canopies. Remote Sensing of Environment 17(3):221–32.

Garbulsky, Martín F. et al. 2010. Patterns and controls of the variability of radiation use efficiency and primary productivity across terrestrial ecosystems. Global Ecology and Biogeography 19(2):253–67. Retrieved November 15, 2013 (http://doi.wiley.com/10.1111/j.1466-8238.2009.00504.x).

Geesing, D., Djibo, H., 2001. Country pasture profiles. Pasture profile for Niger. FAO, http://www.fao.org/ag/AGP/AGPC/doc/Counprof/niger.htm.

Gentine, Pierre, Dara Entekhabi, Abdelghani Chehbouni, Gilles Boulet, and Benoît Duchemin. 2007. Analysis of evaporative fraction diurnal behaviour. Agricultural and Forest Meteorology 143(1-2):13–29..

Giannini, A., Biasutti, M., Verstraete, M.M., 2008. A climate model-based review of drought in the Sahel: Desertification, the re-greening and climate change. Global and Planetary Change 64, 119-128.

Giannini, A., Saravanan, R., Chang, P., 2003. Oceanic forcing of Sahel rainfall on interannual to interdecadal time scales. Science 302, 1027-1030.

Goetz, S. J. 2000. Interannual variability of global terrestrial primary production: Results of a model driven with satellite observations. Journal of Geophysical Research 105(D15):20077–91.

Gomez, M., A. Olioso, J. Sobrino, and F. Jacob. 2005. Retrieval of evapotranspiration over the Alpilles/ReSeDA experimental site using airborne POLDER sensor and a thermal camera. Remote Sensing of Environment 96(3-4):399–408.

Grove, A.T., 1958. The Ancient Erg of Hausaland, and Similar Formations on the South Side of the Sahara. The Geographical Journal 124 (4).

Guyot, Adrien, Jean-Martial Cohard, Sandrine Anquetin, and Sylvie Galle. 2012. Long-term observations of turbulent fluxes over heterogeneous vegetation using scintillometry and additional observations: A contribution to AMMA under Sudano-Sahelian climate. Agricultural and Forest Meteorology 154-155:84–98. Retrieved September 27, 2013 (http://linkinghub.elsevier.com/retrieve/pii/S0168192311003078).

Haas, E.M., 2010. Temporal water bodies as ecological indicators in West African drylands. Phd thesis Université Catholique de Louvain, Belgium.

Hadria, R., and B. Duchemin. 2006. Monitoring of irrigated wheat in a semiarid climate using crop modelling and remote sensing data: Impact of satellite revisit time frequency. International Journal of Remote Sensing (August 2012):37–41. Retrieved November 10, 2013 (http://www.tandfonline.com/doi/abs/10.1080/01431160500382980).

Ham, F. 2011, Analyse de la production de biomasse en zone pastorale au Niger / Saison des pluies 2011. pp. 1-6 (Niamey: Réseau National des Chambres d'Agriculture du Niger).

Ham, Frédéric, and Erwann Fillol. 2010. Pastoral surveillance system and feed inventory in the Sahel. Pp. 83–114 in Conducting national feed assessments, vol. 1998, edited by FAO. Rome.

Hein, L. 2006. The impacts of grazing and rainfall variability on the dynamics of a Sahelian rangeland. Journal of Arid Environments 64(3):488–504.

Hein, L. et al. 2011. Desertification in the Sahel: Towards better accounting for ecosystem dynamics in the interpretation of remote sensing images. Journal of Arid Environments 75(11):1164–72.

Hein, Lars, Marc J. Metzger, and Rik Leemans. 2008. The local impacts of climate change in the Ferlo, Western Sahel. Climatic Change 93(3-4):465–83.

Heinsch, F. a. et al. 2006. Evaluation of remote sensing based terrestrial productivity from MODIS using regional tower eddy flux network observations. IEEE Transactions on Geoscience and Remote Sensing 44(7):1908–25.

Helldén, U., Tottrup, C., 2008. Regional desertification: A global synthesis. Global and Planetary Change 64, 169-176.

Herrmann, S.M., Anyamba, A., 2005, Recent trends in vegetation dynamics in the African Sahel and their relationship to climate. Global Environmental Change Part A, 15(4), pp. 394-404.

Heumann, B., J. Seaquist, L. Eklundh, and P. Jonsson. 2007. AVHRR derived phenological change in the Sahel and Soudan, Africa, 1982–2005. Remote Sensing of Environment 108(4):385–92.

HIC Darfur 2004: map of the administrative units; Humanitarian Information Center for Darfur, Karthoum. Available on www.reliefweb.int

Hiernaux, P., Ayantunde, A., Kalilou, A., Mougin, E., Gérard, B., Baup, F., Grippa, M., Djaby, B. 2009, Trends in productivity of crops, fallow and rangelands in Southwest Niger: Impact of land use, management and variable rainfall. Journal of Hydrology, 375, pp. 65-77.

Hiernaux, Pierre, and Augustine Ayantunde. 2004. The Fakara : a semi-arid agro-ecosystem under stress Report of research activities.

Hiernaux, Pierre, Henry Noël, and Le Houérou. 2006. Les parcours du Sahel. Africa 17:51–71.

Higuchi, A., A. Kondoh, and S. Kishi. 2000. Relationship among the surface albedo, spectral reflectance of canopy, and evaporative fraction at grassland and paddy field. Advances in Space Research 26(7):1043–46.

Hilker, Thomas, Nicholas C. Coops, Michael a Wulder, T. Andrew Black, and Robert D. Guy. 2008. The use of remote sensing in light use efficiency based models of gross primary production: a review of current status and future requirements. The Science of the total environment 404(2-3):411–23.

Hoedjes, J. C. B., a. Chehbouni, F. Jacob, J. Ezzahar, and G. Boulet. 2008. Deriving daily evapotranspiration from remotely sensed instantaneous evaporative fraction over olive orchard in semi-arid Morocco. Journal of Hydrology 354(1-4):53–64.

Hollander, D., and A. Wolfe. 1999. Nonparametric Statistical Methods. 2nd Editio. edited by John Wiley & Sons. New York.

Huber, S., Fensholt, R., Rasmussen, K., 2011. Water availability as the driver of vegetation dynamics in the African Sahel from 1982 to 2007. Global and Planetary Change 76, 186-195.

Ibrahim, F.N., 1978. Anthropogenic causes of desertification in western Sudan. Geojournal 2, 243–254.

INS, 2010. La région de Mopti – Résultats Provisiores du Recensement Général de la Population et de l'Habitat. Bamako, 2p.

INSD, 2008. Recensement général de la population et de l'habitation 2006. Min. Eco & Finances, Ouagadougou, 52 p.

Irmak, Ayse, Ian Ratcliffe, and Kenneth Hubbard. 2011. Estimation of Land Surface Evapotranspiration with a Satellite Remote Sensing Procedure.

Jarlan, L., Mangiarotti, S., Mougin, E., Mazzega, P., Hiernaux, P., LE Dantec, V., 2008, Assimilation of SPOT/VEGETATION NDVI data into a Sahelian vegetation dynamics model. Remote Sensing of Environment, 112(4), pp. 1381-1394.

Jiang, Le et al. 2009. A satellite-based Daily Actual Evapotranspiration estimation algorithm over South Florida. Global and Planetary Change 67(1-2):62–77.

Justice, CO, and PHY Hiernaux. 1986. Monitoring the grasslands of the Sahel using NOAA AVHRR data: Niger 1983. International Journal of Remote … (August 2012):37–41

Kandji, ST, L. Verchot, and J. Mackensen. 2006. Climate change and variability in the Sahel region: impacts and adaptation strategies in the agricultural sector.

Kanniah, K. D., J. Beringer, L. B. Hutley, N. J. Tapper, and X. Zhu. 2009. Evaluation of Collections 4 and 5 of the MODIS Gross Primary Productivity product and algorithm improvement at a tropical savanna site in northern Australia. Remote Sensing of Environment 113(9):1808–22.

Key, C.H., Benson, N. C. 1999. Measuring and remote sensing of burn severity: the CBI and NBR. P. 284 in Joint Fire Science Conference and Workshop, edited by K.C. (Eds.) Neuenschwander, L.F., Ryan. Boise: University of Idaho and International Association of Wildland Fire.

Kiage, L.M., Liu, K. B., Walker, N. D., Lam, N., Huh O. K., 2007, Recent land-cover/use change associated with land degradation in the Lake Baringo catchment, Kenya, East Africa: evidence from Landsat TM and ETM+. International Journal of Remote Sensing, 28(19), pp. 4285-4309.

Kicklighter, DW, and A. Bondeau. 1999. Comparing global models of terrestrial net primary productivity (NPP): Global pattern and differentiation by major biomes. Global Change Biology 5:16–24.

Kiniry, J. R., B. Bean, Y. Xie, and P. Chen. 2004. ,Maize yield potential: critical processes and simulationmodeling in a high-yielding environment. Agricultural Systems 82:45–56.

Kizito, F., Dragila M., Sène M., Lufafa, A., Diedhiou, I., Dick, R.P., Selker, J.S., Dossa, E., Khouma, M., Badiane, A., Ndiaye, S., 2006, Seasonal soil water variation and root patterns between two semi-arid shrubs co-existing with Pearl millet in Senegal, West Africa. Journal of Arid Environments, 67 (3), pp. 436-455.

Knorr, W. Heimann, M. 1995. Impact of drought stress and other factors on seasonal land biosphere CO2 exchange studied through an atmospheric tracer transport model. Tellus B 47:471–89.

Krätli, Saverio. 2007. Cows Who Choose Domestication. Generation and management of domestic animal diversity by WoDaaBe pastoralists (Niger). A thesis submitted for the degree of Doctor of Philosophy June 2007 Institute of Development Studies University of Sussex.

Krätli, Saverio. 2008. Cattle Breeding, Complexity and Mobility in a Structurally Unpredictable Environment: The WoDaaBe Herders of Niger. Nomadic Peoples 12(1):11–41. Retrieved October 13, 2011

Kumar, M., and J. L. Monteith. 1981. Remote sensing of crop growth. edited by Academic Press. New York.

Kurc, Shirley a., and Eric E. Small. 2004. Dynamics of evapotranspiration in semiarid grassland and shrubland ecosystems during the summer monsoon season, central New Mexico. Water Resources Research 40(9)

Kustas, WP, and TJ Schimugge. 1993. Relationships between evaprorative fraction and remotely sensed vegetation index and microwave brightness temperature for semiarid rangelands. Journal of Applied Meteorology.

Lambin, EF, Pamela Cashman, and Aaron Moody. 1993. Agricultural production monitoring in the Sahel using remote sensing: Present possibilities and research needs. 298(38):301–22.

Lamprey, H.F., 1988, Report on desert encroachment reconnaissance in Northern Sudan: 21 October to 10 November 1975. Desertification Control Bulletin, 17, pp. 1–7.

Lasanta, Teodoro, and Sergio M. Vicente-Serrano. 2012. Complex land cover change processes in semiarid Mediterranean regions: An approach using Landsat images in northeast Spain. Remote Sensing of Environment 124:1–14.

Le Houerou, H. N. 1980. The rangelands of the sahel. Journal of Range Management 33(41):41–46.

Lebel, T. et al. 1992. Rainfall estimation in the Sahel: the EPSAT-NIGER experiment. Hydrological Sciences Journal 37(3):201−215.

Leblanc, M. J., Lemoalle, J., Bader, C., Tweed, S., 2011. Thermal remote sensing of water under flooded vegetation: new observations of inundation patterns for the Small Lake Chad. Journal of Hydrology 404, 87-98.

Leblanc, Marc J. et al. 2008. Land clearance and hydrological change in the Sahel: SW Niger. Global and Planetary Change 61(3-4):135–50. Retrieved October 7, 2011 (http://linkinghub.elsevier.com/retrieve/pii/S0921818107001336).

Leblon, B., M. Guerif, and F. Baret. 1991. he use of remotely sensed data in estimation of PAR use efficiency and biomass production of flooded rice. Remote Sensing of Environment 38:147–58.

Legendre, P., and L. Legendre. 1998. Numerical ecology. 2nd Englis. Amsterdam: Elsevier Science BV.

Li, Xingmin, Ling Lu, Wenfeng Yang, and Guodong Cheng. 2012. Estimation of evapotranspiration in an arid region by remote sensing—A case study in the middle reaches of the Heihe River Basin. International Journal of Applied Earth Observation and Geoinformation 17:85–93.

Lillesand, T. M., Kiefer, R. W., 2000, Remote sensing and image interpretation (4th ed.). (New York: Wiley).

Lindroth, Anders et al. 2008. Leaf area index is the principal scaling parameter for both gross photosynthesis and ecosystem respiration of Northern deciduous and coniferous forests. Tellus B 60(2):129–42.

Loague, K.M., Green, R. E. 1991. Statistical and graphical methods for evaluating solute transport models: overview and application. J. Contam. Hydrol. 7:51–73.

Lobell, David B., Gregory P. Asner, J. Iva. Ortiz-Monasterio, and Tracy L. Benning. 2003. Remote sensing of regional crop production in the Yaqui Valley, Mexico: estimates and uncertainties. Agriculture, Ecosystems & Environment 94(2):205–20. Retrieved (http://linkinghub.elsevier.com/retrieve/pii/S016788090200021X).

Luo, Jianwen, Kui Ying, and Jing Bai. 2005. Savitzky–Golay smoothing and differentiation filter for even number data. Signal Processing 85(7):1429–34. Retrieved May 23, 2013 (http://linkinghub.elsevier.com/retrieve/pii/S0165168405000654).

Manfron, Giacinto, and Alberto Crema. 2012. Testing automatic procedures to map rice area and detect phenological crop information exploiting time series analysis of remote sensed MODIS data edited by Karin Stein and John Gonglewski. Proc. of SPIE 8531:85311E–85311E–11.

Marteau, Romain et al. 2011. The onset of the rainy season and farmers' sowing strategy for pearl millet cultivation in Southwest Niger. Agricultural and Forest Meteorology 151(10):1356–69.

Martínez, B., Gilabert, M.A., 2009. Vegetation dynamics from NDVI time series analysis using the wavelet transform. Remote Sensing of Environment 113, 1823-1842.

Mayaux, P., Bartholomé, E., Fritz, S., Belward, A., 2004, A new land-cover map of Africa for the year 2000. Journal of Biogeography, 31, pp. 861-877.

Mecikalski, JR, and GR Diak. 1999. Estimating fluxes on continental scales using remotely sensed data in an atmospheric-land exchange model. Journal of Applied Metereology (1997):1352–69.

Mertz, Ole et al. 2010. Climate Factors Play a Limited Role for Past Adaptation Strategies in West Africa. Ecology And Society 15(4).

Mertz, Ole et al. 2012. Climate Variability and Environmental Stress in the Sudan-Sahel Zone of West Africa. Ambio 41(4):380–92.

Middleton, N., Thomas, D., 1997. World atlas of desertification. United Nations Environmental Programme, Arnold, London.

Mohino, Elsa, Serge Janicot, and Juergen Bader. 2010. Sahel rainfall and decadal to multi-decadal sea surface temperature variability. Climate Dynamics. Retrieved July 19, 2011 (http://www.springerlink.com/index/10.1007/s00382-010-0867-2).

Monod, T. 1985. The Sahel Zone north of the equator. in Hot Deserts and Arid Shrublands, edited by D. (Eds.) Evenari, M., Noy-Meir, I., Goodall. New York: Elsevier.

Monteith, J. L. 1964. Evaporation and environment. The state of movement of water in living organisms. Pp. 205–34 in Symposium of the society of experimental biology.

Monteith, J. L. 1972. Solar radiation and productivity in tropical ecosystems. Journal of Applied Ecology 9:747–66.

Mortimore, M.J., Adams, W.M., 2001. Farmer adaptation, change and crisis in the Sahel. Global Environmental Change 11, 49-57.

Mortimore, Michael. 2010. Adapting to drought in the Sahel : lessons for climate change.

Mutanga, Onisimo, and AK Skidmore. 2004. Merging Double Sampling with Remote Sensing for a Rapid Estimation of Fuelwood. Geocarto International (1):49–55.

Muthuwatta, Lal P., Mobin-ud-din Ahmad, M. Rientjes, and Marinus G. Bos. 2010. Estimating the spatial variability of water consumption in the Karkheh river basin , Iran - using MODIS data. AQUAmundi 115 – 122.

Nicholson, S.E., 1995. Sahel, West Africa. In Nierenberg, W.A. (Ed.), Encyclopedia of Environmental Biology, vol. 3. Academic Press, San Diego, 261–275.

Nicholson, S.E., Grist, J.P., 2001. A conceptual model for understanding rainfall variability in the West African Sahel on interannual and interdecadal timescales. International Journal of Climatology 21, 1733–1757.

Nicholson, S.E., Tucker, C.J., Ba, M.B., 1998. Desertification, drought, and surface vegetation: An example from the West African Sahel. Bulletin of the American Meteorological Society 815, 79, 815–829.

NOAA CPC, 2001. The NOAA Climate Prediction Center African Rainfall Estimation Algorithm Version 2 .0. on line: http://www.cpc.ncep.noaa.gov/products/fews/RFE2.0_tech.pdf.

Novák, V., and MT van Genuchten. 2008. Using the transpiration regime to estimate biomass production. Soil Science 173(6).

Nutini, F., Boschetti, M., Brivio, P.A., Bartholomé, E., Hoscilo, A., Stroppiana, D., Bocchi, S., 2010, Analysis of vegetation pasture climate response on Sahel region through 10 years remote sensed data. In Remote Sensing for Agriculture, Ecosystems and Hydrology, (C.M. Neale, A. Maltese, Eds) Proc. SPIE Vol. 7824, 782404 (Oct. 21, 2010), ISSN: 0277-786X.

Nutini, F., M. Boschetti, PA Brivio, S. Bocchi, and M. Antoninetti. 2013. Land-use and land-cover change detection in a semi-arid area of Niger using multi-temporal analysis of Landsat images. International Journal of Remote Sensing (April):37–41.

Nutini, F , Boschetti, M, PA Brivio, 2010. Analysis of vegetation pasture climate response on Sahel region through 10 years of remotely sensed data. Pp. 782404–782404–9 in Proc. of SPIE, vol. 7824.

Olson, D.M., Dinerstein, E., E.D. Wikramanayake, N.D. Burgess, G.V.N. Powell, E.C. Underwood, J.A. D'Amico, I. Itoua, H.E. Strand, J.C. Morrison, C.J. Loucks, T.F. Allnutt, T.H. Ricketts, Y. Kura, J.F. Lamoreux, W.W. Wettengel, P. Hedao, Kassem, K.R., 2001. Terrestrial ecoregions of the world: A new map of life on earth. BioScience 51, 933-938.

Olson, David M. et al. 2001. Terrestrial Ecoregions of the World : A New Map of Life on Earth. BioScience 51(11):933–38.

Olsson, L., L. Eklundh, and J. Ardo. 2005. A recent greening of the Sahel—trends, patterns and potential causes. Journal of Arid Environments 63(3):556–66. Retrieved June 15, 2011 (http://linkinghub.elsevier.com/retrieve/pii/S0140196305000522).

Omuto, C. T. 2012, A new approach for using time-series remote-sensing images to detect changes in vegetation cover and composition in drylands : a case study of eastern Kenya. International Journal of Remote Sensing, 32 (21), pp. 37-41.

Onyewotu, L.O.Z., Stigter, C.J., Oladipo, E.O., Owonubi, J.J., 1998, Yields of millet between shelterbelts in semi-arid northern Nigeria , with a traditional and a scientific method of determining sowing date , and at two levels of organic manuring. NJAS - Wageningen Journal of Life Sciences, 46(1), pp. 1-10.

Orange, D., Wesselink, A.J., Make, G. and Feizure, C. T. 1997. The effects of climate changes on river baseflow and aquifer storage in Central Africa. Sustainability of Water Resources under Increasing Uncertainty. Pp. 113–23 in Proc. Rabat Symposium S1. IAHS Publ.

Ould Sidi, H., 2004. Etude de mise en oeuvre du plan-cadre des N. U. pour l'aide au développement (UNDAF) – Wilaya-pilote: Assaba. Système des N. U. - bureau de coordination, Nouakchott, 70 p.

Penman, H. L. 1948. Natural evaporation from open water, bare soil and grass. in Proceedings of the Royal Society of London Series a-Mathematical and Physical Sciences.

Peugeot, Christophe, Bernard Cappelaere, Baxter E. Vieux, Luc Séguis, and Ana Maia. 2003. Hydrologic process simulation of a semiarid, endoreic catchment in Sahelian West Niger. 1. Model-aided data analysis and screening. Journal of Hydrology 279(1-4):224–43.

Potter C.S. et al. 1993. Terrestrial ecosystem production —a process model-based on global satellite and surface data. Glob Biogeochemical Cycles 7(4):811–41.

Potter, Christopher, Steven Klooster, and Vanessa Genovese. 2012. Net primary production of terrestrial ecosystems from 2000 to 2009. Climatic Change 115(2):365–78.

Powell, J. 1996. Nutrient cycling in integrated rangeland/cropland systems of the Sahel. Agricultural Systems 52(2-3):143–70.

Priestley, C. H. B., & Taylor, R. J. 1972. On the assessment of surface heat flux and evaporation using large-scale parameters. Monthly Weather Review 100:81–82.

Prince, S. D., and S. J. Goward. 1995. Global primary production: a remote sensing approach. Journal of Biogeography 22:316–36.

Prince, S.D., 1991. Satellite remote sensing of primary production: Comparison of results for Sahelian grasslands 1981–1988. International Journal of Remote Sensing 12, 1901-1311.

Proud, Simon Richard, and Laura Vang Rasmussen. 2011. The influence of seasonal rainfall upon Sahel vegetation. Remote Sensing Letters 2(3):241–49.

Ramankutty, N., 2004. Croplands in West Africa: A geographically explicit dataset for use in models. Earth Interactions 8, 1-22.

Ramier, David et al. 2009. Towards an understanding of coupled physical and biological processes in the cultivated Sahel – 1. Energy and water. Journal of Hydrology 375(1-2):204–16.

Rasmussen, Kjeld, and Anette Reenberg. 1992. Satellite Remote Sensing of Land-use in Northern Burkina Faso - The Case of Kolel Village. Danish Journal of Geography 92:86–93.

Rasmussen, L. V., Reenberg, A., 2012, Land use rationales in desert fringe agriculture. Applied Geography 34, pp. 595-605.

Rasmussen, M. S. 1998. Developing simple, operational, consistent NDVI-vegetation models by applying environmental and climatic information. Part II: Crop yield assessment. International Journal of Remote Sensing 19(1):119–39.

Reenberg, A., Nielsen, T. L., Rasmussen, K., 1998, Field expansion and reallocation in the Sahel – land use pattern dynamics in a fluctuating biophysical and socio-economic environment. Global Environmental Change, 8, pp. 309-327.

Ricotta C., Avena G. and De Palma A. 1999. Mapping and monitoring net primary productivity with AVHRR NDVI time-series: statistical equivalence of cumulative vegetation indices. ISPRS Journal of Photogrammetry & Remote Sensing 54, 325–331

Roebeling, R. a., E. van Putten, G. Genovese, and A. Rosema. 2004. Application of Meteosat derived meteorological information for crop yield predictions in Europe. International Journal of Remote Sensing 25(23):5389–5401.

Roerink, G., Z. Su, and M. Menenti. 2000. S-SEBI: A simple remote sensing algorithm to estimate the surface energy balance. Physics and Chemistry of the Earth, Part B: Hydrology, Oceans and Atmosphere 25(2):147–57

Rouse, J. W., Haas, R. H., Schell, J. A., Deering, D. W., 1973, Monitoring vegetation systems in the Great Plains with ERTS. Third ERTS Symposium, NASA SP-351 I, 309-317.

Ruelland, Denis, Florent Levavasseur, and Antoine Tribotté. 2010. Patterns and dynamics of land-cover changes since the 1960s over three experimental areas in Mali. International Journal of Applied Earth Observation and Geoinformation 12:11–17.

Rufino, M. C., Rowe, E. C., Delve, R. J., Giller, K. E. 2006, Nitrogen cycling efficiencies through resource-poor African crop–livestock systems. Agriculture, Ecosystems & Environment, 112, pp. 261-282.

Ruhoff, Anderson L. et al. 2012. A MODIS-Based Energy Balance to Estimate Evapotranspiration for Clear-Sky Days in Brazilian Tropical Savannas. Remote Sensing 4(12):703–25. Retrieved May 23, 2013 (http://www.mdpi.com/2072-4292/4/3/703/).

Ruhoff, Anderson L. et al. 2012. A MODIS-Based Energy Balance to Estimate Evapotranspiration for Clear-Sky Days in Brazilian Tropical Savannas. Remote Sensing 4(12):703–25.

Ruimy, A., G. Dedieu, and B. Saugier. n.d. TURC: A diagnostic model of continental gross primary productivity and net primary productivity. Global Biogeochemical Cycles 10(2):269–85.

Ruimy, A., L. Kergoat, and A. Bondeau. 1999. Comparing global models of terrestrial net primary productivity (NPP): Analysis of differences in light absorption and light-use efficiency. Global Change Biology 5:56–64. Retrieved November 29, 2013 (http://onlinelibrary.wiley.com/doi/10.1046/j.1365-2486.1999.00007.x/full).

Saidou, O., Douma, S., Djibo, A.Z., Fortina, R., 2010, Analysis of herbaceous populations at the Toukounous Sahelian experimental station (Niger): Floral composition and pastoral value. Science et changements planètaires secheresse, 21 (2), pp. 154-60.

Samaké, K. 2006. Etude de la gestion communautaire transfrontalière des ressources naturelles: cas des villages de Bih (Mali) et Douari (Burkina Faso) – Rapport final. 28 p

Sandholt, Inge, Kjeld Rasmussen, and Jens Andersen. 2002. A simple interpretation of the surface temperature/vegetation index space for assessment of surface moisture status. Remote Sensing of Environment 79(2-3):213–24

Schimmer, R., Geerken, A., Kiernan, B., 2008. Tracking the genocide in Darfur: population displacement as recorded by remote sensing. Genocide Studies Working Paper 36, Yale University, 51 p.

Schlecht, E., Hiernaux, P.. 2006. A spatio-temporal analysis of forage availability and grazing and excretion behaviour of herded and free grazing cattle, sheep and goats in Western Niger. Agriculture, Ecosystems and Environment 113, 226-242.

Seaquist, J. 2003. A remote sensing-based primary production model for grassland biomes. Ecological Modelling 169(1):131–55.

Seaquist, J.W., Hickler, T., Eklundh, L., Ardo, J., Heumann, B.W., 2009. Disentangling the effects of climate and people on Sahel vegetation dynamics. Biogeosciences, 6, 469-477

Sen, P., 1968. Estimates of the regression coefficient based on Kendall's tau. Journal of the American Statistical Association 63, 1379-1389.

Sepulcre-cantó, Guadalupe et al. 2013. Estimating crop-specific evapotranspiration using remote-sensing imagery at various spatial resolutions for improving crop growth modelling. International Journal of Remote Sensing (February):3274–88.

Sjöström, M. et al. 2011. Exploring the potential of MODIS EVI for modeling gross primary production across African ecosystems. Remote Sensing of Environment 115(4):1081–89.

Sjöström, M. et al. 2013. Evaluation of MODIS gross primary productivity for Africa using eddy covariance data. Remote Sensing of Environment 131:275–86. Retrieved November 19, 2013 (http://linkinghub.elsevier.com/retrieve/pii/S0034425712004890).

Smets, B., H. Eerens, T. Jacobs, and A. Royer. 2010. BioPar Dry Matter Productivity (DMP) Product User Manual.

Sobrino, J. a., M. Gómez, J. C. Jiménez-Muñoz, and A. Olioso. 2007. Application of a simple algorithm to estimate daily evapotranspiration from NOAA–AVHRR images for the Iberian Peninsula. Remote Sensing of Environment 110(2):139–48.

Soler, C. M. T., N. Maman, X. Zhang, S. C. Mason, and G. Hoogenboom. 2008. Determining optimum planting dates for pearl millet for two contrasting environments using a modelling approach. The Journal of Agricultural Science 146(04):445–59.

Song, C., Woodcock, C.E., Seto, K.C., Lenney, M.P., Macomber, S.A. 2000. Classification and Change Detection Using Landsat TM Data: When and How to Correct Atmospheric Effects? Remote Sensing of Environment 75, 230-244.

Stroppiana, D., M. Boschetti, P. A. Brivio, F. NUtini, and E. Bartholomè. 2011. Analysis of earth observation time series to investigate the relation between rainfall, vegetation dynamic and streamflow in the Uele'basin (Central African Republic). Analysis of Multi- 177–80. Retrieved December 9, 2013 (http://ieeexplore.ieee.org/xpls/abs_all.jsp?arnumber=6005077).

Sturges, HA. 1926. The choice of a class interval. Journal of the American Statistical Association 21(153):65–66. Retrieved September 30, 2013 (http://www.aliquote.org/cours/2012_biomed/biblio/Sturges1926.pdf).

Su, Z. 2002. The Surface Energy Balance System (SEBS) for estimation of turbulent heat fluxes. Hydrology and Earth System Sciences 6(1):85–99.

Sun, Zhongping et al. 2011. Evapotranspiration estimation based on the SEBAL model in the Nansi Lake Wetland of China. Mathematical and Computer Modelling 54(3-4):1086–92. Retrieved May 23, 2013 (http://linkinghub.elsevier.com/retrieve/pii/S0895717710005303).

Suttie, J.M., Reynolds, S.G., Batello, C., 2005. Grassland of the world. FAO-UN, Rome, 419-424.

Taddei, R., 1997, Maximum value interpolated (MVI): a maxi-mum value composite method improvement in vegetation index profile analysis. International Journal of Remote Sensing, 18(11), pp. 2365-2370.

Tang, Ronglin et al. 2013. Spatial-scale effect on the SEBAL model for evapotranspiration estimation using remote sensing data. Agricultural and Forest Meteorology 174-175:28–42.

Tang, Ronglin, Zhao-Liang Li, and Bohui Tang. 2010. An application of the Ts–VI triangle method with enhanced edges determination for evapotranspiration estimation from MODIS data in arid and semi-arid regions: Implementation and validation. Remote Sensing of Environment 114(3):540–51.

Tao, F., M. Yokozawa, Z. Zhang, Y. Xu, and H. Yousay. 2005. Remote Sensing of Crop Production in China by Production Efficiency Models: Models Comparisons, Estimates and Uncertainties. Ecological Modelling 183:385–96.

Teixeira, a. H. De Castro, W. G. M. Bastiaanssen, M. D. Ahmad, M. S. B. Moura, and M. G. Bos. 2008. Analysis of energy fluxes and vegetation-atmosphere parameters in irrigated and natural ecosystems of semi-arid Brazil. Journal of Hydrology 362(1-2):110–27.

Therneau, TM, and EJ Atkinson. 2013. An introduction to recursive partitioning using the RPART routines.

Thrupp, N., and L. A. Megateli. 1999. Critical Links: Food security and the environment in the Greater Horn of Africa. edited by ILRI. Washington.

Tou, J. T., Gonzalez, R. C., 1974, Pattern Recognition Principles, (Addison- Wesley-Longman, Reading, Mass).

Tucker, C. J., J. R. Townshend, and T. E. Goff. 1985. African land-cover classification using satellite data. Science (New York, N.Y.) 227(4685):369–75.

Tucker, C., C. Vanpraet, E. Boerwinkel, and a Gaston. 1983. Satellite remote sensing of total dry matter production in the Senegalese Sahel. Remote Sensing of Environment 13(6):461–74.

Tucker, C.J., Nicholson, S.E., 1999. Variations in the size of the Sahara desert from 1980 to 1997. Ambio 28, 587–591.

Tucker, C.J., Vanpraet, C.L., Sharman, M.J., Van Ittersum, G., 1985. Satellite remote sensing of total herbaceous biomass production in the senegalese sahel: 1980–1984. Remote Sensing of Environment 17, 233-249.

Turner, David P., Stith T. Gower, Warren B. Cohen, Matthew Gregory, and Tom K. Maiersperger. 2002. Effects of spatial variability in light use efficiency on satellite-based NPP monitoring. Remote Sensing of Environment 80(3):397–405.

UNHCR (2012). Global Appeal 2012-2013, Africa, Chad, pp. 50-53, http://www.unhcr.org/4ec230faa.html, last access April 2012.

US Dept. of State, 2010. Darfur, Sudan: confirmed damaged and destroyed villages, February 2003 – December 2009 (map). Humanitarian Information Unit, ref U179 4-10 STATE (HIU).

Van Vliet, Nathalie, Anette Reenberg, and Laura Vang Rasmussen. 2013. Scientific documentation of crop land changes in the Sahel: A half empty box of knowledge to support policy? Journal of Arid Environments 95:1–13.

Venturini, V., S. Islam, and L. Rodriguez. 2008. Estimation of evaporative fraction and evapotranspiration from MODIS products using a complementary based model. Remote Sensing of Environment 112(1):132–41.

Vermote, E. F., Tanrè, D., Deizè, J. L., Herman, M., Morcrette, J. J., 1997, Second Simulation of the Satellite Signal in the Solar Spectrum, 6S: An Overview. IEEE Trans. Geoscience and Remote Sensing, 35, pp. 675-686.

Verstraeten, Willem W., Frank Veroustraete, and Jan Feyen. 2005. Estimating evapotranspiration of European forests from NOAA-imagery at satellite overpass time: Towards an operational processing chain for integrated optical and thermal sensor data products. Remote Sensing of Environment 96(2):256–76.

Verstraeten, Willem W., Frank Veroustraete, and Jan Feyen. 2006. On temperature and water limitation of net ecosystem productivity: Implementation in the C-Fix model. Ecological Modelling 199(1):4–22.

Vinukollu, Raghuveer K., Eric F. Wood, Craig R. Ferguson, and Joshua B. Fisher. 2011. Global estimates of evapotranspiration for climate studies using multi-sensor remote sensing data: Evaluation of three process-based approaches. Remote Sensing of Environment 115(3):801–23.

Wang, Jing, Xin Li, Ling Lu, and Feng Fang. 2013. Estimating near future regional corn yields by integrating multi-source observations into a crop growth model. European Journal of Agronomy 49:126–40.

Wang, Jing, Xin Li, Ling Lu, and Feng Fang. 2013. Estimating near future regional corn yields by integrating multi-source observations into a crop growth model. European Journal of Agronomy 49:126–40.

White, F., 1983. The Vegetation of Africa. A Descriptive Memoir to Accompany the UNESCO/AETFAT/UNSO Vegetation Map of Africa, UNESCO, Paris.

Wickens, G.E., 1997. Has the Sahel a future?, Journal of Arid Environments 37, 649-663.

World Bank (2010) Local Development, Institutions and Climate Change in Niger. Situation Analysis and Operational Recommendations pp 88. Available at http://siteresources.worldbank.org/EXTSOCIALDEVELOPMENT/Resources, last access May 2011.

WORLD METEOROLOGICAL ORGANIZATION. 2000. world climate programme data and monitoring world climate programme – water detecting trend and other changes in hydrological data. Pp. 1–158 in, edited by Zbigniew Kundzewicz and Alice Robson. Geneva.

Yang, Da-wen, He Chen, and Hui-min Lei. 2013. Analysis of the Diurnal Pattern of Evaporative Fraction and Its Controlling Factors over Croplands in the Northern China. Journal of Integrative Agriculture 12(8):1316–29.

Yuan, Wenping et al. 2007. Deriving a light use efficiency model from eddy covariance flux data for predicting daily gross primary production across biomes. Agricultural and Forest Meteorology 143(3-4):189–207.

Zecchini, M., and A. Cantàfora. 2010. Prudurre latte in africa subsahariana.

Zhao, M. 2005. Improvements of the MODIS terrestrial gross and net primary production global data set. Remote Sensing of Environment 95(2):164–76.

Zorom, Malicki, Bruno Barbier, Ole Mertz, and Eric Servat. 2013. Diversification and adaptation strategies to climate variability: A farm typology for the Sahel. Agricultural Systems 116:7–15.